

Combustion of Bio-oil and Heavy Fuel Oil

Farooq Abubakar Atiku

**Submitted in accordance with the requirements for the degree of
Doctor of Philosophy**

The University of Leeds

**Energy Research Institute
School of Chemical and Process Engineering**

November 2015

Intellectual Property and Publication Statements

The candidate confirms that the work submitted is his own, except where work which has formed part of jointly-authored publications has been included. The contribution of the candidate and the other authors to this work has been explicitly indicated below. The candidate confirms that appropriate credit has been given to within the thesis where reference has been made to the work of others. Further details of the jointly-authored publications and the contributions of the candidate and the authors to the work are listed below.

1. Lea-Langton AR; Baeza-Romero MT; Boman GV; Brooks B; Wilson AJM; Atiku FA; Bartle KD; Jones JM; Williams A (2014): A study of smoke formation from wood combustion. *Fuel Processing Technology*, vol. 137, pp.327-332.

I performed much of the experimental work (Wick burner experiments, Ultimate analysis, thermogravimetric combustion TGA, pyrolysis gas chromatography mass spectrometry Py-GCMS, transmission electron microscopy TEM, and differential mobility spectrometry DMS, and was the lead co-ordinator for collecting a large part of the analysed experimental data.

Alan Williams was the lead author. The aerosol time of flight mass spectrometry work, ATOFMS, was conducted by G.V; Boman.

2. A.R. Lea-Langton, F. A. Atiku, K.D. Bartle, J.M. Jones, M Pourkashanian, A Williams, I. Burns, G. Humphries (2015): Mechanism of the formation of smoke from the combustion of wood MCS-2015: *Ninth Mediterranean Combustion Symposium 7-11 June 2015*. Page 10, Sheraton Rhodes Resort, Rhodes, Greece.

I carried out all the experimental work (fuel combustion and diffusion flames photography/image analysis, designed the novel soot sampling device, TEM, Py-GCMS, DMS, burning rate calculations and analysis of all the generated results and some part of the research group discussion.

Chapter four is based on this conference paper but with the complete data set of results included.

3. A.R. Lea-Langton, F.A. Atiku, K.D. Bartle, J.M. Jones, M. Pourkashanian and A. Williams (2015): Some Aspects of the Combustion of High Asphaltene Heavy Oils. 10th European Conference on Industrial Furnaces and Boilers. ISBN: 978-972-99309-7-3) 7th -10th April, 2015, Lisbon, Portugal.

I conducted some of the major experiments and data analysis for this work.

Amanda Lea-Langton was the lead author and co-coordinator for the experimental work.

4. A.R. Lea-Langton, F.A. Atiku, K.D. Bartle, P. Biller, J.M. Jones, A.B. Ross and A. Williams.,(2015): Asphaltene Structure and its Effect on the Combustion of Heavy Fuel Oils. 1st Chemistry in Energy Conference, 20th to 23rd July, 2015 Heriot-Watt University Edinburgh, UK.

Chapter five is based on this conference paper, but with the complete data set of results included.

5. F.A. Atiku, E.J.S. Mitchell, A.R. Lea-Langton, J.M. Jones, A. Williams and K.D. Bartle., (2016): The Impact of Fuel Properties on the Composition of Soot Produced by the Combustion of Biomass and Some other Solid Fuels. Submitted for publication in Fuel Process Technology; FUPROC-D-16-00274.

I was lead author and also lead conductor and co-ordinator of experiments and experimental data respectively.

This copy has been supplied on the understanding that it is copyright material and that no quotation from the thesis may be published without proper acknowledgement.

Acknowledgements

First and foremost I would like to thank my brilliant supervisor Professor Jenny M. Jones; for the guidance and support she provided throughout the course of this work. Jenny was a great supervisor and I am very grateful for all the hard work and guidance she has provided throughout my PhD. I would like to thank my co-supervisors. Professor Alan Williams ‘ambitious parent’. Alan’s discussions on this work were of great importance, without his cool persuasion this work would not have produced the papers. I thank him for the push when required. Many thanks also to Dr Amanda R Lea-Langton who was my third supervisor throughout my PhD, without her experience, ideas and unlimited assistance; most of my experimental work would have been nearly impossible.

For financial support under tertiary education trust fund TETFUND. Thanks are due to Kebbi State University of Science and Technology, Aliero, Nigeria. Also many thanks go to EPSRC and Supergen Bioenergy Hub under the grant number RG/ERI 483135. At this juncture I would also like to say a big thank you to the Coal Research Council UK, and the Royal Society of Chemistry for their financial support in attending conferences.

Thanks to Professor Keith Bartle whose wealth of chemistry knowledge was very crucial towards mechanistic aspect of the discussions. A big thank you to Dr Robert Fowell (Bob) for his unlimited advises and encouragements towards this great achievement. Thanks are also due to Dr Nicole Hundow for her assistance with transmission electron microscopy. Also special thank you to our technician Simon Lloyd who was always there for me with any query I had. This work would not have been possible without the help of numerous people in the laboratory and office. Therefore I would like to thank Dr Adrian Cunliffe, Sara Dona, Karin Alves Thorne, Ed Woodhouse, Chris Day, and Tersem Hudson for all their technical assistance. Thanks to Heather Strachan, Sheilagh Ogden, and David Haynes for clerical assistance.

I have also been lucky in having great friends and colleagues in my research group. Thanks to Eddy Mitchel, Ben Dooley, Leilani Darvell, Patrick Biller (A special thank you for the AED work), Surjit Singh, Bijal Gudka, Femi Akinrinola, Thomas Robin, Patrick Mason, Paula

McNamee, Yessing Chin, Douglas Phillips, Kasturi Shikhapure, Kiran Parmer, Peinong Xing, and Paul Straker - with your support I got everything done.

A special thanks is due to my wife, son and daughter; Dr Asmau Mohammed Wali, Abdullahi Farooq, and Maryam Farooq for their utmost support, endurance, love and care, and above all, their prayers.

Finally, the most important people I need to thank, my wonderful Mother Aisha Abubakar Atiku for support (prayers) to this point; and also the rest of my family. Thank are due to Hajia Saudi Abubakar Atiku, Engr. Mohammed Murtala Atiku, Dr Chika Abubakar Atiku, Hajia Rukayya Abubakar Atiku, Rafia Abubakar Atiku, Hadiza Abubakar Atiku, Zainab Abubakar Atiku, Aisha Abubakar Atiku, Abdulrahman Abubakar Atiku, and last but not the least of the family Abbas Abubakar Atiku. Finally, I thank my friends and colleagues for their friendship and support.

Table of contents

Contents

Combustion of Bio-oil and Heavy Fuel Oil.....	1
Intellectual Property and Publication Statements	2
Acknowledgements.....	4
Table of contents.....	6
List of abbreviation.....	13
List of tables.....	14
List of figures.....	16
Abstract.....	22
Chapter 1 General introduction.....	23
1.1 Global carbon emissions	23
1.2 Fossil fuels	24
1.3 Fuel oil	24
1.4 Bio-fuels combustion in relation to fossil fuels	25
1.4.1 Pyrolysis of biomass and bio-oil.....	25
1.4.2 Pyrolysis leading to bio-oil production.....	27
1.5 Fuel oil and climate change	27
1.5.1 Classification of emissions	28
1.5.2 Black carbon (BC).....	28
1.5.3 Black carbon emissions and their abundance	29
1.5.4 Organic carbon, reactions and formation of polycyclic aromatic hydrocarbons PAHs	30
1.5.5 Emission of organic carbon aerosol from fossils fuel combustion.....	31
1.5 Thesis overview	32
1.6 Research aim.....	33
1.7 Research objectives.....	33
1.8 Thesis Outline	35

Chapter 2 Literature survey	38
2.1 Current use of fossils fuels.....	38
2.2 Combustion of sprays and oil droplets.....	46
2.2.1 Combustion of droplet liquid fuels and biomass particles.....	46
2.2.2 Nature of spray combustion.....	49
2.3. Liquid fuels used in spray combustion and their sources	53
2.3.1 Fuel oil from crude oil.....	54
2.3.2 Oil from shale and oil sands	55
2.3.3 Liquids from coal.....	56
2.3.3.1 Coal pyrolysis.....	56
2.3.4 Biomass liquid fuels	57
2.4. The nature and properties of Fuel Oils.....	59
2.4. Chemical and physical properties	59
2.4.1 Smoke point.....	59
2.4.1.1 Smoke point or soot threshold.....	60
2.4.3 Volatility	63
2.4.5 Viscosity	63
2.4.7 Pour point and cloud point.....	64
2.4.8 Heat of combustion.....	64
2.4.9 Sulphur content.....	65
2.4.10 Asphaltenes.....	66
2.4.11 Flash and fire point.....	66
2.5. Light oils (LOs)	66
2.6 Diesel fuels and gas oil	67
2.7. Heavy fuel oils (HFO)	68
2.7.1 Industrial application of fuel oil	69
2.8 Smoke emissions.....	71
2.8.1 Origin and general description of soot.....	71
2.8.2 Mechanisms of soot formation and oxidation for hydrocarbons	72

	8
2.8.2.1 Structure and properties of soot.....	72
2.8.2.2 Soot formation mechanisms/stages	75
2.8.2.3 Fuel Pyrolysis.....	76
2.8.2.4 Nucleation	78
2.8.2.5 Surface growth	80
2.8.2.6 Coalescence and agglomeration	81
2.8.2.7 Oxidation.....	82
2.8.2.8 CO formation.....	83
2.9 Bio-fuels.....	84
2.9.1 Pyrolysis oils from wood.....	84
2.9.2 Pyrolysis of biomass and bio-oil Pyrolysis.....	85
2.9.3 Pyrolysis leading to bio-oil production.....	86
2.9.3.1 Types of Pyrolysis.....	86
2.9.3.2 Conventional/slow pyrolysis.....	86
2.9.3.3 Fast pyrolysis.....	87
2.9.4 Pyrolysis process reactions	88
2.9.5 Pyrolysis oil upgrading reactions.....	90
2.9.6 Co-pyrolysis and atmospheric distillation of bio-oil	91
2.10 Factors affecting the pyrolysis of biomass.....	93
2.10.1 Effect of sample composition and size	93
2.10.2 Effect of heating rate and temperature.....	94
2.10.3 Effect of volatile and solid residence time	94
2.11 Pyrolysis reactors.....	95
2.11.1 Bubbling fluidized bed reactors.....	95
2.11.2 Auger reactors.....	96
2.11.3 Ablative pyrolysis reactors	97
2.11.4 Vacuum pyrolysis reactor	98
2.11.5 Entrained flow reactors.....	99
2.12. Steps in biomass combustion.....	100

2.12.1 Combustion steps.....	101
2.12.1.1 Drying	102
2.12.1.2 Pyrolysis.....	102
2.13 Gasification.....	103
2.14 Liquefaction.....	103
Chapter 3 Experimental methods.....	104
3.0 Introduction.....	104
3.1 Fuels.....	104
3.1.1 Asphaltene extraction	104
3.2 Soot sampling methods.....	107
3.3 Smoke point	108
3.2.1 Experimental method.....	108
3.3.2 Smoke point (SP) experimental procedure.....	109
3.4 Elemental analysis	112
3.5 Size exclusion chromatography (SEC).....	113
3.6 Transmission electron microscopy (TEM)	113
3.7 Scanning electron microscopy, SEM.....	115
3.8 Differential mobility spectrometry DMS and soot sampling.....	116
3.8.1 DMS Instrumentation and its basic operations.....	116
3.8.1.1 System dilution.....	117
3.9 Laser induced incandescence (LII)	119
3.9.1 Time-resolved laser induced incandescence (T-R LII).....	120
3.10 Pyrolysis Gas Chromatography Mass Spectrometry (Py-GCMS).....	122
3.10.1 Pyrolysis GCMS Sample preparation.....	122
3.10.2 Pyrolysis method for soot sample.....	123
3.10.3 Sequential Temperature Application (STA).....	124
3.11 Thermogravimetric analysis TGA.....	125
Chapter 4 Combustion of model compounds.....	126
4.1 Introduction.....	126

	10
4.2 Composition of black carbon /organic carbon and its effect	127
4.2.1 Experimental Methods.....	129
4.2.1.1 Soot sampling.....	129
4.2.1.2 Thermogravimetric analysis TGA.....	129
4.2.1.3 Pyrolysis gas chromatography Py-GCMS.....	129
5.3 Experimental Results	130
4.3.1 TGA-FTIR Analysis	130
4.3.2 Pyrolysis-GC-MS	132
4.4 Discussion.....	139
4.4.1 Determination of EC/TC ratios by different methods.	139
4.4.2 Variation of EC/TC ratios with fuel, combustion conditions and sample collection method.	141
4.4.3 Chemical composition of soot pyrolysis products.....	141
4.5 Conclusions.....	142
4.6 Particle size distributions and volatile composition of soot from diffusion flames.....	143
4.6.0 Introduction	143
4.6.1 Experimental methods	145
4.6.1.1 Pyrolysis gas chromatography mass spectrometry (Py-GC-MS).....	145
4.6.1.2 Differential mobility spectrometry and soot sampling.....	145
4.6.2 Results and discussion.....	146
4.6.2.1 Particle size distribution of soot (PSDS).....	146
4.6.2.2 Pyrolysis- Gas Chromatography Mass Spectrometry (Py-gcms).....	153
4.6.3 Discussion.....	158
4.6.4 Conclusions	158
4.7 Elemental analysis of soot fuel properties and burning characteristics	159
4.7.1 Results and discussion.....	159
4.8 Model fuel burning rate, emission factors and morphological structure of soot and its formation mechanisms.....	162
4.8.1 Introduction	162

	11
4.8.2 Material and methods	163
4.8.3 Analytical technique	164
4.8.3. Design of thermophoretic soot sampling device and testing	164
4.8.4 Results and discussion	165
4.8.4.1 Scanning electron microscopy.....	165
4.8.4.2 Transmission electron microscopy.....	166
4.8.5 Flame photography of the combusted fuels.....	179
4.8.5.1 Direct photography.....	179
4.8.5.2 CH* emission from flames.....	180
4.8.5.3 C ₂ * emission from flames.....	181
4.8.5.4 Smoke point, mass burning rate and soot emission factor	182
4.8.6 Discussion.....	183
4.8.7 Conclusion.....	184
Chapter 5 Heavy Fuel Oil Combustion.....	185
5.0 Introduction.....	185
5.1 Background.....	186
5.2 Experiments conducted.....	187
5.2.1 Extraction of asphaltenes and their characterisation.....	187
5.2.2 Ultimate analysis	187
5.2.3 Size exclusion chromatography.....	188
5.2.4 Thermogravimetric analysis (TGA).....	190
5.2.5 Pyrolysis - GC of asphaltenes	190
5.3 Experimental results and discussion	191
5.3.1 Pyrolysis of asphaltenes.....	191
5.3.2 Thermal reactions of asphaltenes.....	201
5.3.3 Structure of asphaltenes: affinities with lower MW petroleum fractions.....	204
5.3.4 Thermogravimetric analysis	206
5.3.5 Routes to smoke formation during the combustion of heavy oils.	208
5.3.6 Environmental significance of heavy oil asphaltene structure	209

	12
5.4 Conclusions.....	211
Chapter 6 Bio-oil combustion and its derived asphaltenes	212
6.1 Introduction.....	212
6.2 Background.....	214
6.2 Aim and objectives	215
6.2.1 Research aims	215
6.3 Experimental techniques.....	215
6.3.1 Preparation and extraction of bio-asphaltene.....	215
6.3.2 Ultimate analysis and some physical parameters	215
6.3.3 Thermogravimetric analysis	216
6.3.4 Pyrolysis of the bio-oil asphaltene via Py-GC-MS.....	217
6.4 Results and discussion	217
6.4.1 Properties of fast pyrolysis bio-oil from pine wood	217
6.4.2 Thermogravimetric analysis results.....	218
6.4.3 Pyrolysis gas chromatography mass spectrometry Py-GCMS	221
6.4.3.1 Pyrolysis of Bio-oil	221
6.4.3.2 Pyrolysis of asphaltene derived from pyrolysis bio-oil	233
6.4.4. Nature and pyrolysis bio-oil asphaltene structure.....	248
6.5 Conclusions.....	251
Chapter 7 Conclusion and future work	253
7.1 Introduction.....	253
7.2 Combustion of model compounds	253
7.2.1 Composition of black carbon /organic carbon and its effect	254
7.2.2 Particle size distribution and volatile composition of soot.....	254
7.2.3 Structure of the soot from bio-oil model compounds.....	255
7.3 Heavy fuel oil combustion.....	256
7.4 Bio-oil combustion	257
7.5 Future work.....	258
References.....	260

Appendix A: Data interrogation for both Shell oil and heavy fuel oil asphaltene chromatograms showing different heavy molecular weight compounds.	287
Appendix B: Data interrogation for both Shell oil and heavy fuel oil asphaltene chromatograms showing different lower molecular weight compounds.	294

List of abbreviation

PPP – Purchasing Power Parity

GDP – Gross Domestic Products

TARFOX – Tropospheric Aerosol Radiative Forcing Observational Experiments

DDC- Destructive Distillation of Coal

List of tables

Chapter 1

Table 1- 1 Characteristic of different pyrolysis types and their variants	27
---	----

Chapter 2

Table 2- 1 Bio-oil compared with crude oil characteristics	90
--	----

Chapter 3

Table 3- 1 Fuel samples used in this study: structures and their properties.....	106
--	-----

Chapter 4

Table 4- 1 Major Species types identified in the Soot Organic Carbon Fraction	138
---	-----

Table 4- 2 Comparison of soot EC/TC determined by Py-GCMS with TGA	139
--	-----

Table 4- 3 ET/TC Comparison of Py-GCMS with ATOFMS	140
--	-----

Table 4- 4 Summary of mean diameters and sizes.....	146
---	-----

Table 4- 5 shows the elemental analysis of the model fuels pyrolysis products (soot) generated from a wick burner.....	161
--	-----

Table 4- 6 Average particle size (Dp) from TEM images using ImageJ	167
--	-----

Table 4- 7 Characteristic properties of soot particle agglomerates generated using ImageJ	179
--	-----

Table 4- 8: Fuel properties and burning characteristics	183
---	-----

Chapter 5

Table 5- 1 Elemental composition of the fuels (wt. %).	187
--	-----

Table 5- 2 Atomic emission detection monitoring wavelengths and reagent gases.....	190
--	-----

Table 5- 3 Aromatic hydrocarbons identified in pyrolysis products of asphaltenes (HFO and SMO)	197
--	-----

Table 5- 4 Percentage total stack solids produced by combustion of heavy oils containing different amounts of asphaltenes as a function of flue gas oxygen content.....	207
---	-----

Chapter 6

Table 6- 1 Physical and chemical properties of pyrolysis bio-oil.....	218
---	-----

Table 6- 2 Elemental composition for Bio-crude asphaltene from fast pyrolysis bio-oil	218
---	-----

Table 6- 3 Compound identification for bio-oil at 300°C pyrolysis temperature	222
---	-----

Table 6- 4 Compound identification for bio-oil at 400°C pyrolysis temperature	223
Table 6- 5 Identification of compound for bio-oil at 500°C pyrolysis temperature.....	224
Table 6- 6 Compound identification for bio-oil at 600°C pyrolysis temperature	225
Table 6- 7 Compound identification for bio-oil at 700°C pyrolysis temperature	226
Table 6- 8 Compound identification for bio-oil at 800°C pyrolysis temperature	227
Table 6- 9 Compound identification for bio-oil at 900°C pyrolysis temperature	228
Table 6- 10 Compound identification for bio-oil at 1000°C pyrolysis temperature	230
Table 6- 11 Compound identification for bio-oil at 1100°C pyrolysis temperature	231
Table 6- 12 Compound identification for bio-oil at 1200°C pyrolysis temperature	232
Table 6- 13 Interrogation of the GCMS data for bio-oil asphaltene from Bio-oil at 300C.....	234
Table 6- 14 Interrogation of the GCMS data for bio-oil asphaltene from Bio-oil at 400°C	235
Table 6- 15 Interrogation of the GCMS data for bio-oil asphaltene from Bio-oil at 500°C	237
Table 6- 16 Interrogation of the GCMS data for bio-oil asphaltene from Bio-oil at 600°C	240
Table 6- 17 Interrogation of the GCMS data for bio-oil asphaltene from Bio-oil at 700C.....	241
Table 6- 18 Interrogation of the GCMS data for bio-oil asphaltene from Bio-oil at 800°C	243
Table 6- 19 Interrogation of the GCMS data for bio-oil asphaltene from Bio-oil at 900°C	245
Table 6- 20 Summary and comparison of petroleum and bio-asphaltene fraction	250

List of figures

Chapter 1

Figure 1- 1 Organic carbon sources	25
Figure 1- 2 Biomass conversion technology	26

Chapter 2

Figure 2- 1 Presents Oil, gas, and coal comparative production scenarios	42
Figure 2- 2 The major ideal bio-oil combustion processes in a spray combustion chamber	53
Figure 2- 3 Crude oil fractions yielding highly asphaltic oil composition.....	70
Figure 2- 4 Residuum (maltenes) subdivisions producing more asphaltene fraction	70
Figure 2- 5 TEM images of agglomerates and primary particles.....	74
Figure 2- 6 Schematic of substructure of carbon particle	74
Figure 2- 7 Schematic diagram of the soot formation steps.....	75
Figure 2- 8 Pathways for the formation of the first benzene moiety from acetylene.....	77
Figure 2- 9 HACA mechanism of polycyclic aromatic hydrocarbon formation.....	79
Figure 2- 10 Combination of benzyl with propargyl	79
Figure 2- 11 Combination of two cyclopentadienyl	80
Figure 2- 12 Combination of cyclopentadienyl and indenyl.....	80
Figure 2- 13 Propargyl radical reactions leading to phenanthrene formation.....	80
Figure 2- 14 General proposed mechanism of soot formation.....	82
Figure 2- 15 Pyrolysis of wood leading to liquid fuels production.....	84
Figure 2- 16 Biomass conversion technology products	85
Figure 2- 17 Structural representation of some compounds of bio-oil	88
Figure 2- 18 Some pyrolysis reactions of bio-oil.....	89
Figure 2- 19 Pyrolysis upgrading reactions of bio-oil	90
Figure 2- 20 Schematic of the direct atmospheric distillation coupled with co-pyrolysis process to produce chemical feedstock.....	92
Figure 2- 21 Photographs of raw bio-oil, different fractions of distillate and the atmospheric distillation residue	93

Figure 2- 22 Bubbling fluidized bed reactor	96
Figure 2- 23 Ablative reactor	97
Figure 2- 24 Vacuum Pyrolysis reactor	99
Figure 2- 25 Entrained flow reactor	100
Figure 2- 26 Steps in biomass combustion	101

Chapter 3

Figure 3- 1 Soot sampling set-up using glass microscope slides	107
Figure 3-2 Show the soot generated from cold glass slides for analysis.....	108
Figure 3- 3 Seta smoke point apparatus lamp	110
Figure 3- 4 Shows the smoke point for pure eugenol fuel.	111
Figure 3- 5 Flame shapes showing the smoke point zone, A- above the SP; B- at the SP and C- below SP.	112
Figure 3- 6 TEM images of agglomerates and primary particles adapted from	114
Figure 3- 7 Shows the thermophoretic soot sampling device for TEM analyses.....	115
Figure 3- 8 Principle of operation for the DMS 500 Series	117
Figure 3- 9 Dilution system during sampling	118
Figure 3- 10 DMS primary dilution system.....	119
Figure 3- 11 Spectral radiance of a blackbody for different temperatures.....	120
Figure 3- 12 Shows the LII set-up for sampling soot volume fraction in the laboratory.....	123

Chapter 4

Figure 4- 1 TGA plot of analysis for: (a) wood stove soot, (b) eugenol soot.	131
Figure 4- 2 Results of TGA, weight percentage of OC, EC and ash for the fuels studied.....	131
Figure 4- 3 Py-GCMS Chromatograms of; (a) wood stove soot and (b) anisole soot, both produced at 400°C.....	134
Figure 4- 4 Py-GCMS Chromatograms of multi-fuel soot at (a) 400°C, (b) 500°C and (c) 600°C	135
Figure 4- 5 Py GCMS Chromatogram of Forecourt wood at 500°C.....	136
Figure 4- 6 Py GCMS Chromatogram of Rape straw at 500°C.	137

Figure 4- 7 The particle size distributions for soot from n-decane combustion sampled at (a) 5cm, (b) 10cm and (c) 15 cm above the flame.....	149
Figure 4- 8 The particle size distributions for soot from n-heptane combustion sampled at (a) 5cm, (b) 10cm and (c) 15cm above the flame.....	150
Figure 4- 9 The particle size distributions for soot from anisole combustion sampled at (a) 5cm, (b) 10cm and (c) 15 cm above the flame	151
Figure 4- 10 The particle size distributions of soot from eugenol combustion sampled at (a) 5cm, (b) 10cm and (c) 15cm above the flame.....	152
Figure 4- 11 Py-GCMS chromatogram of eugenol soot (5cm) adsorbed at 300 ⁰ C	154
Figure 4- 12 Py-GCMS chromatogram of eugenol soot (10cm) adsorbed at 300 ⁰ C	154
Figure 4- 13 Py-GCMS chromatogram of eugenol soot (15cm) adsorbed at 300 ⁰ C	154
Figure 4- 14 Py-GCMS chromatogram of anisole soot (5cm) adsorbed at 300 ⁰ C.....	155
Figure 4- 15 Py-GCMS chromatogram of anisole soot (10cm) adsorbed at 300 ⁰ C.....	155
Figure 4- 16 Py-GCMS chromatogram of anisole soot (15cm) adsorbed at 300 ⁰ C.....	155
Figure 4- 17 Py-GCMS chromatogram of n-decane soot (5cm) adsorbed at 300 ⁰ C.....	156
Figure 4- 18 Py-GCMS chromatogram of n-decane soot (10cm) adsorbed at 300 ⁰ C.....	156
Figure 4- 19 Py-GCMS chromatogram of n-decane soot (15cm) adsorbed at 300 ⁰ C.....	156
Figure 4- 20 (a) Py-GCMS chromatogram of n-heptane soot (5cm) adsorbed at 300 ⁰ C.....	157
Figure 4- 21 Py-GCMS chromatogram of n-heptane soot (10cm) adsorbed at 300 ⁰ C	157
Figure 4- 22 (c) Py-GCMS chromatogram of n-heptane soot (15cm) adsorbed at 300 ⁰ C.....	157
Figure 4- 23 Van Krevelen analysis of soots showing hydrogen /carbon to oxygen carbon ratio generated from the model fues.....	160
Figure 4- 24 Schematic diagram of soot sampling device	164
Figure 4- 25 Scanning electron microscopy (SEM) images of soots deposited on glass slides of diffusion flames for (a) anisole (b) n-decane (c) furfural and (d) eugenol.	166
Figure 4- 26 TEM micrographs of (a1-2) anisole, (b1-2) eugenol, (c1-2) furfural, (d1-2) decane and (e1-2) heptane.....	172
Figure 4- 27 Image analysis of Heptane soot TEM micrographs using ImageJ	174
Figure 4- 28 Image analysis of Decane soot TEM micrographs using ImageJ.....	175

Figure 4- 29 Image analysis of Eugenol soot TEM micrographs using ImageJ	176
Figure 4- 30 Image analysis of furfural soot TEM micrographs using ImageJ	177
Figure 4- 31 Image analysis of anisole soot TEM micrographs using ImageJ	178
Figure 4- 32 Direct photography of flames for the model fuels	180
Figure 4- 33 CH* filtered flames for different oils using a 430 nm optical filter	181
Figure 4- 34 C ₂ * analysis of the soots of the pyrolysis oils using 520nm optical filter.....	182

Chapter 5

Figure 5- 1 Size exclusion chromatogram showing the molecular weight distribution in the asphaltene fraction of Shell Marine oil.....	188
Figure 5- 2 Size exclusion chromatogram showing heavy molecular weight of organic fraction of SMO asphaltene.....	189
Figure 5- 3 Size exclusion chromatogram showing heavy molecular weight of organic fraction of HFO asphaltene	189
Figure 5- 4 TGA of Bunker C fuel oil asphaltene.....	191
Figure 5- 5 TGA of Heavy fuel oil asphaltene.....	192
Figure 5- 6 Derivative weight loss for H F O asphaltene	192
Figure 5- 7 Derivative weight loss for Bunker C fuel oil asphaltene.....	193
Figure 5- 8 TGA profiles comparing the three asphaltene fractions in temperature programmed pyrolysis under nitrogen, followed by combustion in air.	194
Figure 5- 9 Derivative weight loss time plots comparing the three asphaltene fractions.	194
Figure 5- 10 Typical Py –GC-MS of asphaltenes at (a) 300, (b) 400 and (c) 500C (d) 600C.	196
Figure 5- 11 Typical Py –GC-MS of asphaltenes at (e) 700, (f) 800 and (g) 900C (h) 1000C.	199
Figure 5- 12 Py-GC-AED of Bunker C Oil Asphaltene with sulphur detection at 181nm.	200
Figure 5- 13 Dimethylnaphthalene region (m/z 156) of pyrolysis product of Bunker C asphaltene at 600 ⁰ C.....	204
Figure 5- 14 General reaction scheme for the pyrolysis of asphaltenes showing the effect on ignition, soot and cenosphere formation.....	205
Figure 5- 15 Vanadium content for Shell marine asphaltene, Heavy fuel oil asphaltene, and Bio-oil asphaltene	208

Figure 5- 16 intrinsic oxidation rate of soot, HFO cenospheres and cokes	209
Chapter 6	
Figure 6- 1 Extraction of Bio-oil-asphaltene	216
Figure 6- 2 TGA for Bio-oil Asphaltene fraction	219
Figure 6- 3 Derivative weight loss for Bio-oil Asphaltene	220
Figure 6- 4 Mass loss curves, derivative of mass loss (DTG) curves and temperature against time for the bio-oil asphaltene sample from TGA pyrolysis using STA	220
Figure 6- 5 Py-GCMS Chromatogram of Bio-oil with marker compounds indicated at 300°C pyrolysis temperature.....	222
Figure 6- 6 Py-GCMS Chromatogram of Bio-oil with marker compounds indicated at 400°C pyrolysis temperature.....	223
Figure 6- 7 Py-GCMS Chromatogram of Bio-oil with marker compounds indicated at 500°C pyrolysis temperature.....	224
Figure 6- 8 Py-GCMS Chromatogram of Bio-oil with marker compounds indicated at 600°C pyrolysis temperature.....	225
Figure 6- 9 Py-GCMS Chromatogram of Bio-oil with marker compounds indicated at 700°C pyrolysis temperature.....	226
Figure 6- 10 Py-GCMS Chromatogram of Bio-oil with marker compounds indicated at 800°C pyrolysis temperature.....	227
Figure 6- 11 Py-GCMS Chromatogram of Bio-oil with marker compounds indicated at 900°C pyrolysis temperature.....	228
Figure 6- 12 Py-GCMS Chromatogram of Bio-oil with marker compounds indicated at 1000°C pyrolysis Temp.....	229
Figure 6- 13 Py-GCMS Chromatogram of Bio-oil with marker compounds indicated at 1100°C pyrolysis temperature.....	230
Figure 6- 14 Py-GCMS Chromatogram of Bio-oil with marker compounds indicated at 1200°C pyrolysis temperature.....	231
Figure 6- 15 Py-GCMS chromatogram of asphaltene extract from Pyrolysis bio-oil at 300°C	233
Figure 6- 16 Py-GCMS chromatogram of asphaltene extract from Pyrolysis bio-oil at 400°C	234

Figure 6- 17 Py-GCMS chromatogram of asphaltene extract from Pyrolysis bio-oil at 500°C 236

Figure 6- 18 Py-GCMS chromatogram of asphaltene extract from Pyrolysis bio-oil at 600°C238

Figure 6- 19 Py-GCMS chromatogram of asphaltene extract from Pyrolysis bio-oil at 700°C239

Figure 6- 20 Py-GCMS chromatogram of asphaltene extract from Pyrolysis bio-oil at 800°C 242

Figure 6- 21 Py-GCMS chromatogram of asphaltene extract from Pyrolysis bio-oil at 900°C244

Figure 6- 22 Py-GCMS chromatogram of asphaltene extract from Pyrolysis bio-oil at 1000°C
..... 246

Figure 6- 23 Py-GCMS chromatogram of asphaltene extract from Pyrolysis bio-oil at 1100°C
..... 247

Abstract

The use of combustion parameters to predict what happens to fuel during burning and its effect on living systems is important. This work is directed towards understanding the fundamental chemistry of soot generated from burning biomass-pyrolysis liquid fuels and its mechanism of formation. In this study, fuels such as eugenol, anisole, furfural and some hydrocarbon fuels are subjected to combustion using a wick burner which allowed the burning rate, smoke point and emission factor to be investigated. Reaction zone analysis of flames by direct photography and by using optical filters for further investigation of C_2^* and CH^* species, was conducted. Additionally, detailed characterization of the soot generated was performed, and comparisons were made with soot from petroleum products and from biomass combustion system. The key aim was to generate experimental data and to capture detailed information regarding sooting tendencies with a view to utilize the information which would eventually allow the formation of a comprehensive bio-oil combustion model. This could provide accurate predictions of the combustion characteristics and pollutant formation. Studies are reported on the significant role of high temperature pyrolysis products in soot formation and acquiring further mechanistic insight. This work has been extended to consider heavy petroleum fuel oils (residual oil) during combustion and the effect of composition on combustion products and on the effect on health and the global environment. Heavy fuel oil, such as Bunker C and vacuum residue, are commonly used as fuel for industrial boilers, power generation, and as transport fuels in, for example, in large marine engines. The combustion of these fuels gives rise to carbonaceous particulate emissions including fine soot (Black Carbon or BC) which, along with associated polynuclear aromatic hydrocarbons (PAH): The structure and thermal reactions of petroleum asphaltene have been studied by analytical pyrolysis.

Additionally, related combustion characteristics of the asphaltene extracted from bio-oil have been investigated by pyrolysis gas chromatography-mass spectrometry. The results showed the difference between bio-asphaltene and the petroleum asphaltene and the different tendency to form smoke. They also showed the presence of markers for the bio-asphaltene structure.

Chapter 1 General introduction

Nowadays, the major factor acting across the global energy scene is the on-going focus on climate and environmental issues that arises from the utilisation of fossils fuel reserves. The British Petroleum Statistics Review of World Energy 2015[1] shows that the total proven reserves of fossils fuels were essentially unchanged in 2014. This means that oil remains one of the most abundant reserves, but discoveries of new sources of energy could supersede its consumption. These results for the total proven oil and gas reserves for 2014 are more than double their suspected levels in 1980. The key issue is not whether oil reserves are to be depleted but rather how to utilize these reserves in an efficient and sustainable way, without being a potential threat to health as well as the environment. This is where the issue of carbon emission resulting from the combustion of these fossils fuel in the course of energy generation needs to be considered.

1.1 Global carbon emissions

The growth of energy demand, together with the modification of the fuel mix, has had significant implications for the increase of carbon emissions. In particular, global carbon emissions from energy use are estimated to have risen by just 0.5% (187 MtCO₂) (1) in 2014, the slowest rate of growth for over 15 years, other than in the immediate aftermath of the financial crisis.

Emissions growth of 0.5% in 2014 compares with an average annual growth rate over the past 10 years of 2.0%. Around a quarter of the lower carbon emissions in 2014 relative to the 10-year average can be attributed to weaker GDP growth: global GDP (on a PPP basis) grew by 3.3% in 2014, compared with a 10-year average of 3.7%. The most important driver – accounting for around half of the lower emissions – was the faster rate of improvement in energy intensity. This largely reflects the changing structure of the Chinese economy, together with last year's unusually mild European winter causing the fall in heating demand. The

remainder of the slower growth reflects the greater than average reduction in carbon intensity associated with the changing fuel mix in 2014, predominantly the slowdown in coal consumption and the greater contribution of gas and non-fossil fuels (2, 3).

1.2 Fossil fuels

Fossil fuels generally refers to the buried combustible geological supplies of organic deposits, originated from decayed living organisms that have been turned into crude oil, natural gas, as well as, coal by exposure to heat and pressure beneath the earth's crust for many millions of years (4). Conventional fuels such as light oils (from heavy distillate fractions) are widely used in different types of combustors for energy, power and transport. Burning these fuels is not enough to meet the energy demand without using the heavy fuel oil fractions as fuel oil, which was put into use for power generation many years ago; the associated environment issues emanating from their combustion is quite a problem.

1.3 Fuel oil

Fuel oil also called higher molecular weight oil is mostly utilized in furnaces, heavy duty engines for power generation and marine applications. However, the high energy demand makes these heavy fuel oils are high in aromatics, and hence high carbon content, and some heteroatom compounds such as S and N. The overall effect of burning these fuels results in releasing emissions of soot (black carbon or BC) which has a detrimental effect on atmospheric chemistry and is a contributor to global climate change (5, 6). Biomass burning in combustors and open fires also releases carbon emissions but the difference between the biomass fuels and the fossil fuels is that, for biomass the carbon dioxide undergoes a recycling process by the plants via photosynthesis. The carbon cycle is depicted in Figure 1-1.

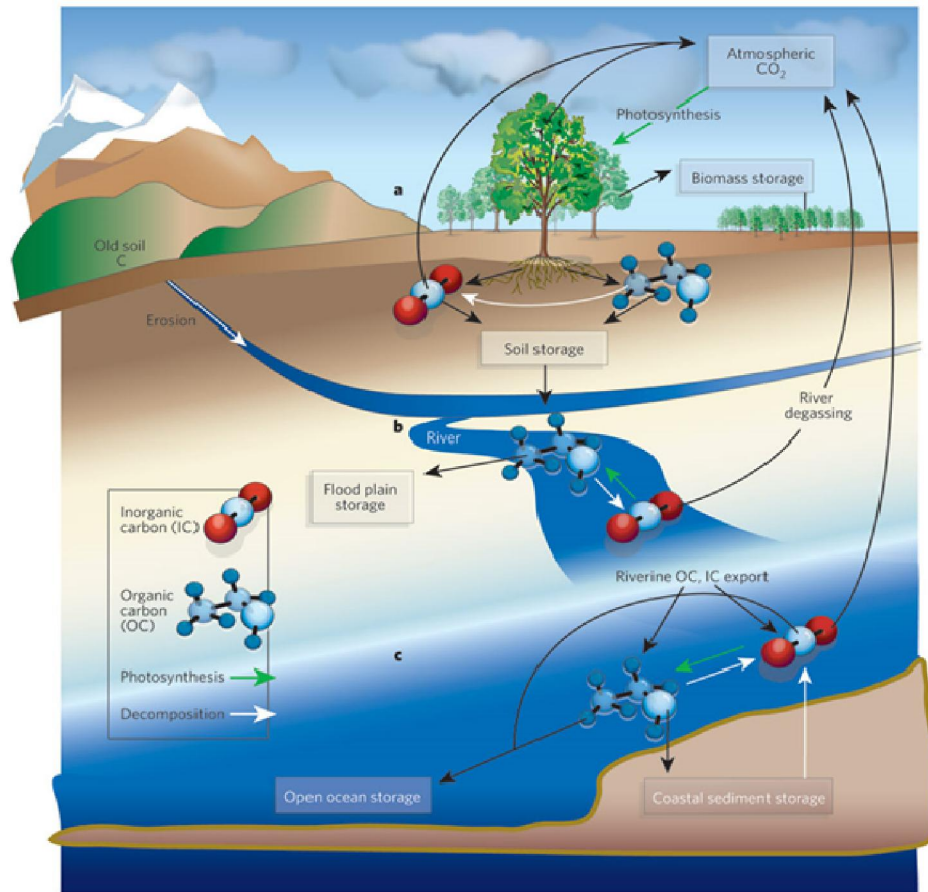


Figure 1- 1 Organic carbon sources [available at: http://www.nature.com/nature/journal/v436/n7050/fig_tab/436469a_F1.html] (7)

1.4 Bio-fuels combustion in relation to fossil fuels

1.4.1 Pyrolysis of biomass and bio-oil

Pyrolysis is the process involving thermal decomposition of biomass such as cheap, local, and abundant lignocelluloses components in grasses and trees into a more economically viable product for various domestic and industrial applications. It involves heating in the absence of air and oxygen at temperatures ranging from 400 – 800°C (8, 9). The product comprises of bio-oil, combustible gases and a carbonaceous char.

Pyrolysis as an endothermic process undergoing thermal conversion of lignocellulosic polymers; their chemical bonds break at elevated temperatures which results in release of a

liquid fraction and gases (10). However, Balat et al, 2009 (11) has pointed out that pyrolysis has the economic advantage of low capital investment and a liquid end product which can be transported and converted (catalytically) to fuels and useful end products such as food flavorings, fertilizers, resins as well as other forms of chemical product which can be fully compatible with existing petroleum materials.

Williams, et al 2005, (9) indicated that, pyrolysis is an interesting thermochemical process due to the flexibility in the operating conditions leading to the production of oils, char or gases as the entire product distribution changes depending on heating rate and temperature. He also pointed out that the end products from pyrolysis have vast application, for instance the char has the potential to be used as a solid fuel as well as being changed to activated carbon. Demibas reviewed shows the different conversion technologies for biomass to produce hydrocarbon products (12). Theodore in his findings suggested routes for the biomass conversion processes as presented in the Figure 1-2 (13).

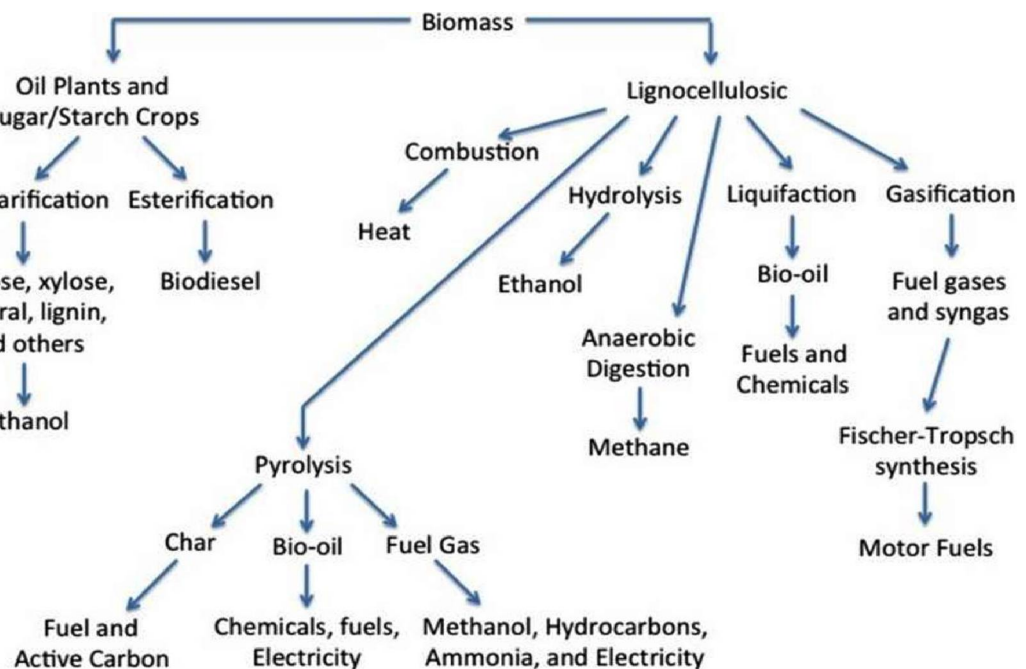


Figure 1- 2 Biomass conversion technology (13)

Additionally, numerous pyrolysis products at different operation conditions (residence time, heating rate, and temperature,) relating to technology type have been identified by Bridgewater, 2012 (14), as demonstrated in Table 1-1.

1.4.2 Pyrolysis leading to bio-oil production

Decomposition of biomass thermochemically at temperatures ranging from 400-650°C in the absence of O₂ yields volatile species, while the solid non-volatiles are collected as char. A fraction of the gas-phase volatile condense into darkish viscous crude oil termed bio-oil (15); Balat, et al 2009, (11) also points out the various synonyms for biomass product oils such as pyrolysis oil, bio-crude oil, bio-fuel oil, wood liquid, wood oil, liquid smoke, wood distillates, pyroligneous tar, and pyroligneous acid. The different pyrolysis approaches differ in their temperature, heating rate and residence time, which affect the percentage yield of gas, char and liquid products in a predictable manner, at the same time making the resultant individual chemical species remaining hard to predict and quantify (11, 15).

Table 1- 1 Characteristic of different pyrolysis types and their variants (16)

Pyrolysis technology	Residence time	Heating rate	Temperature (°C)	Products
Carbonization	Days	Very low	400	Charcoal
Conventional	5-30 min	Low	600	Oil, gas, char
Fast	0.5-5s	Very high	650	Bio-oil
Flash liquid	<1s	High	<650	Bio-oil
Flash gas	<1s	High	<650	Chemicals, gas
Ultra	<0.5	Very high	1000	Chemicals, gas
Vacuum	2-30s	Medium	400	Bio-oil
Hydro-pyrolysis	<10s	High	<500	Bio-oil
Methano-pyrolysis	<10s	High	>500	Chemicals

Burning fossils fuels results in converting stable carbon produced millions of years ago into atmospheric carbon dioxide. Whilst burning biomass is much lower in carbon emissions since the carbon dioxide returns to the atmosphere and is taken up by the growing plants, as replacement growth. This is why biomass is used for energy production, for example, if wood fuel is obtained from well managed woodlands, then carbon released from the wood during the combustion will be removed from the atmosphere as the remaining trees and seedlings photosynthesize.

1.5 Fuel oil and climate change

Combustion of fossil fuels is driven in most economies by the need to supply energy. Conversion of the carbon and hydrogen in fossil fuels by combustion into carbon dioxide and water results in heat which is used directly or indirectly to produce mechanical energy, and then subsequent conversion to generated electrical energy or for transport use. The sector that usually considered as the most important in greenhouse emission production is the energy sector which typically contributes over 90% of carbon dioxide emissions and 75% of the greenhouse gas emissions in developed countries (17, 18). 70% of greenhouse gas emissions (GGE), from the energy sector is due to stationary combustion plants and almost half of the emissions were generated from combustion in the energy industries i.e. power plants and refineries of which a quarter of these emissions comes from portable combustion facilities (transport).

1.5.1 Classification of emissions

The sectors in energy comprise; (a) exploration, exploitation of primary energy sources (b) conversions of (a) into more useful energy forms in refineries and power plants, (c) transmission and distribution of fuels, and (d) application of (c) into stationary and movable activities.

Emissions emanates from the above applications via combustion and as a transient emissions, or escape as uncombusted substances. These definitions enable the separation of the combustion of fuels for distinct and productive energy use from the use of hydrocarbons (HCs) in chemical reactions resulting from industrial chemical processes.

1.5.2 Black carbon (BC)

Soot is released in different ways from combustion processes spread widely throughout the world. Soot or black carbon (BC) has a unique and advantageous role in the Earth's climate system because it absorbs incoming and outgoing radiation which contributes to "dimming" at

the Earth's surface. It also influences cloud processes, and the reflecting of snow and ice cover if deposited (accelerating melting). Anthropogenic activities result in accumulations of large black carbon concentrations in the atmosphere. Concentrations respond quickly to reduction in emissions due to the fact that BC is rapidly removed from the atmosphere through deposition. Hence black carbon emission reductions represent a potent mitigation strategy that could abate global climate forcing from anthropogenic activities in the short term and consequently slow down the associated rate of climate change.

Studies have shown large differences between estimations of the effect of black carbon (soot) on climate change and the reasons behind these differences are still under serious investigation. It is therefore, very timely to undertake an assessment of the formation of routes to emission of black carbon (BC).

Black carbon is a clear-cut type of carbonaceous materials that is formed primarily in flames, which is directly released into the atmosphere. It has an intense absorption of visible light with mass cross section of at least $5\text{m}^2\text{g}^{-1}$ at a wave length of 550nm. It is a refractory material with a vaporization temperature of about 4000k, it also exists as aggregates of small spheres and is insoluble in water and simple organic solvents.

1.5.3 Black carbon emissions and their abundance

Firstly, the sources whose emissions are rich in black carbon can be grouped into a few classifications, broadly described as diesel engines, industrial, residential-solid fuels and open fires. The largest global contributor source is open burning of forest and savannas. A dominant emission of black carbon come from different types of combustion processes (biomass- derived fuels, fossil and other combustible fuels) and depends on location.

Global total black carbon emissions through a bottom-up inventory method are 7500Gg yr^{-1} with an uncertainty range of $200\text{-}2900\text{Gg yr}^{-1}$ (18) and $4800(1200\text{ to }15000)\text{Gg yr}^{-1}$ of the emitted black carbon emanates from energy related combustion. This may include all but open burning, and open burning from forests, grass lands and agriculture makes up the remainder.

Knowledge of black carbon abundances in a pre-industrial year provides a background estimate to evaluate climate effects. This assessment was done by the IPCC in terms of the industrial era in order to estimate changes in the atmospheric state between present day and the year 1750. It assumed a pre-industrial era value of 1400Gg yr^{-1} (18) of black carbon from bio fuel and open biomass burning, even though some fraction was anthropogenic at that time. Currently, emissions are estimated from major sources and emitting regions with the existence of the some uncertainties. An information gap includes the amount of bio fuels or biomass combusted as well as the type of combustion processes they have undergone and/ or burning locations (17).

1.5.4 Organic carbon, reactions and formation of polycyclic aromatic

hydrocarbons PAHs

Organic carbon associated with soot originates from incomplete combustion; it is a mixture of elemental compounds and complex hydrocarbons. It has been widely proved that carbonaceous aerosols (soot particles) in the atmosphere interfere and are partly the genesis for global climate change. The contribution of soot to climate change resulting from direct absorption of solar radiation is estimated as second only to that of carbon dioxide. Also it is pointed out that organic carbon soot contributes to regional climate change and quality of air in general (19). In fact, it has been related to the increase in drought or floods in China over the past 20 years (20, 21) and with haze formation off South Asia

, as well as a health risk through enhancing respiratory, cardiovascular and allergic diseases (22, 23). Once it is released into the atmosphere, it undergoes an aging process via the reaction with reactive species, such as OH, O₃, NO₂, NO₃, N₂O₅, HNO₃ and H₂SO₄ (19), and photochemical reaction (24). In addition, the organic compounds associated with soot, i.e. polycyclic aromatic hydrocarbons (PAHs) such as anthracene, phenanthrene, fluoranthene, and pyrene are excellent acceptors of singlet molecule oxygen which can then undergo further reaction via an energy transfer mechanism and subsequent thermal decomposition of an unstable peroxide product leading to the formation of various aromatics, aldehydes, acids and quinones (19). PAHs like fluorene are not good acceptors of singlet molecular oxygen but undergo photolysis rapidly at

the solid-air interface via an electron transfer mechanism (19). Hence, the consumption of polycyclic aromatic hydrocarbons adsorbed on soot (organic carbon) also impact on atmospheric chemistry.

Oxygenated aromatic compounds (anthraquinones, and aromatic carbonyls) which can be derived directly by combustion processes or from PAH oxidation, are quite common photosensitizers and therefore induce the photodegradation of aliphatic hydrocarbons(19, 25). Furthermore, combustion operation conditions particularly the fuel-oxygen ratio, have a very important role to play on the composition and properties of organic carbon (soot) (26).

1.5.5 Emission of organic carbon aerosol from fossils fuel combustion

A complex mixture of chemical compounds containing carbon – carbon bonds are formed from burning fossil fuels and biofuels; these together with natural biogenic emissions are known as organic aerosols. Organic aerosols are discharged as primary aerosol particles or formed as secondary aerosol particles resulting from reaction and nucleation of organic vapours considered semi-volatile or having low volatility. Hundreds of heterogeneous atmospheric organic compounds have been identified in the atmosphere (18, 27) which makes descriptive modeling of the direct and indirect effects highly challenging. Emissions of primary organic compounds originating from fossil fuels burning, have been estimated to be 10-30 T g C yr⁻¹ (16, 18). Most recently, a detailed analysis of primary organic carbon emission generated from fossil fuels, bio-fuels, and open burning (agricultural bush burning) has been provided and an estimation made that the sum of fossil fuels and bio-fuel emissions was in the range of 5 to 17 TgCyr⁻¹ with fossil fuels showing a value of 2.4TgCyr⁻¹. Research findings have also shown that the estimated global fossil fuel particulate organic matter (POM) i.e. the sum of the organic carbon and the other related chemical components; emissions are around 2.2 Tg(POM)yr⁻¹ and the resulting global bio-fuel emissions are around 7.5Tg(POM)yr⁻¹. In addition, there has been an overall increment by a factor of three over the period 1870 – 2000 of emissions from fossil fuels and bio-fuel organic carbon. After emission, the hygroscopic, chemical and optical

properties of organic carbon particles continue to undergo transformation due to the chemical reactions in the gas-phase oxidation, for instance ozone, OH, and the nitrate radical (NO_3). Similarly, atmospheric concentrations of organic aerosols are frequently comparable to those of industrial sulphate aerosols. Measurement of organic carbon on the East Coast of the USA during the TARFOX campaign [16] found that organic carbon primarily from fossil fuels combustion contributed up to 40% of the total submicron aerosol mass (18).

1.5 Thesis overview

Biomass combustion has the potential to contribute to 150-400EJ/yr .i.e. up to 25% of the total energy requirement by 2050. Sustainable biomass will, thus help the UK achieve its legally-binding target for carbon reduction. Biomass has potential to contribute to all sectors- electricity, fuels and heat, but the latter is the most under- developed in the UK. There are concerns regarding to the impact of wide-spread small-scale biomass on airborne emission, and in many developing countries emissions have adverse effect on air quality and human health. This thesis concerns a fundamental study of soot polycyclic aromatic hydrocarbons (PAH) and volatile organic compounds (VOC) formation during biomass combustion, in comparison to fossil fuel combustion. This fundamental knowledge is gained through measurement of the size, chemical and physical properties, formation rate and basic mechanisms of formation of different biomass derived soot formed using flames from a wick burner and smoke point lamp. Soot index measurements were made in two ways - by direct photography and via deposition onto a glass slide. A differential mobility spectrometer (DMS 500 series) was used to obtain information on particles size distribution, together with electron transmission microscopy. Pyrolysis and GC-MS analysis is used to study the intermediate species leading to soot formation. This research will focus on generating extensive experimental data and capture detailed information regarding sooting tendencies in flame environments as a function of fuel type, temperature, residence time and velocity. The relationship between the composition of the burning biomass fuels or the petroleum based products and soot formation will assist in the

design of a comprehensive bio-oil combustion model. This will eventually define compositional requirements for fuels in order to mitigate emission levels. This research contributes to the SUPERGEN bioenergy hub (www.supergen-bioenergy.net) concerning the impact of feedstock parameters on airborne emissions from biomass combustion. In addition, the effects of asphaltenes on the combustion of heavy fuel oil have been examined.

1.6 Research aim

The main aim is to generate a wide experimental data base and to capture detailed information regarding sooting tendencies from conventional and bio-oils. This has been undertaken with a view to use the information to eventually design a comprehensive bio-oil combustion model in order to provide accurate predictions of combustion characteristics and pollutant formation.

The work has two strands. Firstly, the sooting tendency and soot characteristics emitted from flames from bio-oil/biomass model compounds are studied and compared with flames from petroleum model compounds. The second strand of research examines the soot formation during combustion of a pyrolysis bio-oil and heavy fuel oil. This second aim includes a study of the role of the heavy components (i.e. asphaltenes in the heavy fuel, and heptane-insoluble in the bio-oil).

1.7 Research objectives

A comprehensive oil combustion model should account for sooting tendencies and soot chemistry as well as the effects of the soot on the combustion products. Soot properties (size and optical constant) are required in order to perform heat transfer calculations. A well understood soot formation mechanism is required to illustrate how soot properties and kinetics are related to reaction conditions during fuel combustion processes. One project objective is to generate a fundamental base of knowledge on the size, chemical and physical properties, formation rate and basic mechanisms of biomass derived soot formed using flames from a wick

burner, with prediction of accurate flame temperature, gaseous formation rate and other important parameters and their influence on soot formation in biomass oil / heavy fuel oil combustion systems. The origin of soot in biomass or heavy fuel oil flames has also been investigated by examining their pyrolysis products, since pyrolysis is one of the initial steps in combustion.

The project objectives for strand one of the research have been achieved via the following identified tasks:

- ❖ Construction of substantial stable flame using a wick burner set-up
- ❖ Construction of a soot sampling device and grid holder sampling probe which allows reliable optical appropriate collection of soot at different flame heights.
- ❖ Examining the physical and chemical properties of soot derived from different biomass oils and compare biomass oil derived soot with conventional hydrocarbon flames.
- ❖ Determination of sooting tendencies in a flame environment as a function of temperature, residence time and velocity. This includes investigation of the gas-phase composition on soot yield.
- ❖ To study the morphology of microscopic soot for measured sooting propensities of the burnt fuel
- ❖ Investigating the structure of the flames and exploration of the effect of soot structure evolution from burning biomass oil and petroleum based products.

To utilize the investigated data using combustion and pyrolysis chemistry to help develop a kinetics modelling to improve the understanding of the mechanisms involved in pollutant formation as well as the fundamental chemistry of bio-oil combustion, while contributing to mitigate emission levels.

For strand two of the research, the objectives are:

These experiments are on the basis the applications which are listed below;

- ❖ To extract bio-oil asphaltenes from fast pyrolysis bio-oil

- ❖ To evaluate the evolution of decomposition products from the pyrolysis of bio-oil in a Pyrolysis GC-MS unit over the temperature range of 300 to 1100°C. The results are compared with those generated from the petroleum heavy fuel oil.
- ❖ To study the nature and structure of the products during the GC-MS pyrolysis of the heavy fraction, bio-asphaltenes, ranging from 300 to 1100°C. TGA studies were also undertaken up to 950°C and the char produced was combusted to replicate practical combustion situations.
- ❖ To observe the pattern of methyl substitution in the naphthalenes and phenanthrenes resulting from bio-asphaltenes pyrolysis and compare to the volatile petroleum fractions from conventional fossil fuels.
- ❖ To investigate whether soots and chars are produced from bio-asphaltenes combustion.
- ❖ To study the deleterious effects of the heavy asphaltene content as a potential health threat from the volatile fragments released during combustion such as carcinogenicity of the PAH liberated by pyrolysis.

1.8 Thesis Outline

Chapter 1

In this chapter an overview of energy demand and consumption trend, supply, security and some of the environmental issues encountered from energy production both globally and in the UK has been addressed briefly.

It also introduces fossil fuels, biomass, its resources, as well as, some of the thermal conversion technologies leading to bio-oil production and also routes to chemical based bio-oils. Additionally, this chapter demonstrates the relevance of the work covered in this thesis and the concept of black carbon and organic carbon emissions from burning fuels are also introduced.

Chapter 2 Contains a literature survey of some of the fossil fuels properties, biomass, and biomass-derived fuels and its combustion characteristics, and hence spray combustion for these fuels.

It reviews previous work concerning the fundamental mechanisms of soot formation and the current understanding of the formation in wick burners and combustors. A detailed study of the literature on bio-oil combustion, carbonization and gas phase composition was performed for the purpose of this thesis. The available literature permits a profound understanding of the work carried out, recognises areas of research that have been covered and the gaps that require further exploration.

Chapter 3 Examines the fuels analysed for this study, the experimental methods employed for their analyses and the equipment and model code used for the analyses. The main objective of this chapter is to outline the methods used allowing others to imitate the experiments. Further, it is significant for readers to have detailed understanding of the sample workup and analysis for the same reason. Also some of the chemical and physical operations of the instruments are covered in this chapter to enable further understanding for the instrumental operations. Additionally this information is freely available and most readers interested in the current work are expected to have some initial knowledge of the technologies involved.

Chapter 4 presents model fuels and biomass combustion results, properties, and emission factors of soot generated from different feed stocks such as eugenol, anisole, furfural and some hydrocarbon fuels. Also raw biomass fuels (pine wood, forecourt wood rape and rape straw) and biomass soots, like wood stove and multi-fuel wood burner soots. Their potential for volatiles release in combustor plants has been investigated and characterised.

It also describes the determination of primary particle diameters. As well descriptions of the different laser diagnostics used to visualize and quantify soot and especially describes the optical techniques used in the experiments. The application of the technique to a laminar diffusion flame in order to validate and develop further understanding and to characterize the soot formation in a diffusion flame is included.

A new analytical technique based on Pyrolysis GC-MS was developed to analyse the black carbon/ organic carbon BC/OC contents of the soot samples. The technique involves pyrolysing not more than 2 mg of soot and separating the pyrolysis products by GC-MS. By fingerprinting

common model compounds of lignin and holocellulose, marker compounds could be identified for each biomass and bio-oil component. This has allowed comparison to be done of the chromatograms from model compound and petroleum based fuels composition. The analysis technique was also assessed as a means to determine concentrations of specific compounds found in soot.

Bulk and surface investigation of soot properties generated from oxygenates and hydrocarbon fuels were made using TEM and SEM as well as DMS. The TEM revealed the alignment direction of the particles, and stacking of soot (black carbon) as it show a little degree of disorder indicating formation of a significant proportion of secondary structures (possibly oxygenated species) as previously indicated in the Py GCMS results. Additionally, SEM was used for morphological structure of soot and DMS for particle distribution. This chapter further studied the CH* and C₂* emission within the flame environment including the reaction zone during fuel combustion.

Chapter 5 outlines the standard principles of extraction of crude asphaltenes from heavy fuel oil with ‘‘bio-asphaltenes’’ from bio-oils in chapter 6. Additionally, this chapter examines the volatile products and solid phase analysis. In this regards the nature of the products generated are studied as follows: Phase 1 effect of the pyrolysis temperature and heating rate on the products and also the phase 2 demonstrates the toxicity. Generally, the aim and objective of this chapter is to examine the constitutional properties of both heavy oil fractions-(Bunker C fuel oil and vacuum residue), and aromatic model fuels under variable temperatures, but controlled conditions. These experiments are on the basis of two applications which are as follows; firstly, to evaluate the development of toxic gases in an enclosed system during the combustion of heavy fuel, and secondly to study the structure and nature of the products during pyrolysis of these heavy fuels (asphaltene) from a lower to higher temperature in large combustors, such as power plants, marine engines, furnaces and boiler for heating and energy generation. An overall aim is to determine the nature of soot black carbon for a range of combustion conditions, with the view to elucidate the combustion mechanism and the way in which fine particulate soot and

cenospheres are produced, and the potential threat of volatile species released during combustion.

Chapter 6 explores the experimental studies of the rates of combustion of droplets of liquid fuels (from conventional and unconventional sources) which could be used as sprays of these fuels; it examines the mechanisms and the way in which fine particulate soot and cenospheres are produced. Also the chemical composition is of paramount importance; in the case of heavy fuel oils the asphaltenes content is a key tool to consider, whilst analogous compounds present in the renewable fuels also play a significant role. Furthermore the chemical structure of Petroleum Asphaltene has been investigated via a pyrolysis technique and with mass spectrometric and atomic emission detection AED.

Chapter 7 concludes with the overall findings from chapters 4 to 6.

Chapter 2 Literature survey

2.1 Current use of fossils fuels

For more than 100 years researchers have been observing the variations of global production, and consumption, as well as emissions from burning fossil fuels leading to the climate threatening greenhouse gases emanating during combustion of these fuels. However, in the latter half of the 20th century and early 21st century there has been a rapid improvement in the standard of living in the western world due to new energy intensive technologies. Along with this, there has been a rapidly increasing global population with an associated increasing energy demand. There has been a drive for emerging technologies to be increasingly more energy efficient. Many researches point out that there have been technological capability to use fossil fuels efficiently without climate threatening greenhouse gases or pollutants (28). Fossil fuels are predictable and currently over three quarters of the world's fuel comes from non-renewable carbon based fuels. Despite this there are also security of supply issues caused by OPEC and Russia having very large quantities of the world's oil and natural gas reserves (2), logically, nations are seeking to improve their local energy production.

Most significantly, fossil fuels are being used at a rate which cannot continue as the combustion of carbon-based fuels creates carbon dioxide, which is a major greenhouse gas (GHG) and contributes to climate change. It is shown that anthropogenic greenhouse gas emissions since the beginning of the industrialisation have increased the proportions of greenhouse gases in the atmosphere which has resulted in an appreciable climate transformation. Detailed knowledge of the mechanisms causing global climate change including the extent of the effect of natural phenomena such as volcanic eruptions and sunspots, makes modelling challenging, but a 0.6^oC rise has already been attributed to GHGs and a further increase of between 1.4-5.8^oC over the present century is forecast(29, 30). The increase in temperatures will lead to rise in sea levels. This is because of; the thermal expansion of the oceans, melting of the ice-caps as well as decrease in fresh snow-fall. Countries in low level coastal regions including those built on or near river flood plains will experience more frequent and more severe flooding. On the other hand, dry climatic regions will experience higher temperatures, shorter rainy seasons and very severe water shortages(29, 31).

Recently, policy makers have generally agreed that the average global temperature rise caused by greenhouse gas emissions should not exceed 2^oC above the average global temperature of

pre-industrial times (32, 33). However, it has been estimated that to have at least a 50 per cent chance of keeping warming below 2°C throughout the next century, the cumulative carbon emissions between 2011 and 2050 need to be limited to around 1,100 gigatonnes of carbon dioxide (Gt CO₂)(30, 34). However, Meinshausen et al, 2009 (30) and Raupach et al, 2014 [34] have suggested that, greenhouse gas emissions contained in present estimates of global fossil fuel reserves are around three times higher than this estimation, and so the unabated use of all current fossil fuel reserves is incompatible with a warming limit of 2°C(30, 35). Research by [39] demonstrated their predictions using a single integrated assessment model that contains estimates of the quantities, locations and nature of the world's oil, gas and coal reserves and resources, and it is shown to be consistent with a wide variety of modelling approaches with different assumptions by the IPCC in 2014. They explore the implications of the emissions limit for fossil fuel production in different regions. The results suggest that, globally, a third of oil reserves, half of gas reserves and over 80 per cent of current coal reserves should remain unused from 2010 to 2050 in order to meet the target of 2°C. This indicated that the development of the resources in the Arctic and any increase in unconventional oil production are not commensurate with efforts to limit average global warming to 2°C(36). They also note that those policy makers' instincts to exploit rapidly and completely their territorial fossil fuels are, in aggregate, inconsistent with their commitments to this temperature limit. Implementation of this policy commitment would also render unnecessary continued substantial expenditure on fossil fuel exploration, because any new discoveries could not lead to increased aggregate production(36).

Recently, climate studies have revealed that average global temperature escalations are closely related to increasing emissions of greenhouse gases emitted over a given period of time (30, 37, 38). This has resulted in the concept of the remaining global 'carbon budget' associated with the probability of successfully keeping the global temperature rise below a certain level. The IPCC, 2014 recently suggested that to have a better-than-even chance of avoiding more than a 2°C temperature rise, the carbon budget between 2011 and 2050 needs to be around 870–1,240 Gt

CO₂. Such a carbon budget will have deep implications for the future utilization of oil, gas and coal (36). However, they establish the quantities and location of those currently estimated to exist with a view to understanding the quantities that are required under different scenarios. This allowed a variety of metrics that are relied upon to report the availability of fossil fuels [10, 11]. The two most common are ‘resources’ and ‘reserves’ with the distinction being recoverable resources are the quantity of oil, gas or coal remaining that is recoverable over all time with both current and future technology, irrespective of current economic conditions, whereas, ‘reserves’ are a subset of resources that are defined to be recoverable under the current economic conditions and have a specific probability of being produced. Estimates have been made of the CO₂ emissions that would result from the combustion of the estimated remaining fossil fuel resources, nearly 11,000 Gt CO₂ (37, 39). Combustion for the remaining reserves alone would total nearly 2,900 GtCO₂; the disparity between what resources and reserves exist and what can be emitted while avoiding a temperature rise greater than the agreed 2⁰C limit is therefore very difficult (36).

While previous researchers have examined the implications that emission mitigation might have on the revenue collected by fossil fuel resource owners, more pertinent to policy and industry are the quantities of fossil fuel that are not used before 2050 in scenarios that limit the average global surface temperature rise to 2⁰C. Such geographically disaggregated estimates of ‘unburnable’ reserves and resources are provided that was based on using the linear optimization, integrated assessment model. This tool provides context to the issue of unburnable fossil fuels and their results. It is useful to examine scenarios provided by other models that quantify separately the volumes of oil, gas and coal produced globally under a range of future emissions trajectories (32). This is done in Figure 2-1 which shows global production of oil, gas and coal over time in the main 2⁰C rise scenario.

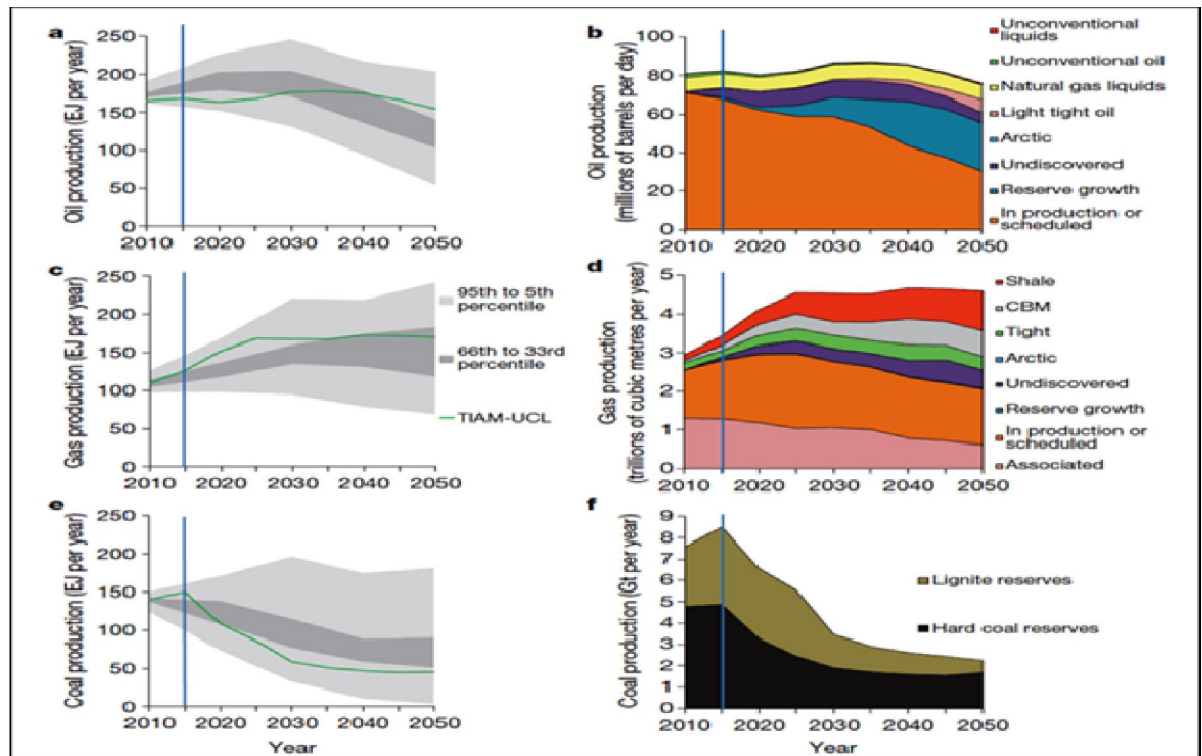


Figure 2- 1 Presents Oil, gas, and coal comparative production scenarios (with CCS) IPCC (16)

The Figure shows production by category, that is, by the individual kinds of oil and gas that make up the global resource base and comparisons are made with total production of the projections from the 2⁰C scenarios. The Figure shows continuing production of oil and gas and declining coal production in particular. After setting out the regional unburnable resources of all coal, gas and oil in the scenario prediction of required CCS can be made by comparing cumulative production of all fossil fuel resources with the resource estimates from combustion, and the combustion CO₂ emissions for these resources. Within these resource estimates, 1,294 billion barrels of oil, 192 trillion cubic metres of gas, 728 Gt of hard coal, and 276 Gt of lignite are classified as reserves globally. These reserves would result in 2,900 Gt of CO₂ if combusted unabated (30). The range of carbon budgets between 2011 and 2050 that are approximately commensurate with limiting the temperature rise to 2⁰C (870–1,240 Gt of CO₂) is also shown. However, the remaining reserves and ultimate recoverable resources RURR of both types of coal and unconventional oil vastly exceed cumulative production between 2010 and 2050, with the overwhelming majority remaining unburned. Additionally, resources of conventional oil are used to the greatest extent, with just under 350 billion barrels of non-reserve resources produced

over the model time frame (39). Conversely, the Middle East again holds the largest share of the unburnable resources of conventional oil, but there is a much wider geographical distribution of these unburnable resources than was the case for oil reserves. Figure 2-1 includes the production of unconventional oil, open-pit mining of natural bitumen in Canada; this rapidly drops to negligible levels after 2020 in all scenarios because it is considerably less economic than other methods of production. Carbonization is also an essential tool to consider; here by in situ technologies continues in the 2⁰C scenario that allows CCS, but this is accompanied by a rapid and total decarbonization of the auxiliary energy inputs required. Even though such a decarbonization would be extremely challenging in reality, for instance, the cumulative production of Canadian bitumen between 2010 and 2050 is 7.5 billion barrels. About 85% of its 48 billion of barrels of bitumen reserves thus remain unburnable if the 2⁰C limit is not to be exceeded. When CCS is not available, all bitumen production ceases by 2040. In both cases, the RURR of Canadian bitumen dwarfs cumulative production, so that around 99% of its resources (640 billion barrels) remains unburnable. Similar results are seen for extra-heavy oil in Venezuela. Cumulative production is 3 billion barrels, meaning that almost 95% of its extra-heavy reserves and 99% of the RURR are unburnable, even when CCS is available. The utilization of unconventional gas resources is considerably higher than unconventional oil. Under the 2⁰C scenario, gas plays an important part in displacing coal from the electrical and industrial sectors and so there is over 50 trillion cubic metres of unconventional gas production globally, over half of which occurs in North America. Nevertheless, there is a low level of utilization of the large potential unconventional gas resources held by China and India, Africa and the Middle East, and so over 80% of unconventional gas resources (247 trillion cubic metres) are unburnable before 2050. Of course, production of these unconventional gas resources is, however, only possible if the levels of coal reserves identified i.e. principal estimation of the remaining reserves as well as, ultimate recoverable resources drop drastically. Researchers estimate there it to be 100 billion barrels of oil (including natural gas liquids) and 35 trillion cubic metres of gas in fields within the Arctic Circle that are not being produced as of 2010. However, none of this is produced in any region in either of the 2⁰C scenarios before 2050 (39). These consequences indicate to us that, all Arctic resources should be classified as

unburnable. Therefore, the findings from (40), demonstrate that a stark transformation in our understanding of fossil fuel availability is necessary. Although according to Yergin, 2009 (41), there have previously been fears over the scarcity of fossil fuels (41), in a climate-constrained world this is no longer a relevant concern: large portions of the reserve base and an even greater proportion of the resource base should not be produced if the temperature rise is to remain below 2°C.

Biomass resources as a new recoverable fuel have significant potential to become a replacement for the shortfall in fossil fuels and as well as reducing carbon dioxide emissions. Biomass is a natural storage of light energy from the sun in the plant via conversion to chemical energy via photosynthesis. Chemical energy is used to add CO₂ and H₂O synthesize to the C₅ sugar i.e. pentose sugar, and oxygen and water as a by-product, thus fixing inorganic carbon to organic carbon (42). The combustion of biomass (such as bio-oil, as well as chars) releases this energy as heat and carbon dioxide, but subsequently the plant had to initially fix the CO₂ from the atmosphere, meaning that the process is CO₂ neutral (provided it is handled and treated efficiently) and the resultant heat released would be the one that is being release during the plants natural degradation.

Emissions reductions in the energy supply sector is a key area in which governments could confidently achieve their greenhouse gas cuts, and a driver to policies to achieve sustainable percentage of electricity supply from renewable energy by 2050. Renewable energy supply includes solar, wind, wave, biomass (such as bio-oils and heavy fuel) generated power. Biomass has advantages over the other renewable energy sources sine the energy can be stored and hence can be used on demand; and this is adaptable to existing combustion technologies, often with slight to no modifications. Also biomass is the only renewable energy source of carbon and it can be easily converted into different phases (solid, liquid, or gaseous fuel which can be used in small or large scale applications, as a motor fuel, for domestic use (rural and urban settings), for either heating, electricity supply, or cogeneration (43-45).

In the UK, biomass and co-fired biomass are both approved fuels that can be used to earn Renewable Obligation Certificates and therefore there has been an increased focus on biomass combustion, and its application as well as its potential problems (44).

There has also been a range of technologies developed for the treatment of biomass as fuel of either a thermal or biological nature. A thermal application treatment includes direct combustion, pyrolysis, and gasification and the application of each of these methods have been previously discussed elsewhere in this thesis. An additional advantage of biomass is the many different types of bio-fuels (such as bio-oil, bio diesel, bio-chars as well as biogas from plant and animal waste and sewage), including plant material from specifically grown forests and energy crops, agricultural and forest wastes, and also refuse derived fuel originating from waste and from waste landfill (43, 44).

It must be stated that while the use of biomass fuel may reduce anthropogenic carbon dioxide emissions, there are other important environmental considerations which need to be considered when deciding to use it as a fuel. A plant that utilizes biomass-derived feedstock must be competitive with the fossil fuel-use plants and meet requirements for emissions, and control; also design features of the plant should be in accordance with the legislative standards.

The first thing to be considered for the effectiveness of pollution control is that carbon dioxide is not the only waste product of a combusted bio-fuel and it has many of the emissions similar to fossil fuel combustion. However, biomass has negligible sulphur content in comparison to coal and oil such as Bunker C oil and heavy fuel oil, and thus creates virtually no SO_x pollutants. Additionally, when co-fired with coal it can actually, due to its alkali metal content, reduce the SO_x pollutants that would be expected from the coal fraction. Depending on the nature, and the fertility of the land as well as the irrigation environment for the grown biomass, the biomass has a variable nitrogen content which is usually lower than the level in coals, and therefore NO_x problems could be reduced. Furthermore, its combustion temperature can often be lower which can reduce the content of NO_x produced.

Another issue in biomass combustion is associated with methane production as well as polycyclic aromatic hydrocarbons (PAH) and particulates emissions. Plant design must be based on limiting these emissions. Ramage and Scurlock, 1996 (43), suggested that an important design aspect is that there exists complete combustion to prevent unburnt hydrocarbons, and effective after-treatment with the help of electrostatic precipitators, scrubbers and catalytic converters to reduce emissions levels.

2.2 Combustion of sprays and oil droplets

2.2.1 Combustion of droplet liquid fuels and biomass particles

Liquid fuels, particularly heavier fuel oil such as Bunker C oil, are used extensively in Marine engines for transportation and other power generation. Residual fuel oil has been widely used over the years. At the same time a number researches have been carried out during the crude oil refining process, where these oils contain a high percentages of high molecular weight (MWt.) aromatic and naphthenic hydrocarbon compounds. The composition includes asphaltenes, which upon combustion releases an increased level of solid particles as emissions into the environment (46-50). The structural arrangement of the composition of asphaltene occurs in different forms as reported in (51-53).

Research findings have shown that fuel properties, particularly the solubility of petroleum asphaltene is mainly influenced by its high molecular weight and its extent of polycondensation associated with cyclization of the constituent aromatic nuclei upon its combustion (54). Furthermore, several works have shown how these structures are increased by thermal cracking during geochemical and hydrotreating processes particularly the hydrodesulphurization (HDS), and hydrodenitrogenation (HDN) process during crude oil refining processes.

During the combustion of heavy fuel oil , smoke (or stack solids) are produced in high levels by thermal decomposition of the liquid phase components and subsequent formation of cenospheres as well as soot from the vaporized hydrocarbons via the gas phase mechanism(55). The amount of cenospheres produced depends upon the percentage of asphaltene component of the droplet (56-61). Similarly, several efforts have been devoted to studying the combustion of droplets of liquid hydrocarbons including biomass-derived fuels as bio-oil, and also heavier fuel such as heavy kerosene, diesel fuel, as well as light fuels such as alcohols or phenols, more especially ethanol and butanol.

Many years of extensive research have been undertaken on the combustion of sprays of conventional fuels for engines and power generation in which a lot of data has been obtained on rates and mechanisms of combustion and of soot and particulate formation. In general it is agreed that after the initial stage, the droplet burns at approximately a rate given by the square of the diameter (d^2). Droplets of multi-component fuels such as commercial fuels which have similar physical properties have been proved by studies both experimentally and theoretically to follow the same law.

In the case of multi-component fuels soot formation is largely dependent on the aromatic composition, even though the burning rate does not vary (51). Of interest is soot formation during combustion of small solid biomass particles which can be considered as burning droplets of bio-oil. In the combustion of a solid biomass particles a larger fraction of the particle dissociates to give a gaseous product which diffuses from the surface of the particle and as it contacts the surrounding air its forms a flame envelope in a similar way to the combustion of an evaporating liquid droplet. The resulting smoke and particulate matter from the burning hydrocarbon fuels has been widely studied. Oil droplet burning studies revealed that for bio-oil, the droplet undergoes different distinctive stages of combustion. According to Wornat, et al, 1994 (62) it is pointed out that initially the droplet of biomass oil burns quietly with a blue flame. However, a broad range of components evaporate, but due to the inadequate mass transfer within the biomass that can occur automatic termination of the quiescent stage and the creation of distortions which results in rapid droplet swelling and occurrences of micro-explosions (63). Droplet coalescence follows, and continuous burning occurs in a pale blue flame with smaller scale bursts of fuel vapour occasionally. At the extreme end stage of biomass oil combustion, a cloud of soot is formed via gas-phase pyrolysis, where the liquid phase polymerization or the pyrolysis of the droplet of biomass oil results in the formation of carbonaceous cenospheres or char which terminates the process.

To have a smooth and clean, economical way of achieving efficient combustion of sprays of these fuels in practical combustors a promising concept involving mixing very heavy crude oils or bitumen with water has been suggested. This is the formation of emulsions of very heavy fuel oil, bitumen and or even heavy bio-oil droplets in a continuous oil-in-water or water in oil-

medium. This produces a reduction of viscosity in the resultant emulsion as compared with the original/ natural sample oil droplet. It has been proved that this has the advantage of easier handling pumping and better elemental investigation via atomization and also provides a means of comparing the mechanism of combustion of the mixed oil droplet (64-66). However, the emulsions may not be stable.

Several investigations proved the development of a fuel from bitumen in the form of water-in-oil emulsion called Orimulsion based on the emulsification of natural bitumen from the Orinoco belt in Venezuela; this type of mixed fuel has been tested industrially and found to have very good performance in combustion (67).

In fact there are numerous studies on the combustion of similar water-in-oil emulsions (48, 68, 69), and even studies of coal water slurries have been reported (70), but there are not many investigations of the basic combustion parameters of water-in-oil emulsions. For example, little has been done on the basic combustion mechanisms in comparison with hard bitumen water slurries (71). The behaviour of the combustion of bitumen-in-water emulsion using suspended and falling droplet techniques together with spray combustion using air blast atomizers have been investigated (71). Single droplet measurements have been made by the use of a commercial soft bitumen-in-water emulsion. Different mixtures with varying amounts of water of hard bitumen-in-water slurry as well as a heavy fuel oil were used, and data has been generated on ignition delay, droplet centre temperature history, mass loss, and flame emission (69). There is great interest in the potential behind the utilization of oil/water emulsion in liquid fuelled combustors for harnessing fuel economy and pollutant reduction. Extensive studies have been made with respect to postulated and observed beneficial effect(64, 66). In general there is resultant improvement in the undesirable mixed fuelled combustion and much is known on characteristics of sprays, as well as understanding the vaporization and combustion of a single oil/water-in-oil droplet (69).

From a fundamental overview, emulsions are effectively multi-phase chemical systems with multi-components, whose heterogeneous characteristics have not been systematically studied. Several theoretical models have been reported (67-71) for emissions from the combustion of droplets, particularly emphasizing the characteristics governing the onset of the phenomena

known as micro-explosions which has been postulated. This involves cataclysmic fragmentation of the droplet as a result of internal bubbling of the embedded water so the emulsion droplet becomes super-heated. In fact in some of these models, vaporization is either replaced by micro-emulsions (71), or based on the conventional pure-oil droplet vaporization at the droplet surface. It is a well-known fact that water does not participate in the main vaporization process but that it is only there to modify the droplet temperature and the combustion characteristics. The onset of micro-explosions, which depend on the droplet temperature, and that means suppression of water vaporization, can qualitatively affect the theoretical predictions.

Murdoch, et al., 1985 (70) reported that vaporization can be accounted for by quasi-steady state droplet combustion behaviour. Micro-explosions occur only with oils whose boiling point is higher than the limit of superheated water, and their occurrence is accentuated by raising the external pressure. The model is a steady-state one, in that it indicates whether or not micro-explosions occur during the droplet heating period. It does not account for the presence of internal circulation. However, studies on multi-component droplet combustion show that as different droplet combustion behaviour results depending on the internal circulation, and the model system applied by Liddy, et al, 1989 (64) to involve the processes of droplet heating and internal circulation is relevant. The droplet combustion behaviour is majorly governed by these three factors; (i) the concentrations of oil in water, (ii) the intensity of water motion, (iii) the fact that water and oil do not form a homogeneous mixture. Based on these considerations various possible combustion modes can be identified.

An aim of this thesis will be to concurrently study the similarities and differences in combustion of bio-oil droplets (an oil in water emulsion) and that of heavy fuel oil with a view to investigate and evaluate the fundamental combustion properties and soot formation routes.

2.2.2 Nature of spray combustion

Liquid fuels for example petroleum based oil as well as biomass derived liquid fuel (such as bio-oil, biodiesel, algae-oil, including biomass pyrolysis oils) need to be atomized into small droplets in order that they can efficiently burn in combustion chambers. Atomization of these liquid fuels is most frequently carried out via injection of the fuel through small orifices at very high pressure or by mixing air or gas with the fuel at high pressure. Additionally, the most successful atomization is achieved by formation of thin liquid sheets which subsequently become unstable and then break up to form a large drops, and then subsequent breaking down of the large drops into small droplets (72).

Combustion of sprays of liquid fuels is of considerable technological importance to a diversity applications starting from steam raising, furnaces, space heating, diesel engines to space rockets (73). Hence, a considerable proportion of the world's total energy requirement comes from spray combustion as it contributed up to 25% of world energy in 1990 although the Figure is more like 10% now.

Spray combustion was first developed and put into use in the 20th century as a powerful method of burning relatively non-volatile liquid fuels. Certainly it remain the major means of burning heavy fuel oils today, although combustion of these oils can also be conducted in a fluidized bed. Twin-fluid atomizers have been widely used for large scale boilers and are designed to have a high velocity gas stream (often steam) to atomize the fuel in a relatively low velocity liquid fuel stream (73). The fundamental process involved is the disintegration or distortion of the liquid fuel to produce a spray of small droplets with a view to increasing the surface area so as to greatly enhance the rate of heat and mass transfer during combustion. The atomization of a 10mm diameter droplet of liquid fuel to droplets of 1/10mm diameter (100 μ m) increases the surface area by a factor of 10,000 (73-75).

Spray burning differs from a pre-mixed gaseous fuel flame, as the latter has a rapid, and instantaneous available combustible gaseous system. The spray is present in the form of discrete liquid droplets with a range of sizes which are also moving in different directions with diverse velocities to that of the main stream of gas. The absence of uniformity in the unburnt mixture results in irregularities of flames during propagation through the spray and therefore the combustion as well as the reaction zones are geometrically poorly understood.

Many researchers have suggested ways of handling applications of flames industrially. These systems of applying flames industrially are highly complicated due to various factors such as complex flow and mixing pattern in the combustor chamber, heat and mass transfer during the combustion process, and the different droplet spray sizes. Studies of fuel droplets vaporizing in gas flames and issues associated with heavy fuel oil spray combustion are on-going. The flame can be considered as a flowing reaction system in which the properties of flow, temperature, surface area and pressure change with the direction of flow and are constant in any cross section at right angles to the direction of flow. Additionally, Onuma and Ogasawara, 1975 (75), demonstrate direct comparisons between the structures of a spray combustion flame and a turbulent gas diffusion flame in a perpendicular cylindrical furnace. Furthermore, studies on measurements for the spatial distribution of droplets, temperatures, velocity, and gas concentrations, as well as turbulent gas diffusion flame have been conducted (74).

Researches have shown that basically the flame of spray combustion could be sub-divided into three main proportions: an initial region consisting of a two-phase mixture where most of the droplets evaporate and subsequently form soot, because of the very rich mixture ratios. In the second region, which is the intermediate portion, they showed that the concentration and sizes of the droplets are very low while the concentration of the unburned gases is very high, specifically with higher percentage concentration of carbon monoxide CO and unburned soot. The third portion is the region where the intermittent burning proceeds as combustion is completed (74-76) and CO and soot may pass through the zone incompletely burned out.

The overall nature of the processes involved in spray combustion in an idealised case (i.e. for the combustion of a mixture or diluted spray) consider the system contain droplet diffusion flames which are characterized by their yellow flame nature. However, this is a one-dimensional situation of the individual droplets that make up the spray. Heterogeneous spray combustion is a system which demonstrates the other major features of a spray flame such as spray atomization, air confinement, flame stabilization, as well as the irregular nature of atomization.

Many authors suggest that the structure and shape of flames of light fuel oils have the following features: the flame front is visible as a diffuse zone across the top part of the flame zone and sprays can burn effectively like a homogenous mixture. Also the droplets evaporates as they are

approaching the flame zone thereby forming clouds of fuel vapour that are actually burning rather than the droplets. Additionally, Williams, [72], suggested that, these flames (such as jet-A fuel flames) are characterized by their bluish colour and are usually associated with small initial diameters of droplet sprays of volatile fuels (66).

For a comprehensive understanding of the process of spray combustion it is however, necessary to generate substantial knowledge of the combustion of the individual droplets making up of the spray, such that the spray is seen as an accumulation of individual burning or evaporating particles. Therefore, there is need for the statistical description of the droplets in the spray with respect to droplets size and distribution in space.

In general, spray (for example bio-oil, and biomass pyrolysis oil such as eugenol, furfural and anisole sprays including hydrocarbon fuels (such as jet-A fuel, decane, and heptane)) combustion have the following essential features of combustion as indicated in Figure 2-2. In this figure the fuel is conveyed from the fuel storage tank via a fuel handling system that incorporates pumps, filters as well as means of control to an atomizer where the fuel is atomised into small droplets; these droplets are injected into the combustion chamber where the burning of the fuel takes place.

The combustion process is very complicated. The mixing of the fuel and oxidant takes place inside the chamber and hence the mechanistic aspects of the mixing process play a key significant role. The extent of the mixing process during combustion is controlled by the geometry of the combustion chamber, the spatial distribution and momentum of the injected spray, as well as the direction and velocity of the air flow, and also the influence of any sources of flame stabilisation devices. Hence the atomiser and the combustion chamber should be designed as an integrated unit rather than as an independent unit.

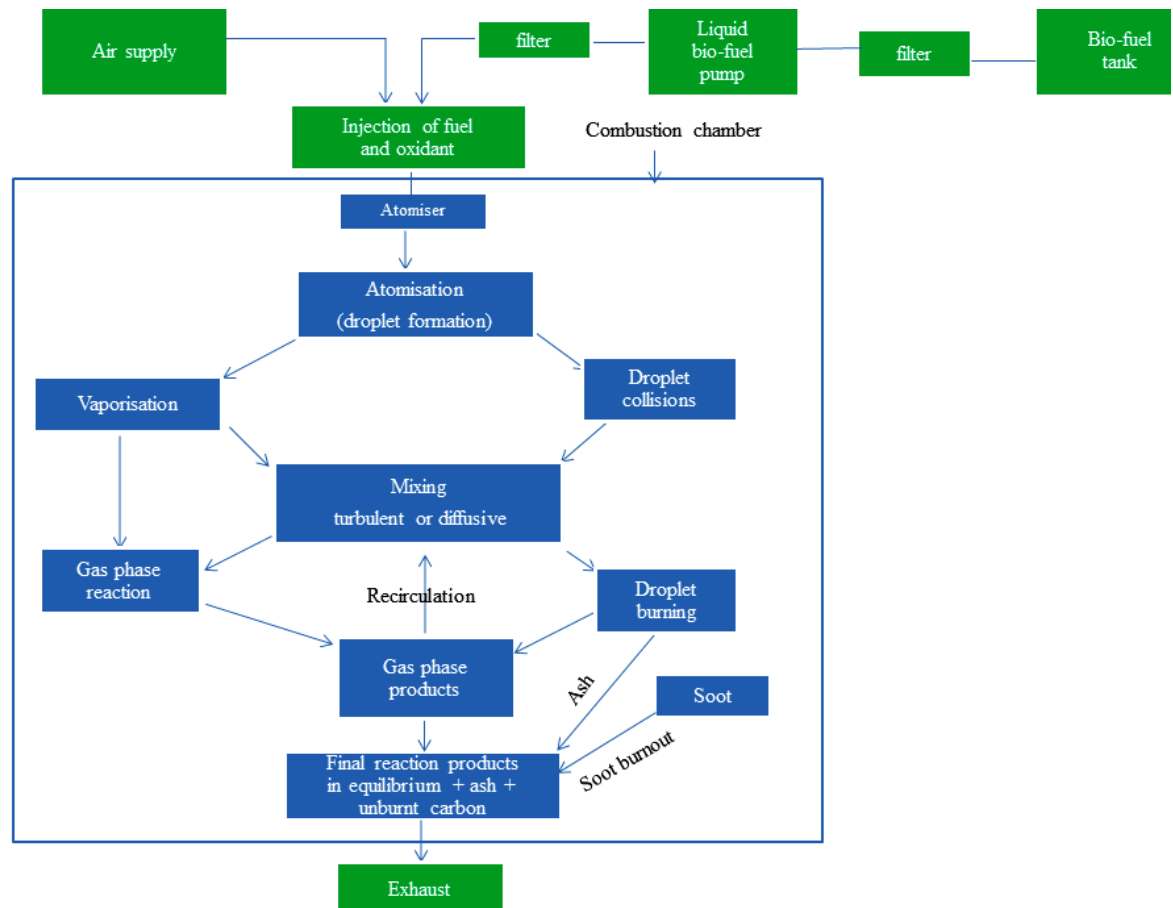


Figure 2- 2 The major ideal bio-oil combustion processes in a spray combustion chamber (adapted from Williams, 2013 with slight modifications)(73)

2.3. Liquid fuels used in spray combustion and their sources

Sprays of fossil fuels (hydrocarbon liquids) are among the most economically important applications of sprays, for instance, using fuel injectors for gasoline and diesel engines, atomizers for jet engines (gas turbine), as well as atomizers for injecting heavy fuel oil into combustion air chambers of steam boilers, and rocket engine injectors. Droplet size is highly important because of the large surface area of the tiny droplets in the atomized spray which trigger rapid evaporation. However, poor atomization of the fuel into the combustor threatens to reduce the efficiency of these systems and increase emissions of pollutants (such as soot, NO_x, CO) levels (76-79).

Nowadays the liquid fuels employed are almost exclusively the fuel oils and their derivatives. The term "fuel oil" signifies different things in different countries but essentially it covers the

range of products of high molecular weight (50). This high molecular weight group incorporates both Jet -A fuel, diesel fuels, and industrial fuels used in furnaces and boilers. The major sources for these fuels are crude oil, but fuel oils can also be derived from coal via a solvent extraction method, as well as the most well-known ways of pyrolysis of oil shale and tar sands.

Several researchers have demonstrated that alternative liquid fuels can also be generated from agricultural residue waste, hard and soft wood, animal wastes (fats) and vegetable oils from plants such as soya bean, palm, sunflower; slurries of very fine powdered particles of coal or bitumen particles dispersed in water have also been considered (56, 65, 76).

Due to the increase in world energy demand and significant importance of the contribution of oil towards the global energy consumption, there has been considerable interest in the global security of oil supplies as well as its price (80). Hence the global supply of oil on a long term basis is of concern and the general suggestions are that the total world ultimately recoverable fuel is of the order of <250 Giga-tonnes. Additionally, about 40 Giga tonnes of this have been already recovered, as well as, approximately 90 Gt tonnes in proved identifiable reserves; the rest are undiscovered resources (80-82). There are also recoverable reserves of extra heavy fuel oil of roughly 8 Gt, of which 7.6 Gt are in Venezuela, with some natural bitumen of about 10 Gt distributed in USA(6Gt) and Ghana (4Gt).

However, many research findings present the possible life-times of these crude oil based on the predictions of (i) Current day demand, and (ii) a continued expansion of oil demand assuming increase rate at 5% per annum. Despite the fact that the future growth rates always remain uncertain it is pointed out that by the next century more alternatives sources of liquids fuels will be developed. Some of these may be based on coal because of its extensive recoverable resource base or even biomass or synthetic fuels generated from other renewable sources such as solar power.

2.3.1 Fuel oil from crude oil

At present, the main sources of liquid fuels are crude petroleum and this originates naturally in sedimentary basins within the geological earth's strata. These oils are derived from vegetable

and animals debris (such as protein, lipids, and hydrocarbons such as terpenoids, terpenes and the derivative of porphyrins because chlorophyll is an important ingredient). During their formation there is substantial loss of the nitrogen and oxygen contents from the organic matter which generates a large mixture of hydrocarbon. The shark liver oil known as pristane, as well as phytane which is a diterpenoids have been used as a biological markers, and also the pristane/phytane ratio has been a powerful tool used to indicate the oxidizing conditions under which the sediments were deposited (53).

Numerous research findings show that crude oil consists essentially of hydrocarbons together with reasonable amount of heteroatom (nitrogen, sulphur, and oxygen) -containing compounds and some proportions of organometallic compounds especially of vanadium and iron. Sodium is also present in the form of sodium chloride. Gaseous, liquid, and solids or semi-solids are present in the crude oil and these are fractionated during refining processes to generate a range of liquid products, part of which gives rise to fuels used in spray combustion (76, 83, 84).

Liquid fuel properties produced are dependent upon the sources of the fuel, the form, and the nature of the refining operations, including the method of blending employed to produce the final product (84).

2.3.2 Oil from shale and oil sands

Large deposits of oil shale and oil sands (tar sand) exist and the world reserves of oil from such sources are considerable. Sunggyu, 2014 and John, 2006, identified the major locations of the world oil shale and tar deposit in sands and their significance. In Canada (Alberta), USA and Venezuela as well as Brazil oil shale deposits were found containing heavy hydrocarbons which are essentially the same as in conventional oil, but having higher viscosities meaning they are tar-like in nature. These oil shales are significantly different to conventional crude oil as they contain no free oil. Rather, it is in form of a solid mixture of organic composites. The insoluble organic matter form in sedimentary rocks called "Kerogen" which is subsequently turned into light oils due to tensional and compressional forces and heating during catagenesis, and metagenesis in petroleum generation processes.

The elemental compositions of the shale in Green river, Colorado, Peace Creek and Dunnet, Scotland have been identified by different authors, and are as follows; Peace Creek is approximately by weight 12.4% Carbon, 0.41% Nitrogen, 0.63 Sulphur and 65.7% Ash while the Dunnet, Scotland shale has almost similar carbon content of about 12.3% but high Ash content of about 77.8% as well as 0.46% and 0.73% of nitrogen and sulphur respectively (84-86). However, Green river, Colorado, is basically higher in all of these compositions since the carbon content is approximately 56% C, 7% H, 13% O, 2.5 % N, and 2.6% S. It appears that these shale oils consist of a different number of multi-ring structures (isoprenoids, thiols, porphyrins) that are held together by crosslinking groups such as -S-, -O-, and -CH₂-. Generating oil from these shale and tar sand deposits requires extensive refining for effective spray combustion.

Due to the complexity of these fractions, a variety of compositional structures, and oil-shale operational conditions each of the oil products from their regions have different refining process. In general, the recovered oil has been found to have a low specific gravity, high viscosity, and high sulphur content which necessitate upgrading prior to its application.

2.3.3 Liquids from coal

Oil generation from coal has been an area of extensive research purposes since the beginning of the Second World War. Coal to oil production methods have been investigated by many researches (73, 87-89), and there exist four different methods (Fischer-tropsch process, coal pyrolysis, slurry fuels, and coal liquefaction). Only the coal pyrolysis method will be discussed in this chapter.

2.3.3.1 Coal pyrolysis

High temperature heating of coal leads to the formation of coke (a solid carbonaceous material) as well as gaseous fuel i.e. coal gas, via the carbonization processes, and also coal tar as products. These products can be used as fuels without undergoing a further conversion process,

such as the flammable coal gas. Further distillation of the remaining products after removing the gas will give rise to a series of fuel oils, the tar fuels from destructive distillation of coal (DDC), and also a benzole fraction, which is a mixture of benzene and toluene that was used in the 1960s for gasoline engines. Additionally, the tar fuel from DDC, also known as coal tar fuels (CTF), are used directly in spray combustors at different atomization temperatures ranging from 10⁰C-205⁰C. The combustion of these fuels generates the usual spray flames. Even though these fuels are highly aromatic in nature they produce highly brilliant flames. However, the aromatics nature of these fuels will tend to release carbonaceous aerosols, smoke, and ash within the combustor and afterwards at the exhaust. Hence blending of DDC with oil is required for effective combustion processes as well as to reduce the emission levels.

Production of liquid fuels via this technique is slightly moderate for small scale purposes about 8 %wt. and this yield can be improved up to 75 %wt. through hydrogenation. The process is slightly complicated as it requires rapid heating of the finely divided coal particles to expel the volatile fragments of both liquid and gaseous form. Frequently, fluidised bed reactors are employed and staged for effectiveness of the pyrolysis conditions which become increasingly severe with each stage. However, research showed that the best among all of these methods is the char oil energy development process, COED, which involved production of char, oil, and gas from coal processing, and subsequently conversion of the char produced to generate more gas product. Additionally, this process yields a low sulphur content fuel oil through hydrotreating the liquid fraction. This method and a number of similar processes have been addressed by different authors (88, 90), and the major disadvantage of this method is, it generates more char about 55-50 Wt.% during the synthesis of fuel oil. Hence the processes must be a concurrent production which uses char or continuous conversion of the char into gaseous fuel which could be used directly as fuel.

2.3.4 Biomass liquid fuels

Biomass is produced in large quantities as a result of plant photosynthesis. In this process the carbon dioxide is converted into sugars and oxygen in plants by the sun light energy. Although,

estimation of the annual mass yield is complicated it has been estimated to be 100 Gt on land and about 50% of this in the ocean.

In historical energy equivalent the total twelve-monthly renewable resources exceeds the current yearly total energy requirements. Wood biomass are the largest biomass resource and are lignocellulose (cellulose, hemicellulose and lignin) which has variable carbon to hydrogen ratio depending on the nature and environmental growth of the plantation. Several research findings revealed that the typical elemental composition for carbon is up to 50%, with 43% oxygen and 6% hydrogen (10, 12, 91). Additionally, estimation have been conducted on the generation of these woody biomass components to be 2 Gt to 13 Gt for wood (ligninocellose), 1.8 Gt, and 0.12 Gt for grain production and sugar production respectively.

The crystalline polymerized glucose proportions of the wood are the cellulose components while hemicellulose is a mixed amorphous polymer of 5- and 6- carbon sugars; the remainder of the cell wall is the random phenolytic polymer comprising lignin. Biomass pyrolysis has received much attention in recent years due to its 'green' properties, which offer important economic benefits. Much research has been conducted once more towards developing pyrolytic methods, specifically concerning rapid heating techniques to generate bio-oil (hydrocarbons) from these materials as, well as chars. Also synthesis gas (CO and H₂) are produced from the char by-product by conventional charcoal production techniques which can be subsequently converted into liquid fuels such as methanol, and hydrocarbon fuels via gas-to-liquid technologies. Furthermore, sugars, and starches are also converted to ethanol by fermentation process and on-going research seeks to convert lignocellulosic biomass via this route (10, 14, 87, 92).

Biomass fuels are also produced in the form of vegetable oils. It has many possible uses ranging from domestic, biomedical, and industrial application and in the field of combustion generally. However, more than 48 Mt are currently produced annually specifically for domestic use as cooking oil such as olive oil, black seed oil, soya bean oil, rapeseed oil and sunflower oil which are all unsaturated, and the largely saturated palm oil and coconut oil. In addition, such fuels have found use in power engines as they are widely tested as diesel fuels and as fuel oils for furnaces and burners (93, 94).

The combustion performance of these fuels has been found to be consistent with the conventional fuel oils although there is a slight change in terms of their viscosity, ignition, and propensities for carbonaceous particle formation, which has to be taken into consideration in practice. Hence in the majority of applications these oils are esterified to generate fatty acid esters, suitable products for diesel fuel applications and for spray combustion use.

2.4. The nature and properties of Fuel Oils

The physical and chemical properties of fuel oils determine their particular application. Automotive and small domestic units require an oil that is economically viable and simply handled and atomised, but large combustion plant can handle fuel oils with higher viscosities that needs preheating.

The major properties relating to the handling, atomisation and combustion patterns of liquid fuel sprays are described briefly here in this section.

2.4. Chemical and physical properties

2.4.1 Smoke point

An approach based on smoke point height has been put into use in this study with a view to examining the sooting propensities and the nature of the chemical or structural components of biomass and hydrocarbon fuels, at same time investigating the consequences of the structures on the generation of heat and chemical compounds in laminar diffusion flames.

Smoke point height is defined as the height of a laminar diffusion flame at which the flame breaks open its apex and emits a stream of smoke. The smoke point is related to the formation or tendencies of soot and the flame is characterized by the nature of each fuel during combustion (95).

Several researches have measured the smoke point height for a large number of hydrocarbons both saturated and unsaturated, aliphatic and aromatic gases and liquid fuels containing different proportions of C, H, O, N, and S atoms in their flame structure (96). In this current study smoke point for biomass pyrolysis fuels and some hydrocarbons including aromatic fuels have been investigated.

2.4.1.1 Smoke point or soot threshold

Soot threshold or smoke point from the fundamental point of view is defined as the point at which any increase in flame height or fuel flow rate results in smoke emission from the tip of the flame. Soot at the threshold emanating from the diffusion flames has been under investigation since the early 20th century and it is still considered today in the specifications for jet fuels, and is relevant to biomass fuels. The early investigations of sooting tendencies were concerned with the ignition quality in kerosene oil lamps. However, determination of the smoke point is made by observing a distinctive change in the flame tip due to flame height adjustment. It is observed that fuels upon combustion that tend to produce more soot, tends to reach the soot threshold at a lower flame height than the less sootier fuels (95, 97).

Research has shown that, the soot threshold can be measured on a Weber Photometer lamp. This burns liquid fuels using a wick of which the height of the flame can be moved up and down until the smoke point is reached. Tendencies to soot for kerosene are measured by height subtracted from the 32mm the upper limit of the scale since a higher value would results in a soot tendency of zero or below (negative value). An improved inverse relationship can be used for calculating smoking tendency:

$$S_t = K/ S_p$$

Equation 2- 1

Where S_t is the smoking tendency, and K is an arbitrary constant. ASTM D1322 gives some measurements of smoke point height SP for pure hydrocarbons and phenols compounds using a Weber Photometer lamp. The correlation applies to the diffusion flame which is roughly

estimated as a cone shape, which is a good approximation when there is the required molecular volume of oxygen for the volume of combustion products.

Minchin, 1931 [98], predicted smoke point height for compounds which had not been measured these were used to make a qualitative ranking of sooting tendencies of groups of compounds with the same or similar molecular structures or hydrocarbon classes such as alkane<alkene<monocyclic cycloalkanes< di-alkenes and di-cyclic – cycloalkane<benzene<naphthalene series. In each of the results obtained it was found that S_t showed a good relationship to carbon number (98).

For paraffinic compounds, S_t decreases as carbon number increases but for other hydrocarbon classes S_t increases with increase in carbon number. This observation is with the assertions that S_t was closely inter-linked with molecular structure of fuel under investigation. [Belvoir, 2006] [100] reported that, two other investigations have been carried out on smoke point for conical pool burners; instead of using a wick, the flame is burned from the surface of the pool of liquid fuel. The approach of varying the flow rate of the fuel seems to be similar in concept to the wick design of exposing more or less wick surfaces, and the trends generally remain the same between compounds, as this plays a significant role to determine the point of smoking.

According to Belvoir, [2006], the smoke point data generated from a wickless conical burner for various hydrocarbons were compared and it was found that the smoke point was consistently higher than the data from the wick lamp; they were similar in qualitative terms and an adequate correlation of sooting tendency with carbon hydrogen ratio was noted. At the same time a significant exception to the C/H ratio correlation was noted in which the branched-chain alkanes have a greater sooting propensity than the normal alkanes despite the fact that they have the same C/H ratio.

Kewley in [1927] (99) reported similar results as Belvoir, [2006] for seven measurements of smoke points. Studies were conducted on the influence of air flow and burner temperature on the smoke point and results suggested that the real actual material values for smoke point depends on apparatus (100).

Minchin, [1931] [98] concluded that C/H ratio does not directly affect the smoke point in their study which further necessitated them to investigate several hydrocarbon's smoke points using

a cylindrical burner with sufficiently large surrounding air flow. Whilst testing the smoke point for to the effect of additives, several mixtures of acetylene plus H_2 , CH_4 , CH_3CH_3 or ethylene were used to match C/H with different compounds in which their results revealed that the mixture with the same C/H ratio did not display the same smoke point and each composition of the two component mixture followed its own distinct trend with C-H ratio.

Clark et al, [1946] [101], measured the fuel consumption rate at the smoke point. They employed a wick fed lamp and 38 hydrocarbons were tested. In order to calculate the mass burning rate or flow rate, the difference in weight of the lamp was measured after reaching the smoke point for a given time interval. Fuel consumption rate results for the smoke point in a wick lamp were compared using the same fuel burned in a pressure lamp in the gaseous phase, and the results of the fuel consumption rate were found to be consistent within $\pm 2\%$ of Clark's 1946 results.

In general, research studies described sooting propensities as the reciprocal of the fuel flow rate and plotted it against carbon number. As the inverse of the estimated smoke point height; had also been conducted by Minchin (98), he also found a linear correlation between compounds of the same hydrocarbons classes. Similarly, from the trend it was noticed that the sooting tendencies increased with carbon number for all the hydrocarbon classes with, the exception of the cycloalkanes. As for normal alkane, their findings were inconsistent with the trends calculated by Minchin, but for alkene and aromatics there is a slight contradiction with Minchin's findings.

While Minchin considered compounds ranging from C6-C17 Clark et al, [1946] (101) measured compounds from C2-C10. However, Clark, et al, went further to find a parameter that would result in a single correlation with a smoke point flow rate for all hydrocarbons fuels. An attempt was made to correlate the smoke point with the average bond strength between the carbon-carbon molecules and the results show that there is a decreasing non-linear relationship that was reasonably successful. However some arguments are still in existence, particularly between sooting tendencies of alkane and isoalkanes. The fact that alkanes and isoalkanes exist in a group with the same type of bond, but the structural arrangement differs, even though they have the same carbon number, their smoke point fuel flow rates were different, which implies that,

the structural arrangement or branching has an effect which was not taken into account (Kewley, [1946] (99)).

2.4.3 Volatility

Volatility is an important parameter for light fuel oils, and usually it is too low to be significant in the event of heavier fuel oils. Vapour pressure can be used to represent the volatility of a liquid fuel. Distillation curves however cannot be applied over the whole temperature range in the case of higher boiling fuel oils, although, they are generally significant at lower temperature. Distillation curves can be obtained by quantifying the amount of distillate while the oil's temperature is being raised at specific conditions set by e.g. Institute of Petroleum, and also ASME. Several researches have been conducted on the volatility parameter for different heavy fuel oils (diesel fuel, gas oil, and aviation kerosene) and as well as some light fuels such as motor gasoline (84).

2.4.5 Viscosity

The viscosity of oil is a measure of its resistance to flow and thus has an effect on the energy needed to pump a fuel via a pipe and significantly affects the atomisation process.

Viscosity is dependent on temperature and previous studies have published the variation of the viscosity with temperature for commercial diesel fuel oils fractions for different engines (like high speed automotive engines, low speed engines, and marine engines). The viscosity characteristics for industrial fuels and how their viscosity varies with temperature have also been measured (73, 84).

There are varieties of subjective methods such as Redwood, Saybolt methods that have been employed previously to quantify viscosities. However, the widely used method currently is the Kinematic method, which quantifies the rate of flow in a standard U-tube viscometer (IP 71/87). The unit of measurement is centistokes (cSt) and in the UK the values are given at 80⁰ C (British

Standard 2869, 1983). The kinematic viscosity and the other usual scales are inter-related in some ways, but the dynamic viscosity (centipoises, cP) is the product of the kinematic viscosity and the oil density (g/cm^3).

The grade for heavy fuel oil regularly used by industry is class G (UK) or No. 5 (USA), while higher viscosity, class H (No. 6 in the USA) fuel oil is used mainly by large scale operators such as the power stations: Refineries may burn highly viscous liquids or pitches such as highly asphaltic cracked by-products in refinery heaters. Nevertheless, in all cases so long as appropriate line heating is given all fuels can be controlled and burned but, taking into consideration the non-Newton characteristic of the highly asphaltic oils (73).

2.4.7 Pour point and cloud point

The temperature at which a haze forms on the cooling of oil is the cloud point, and it is an indication of the formation of wax crystals capable of blocking filters. Obviously this test can only be performed on transparent fuel oils. On the other hand, the pour point is lower than the cloud point by several degrees and is defined as the temperature which is 3°C (5°F) beyond that temperature at which the oil just stops flowing when cooled. This is generally as a result of the separation of wax from the oil(84).

2.4.8 Heat of combustion

The determination of the net heat of combustion, Q_n , can be done directly using bomb calorimetry (IP 12/79) which is the most commonly used and most precise method. Also, it can be done concurrently with the determination of sulphur content. Conversely, the heat of combustion could be obtained indirectly from density correlations for fuel oil or from the elemental analyser. In the first instance, using the Dulong formula, the net heat of combustion, Q_n , is expressed as:

$$Q_n = (46.428 - 8.792 \rho_L^2 + 3.170 \rho_L) (1 - x - y - s) + 9.4205 - 2.449x \text{ (MJ/kg) ...Equation 2- 2}$$

Where ρ_L denote density at 15⁰C, g/cm³ and x, y, and s stands for mass proportions for water, ash, and sulphur respectively.

Calorific values can be obtained rapidly and easily through chemical analysis determined with the use of an elemental analyser. Rather than obtaining the values from direct combustion of the fuels, this indirect method analyses the percentages of carbon, hydrogen, nitrogen and sulphur that are present in the fuel. Moreover, this indirect method can also give information about the viscosity, density and also on the flash and flame points of liquid fuels by using different correlations. According to Colombo et al, 1988 in (73) a modified Dulong equation for liquid fuels is;

$$Q_g = 0.339 C\% + 1.256(H\% - 1/8 O\%) + 0.105 S\% \text{ (MJ/kg)} \dots \text{Equation 2- 3}$$

$$\text{and } Q_n = Q_g - 0.224 H\% \text{ MJ/kg} \dots \text{Equation 2- 4}$$

Where C%, H%, S% denotes mass percentage for carbon, hydrogen, and sulphur present in the liquid fuel.

2.4.9 Sulphur content

Sulphur is to a certain degree present many in liquid fuel fractions in the form of organo-sulphur compounds. As a result of this the calorific value is reduced to some extent since the heat of combustion of carbon is greater than that of sulphur. Nevertheless, formation of sulphur oxides is the main relevance of the sulphur content. Several researches have been conducted on organo-sulphur species for different oils including bio-fuels which have been proved to have very low sulphur contents. Its measurement could be with the use of Bomb calorimetry method (IP 61/84), with a variety of chemical methods or on a routine basis with x-ray fluorescence spectrometry.

2.4.10 Asphaltenes

Asphaltene content is defined as that percentage of the fuel oil that forms precipitate on addition of a non-polar solvent which is usually n-heptane (IP 143/84). The asphaltenes are fairly huge condensed aromatic hydrocarbons that also contain heteroatoms (S, N, and V) and, have long paraffinic side chains. They exist in residual fuel oils and during the oil phase they are insoluble but held in suspension (73, 87, 102, 103).

2.4.11 Flash and fire point

Flash point and fire point are empirical tests that are carried out to show the ease of fuel oil ignition and they are relevant in terms of fuel handling as well as safety of storage. Commonly, the flash point is obtained by heating an oil to establish the temperature at which the vapour just bursts into flames and then goes out. This procedure is done with the use of the Pensky-Martens apparatus (IP35/63). The fire point is the temperature which is a few degrees higher, at which the vapour bursts into flames and continues burning (73, 87, 102, 103).

2.5. Light oils (LOs)

Light oils also known as petroleum light oils (which are observed to flows freely at very low temperature) are the first portion generated during crude oil distillation process due to their low boiling point. They consist of C₁ to C₅ hydrocarbons and benzene, toluene, and xylene (BTX), as well as small molecular weight alcohols which have been identified to have high API gravity between 37⁰API and 42⁰. This is because it contains light hydrocarbon fractions which have low values of density, viscosity, specific gravity at room temperature and low wax content.

Physically these fractions are smaller molecular size, colourless and have high flammability. The chemical and physical nature of these petroleum fractions have been exposed to numerous investigations. Light oils do contain some heteroatoms (S, N, and O) which exist as compounds

but these compounds undergo hydrotreating industrially in the refinery. Sulphur in light oils is removed via hydrodesulphurization (HDS) and nitrogen through (HDN). However, HDN of light oils has been an issue as it requires many steps and involved catalysis but many of these techniques are successful. The removal of these components needs to be carried out so as to prevent emission of pollutants especially when using them as domestic oils(104, 105).

2.6 Diesel fuels and gas oil

The production of diesel fuels by refineries differs according to the configuration of each refinery crude distillation unit (RCDU) and is dependent on the availability of catalytic cracking and visbreaking units. The fraction of cracked components present in automotive gas oil is gradually rising. This will result in production of higher density but lower stability fuels which will in turn lessen the ignition quality (that is cetane number).

The relevance of diesel engine as a power unit of vehicles particularly in commercial sectors, is steadily increasing. This is due its good fuel economy, reliability and also durability.

Diesel fuels are essentially straight-run products that are directly obtained from the crude oil distillation. Additionally, they contain different quantity of cracked distillates in order to increase the yield. Additives may be present in diesel fuel so as to enhance their cold flow characteristics and prevent the development of paraffin wax crystals at low temperatures (Clarke et al, 2002) (106).

The distillate fractions, the gas oils, differ extensively in terms of their composition however. The aromatic contents are generally within the range of 15 – 30% by weight, and the compositions by weight in the paraffins might be from 25 – 70 % while as in the case of naphthenes the variation may range from 4 – 60% though, this depends on the source. Clearly these differences have a significant effect on fuel properties, especially the cetane number. Additionally, the fuel oil for low speed high power engines may comprise residual fuel oils which are compound mixtures of higher hydrocarbons that could be paraffinic or asphaltic in nature.

Different classes of diesel fuel exist, these largely are:

- i) A volatile distillate fuel oil that is mostly used for road transport automobiles. Its boiling point range from 200 - 350^oC
- ii) A lower volatility distillate fuel oil is used for heavy mobiles or industrial diesel engines such as railways, tractors, locomotives, earth moving equipment); also, it can be used for industrial gas turbines. The boiling range for this diesel is ca. 200 – 370^oC.
- (iii) A distillate fuel used for marine purpose which is similar to (ii).
- (iv) Fuels which contain a certain quantity of residuum and used for heavy duty engines of low or medium speeds which are usually applied in marine or industrial generation fields. It is also applicable to industrial gas turbines.

The most widely accepted diesel fuels are those defined by the British standard and the ASTM standard, although, diesel fuel specification differs from country to country. There is the possibility that in the future the cetane number may be lowered by a few points with an increasing interest on cetane enhancers. These enhancers are compounds that easily decompose to release free radicals and promote the chain initiation rate for hydrocarbon oxidation in the event of diesel ignition. Several alkyl nitrates and ether nitrates are appropriate compounds. The most effective additives that are employed in practice for usual application are iso-octyl nitrate or precisely 2-ethyl hexyl nitrate. Such kind of cetane enhancers offer refiners a simple means of attaining flexibility in the realization of specifications on a daily basis precisely when cracked components are used.

2.7. Heavy fuel oils (HFO)

This fuel oil category is generated essentially from crude oil as the bottom fraction called no. 5 and no. 6 fuel oil. Hence, they have vast industrial and marine engines applications. Some of these fuel oil uses such as industrial spray combustion application are described below.

2.7.1 Industrial application of fuel oil

Here the fuels that are taken into consideration are exclusively those that are used in spray combustion application and vary from those used for domestic heating which are the distillate fuels of the gas oil type, and extend through to heavy residual fuels. “Domestic heating oil” is the term commonly used to describe a gas oil type product that is used with spray combustion type domestic heating equipment and its boiling point ranges from 160 – 370 °C.

The residue that forms following the removal of the more volatile components during the distillation process are the residual fuel oils which contain in addition a range of other products which are mixed with it. Therefore, the crude oil source and the constituent of the fuel oil blends basically determine the properties of the residual fuels. Ash and sulphur contents, viscosity and volatility are the major properties of relevance to the spray combustion. However, water content, acidity, inorganic material (like rust), cloud formation and the stability to sludge formation are other significant factors with respects to fuel filter blockage, pumps and pumpability and erosion of tips of burners. There are specific guidelines governing the determination of the upper limit of the major properties of fuel oils, the more relevant ones are the British standard specification 2869:1970 and the ASTM D396-69.

Fuel oils are generally divided into two major types; the distillate fuel oils and the residual fuel oils. Distillate fuel oils are derived from vaporisation and condensation processes and thus do not comprise of compounds with high boiling points or asphaltic components. On the other hand, residual fuel oils contain residue from thermal cracking processes or crude distillation but they could be mixed with some fuels that are lighter. Consequently, residual fuels behave in a more complex manner and can be problematic during handling, combustion and storage; further details are given below.

Separation of crude oil fractions to yield highly asphaltic oil with regards to the refinery processes would be as shown in Figure 2-3.

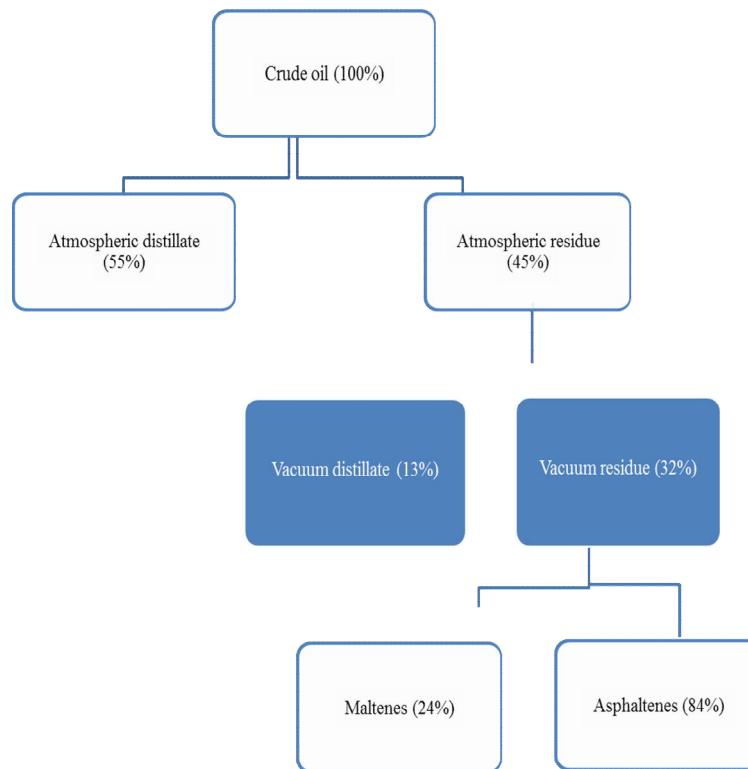


Figure 2- 3 Crude oil fractions yielding highly asphaltic oil composition (73)

Residual fuel oil which is a complex mixture of hydrocarbons could be prepared by blending a residuum component with a flux stock which is a distillate component diluent, in order to achieve the desired viscosity of the produced fuel oil. Hence, the simple model of a fuel oil can be thought to comprise of two parts, an asphaltene constituent and a non-asphaltene constituent or maltenes. Furthermore, the maltenes can be subdivided as illustrated in Figure 2-4.

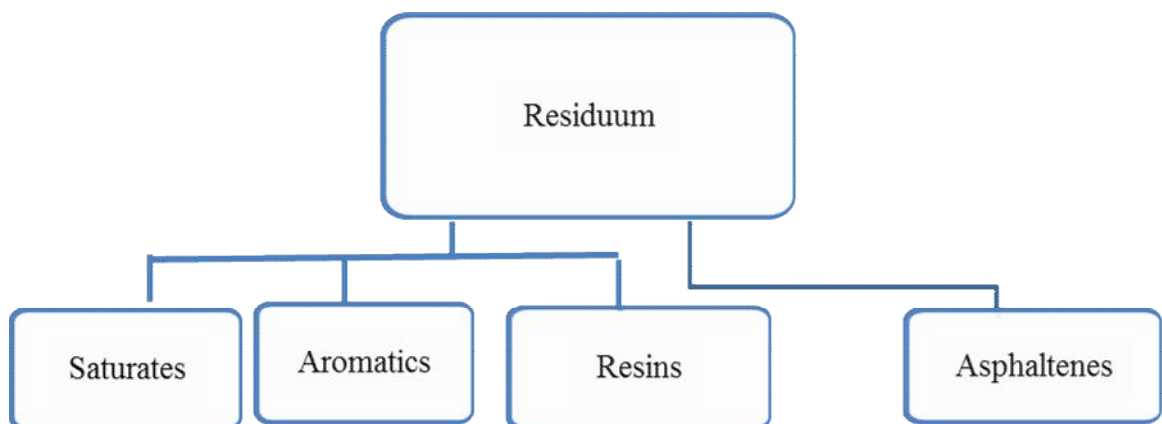


Figure 2- 4 Residuum (maltenes) subdivisions producing more asphaltene fraction

There are various forms of fractionation procedure based on physical or solvent method, though it is only the n-heptane-based asphaltene measurement that forms a standard test known as IP 143/84. Further methods exist which indicate different proportions of these fractions. It must be acknowledged that the asphaltenes constitute a solubility class, hence slightly different results may be obtained when other solvents are used. Also, the use of the term soft resin and hard resin are used by some methods which define asphaltenes as n-pentane insoluble rather than n-heptane.

Asphaltenes can be considered as soluble in the non-asphaltene phase in a fuel that is steady and compatible. Conversely, the insoluble asphaltenes contribute to the overall sediment level in the fuel (in combination with metal and carbon particles) Visbroken fuels are higher in asphaltene composition and in principle precipitation problems can be enhanced unless care is taken in fuel blending (eg. by adding some lighter oil) so that the available solvency power of the base oil is maintained at a high level.

2.8 Smoke emissions

2.8.1 Origin and general description of soot

Soot formation has also been observed in many biomass and coal utilization processes, including biomass gasification and combustion. Sooting in laminar diffusion flames has been under investigation since the 1930s. The main effort for this research really started in aviation. Controlling of smoke and, carbon deposits and radiant heat transfer in gas-turbine design is of great importance. Soot and radiant heat transfer can make hotspots in the turbine and increases wear.

The formation of small submicron carbonaceous particles in the combustion and pyrolysis of both simple and complex hydrocarbons has been observed since the utilization of fossil fuels to generate energy started. Soot is formed in different practical combustion systems ranging from

wick burners and candle burning to more complicated combustors such as gas turbine and internal combustion engines (power generator, transport and heavy duty engines).

Based on the simple hydrocarbon flames experiments, for instance using the diffusion flames and pre-mixed flames, researchers have shown that formation of soot usually is when all the conditions for combustion are achieved. Then, sufficiently fuel rich conditions will allow condensation, polycondensation or polymerization of the fuel fragments including its first decomposition product to compete with oxidation (97). Additionally, soot from hydrocarbon flames usually exists in the form of both individual particles and agglomerates comprises of different primary particles.

2.8.2 Mechanisms of soot formation and oxidation for hydrocarbons

The general mechanisms of formation and oxidation of soot is going to be reviewed based on the studies of simple hydrocarbon pyrolysis and combustion, as a result of limited relevant knowledge in bio-oil derived soot. The bulk amount of research on soot in simple hydrocarbon flames provides a fundamental bases for understanding soot formation in biomass oil derived combustion and heavy fuel oil as well. Secondary reactions of oil volatiles and evolved gases are going to be presented in this section including a brief review of soot sampling techniques.

2.8.2.1 Structure and properties of soot

Soot from typical hydrocarbon pyrolysis and combustion systems consists of agglomeration of a number of primary spheres with a typical diameter in the range of 10-15 nm for a wide variety of operation conditions (107, 108). The size distribution depends upon the primary spheres. Haynes and Wagner, 1981, (97) reported that matured soot has similar physical and chemical characteristics in respect of precursors despite the fact that the pathways to form the matured soot are different. It has been reported that, the earliest particles could have diameters as small as 2nm (109).

The morphology of soot particles from flames of various fuels have been studied using scanning electron microscopy (SEM) and transmission electron microscopy (TEM). The earliest particles from benzene and methane flames contain chain-like agglomerates of individual spheres, which appear as irregularly shaped pieces with sharp edges (110, 111).

The soot internal structures have been examined by high-resolution phase-contrast electron microscopy (108). The edge of the particles have been reported to have an approximate edge, and bent carbon layers follow the shape of the particle surface. The inner part of the particle lattice structures seem to be located less regularly near the centres within which the structure is less ordered and dislocations and other lattice defects are presents.

Heat treatment of soot provides internal order of the particles, and the inter-planar spacing approaches that of graphite. The graphitization rate depends upon temperature, such that the age of a particle as well as its degree of order is linked closely. Soot particle ordering may occur at high temperature as soot particles continue to grow.

Chemically, carbon is the major constituent of soot but hydrogen and other elements can be present as well. Premature soot particles from simple hydrocarbon fuels have carbon hydrogen mole ratio less than or equal to 1, while mature particle have C/H ratio as high as 10. In (97) it is reported that, X-ray photoelectroscopy (XPS) was used to determine whether the soot samples were primarily aromatics or non-aromatics compounds. The earliest particles from methane and benzene flames were non-aromatics, subsequently changing to aromatic under the condition of higher residence times in the flame. A fraction of oxygen was found to be chemically bound to carbon atoms, but not found incorporated into aromatics rings. There is a dramatic decrease of oxygen ratio to carbon with increasing time in the flame. Nitrogen has been found in the structure of soot from coal pyrolysis but has not been reported in the soot of simple hydrocarbon fuels that do not contain nitrogen (112, 113).

Transmission electron microscopy (TEM), for soot particles (shown in Figure 2-5) have shown a chain structure composed of up to 4000 of smaller spherical particles (spherules). These primary particles agglomerate in clusters and are found to contain between 10^5 to 10^6 carbon atoms.

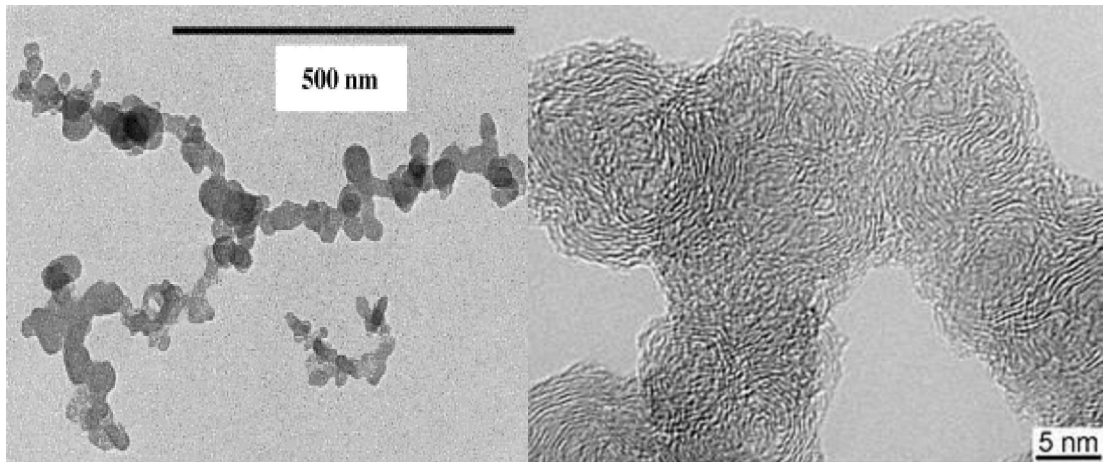


Figure 2- 5 TEM images of agglomerates and primary particles (114-117).

Agglomeration size can fluctuate from 10 to 1000 nm with a surface area of about $200 \text{ m}^2\text{g}^{-1}$. Nanoparticles within the agglomerates are more or less spherical with diameter typically from 10 - 80 nm, but most of them are between 15 to 30 nm. These spherules are composed of concentric lamellae structures arranged around the center reminiscent of carbon black or graphite structures. The carbon atoms are bonded together in hexagonal face-centered plane arrays (platelet) in which the space between two platelets is 0.355 nm on average (slightly higher than graphite). 2-5 platelets overlay in layers leading to crystallite formation, and thousands of crystallites in unordered layers (turbostratic) constitute a spherule (Fig. 2-6) (118). Soot density is estimated to be close to graphite which is around 2 gcm^{-3} .

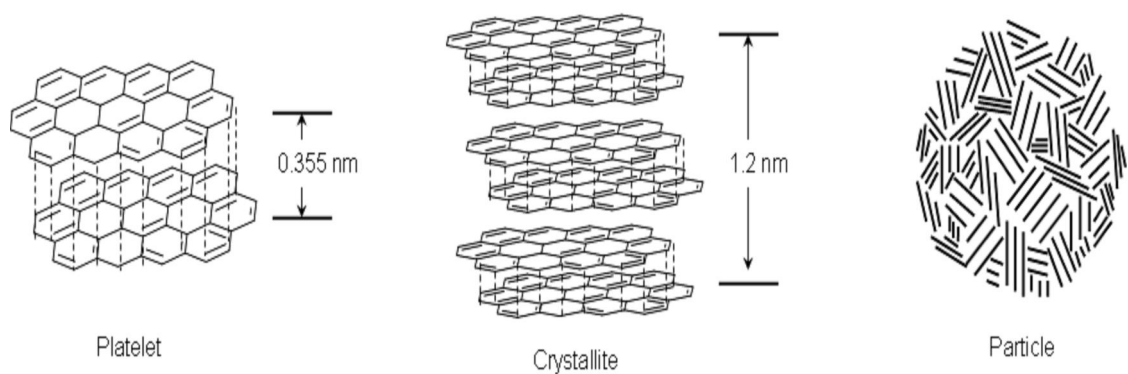


Figure 2- 6 Schematic of substructure of carbon particle (117, 118).

The particle sizes are dependent upon different factors such as nature of the fuel burnt, flame, or engine injector types, and operation conditions, as well as sampling site i.e. where and how the soot particles have been sampled and measured. For instance in a diesel engine, at the exhaust, primary particle size was found to be from 20-50 nm with a mean diameter around 30 nm (119, 120), and also 30-50 and 40-65 identified (121, 122). Researches revealed that, soot agglomerate sizes have been found to be between 100 nm and 2 μ m at the end of combustion (123, 124). Also Bruce, et al., 1991(123), reported that, sizes were found up to a range between 30-70 nm.

2.8.2.2 Soot formation mechanisms/stages

Combustion from liquid or vapour phase hydrocarbons resulting in the evolution of soot particles comprises five process steps namely; pyrolysis, nucleation, coalescence/ surface growth, agglomeration, and oxidation as indicated in the Figure 2-7. These mechanistic stages occur in the previously cited sequence order; however, only the oxidation converts hydrocarbons to CO, CO₂ and H₂O at a given time within the sequence. Hence, the net soot formation involves the formation and oxidation of soot, while the overall process can proceed in a spatial and separate sequence as in the case of a laminar flame, or simultaneously in premix combustors. However, in internal combustion engine, it appears that this sequence varies between two limits.

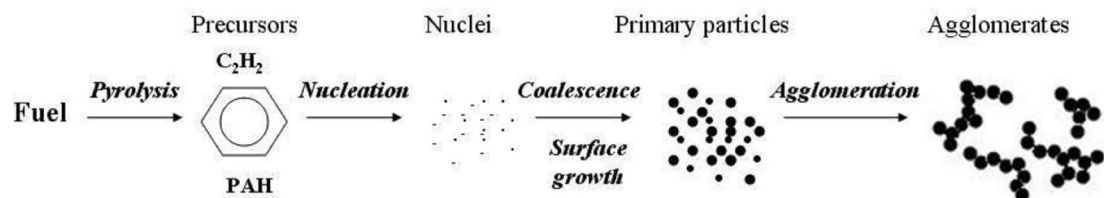


Figure 2- 7 Schematic diagram of the soot formation steps (adapted from (125))

2.8.2.3 Fuel Pyrolysis

Pyrolysis is an endothermic reaction in which the rate depends upon temperature and concentrations. Pyrolysis at high temperatures alters the molecular structure of the fuel, and these alterations start with the decomposition of carbon bonds followed by radical reactions such as recombination. Moreover, the absence of oxygen means there is limited/ no significant oxidation. Pyrolysis results in the production of soot precursors which are the building blocks of soot formation; these include species such as polycyclic aromatic hydrocarbons (PAH) and acetylene.

The formation of the soot precursors depends on the fuel pyrolysis rate compared to the fuel and precursor oxidation rate by OH. All these rates increase with temperature despite the fact that the premixed flame (large quantity of oxygen present) produces less soot than the diffusion flames (absence of oxygen in the pyrolysis region) even though the temperature increases (117). In diffusion flames, radical diffusion is important, for instance if the radical OH diffuses into the fuel-rich zone it can accelerate the pyrolysis. A small amount of atomic oxygen, oxygen molecule or hydroxyl can also influence the increase in the pyrolysis rate, since most of the reactions take place by means of a free radical mechanism.

Typically pyrolysis products in a laminar diffusion flame are C_2H_2 , C_2H_4 , CH_4 , C_3H_6 , and C_6H_6 . Acetylene is largely present in fuel-rich combustion; the reaction of these monomers results in polymers, and formation of PAHs is considered to be the main soot precursor. The initial reaction begins phenyl or acetylene to produce the first aromatic ring as shown in the Fig 2-8 which will play an important role in polycyclisation of the molecules.

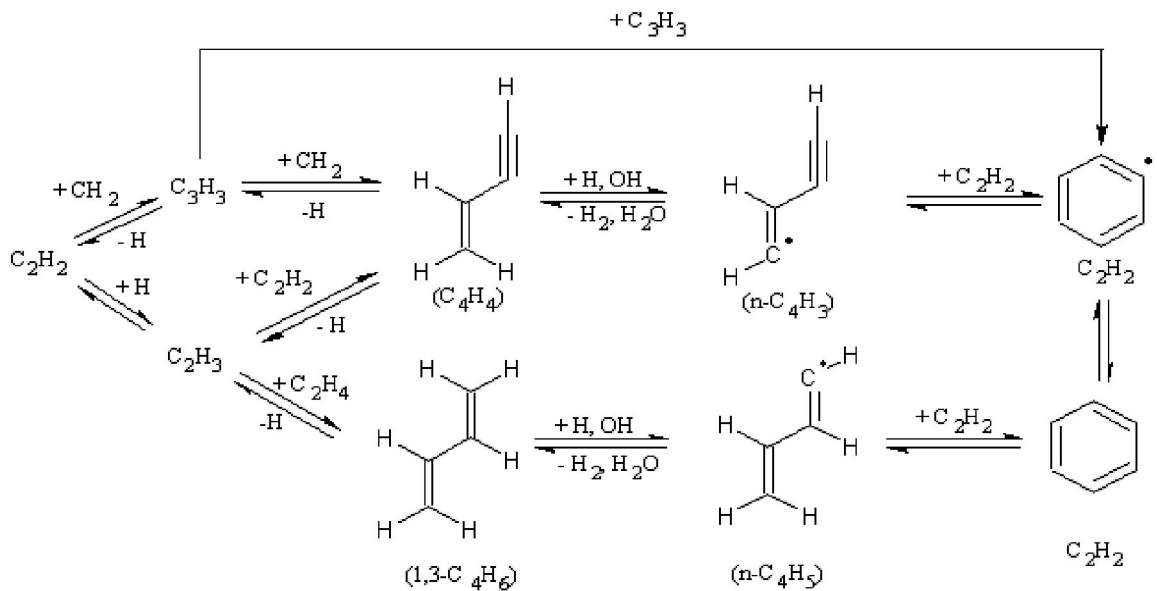


Figure 2- 8 Pathways for the formation of the first benzene moiety from acetylene

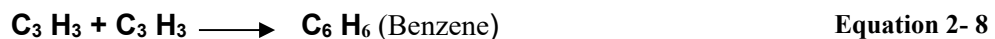
The first part of the formation of benzene is shown in equations 2-5 to 2-6 (126)



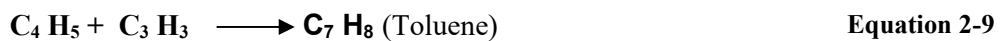
A second stepwise reaction for the benzene formation can occur via a C_3H_3 route: (127).



or



3rd possible way (128) is:



The rates of the above reactions are highly influenced by temperature, and the formation rate is maximum at temperatures around 700 K for the first way (via C_4+C_2), but for the second way (via C_3+H_3) is around 1600 K whilst for the third way is as low as room temperature.

The Frenklach model provides an insight of the detailed kinetic model containing about 600 possible elementary reversible reactions and 180 species [105]. In this, the principal routes for the particle inception include first ring formation, production of two rings aromatics and the continuous growth of fused polyaromatization. Non-radical and radical cyclizations are the two

possible cyclization reactions. The latter, is also subdivided into: (a) cyclization of a more stable radical; (b) cyclization of a less stable radicals; and (c) radical cyclization via interaction due to unpaired electron with a triple bond. The results of computational studies show that (c) is several orders of magnitude faster than reactions (a), (b) and non-radical cyclization as well.

Generally there are physical parameters influencing soot formation for instance temperature, pressure, stoichiometry, fuel structure and composition, and in diesel engines soot formation also depends on injectors, injection timing, cylinder pressure and temperature, multiple injection, combustion chamber design and engine transients.

2.8.2.4 Nucleation

Nucleation is also known as soot particle inception. It is the formation of solid particle (nuclei) from gas phase reactant(s), and the reaction mechanisms are irreversible. The smallest nuclei detected in a luminous flame are in the range of 1.5-2nm in diameter. Researches also revealed that nucleation is likely due to the addition of small, aliphatic hydrocarbons to larger aromatic (PAH) particles at 1300 to 1600 K or by two PAH combining. The nuclei mass has a negligible contribution to the total mass of soot, but they have an important role to play in the mass added later by providing sites for the surface growth. Nucleation only occurs close to the primary reaction zone where the operation conditions are optimum for instance, the temperature, and concentrations of radicals.

The first monocyclic hydrocarbons produced will evolve in to polycyclic aromatics. The growth of the aromatics is substantiated through the hydrogen-abstraction-acetylene-addition (HACA) (129) mechanism given in Fig 2-9.

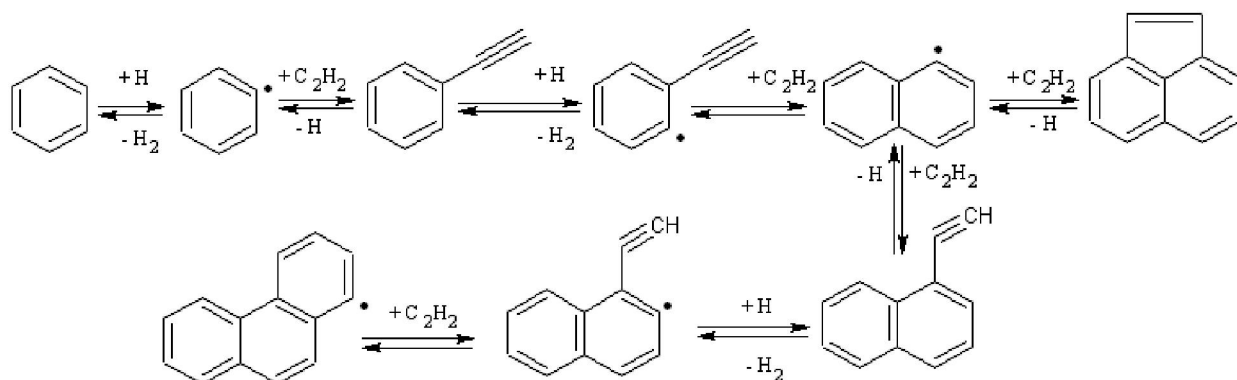


Figure 2- 9 HACA mechanism of polycyclic aromatic hydrocarbon formation

The above Figure 2-9 shows the following steps, firstly the release of a hydrogen atom which creates the radical centre, followed by the addition of acetylene to the aromatic radical such as phenyl leading to the bonding of an ethynyl ($-C_2H$) group to the aromatic ring. Subsequent continuation of the mechanism results in planar, stable, condensed, and irreversible aromatic rings. The competition which occurs between two mechanisms is determined by the quantitative ratio of acetylene to benzene. Depending upon the concentration of aromatic species PAHs can cultivate through the direct ring-ring condensation (130). Nevertheless, when equal volume of acetylene and benzene are present then the HACA mechanisms becomes dominant. The presences of other formation pathways have been described and reviewed (131).

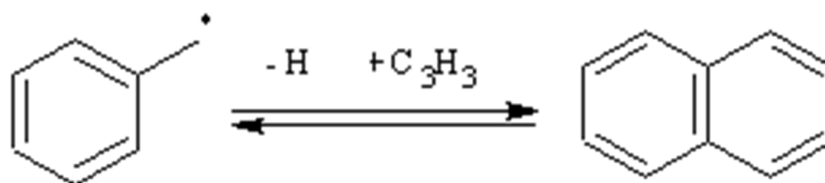


Figure 2- 10 Combination of benzyl with propargyl

Figure 2-10 shows the combination of benzyl and propargyl leading to the naphthalene formation (66). A combination of two cyclopentadienyl radicals (from oxidised benzene) also results in a naphthalene molecule (132) as shown in Figure 2-11.

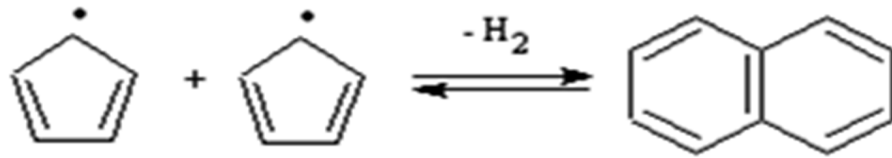


Figure 2- 11 Combination of two cyclopentadienyl

Cyclopentadienyl radical can also propagate PAH growth via the reaction given in Figure 2-12.

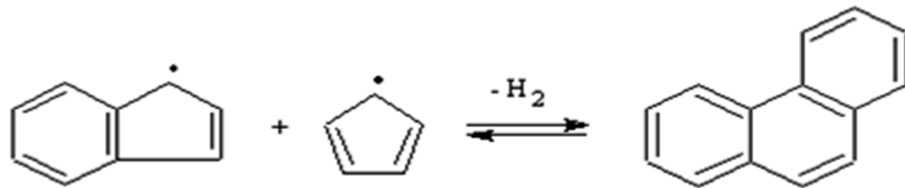


Figure 2- 12 Combination of cyclopentadienyl and indenyl

Sequential addition of propargyl radicals leads to the formation of phenyl radicals and biphenyl, while the polycyclisation in phenanthrene is achieved with the addition of acetylene as shown in Figure 2-13.

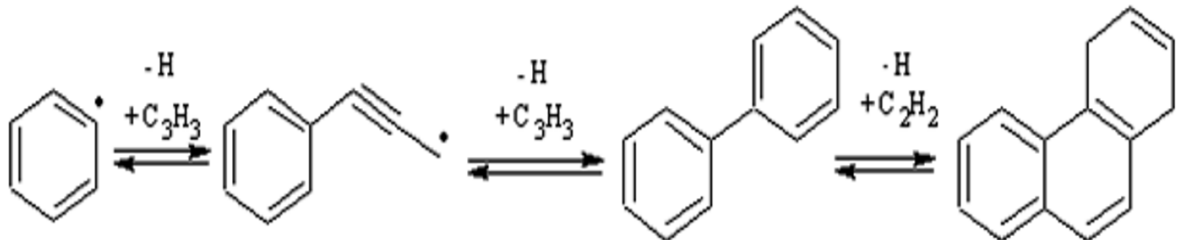


Figure 2- 13 Propargyl radical reactions leading to phenanthrene formation

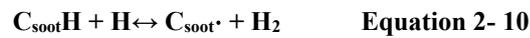
2.8.2.5 Surface growth

Surface growth is the process of adding weight to the nuclei which occur in numerous numbers (but without significant load of soot). There is no sharp line between the end of nucleation and the beginning of surface growth but the gas-phase hydrocarbons are deposited on the reactive surface of the nuclei. After leaving the primary reaction zone into cooler and less reactive

regions, there is still occurrence of surface growth, and there is no increase in number of particles but the weight of soot and its volume fractions increases.

The major part of the soot mass growth is produced during this step, and the time allowed for surface growth is an important consideration in reducing soot production. The size of the nuclei determines the surface growth, hence the smaller the nuclei the higher the surface growth because smaller nuclei have more reactive radical sites (133). According to Heywood, (1988), the formations of the initial carbon particles start from growth of the PAH in three dimensions, and the reactive surface of the soot particles readily accepts hydrocarbons usually from the gas phase.

The higher reactivity of the soot surface is such that the presence of the soot can accelerate the decomposition of benzene and acetylene as well during pyrolysis. The surface rate of deposition when methane is pyrolysed on soot particles is an order of magnitude higher than it is on graphite and aluminium. It is suggested that the main species being attached to the surface are acetylene and polyacetylene. The surface reactions are as follows:



Where: $C_{\text{soot}}H$ and C_{soot}^*H represent an arm-chair site on the soot particle surface and $C_{\text{soot}}\cdot$ represents the corresponding radical. Estimation of the rate coefficients for the above heterogeneous reactions is based on analogous gas-phase reactions of two one- ring aromatics (benzene and phenyl radical).

2.8.2.6 Coalescence and agglomeration

Coalescence and agglomeration are processes in which the particles are amalgamated. Coalescence, also known as coagulation it occurs when the particles collide and coalesce thereby reducing the number of particles without changing the soot mass. Particle coagulation is due to the collision and striking of particles undergoing Brownian motion, which lead to the

increase in the characteristic dimension of the particles without harming the soot loading. Particles collision is effective and coalescence for particles with diameter up to many tens of micrometers results in a decrease in the number of particles (134).

2.8.2.7 Oxidation

The transformation of carbon or hydrocarbons into combustion product is called oxidation. When the carbon has undergone a partial oxidation process, it will not evolve into a soot particle even if the molecule went through a fuel-rich zone. Occurrence of this phenomenon is at the moment starting from pyrolysis through agglomeration, and depends upon the species present and operating temperature. Soot oxidation occurs at elevated temperature up to above 1300K (135). O_2 , O , OH , CO_2 , and H_2O species can cause soot oxidation. Figure 2-14 below shows the generalized soot formation mechanism for model fuels and some hydrocarbon fuels.

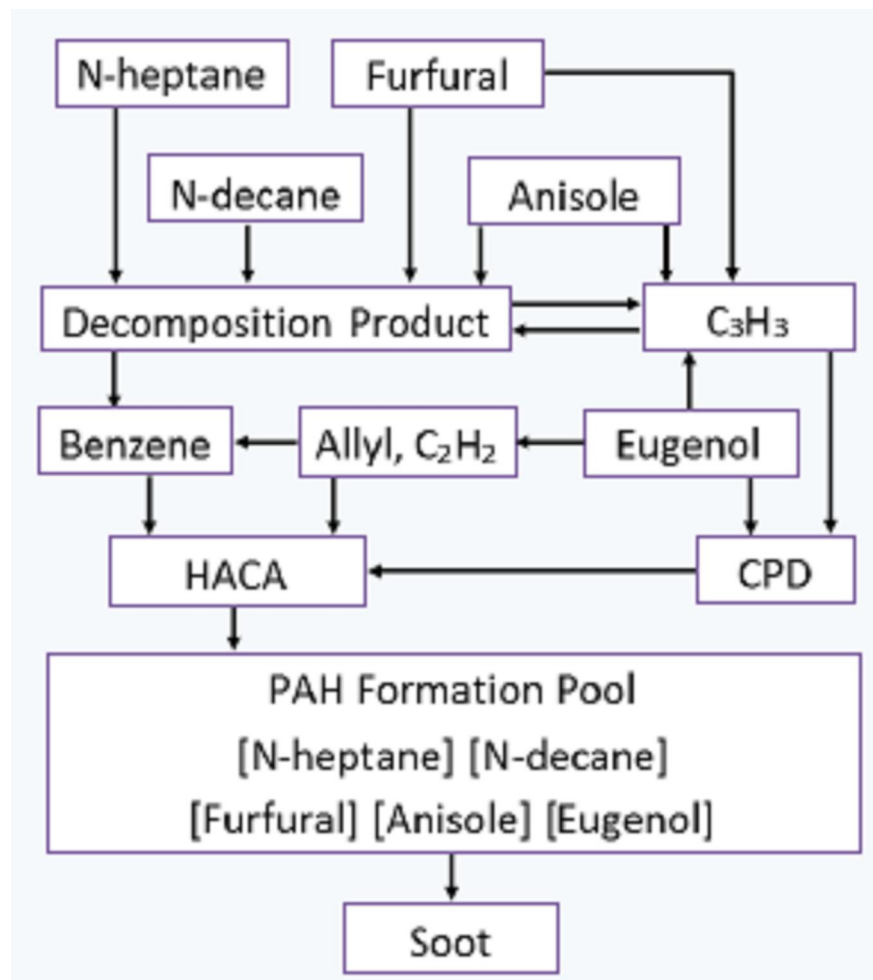


Figure 2- 14 General proposed mechanism of soot formation

2.8.2.8 CO formation

Formation of carbon monoxide CO is seen in the products resulting from combustion of all carbonaceous fuels with a concentration that is usually higher than what is anticipated from the equilibrium point of view. The concentration of carbon monoxide for any system within equilibrium is expressed in the overall reaction below



Therefore, $[\text{CO}] = K_1 [\text{CO}_2] / [\text{O}_2]^{0.5}$ Where K_1 is the equilibrium constant and $[\text{CO}]$ etc. are the concentration of the gases in appropriate units

It is apparent that temperature and the level of excess air determine the equilibrium level of carbon monoxide. At a constant temperature and low level of excess air the carbon monoxide concentration becomes higher.

Formation of carbon monoxide occurs in flames via rapid oxidation of hydrocarbons by oxygen and this takes place in the reaction zone. Thereafter, the carbon monoxide becomes slowly oxidized to form carbon dioxide as can be seen in the two reactions below. However, these two reactions together formulate the water-gas equilibrium reaction.



As formation of carbon monoxide occurs rapidly in the reaction zone, and is consumed slowly the carbon monoxide concentration existing in the reaction zone are beyond the equilibrium values. Thus, the slow conversion of carbon monoxide to carbon dioxide in the post-flame zone gases is called after-burning. The rate at which this conversion occurs has been described in (136-138) and in Dryer and Glassman, 1973(137).

2.9 Bio-fuels

2.9.1 Pyrolysis oils from wood

Wood and its product fuels are widely used in combustors to generate energy and power for domestic, commercial, and industrial heating units. ‘Soot’ particles -agglomerated chains of carbonaceous spherules of ‘Elemental Carbon’ (EC) become a niche for volatile organic species known as ‘Organic Carbon’ (OC). Small-scale combustors may contribute significantly to ambient air pollution including EC and BC, although feedstock parameters significantly influence emissions of NO_x, CO and PM (139)

Liquid fuels such as eugenol, furfural, anisole, as well as light chemical base fuels are essentially generated from the pyrolysis of woody biomass for combustors. Figure 2-15 below indicates simplified stages involved during pyrolysis of wood in which each of the wood polymers gives rise to a valuable product. The details of these components are discussed later.

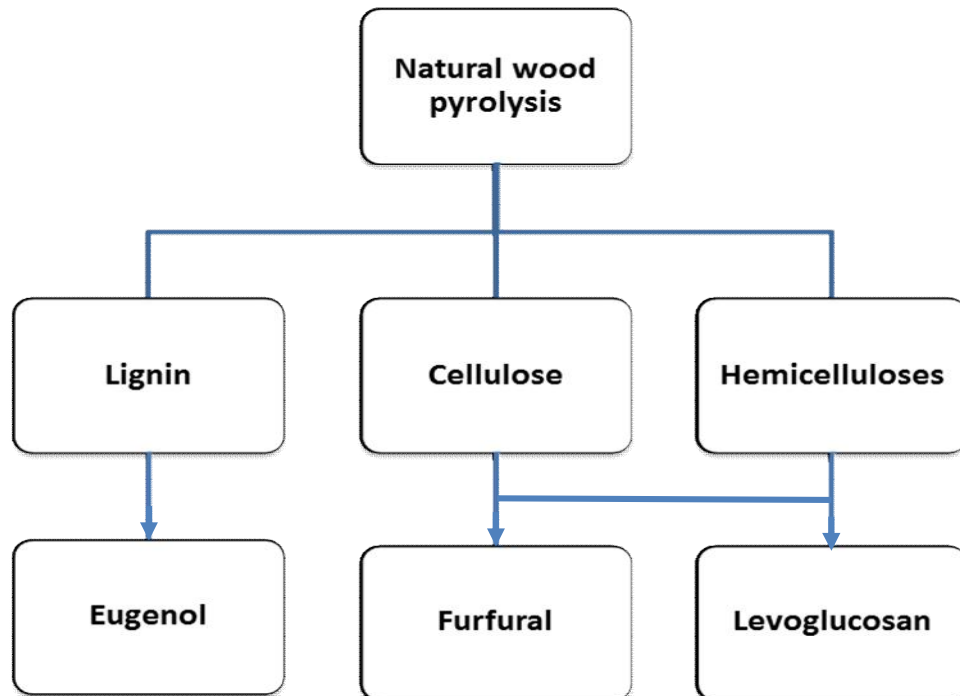


Figure 2- 15 Pyrolysis of wood leading to liquid fuels production

2.9.2 Pyrolysis of biomass and bio-oil Pyrolysis

The process involves thermal decomposition of biomass in the absence of air and oxygen at temperatures ranging from 400–800°C (9, 140). Numerous biomasses have been studied (cheap, local, and abundant lignocellulosic components in grasses and trees). The finished product usually comprises of bio-oil, combustible gases and carbonaceous char.

Pyrolysis is an endothermic process involving thermal and unstable conversion of hydrocarbon molecules into forms of organic compounds; chemical bonds break down at elevated temperatures. This results in release of a liquid fraction and gases (10). Balat, et al 2009, (11) has pointed out that pyrolysis has the economic advantage of low capital investment and a liquid end product which can be transported and catalytically converted into fuels and useful end products. These include food flavorings, fertilizers, resins as well as other forms of chemical product which can be fully compatible with existing petroleum products.

Williams, 2005., (9) mention that, pyrolysis is an interesting thermochemical process due to its flexibility; manipulation of process or operating conditions leads to production of oils, char or gases by changing its heating rate and temperature. He also mentioned that end products from pyrolysis have vast application, for instance the char has the potential to be used as a solid fuel as well as changed to activated or black carbon. The schematic diagram in Figure 2-15 shows the different conversion technologies of biomass to produce diversified hydrocarbon products (12).

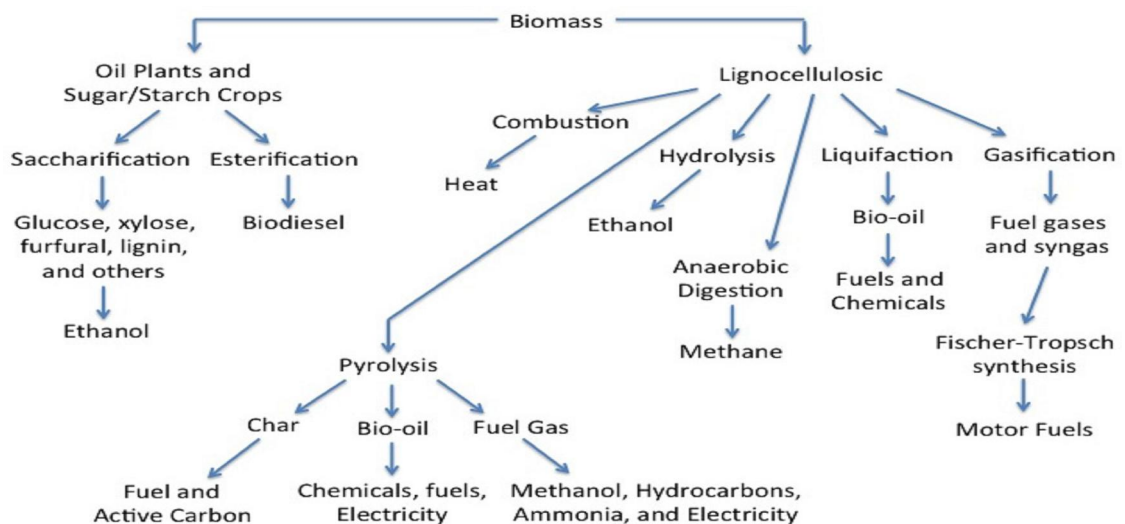


Figure 2- 16 Biomass conversion technology products (13).

Bridgewater, 2012 (14) in his major studies, identified five characteristics of different Pyrolysis types as listed below.

Pyrolysis type technologies				
1. Bubbling fluidized bed	2. Ablative pyrolysis	3. Augers pyrolysis	4. Vacuum pyrolysis	5. Entrained flow pyrolysis

2.9.3 Pyrolysis leading to bio-oil production

Thermochemical decomposition of biomass at temperatures ranging from 400-650°C in the absence of O₂ yields volatile species, while the solid non-volatiles are collected as char. A fraction of the gas-phase volatile condense into a black viscous crude oil termed bio-oil(15); Balat, et al., 2009, pointed out various synonyms for biomass product oil such as pyrolysis oil, bio-crude oil, bio-fuel oil, wood liquid, wood oil, liquid smoke, wood distillates pyroligneous tar, and pyroligneous acid. These different pyrolysis liquids differ in their temperature, heating rate and residence time of production. The percentage yield of gas, char and liquid products is nearly predictable manner with process conditions but the resultant individual chemical species are hard to predict and quantify (11, 16).

2.9.3.1 Types of Pyrolysis

Pyrolysis can be categorized into two main groups, namely conventional/slow and flash/fast pyrolysis.

2.9.3.2 Conventional/slow pyrolysis

It has been reported in (141) that conventional/slow pyrolysis is known for its very low maximum temperature, heating rates and huge solid and gas residence time. Also it is mentioned by (9) that it is the process which produces a small amount of oil and gas product

concentrations as by-products and a higher percentage yield of char. [8] also reports that, pyrolysis at a heating rate ranging from 20⁰C/min to 100⁰C/min depending upon system and temperature of about 600⁰C will eventually result in an equal proportion of char, oil and gases. Sadaka, et al., 2008 in their analysis of slow pyrolysis found that the residence time for gas may be more than 5 seconds, while that of biomass could range from minutes to days. In slow pyrolysis, the biomass devolatilizes slowly, while making the char and tars the major products. When the primary reaction occurs – repolymerisation reaction also occurs at the same time. Williams, 2005., (9) reported that with both slow heating rate and slow product removal from the hot reactor, secondary reactions may occur leading to the formation of more complex products.

In-general, slow pyrolysis has been known to be a promising reaction leading to desirable product under the following operating conditions; heating rate of 0.1-1⁰C/s a range anywhere from hours to minutes of residence time and temperature range of 400-600⁰C. The previous pyrolysis operating conditions have been used for centuries to produce methanol and also yield approximately equal amounts of char, gas and liquid (11, 16, 136).

2.9.3.3 Fast pyrolysis

This is relatively a new promising technology with the following advantage; a high yield of liquid product, achieved through rapid heating rate of about 10-1000⁰C/s, very short residence time of < 2 seconds; and 400-650⁰C operating temperature and rapid quenching of the vapours (11, 140).

Bio-oil varies according to the nature of the process, process conditions as well as the feedback involved. Recently studies have put more emphasis on fast pyrolysis oil, which generally involves a series of complex reactions to produce different chemical components such as hydroxyaldehydes, hydroxylketones, carboxylic acids, pyran/furan ring containing compounds, anhydrous sugar, phenolic compounds and oligometric fragment of lignocellulosic polymers. Some other examples are also listed in Figure 2-17. All these products stem from the original

biomass composition consisting of cellulose, hemicelluloses, lignin, extractives, lipids, proteins, simple sugars, starches, water, hydrocarbons, ash, organic carbon and other compounds (11).

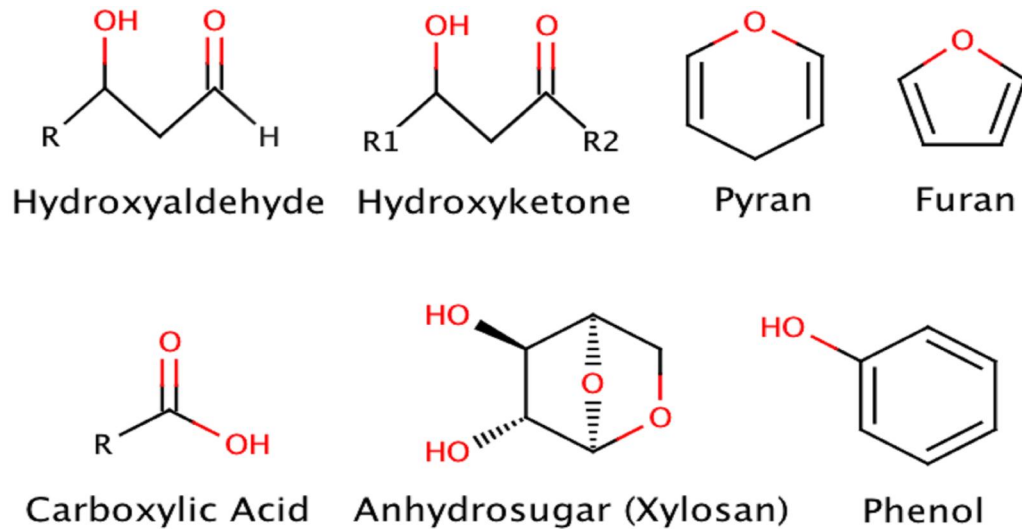


Figure 2- 17 Structural representation of some compounds of bio-oil

2.9.4 Pyrolysis process reactions

During pyrolysis processes the mechanism of pyrolysis indicates that there is change in colour and reduction of weight in the biomass as well as loss of flexibility [36]. It has also been reported that at an operating temperature of 350°C, almost 80% weight loss is observed and the remaining mass is char product. Heating at 600°C conversely results in a decrease in char to about 9% of the initial biomass weight and increases the yield of pyrolysis oil. However, reactions under pyrolysis operating conditions are complex and not well understood because it involves various reaction temperatures as well as the complex biomass. Yet they are generally termed as simultaneous reactions comprising water elimination, or dehydration, depolymerization, repolymerization, fragmentation rearrangement and condensation as indicated in Figure 2-18, and these reactions result in a bio-oil containing over 300 different compounds (142).

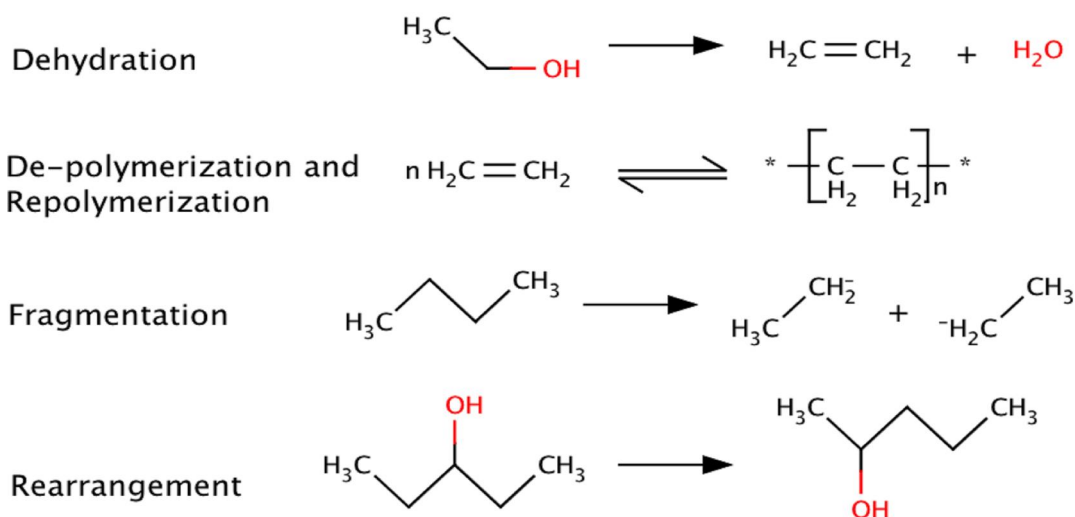


Figure 2- 18 Some pyrolysis reactions of bio-oil (13)

Based on the applied perspective, bio-oil can be burned directly to generate energy, used for chemicals or as a substitute for fuel oil for various use in boilers and furnaces (8). (143) Bio-oil is not miscible with fossil fuels but miscible with water to 35-40%. The liquid gradually changes with the formation as it is a polyphenone polymers, resulting in a variable viscosity, ranging from 10 to 10,000cP. It changes faster when exposed to light, oxygen and temperatures greater than 80⁰C, leading to storage issues. It has a low pH due to the presence of organic acids which further increases corrosion and storage issues. Solid suspension ranging from 0.3-3% within the oil has the potential to affect the combustion characteristics negatively by plugging nozzles. The presence of oligomeric fragments can lead to solid, tar-like organic carbon deposit in pipes and reactors (143).

Bio-oil is compared with petroleum in the Table 2-1 below and it is clear that some upgrading is necessary to improve certain properties.

Bio-oil can be modified chemically or upgraded by eliminating or modifying the unwanted compounds and also those compounds with high percentage of oxygen. The upgrading strategy mostly involves improving the H/C ratios and decreasing the O/C ratio in order to obtain higher quality liquid products. These ratio considerations are important especially when bio-oil is to be used as a substitute for the demanding petrochemical applications such as transport fuels which need to be clean, homogenous fuels (144).

Table 2- 1 Bio-oil compared with crude oil characteristics (13).

Composition	Bio-oil	Crude Oil
Water (wt %)	15–30	0.1
pH	2.8–3.8	-
density (kg/L)	1.05–1.25	0.86
viscosity 50 °C (cP)	40–100	180
HHV (MJ/kg)	16–19	44
C (wt %)	55–65	83–86
O (wt %)	28–40	<1
H (wt %)	5–7	11–14
S (wt %)	<0.05	<4
N (wt %)	<0.4	<1
Ash (wt %)	<0.2	0.1
H/C	0.9–1.5	1.5–2.0
O/C	0.3–0.5	≈0

2.9.5 Pyrolysis oil upgrading reactions

Catalyst addition to pyrolysis systems speeds up the reactions that include cracking, decarbonylation, decarboxylation, hydrocracking, hydrodeoxygenation, hydrodenitration, and hydrogenation as shown in the Figure 2-19.

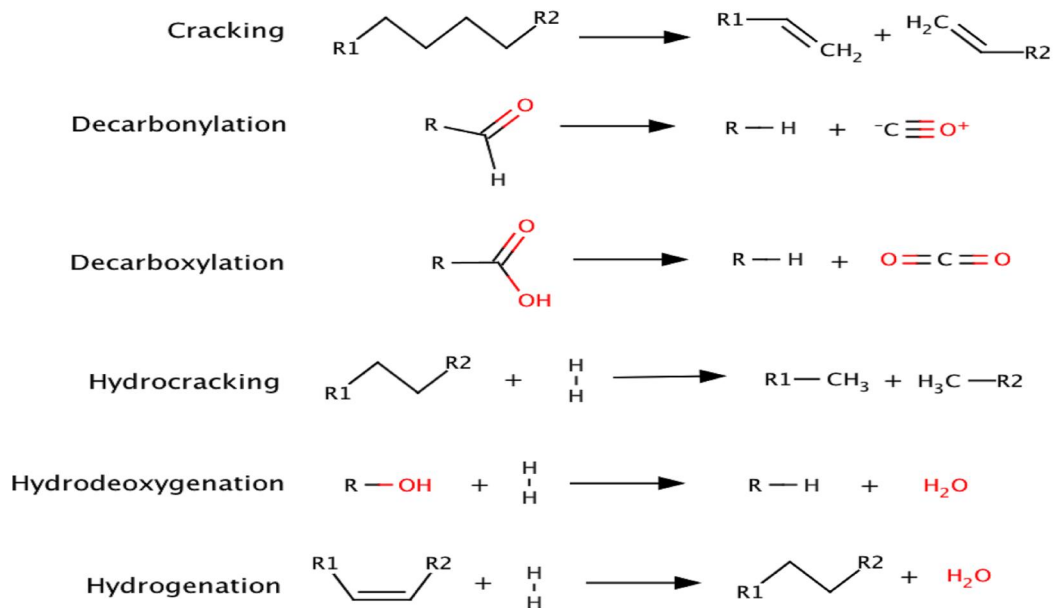


Figure 2- 19 Pyrolysis upgrading reactions of bio-oil (145)

The above reactions show catalytically upgraded properties with the view to enhance the properties of bio- oil through elimination of the oxygenated compounds H_2O and CO_2 . This also

reduces the molecular weight and alters the chemical structures to resemble those of petrochemical products. Interestingly, the chemical framework of biomass composition has naturally occurring ions that can have a catalytic effect under pyrolysis reaction conditions, (146) for instance reducing the bio-oil yield in favour of char and gaseous species (13). The effect was realised with the most abundant inorganic components present in bio-oil such as Na, K, Mg, and Ca ions which have an effect on the pyrolysis products (147). Demineralization was therefore considered in order to increase the yield of anhydrous sugar and other liquid products (147, 148).

2.9.6 Co-pyrolysis and atmospheric distillation of bio-oil

Conversion of carbonaceous materials such as coal and biomass thermochemically is a complex process which involves a lot of homogenous and heterogeneous reactions. Conversion begins with pyrolysis or devolatilization reactions, thermal decomposition processes leading to the release of various gases and tar from the feedstock and a residue containing a high percentage of carbon, char.

Pyrolysis of biomass releases gases more rapidly than coal. This is due to relatively lower bond energy of the biomass components which is either (R-O-R) and C - C bonds associated with lignocellulosic biomass compared with the coal having aromatic composition of C = C bonds in the molecular structure (149).

Thermogravimetric analysis (TGA) has produced valuable co-pyrolysis findings (150-156) even though the high heating rate approach is more representative of actual conditions in most of the types of gasifiers.

Xue-Song, et al, 2012., (155) in their studies of co-pyrolysis of biomass/coal found that rapid pyrolysis of biomass/coal product produces hydrogen which stabilizes large radical structures produced during the early stage of coal pyrolysis, resulting in release of the structures as tar due to stabilization, rather than cross linking with one another to produce secondary char and gases. For this to be achieved, coal and biomass particles have to undergo rapid heating during co-

pyrolysis. Some studies have shown that additional gas is the primary product of co-pyrolysis. (155) also reported studies of chemicals from biomass- derived oil applied to fast pyrolysis and atmospheric distillation in which the oil was heated gently to 513K under vigorous magnetic stirring. It was found that, volatiles moved upwards while bio-oil continued to condense with the elevation of temperature, with the residue at the bottom becoming increasingly viscous and it was termed atmospheric distillation residue (ADR). The oil produced by fast pyrolysis mixed with certain proportions of ADR have been studied in a downdraft fixed-bed, fast pyrolyzer under nitrogen atmosphere at 723K. The process strategy is shown in the Figure 2-20 and example products in Figure 2-21 (155).



Figure 2- 20 Schematic of the direct atmospheric distillation coupled with co-pyrolysis process to produce chemical feedstock [155]

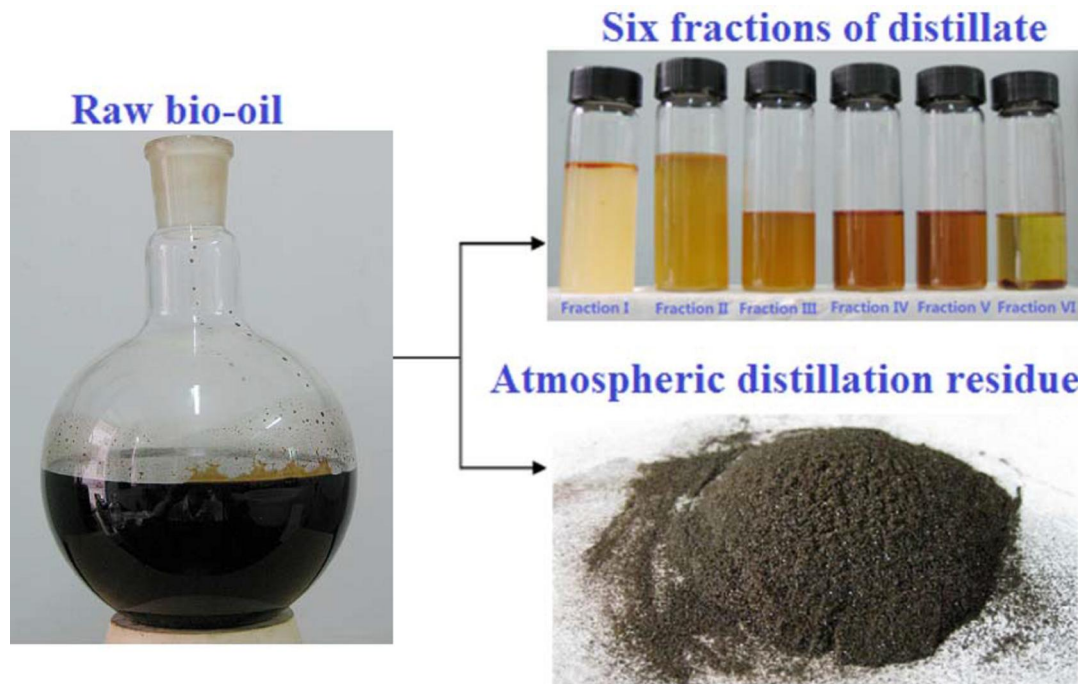


Figure 2- 21 Photographs of raw bio-oil, different fractions of distillate and the atmospheric distillation residue [155]

2.10 Factors affecting the pyrolysis of biomass

Various operating conditions have an impact on the mechanism of pyrolysis reactions, such as ash, temperature, heating rate, feedstock composition, side reactions, reaction atmosphere, volatiles and solid residence time (141). These factors have a great effect on the kinetics and sequence of the reactions and product yield. However, depending on the product yield, these conditions may be controlled along with side reactions.

2.10.1 Effect of sample composition and size

Composition and particle size of a sample plays an important role in pyrolysis due its effect on secondary reactions occurring within the particle, i.e. mass and heat transfer. In general, pyrolysing small particle sizes leads to a decrease in char, tar and water products while increasing the gas yield due to the increase in heating rate (157).

However, studies by Sadaka, 2008., (141) point out that, reduction of the particle size leads to an increase in ash content which in turn increases the char yield. Heterogeneous biomass samples are the genesis of the major problems to its chemical use since it is difficult to predict the yields of individual products, and also char yields and other pyrolysis products.

2.10.2 Effect of heating rate and temperature

The relationship between bio-oil yield, temperature and heating rate has been widely investigated [54]. The temperature of the reaction and heating rate are important parameters which play a very important role in both slow/conventional and fast pyrolysis. These parameters are interdependent, meaning that higher heating rate leads to higher temperatures even though heating rate is controlled by the nature of the sample composition and particle size. Fundamentally, the heating rate affects the attainment of the desired particle temperature (158). It has also been found that the temperature is a key to bio-oil stability, thermal decomposition rate and reaction products. Higher temperatures, $> 600^{\circ}\text{C}$, associated with vacuum pyrolysis enhance small gaseous molecule production, while a temperature $< 400^{\circ}\text{C}$ leads to higher coking propensity, a viscous liquid product, a higher pyrolysis rate, and various secondary reactions and dehydrogenation. Similarly, reported by (158) an increase in temperature influences the increase in production of hydrocarbons (CH_4 and C_2H_4) which may be from the decomposition of other products.

2.10.3 Effect of volatile and solid residence time

The volatile residence time is the amount of time it takes to generate a volatile compound within the reactor until the time it leaves the reaction hot zone. The solid residence time is the time the solid sample is in the hot reaction zone. In (159) this has also been investigated showing that both features especially volatile residence time permit secondary reactions (157). High volatile residence time result in further reduce and cracking, hence resulting in an increase in the amount

of gaseous products (160), while the contrary reduces secondary reactions leading to an increase in liquid and char products.

2.11 Pyrolysis reactors

Reactors are indispensable tools in both slow and fast pyrolysis; this drives researchers towards developing more economic and productive reactors. Depending on the pyrolysis operating conditions, there are different types of pyrolysis reactors: bubbling fluidized-bed reactors, transported and circulating fluidized-bed reactors, ablative (vortex and rotating blade) reactors and pyroprobe, rotating cone reactors, vacuum reactors, auger reactors, fixed-bed reactors, entrained flow reactors (92). The above reactors were also classified based on commercialization into four main technologies which generate acceptable yield of liquid products as follows; (a) shallow fluidized bed reactor, (b) vacuum pyrolysis reactors, (c) ablative reactors both cyclonic and plate type, and (d) circulating fluidized bed reactor (both dilute and dense type). Apart from the above four classifications, it has been also reported that, (e) Auger reactors are also considered as the fifth reactor (16). A discussion of some of these reactors follows:

2.11.1 Bubbling fluidized bed reactors

Bubbling fluidized beds are also known as fluidized bed as opposed to circulating fluidized bed. This type of technology is well understood, as it is easy to construct and simple to operate, they are constructed in such a way that they provide a stable temperature control, with very effective heat transfer to the biomass particles due high solid density in the bed (16). It also produces an acceptable quality bio-oil with high liquid yield, and no accumulation of char in the bed, since it is quickly eluted. Shallow fluidized bed reactors can be scaled up, even though Scott, et al 1999., (161) pointed out that, the low bed height –to- diameter ratio causes transverse temperature and concentration gradients to develop in large reactors. Hence there is need for

new special design requirements to eliminate the processing problems which occur during scale up.

Residence time of solid and vapours is controlled by the fluidizing gas flow rate. It is also reported that char has higher residence time than vapours and it acts as an effective vapour cracking catalyst at fast pyrolysis reaction temperatures. Char separation is done by ejection followed by separation in one or more cyclone separators. The diagram of the reactor is shown in Figure 2-22.

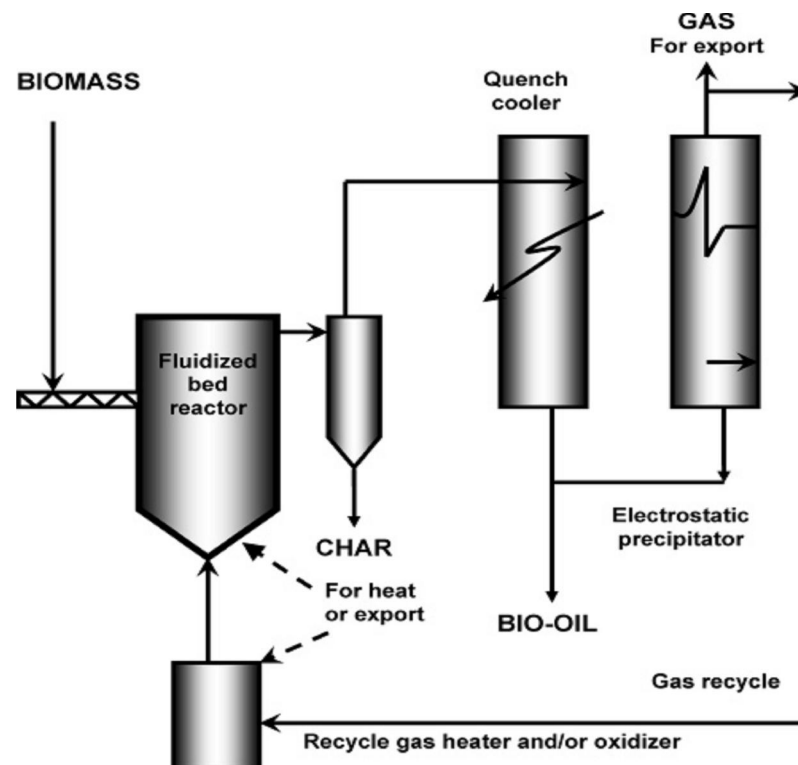


Figure 2- 22 Bubbling fluidized bed reactor (162)

2.11.2 Auger reactors

Recently, an auger feed pyrolysis reactor was constructed by the Mississippi State University and is typically of auger reactors. It has the following designed features;

- The reactor is compact and does not need any carrier gas
- It operates at low process temperature (400 °C)
- It also operates as a continuous process

- It makes use of the auger-feed to move biomass feedstock (wood, organic residue, and/or agricultural residue, plastic waste) via an oxygen-free cylindrical heated tube, while a passage inside the tube raises the feedstock to achieve the desired pyrolysis temperature (which ranges from 400 – 800 °C). This causes the feedstock to volatilize and gasify leading to the formation of char as a product and the vapours are condensed to turn into bio-oil. Non-condensable products are collected as biogas. Modification of vapour residence time can be done by increasing the length of the heated zone through which vapours pass before entering the condenser train (16).

2.11.3 Ablative pyrolysis reactors

Bridgwater, et al, 1999 (92) describes studies of fast pyrolysis reactions utilizing ablative reactors which involve the pressing of wood against hot surfaces resulting in an oil film which later evaporates. The reactor uses larger wood particle and the process heat supply rate to the reactor is limited resulting in an intensive and compact pyrolysis reactor which does not need any carrier gas. The reactor is shown in the Figure 2-23 below;

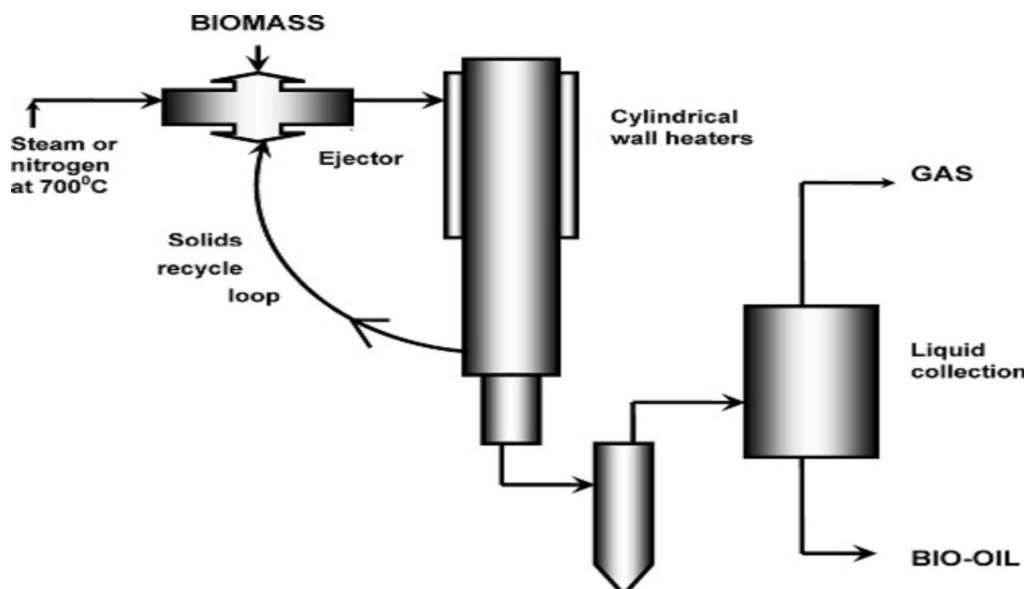


Figure 2- 23 Ablative reactor (146, 162, 163)

2.11.4 Vacuum pyrolysis reactor

The above named reactor actually is not a real fast pyrolysis reactor, due to the fact that, the heat and mass-transfer rate both to and from the solid biomass, are very much slower than the ones observed in other reactors (163). Hence, the pyrolysis product discharges from the solid phase over a long time frame. Furthermore, larger samples are needed and the vacuum unit will be very large which in turn requires a greater cost, but it yields up to 60-65% liquid yields (92). However, only one parameter is comparable to those of fast pyrolysis which is the vapour residence time. Vacuum pyrolysis involves the thermal decomposition of biomass under highly reduced pressures. Complex organic molecules decompose into primary fragments when heated in the reactor, followed by vaporization of the fragmented product and subsequent rapid removal from the reactor by the vacuum, to be recovered in the form of pyrolytic oil through condensation. Without the reduced pressure these fragments undergo further cleavage to lower boiling point –fragment while cooling. Thus their rapid volatilization under vacuum reduces the extent of secondary decomposition reactions. The chemical structure of the pyrolysed product most likely resembles the original structure of the complex organic biomolecules which constitute the original biomass.

In general, it has also been reported that, vacuum pyrolysis of biomass is conducted at a temperature of 450⁰C and a total pressure of 15 kPa. One of the most important features of the vacuum pyrolysis reactor is that the short residence time of the volatile molecules is achieved easily. Hence, the volatile residence times are not coupled to that of the biomass particles which in turn decompose in the reactor. This technique suffers from poor-heat and mass transfer which eventually results in the need for large scale equipment (16, 163). The set-up is shown in Figure 2-24.

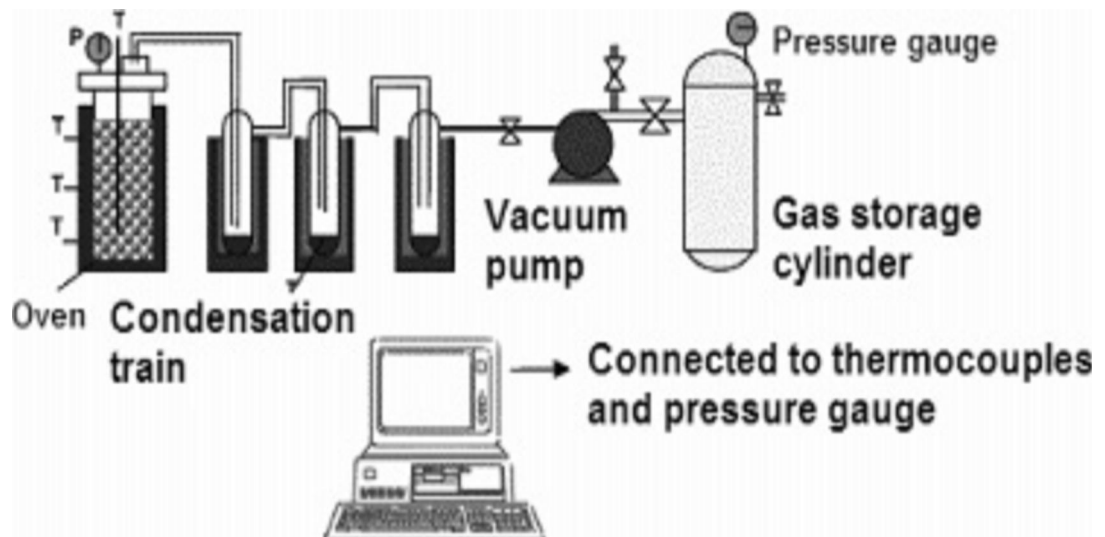


Figure 2- 24 Vacuum Pyrolysis reactor (16)

2.11.5 Entrained flow reactors

The entrained flow pyrolysis reactor is a widely used reactor but is still under development and extensively studied for the processing of biomass (158, 160). Several research papers have shown that, this reactor has an extremely high heating rate, high operation temperature with short sample and gas residence times ranging from milliseconds to a few seconds (160, 164). The reactor has a feed mechanism which sends the feedstock to the reactor hot zone, which comprises a tubular length usually heated through electrical heaters. The tube of the reactor is connected to different operation compartments like the char receiver, the gas filter, condenser and gas collection system. The carrier gas is usually transported to the reactor via the feed mechanism of the reactor, while the length of the heated section is used to control the sample's residence times (164, 165).

Goyal, et al., 2008 (166) in findings of the entrained reactor pointed out that heat is supplied to the sample by the carrier gas at the same time moving it through the heated zone. Hence a small particle size of approximately 2mm is of great importance for rapid heating upgrading.

However, this reactor has its own problem, like the heat and mass transfer between hot carrier gas and sample particles within the short residence time. In addition, preparation of the sample can be cost intensive (91). The entrained flow reactor is shown in Figure 2-25.

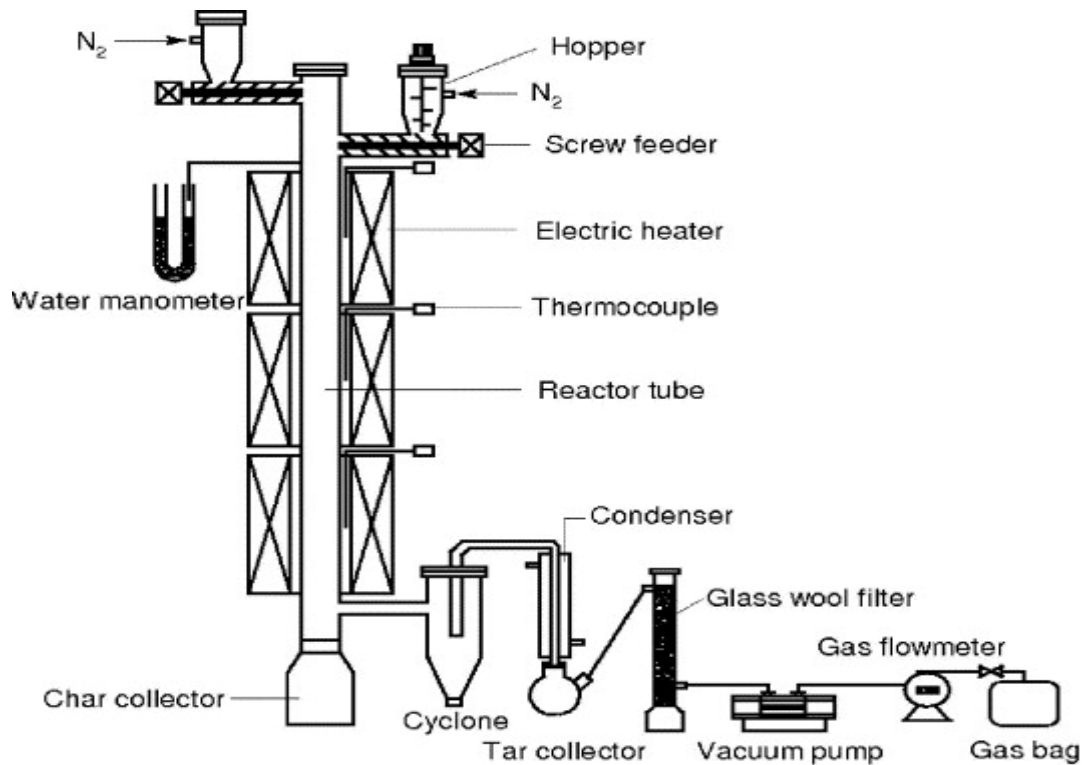


Figure 2- 25 Entrained flow reactor (165).

2.12. Steps in biomass combustion

Combustion may be defined as a chemical reaction that occurs between a fuel and oxidizing agent that produces energy, usually in the form of heat and light. Similarly, it is a rapid chemical reaction the oxidation – reduction type with large energy release. These reactions mainly comprise of the carbon and hydrogen elements of any type of fuel and the oxygen / air as the oxidizer. The main experimental objective of combustion is to alter the chemical energy of the reactant (heating value) into high temperature products which can be cooled by direct conduction to the wall of the combustion chamber and / or via convection using the reaction products as the heat carrier, or directly converted to mechanical work in a thermodynamic process (167).

2.12.1 Combustion steps

Biomass combustion involves a complex process that consists of a series of heterogeneous and homogenous reactions. The major process steps are drying, devolatilization, gasification, char combustion and gas phase oxidation. The time taken for each reaction step depends on the fuel size and properties, on temperature and on combustion operation conditions (167, 168).

However, according to Jones, et al, 2007., (169) the extremely complex process depends on these key factors: composition of lignocellulosic materials, heating rate, and inorganic matter content.

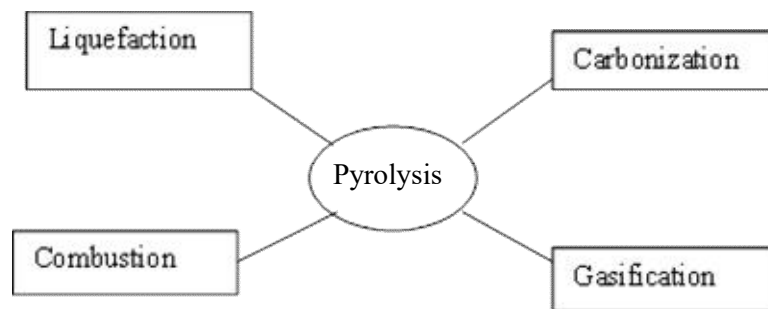


Figure 2- 26 Steps in biomass combustion (169).

Sjaak and Jaap, 2008 (167) suggested that the process of combustion occurs in general subdivisions, namely drying, pyrolysis, gasification and combustion. The general form of the process of combustion maybe continuous or batch process with the addition of air via forced or natural convection. For virtually all medium to large scale units combustion always uses continuous combustion with forced drought air supply (167).

Jones, et al 2007, [169], pointed out that, the relative significance of the above process steps vary depending on the following (1) the combustion process technology adopted (2) properties of the fuel (3) combustion process conditions. Drying pyrolysis/gasification and gas and char combustion stages may overlap. The following features are applicable for the large scale biomass combustion which requires a continuous fuel feed. For a moving grate the different processes occur usually in various sections of the grate. However, distinct separation occurs in

batch combustion processes between the volatile and char combustion phases. A summary of the detailed combustion steps involved are described below:

2.12.1.1 Drying

Evaporation of the moisture content occurs at lower temperatures ($<100\text{ }^{\circ}\text{C}$). Since the combustion process releases energy, some of it is used for vaporization of moisture thereby lowering the temperature of the combustion chamber, which slows down the combustion process. For instance, in wood fired boilers, it has been found that the combustion process will not continue to occur if the wood moisture content is above 60% on a wet basis (w.b). Therefore, wood drying requires much more energy for evaporating the moisture in it and following that, the heating of the water vapour. The temperature maybe lowered to below the required minimum temperature needed to maintain combustion. Hence, moisture content is a very significant fuel variable (167).

2.12.1.2 Pyrolysis

As shown in Figure 2-26 pyrolysis is central to the different thermal conversion processes. Thermal degradation (volatile loss) without any oxidizing agent results in the formation of tar and carbonaceous char, and lower molecular weight gases. Additionally, CO and CO₂ may be formed in reasonable quantities, mostly from oxygen rich fuels, like biomass. Usually the following variables affect the quantity and properties of the product formed: pressure, temperature, heating rate, fuel type and reacting time. Jones, et al 2007, [169], studied single particle combustion of four different willow samples. When the particle are exposed to the flame the rise in temperature leads to sample drying and devolatilization occurring at 473K and the rate of devolatilization increases with increasing temperature. The volatiles escape and the devolatilization rate decreases.

Pyrolysis products have a variety of applications, for instance they can be upgraded to activated carbon, to be used in the metallurgical industry also as a domestic cooking fuel. While the

pyrolysis gas can be used for electricity generation and also for production of methanol via synthesis, the liquid crude oil or bio-oil can be upgraded to a multi grade hydrocarbon liquid fuel for combustion engines with low emissions, for transport, or directly used in boilers or furnaces for electricity generation (14, 149, 167, 170).

2.13 Gasification

Gasification is the partial combustion of biomass to give a low CV gas and bio-chars. It's the thermal conversion in the presence of an oxidizing agent such as air, or oxygen, or steam and O_2 . It gives good char and tar yield and gasification deals with improving the gas yield, under a temperature of about 1073-1373K. The composition of the gas is mainly CO, CO_2 , H_2O , H_2 , CH_4 , and other small HCs. In gasification, steam and CO_2 can replace oxygen or air. Hence the use of air or steam and others depends on application. For example, air gasification produces a low calorific value gas of 4-7 mega joules per normal cubic metre (MJ/m^3 dry) and about 10-18 MJ/m^3 with oxygen and with synthesis, upgrading of the fuel gas can be done to produce methanol. It can be burned externally in a boiler to obtain hot water/ steam, in a gas turbine for production of electricity and for transport and combustion engines, after the gas has to be purified by removing the tar, char particles, ash, and alkali, compounds as contaminants. Likewise the hot flue gas is also applicable in a steam turbine or in an Integrated gasification combined cycle unit (IGCC) (167).

2.14 Liquefaction

Liquefaction can be defined as thermochemical conversion to the liquid phase and is accomplished at low temperature usually 523-623K and at high pressure of about 100-200 bar, also together with a high hydrogen partial pressures and a catalyst to influence rate of reaction or to upgrade the selectivity of the process. In contrast with pyrolysis, these have a higher liquid yield and also the liquid has higher calorific value and a very low oxygen content (167, 169).

Chapter 3 Experimental methods

3.0 Introduction

Soot investigation techniques have been in existence for many years. Some of these measurements can be in-situ or online; ex-situ, invasive or non-invasive and measured at, domestic or industrial scale. Usually domestic measurements include small scale, relevant for this research where wick burners and wood stoves are considered. Industrial measurements include heavy duty engine exhausts, which frequently are ex-situ measurements. However, the aim for this research is to further understand the processes involved in soot formation, along with the reaction mechanisms involved. Investigations in a non-invasive way which have been used in this research are on-line sampling in the flame by means of both optical and non-optical diagnostics and are described in this chapter. Ex-situ methods were also used and these are also described in this chapter.

3.1 Fuels

A number of fuels were utilised in this research: Model compounds for biomass pyrolysis products included anisole, furfural, and eugenol, models for productions from decomposition of lignocellulose. Models compounds for petroleum fractions includes heptane and decane. Also studied were a heavy fuel oil and bio-oil from a demonstration fast pyrolysis unit. Properties of the model compounds are given in the Table 3-1.

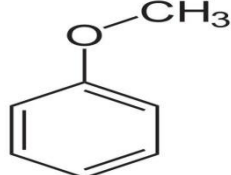
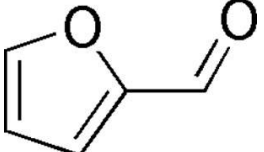
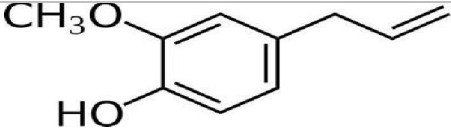
3.1.1 Asphaltene extraction

A sample of bio-oil was obtained commercially and produced by a fast pyrolysis method from pine wood.

Asphaltene was prepared with *n*-heptane as an extracting solvent. The asphaltene separation process involved three steps. Firstly, bio-oil, i.e., fast pyrolysis bio-oil, was weighed and poured

into a round-bottom flask. The solvent (*n*-heptane) was added according to the proportion of 30 mL *n*-heptane per 1 g bio-oil and the mixture was heated to reflux for 65 minutes, cooled down, and placed in the dark for 150 min calculated from the time of its removal from reflux. Secondly, the precipitate was decanted without agitation quantitatively into the filter paper folded as shown in figure 6-1 so as to prevent loss of asphaltene. The precipitate was wrapped with the double-layer filter paper and placed into a reflux extractor. Thereafter, the extraction was continued with *n*-heptane using a different flask, and at rate of 2 drops/s to 4 drops/s dropping from the condenser end until the liquid drops were colourless and subsequently no residue on evaporation. Finally, the flask was replaced by the initial flask containing toluene, and reflux was continued until the filter paper turned colourless and the contents were removed and weighed into dishes. Asphaltene was obtained after removal of the solvent via evaporation in a dark environment to prevent the asphaltene reacting with light energy ASTM D6560 (171).

Table 3- 1 Fuel samples used in this study: structures and their properties

Samples	Compound structure	Boiling point °C	Molecular formula	Molecular weight	Viscosity cP 25 °C	IUPAC Name	Density 20 °C kg/m ³
Heptane		98.4	C ₇ H ₁₆	100.21 g/mol	0.376	n-heptane	684
Decane		174.1	C ₁₀ H ₂₂	142.29 g/mol	0.859	n-decane	730
Anisole		153.8	C ₆ H ₅ OCH ₃	108.14 g/mol	1.05	Methoxybenzene	995
Furfural		161.7	C ₅ H ₄ O ₂	96.09 g/mol	1.49	Furan-2-carbaldehyde	1160
Eugenol		254	C ₁₀ H ₁₂ O ₂	164.2 g/mol	0.839	4-Allyl-2-methoxyphenol	1060
50/50 eugenol furfural mixture	Not applicable		Not applicable	Not applicable		Not applicable	Not applicable

3.2 Soot sampling methods

Soot samples were obtained from diffusion flames for the model compounds given in Table 3-1 burning on a wick burner. The burner had the following wick dimensions; 2mm height and 7mm diameter. The samples were collected using a glass microscope slide of dimensions 76x26mm and thickness 1.0/1.2mm with ground edges, Figure 3-1. The slides were fixed using a clamp at a known height above the diffusion flame: namely 50mm, 100mm or 150mm. The soot deposition was typically carried out for 5min, 10min, 15min or 20min for each fuel. The slides were allowed to cool for a few minutes and then weighed. The generated soot was immediately scraped off using a spatula into an air tight sample bottle and labelled, Fig 3-2. Finally, the soot samples were then stored under inert argon prior to analysis to prevent secondary reactions.

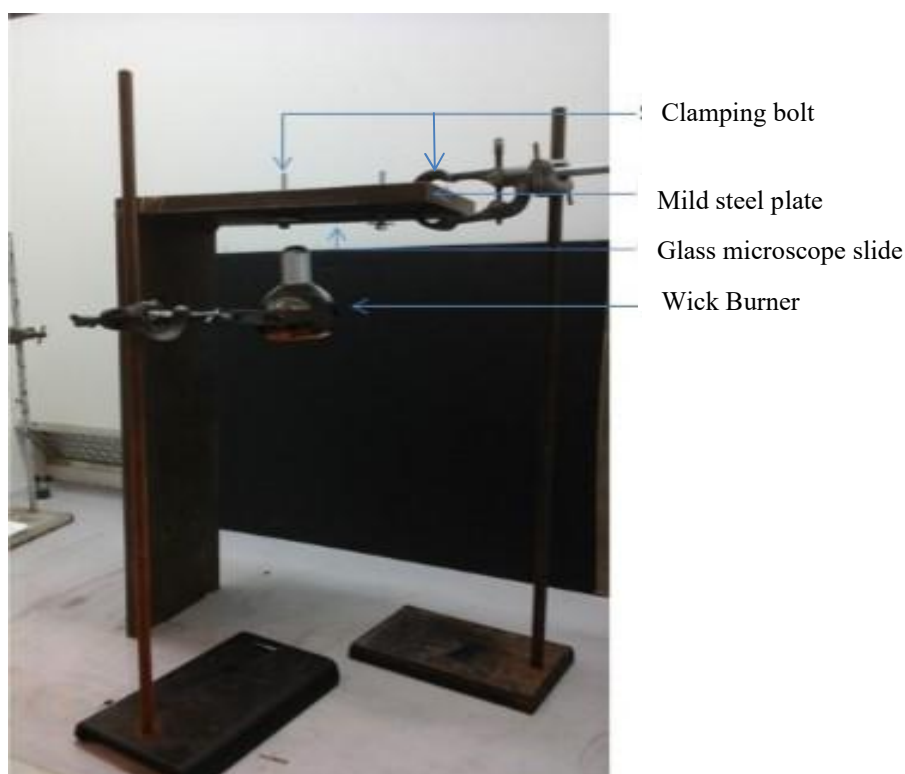


Figure 3- 1 Soot sampling set-up using glass microscope slides



Figure 3-2 Show the soot generated from cold glass slides for analysis

3.3 Smoke point

3.2.1 Experimental method

A standard smoke point lamp for liquid fuels as specified by [ASTM D1322-97] was employed. The standard testing method for smoke point of aviation kerosene and aviation turbine fuel [ASTM D1322] was used to explore results from smoke point height of the fuel samples. In this research the Seta smoke point apparatus was employed and it can be seen in Figure 3-3. The fuel was stored in the reservoir marked candle and burned from cotton wicks. ASTM D1322-97 provides the specification for the standard wick. The wicks were obtained together with the Seta smoke point apparatus from Stanhope-seta.co.uk. The wicks were also prepared in accordance with the ASTM D1322 method. The candle was assembled and adjusted up and down to expose more or less of wick through the screw mechanism at the bottom of the candle, thereby providing reasonable control of the flame height. The flame height was measured via a 50mm scale mounted on the surface of the lamp behind the flame. The top wick guide was level with the zero mark on the scale. The glass door fixed at the front of the apparatus was covered to prevent flickering of the flame and also multiple images formation. The chimney, and also an outer black painted steel frame surrounding the apparatus on three sides provided a repeatable experiment and improved flame stabilization.

3.3.2 Smoke point (SP) experimental procedure

SP measurements were made in accordance with ASTM D1322-97[160] for the fuel sample compounds and their mixtures given in the Table 3-1. 20ml of each sample was obtained and poured into a 25ml graduated cylinder. The newly-prepared cotton wick was dipped into the sample making the entire wick submerge. Then a wick trimmer assembly was used to pull the soaked wick to the top of the candle. A razor blade was then used to cut the excess to obtain a flat edge, leaving about 6mm protruding through the end of the candle. The tail end of the wick was dipped back into the sample so that it would not dry off, then the remaining sample fuel was poured into the candle reservoir. Once the candle reservoir and wick were assembled, then the top of the candle was constricted and placed on the apparatus. After igniting the candle, the door was immediately closed and the wick was lowered until the smoke stopped emanating from the flame. For the actual smoke point determination, the wick was raised just above the smoke point and then lowered back to the smoke point. The smoke point was obtained when the shape of the flame tip changed from elongated with concave upward edge, to a slightly blunted straight tip (without concave downward) edge as shown in the Figure 3-4 and Figure 3-5.

In some instances the elongated tip, was observed above the smoke point including the sooting wings on the sides where soot breakthrough was clearly visible. When it was exactly at the smoke point, the soot wings and flame merged together to form a smoothly curved edge with the entire flame. Generally, the smoke point of very heavily sooting compounds were short and very easy to identify due to the lower flow rate associated with the smoke point height, which resulted in a definite stable flame with a cone shaped edge. The flame height was measured by lining up the top of the flame which was reflected on either sides of the vertical scale line as depicted in the Figure 3-4. The value was then recorded to the nearest millimetre which marked the end of a smoke point test. The remaining sample fuel was put back into the main sample bottle for future use. The wick was removed, the metallic part of the candle and the trimmer was washed with n-heptane and all glassware were rinsed with dichloromethane (DCM). Finally the raised parts were blown dry with compressed air and a new wick was employed for the second

test until three sets of results were obtained and the average was calculated for all fuels under investigation. During some of these experiments it was noticed that, the results for smoke point changed over time especially for the mixtures. Readings for the mixture 50:50, furfural-eugenol (by volume) were taken every minute, during a particular test. The final reading or value of smoke point for a mixture is usually reached after three minutes. This length of time varied for different fuels, ranging from less than one minute for straight chain hydrocarbon compounds and up to three minutes for fuel mixtures. Moreover, the smoke point of some fuels increases to a final value and others decreases depending upon the nature, structural composition, and the bond type of the fuel under investigation.

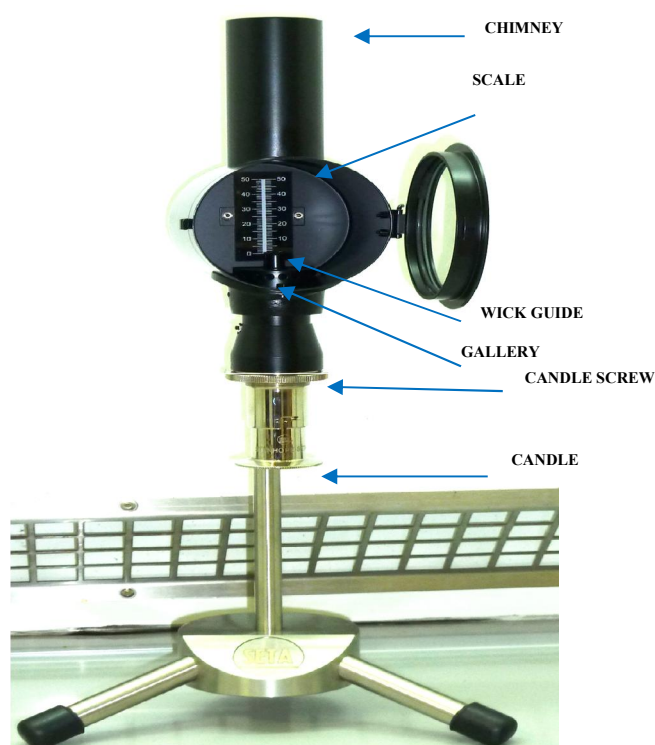


Figure 3- 3 Seta smoke point apparatus lamp

A change in smoke point for pure compounds can be derived from the time to reach the steady state. In the case of a mixture this may be attributed to the composition of the gaseous fuels just above the wick not being the same as the composition of the fuel at the middle, and also the level of the fuel saturation may be varying as well as the mixture of fuel during this transient period. This could be possible due to the difference in boiling points of the fuel mixture components, and that is why the smoke point of furfural-eugenol was above that of pure eugenol and does not reach that of furfural. Therefore as the composition of the gaseous fuel mix adjusts the smoke point changes drastically and only the values measured after the system reached steady state were recorded as actual smoke points, since it was found at least fuel burning for three to five minute was sufficient to reach the steady state. The value was then recorded to the nearest millimetre which marked the end of a smoke point test. The remaining sample fuel was put back into the main sample bottle for future use.

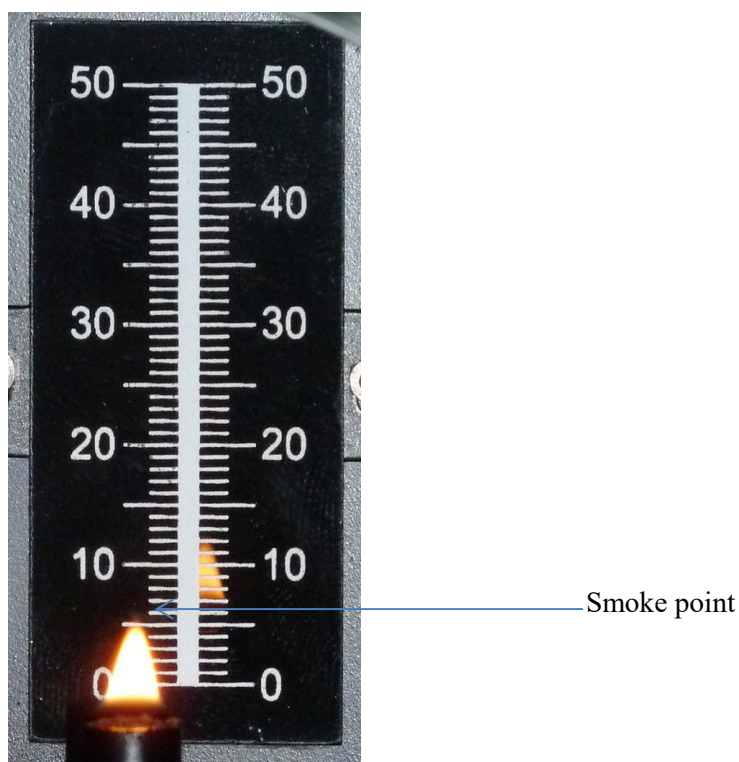


Figure 3- 4 Shows the smoke point for pure eugenol fuel.

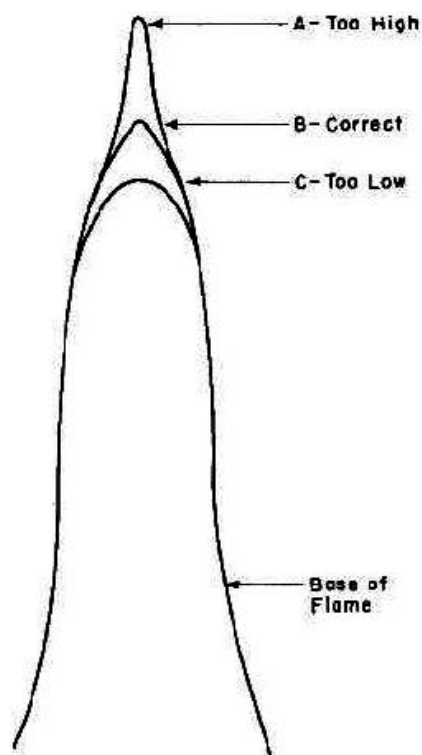


Figure 3- 5 Flame shapes showing the smoke point zone, A- above the SP; B- at the SP and C- below SP. [ASTM D1322]

3.4 Elemental analysis

Ultimate analysis was carried out on the samples under investigation for the elemental contents for C, H, N, S, and O using a CE Instruments Flash EA 1112 series elemental analyser. Calibration of the instrument using a BBOT standard (2,5-Bis (5-tertiary-butyl-benzoxazol-2yl) thiophene); 72.53 wt.%, 6.09 wt.%, 6.51 wt.%, 7.44 wt.%, and 7.43 wt%, for Carbon, Hydrogen, Nitrogen, Sulphur, and Oxygen respectively. The BBOT was followed by four standards (Atropine; N=4.84, C=70.56, H=8.01, S=0, 16.59 all in Wt.%, Methionine, Sulfonamide, and L-Cystine; N=11.61, C=29.95, H=5.1, S=26.68, and O=26.67 Wt.%). Between 2.5 to 3.5 mg of the samples and standards were weighed out into tin capsules in duplicate. Combustion of the tin capsule took place under excess oxygen in the reactor of the elemental analyser. The analyser automatically calculated the composition of the elements in the sample through the measurement of CO₂, NO_x, and SO₂ concentrations of the generated gas product (172). The elemental composition was employed to calculate the high heating value, HHV, using the Dulong formula eqn 3-1 (172) as follows:

$$\text{HHV (MJ/Kg)} = 0.3383 \times C + 1.443 \times (\text{H}-0/8) + 0.0942 \times S$$

Equation 3- 1

Where:

C = Carbon Wt. %, H = Hydrogen Wt. %, O = Oxygen Wt. %,

S = Sulphur Wt. % Note: All the mass fractions of the elements are in Weight % and on a dry basis.

3.5 Size exclusion chromatography (SEC)

Size exclusion chromatography of the asphaltene was performed on a Perkin-Elmer Series 200 HPLC instrument. The machine had the following specification: a Varian PGel column of 30 cm length and 7.5 mm diameter with a 3 μ m particle size. The mobile phase flow rate was 0.8ml/min tetrahydrofuran, THF. About 20 to 25 mg of the asphaltene sample was dissolved in the 1.5 ml of THF and this was eluted followed by detection at the refractive index detector. A comparison was made by dividing the chromatograms by the sample mass injected. The instrument calibration was achieved by using a polystyrene molecular weight standard.

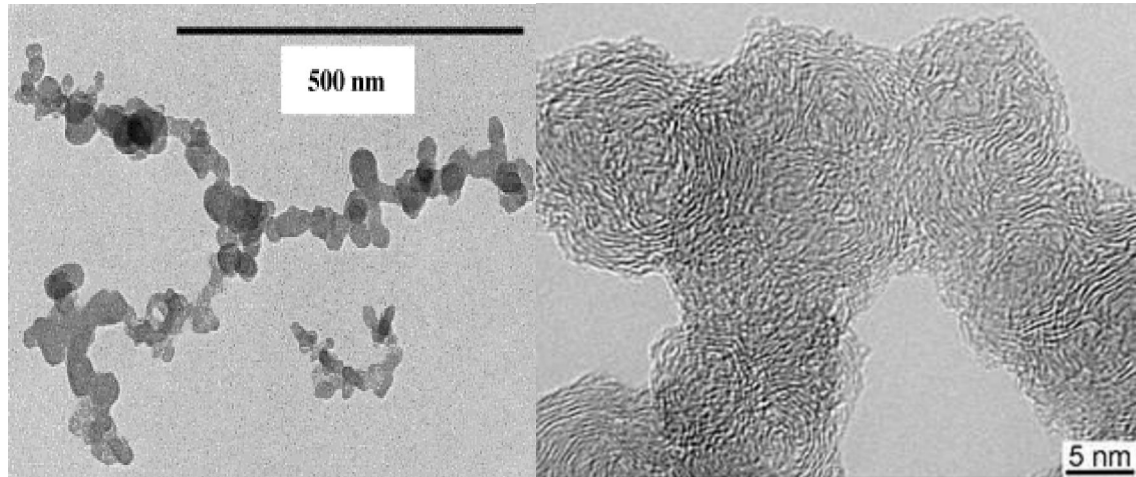
3.6 Transmission electron microscopy (TEM)

Soot particles via microscope analysis give an image of the aggregates and the initial primary particles. Hence size and structure of the primary particles, shape of the agglomerate, and numbers of particles per agglomerate and particle size distribution can be studied.

Transmission electron microscopy (TEM), for soot particles was found to have a chain structure composed of up to 4000 smaller spherical particles (spherules). These primary particles agglomerated in clusters and are found to contain between 10⁵ to 10⁶ carbon atoms Figure 3-6.

Soot particles are collected from the flame using thermophoresis sampling Figure 3-7, and analysed afterwards by means of transmission electron microscopy TEM (139). This technique is an ex-situ technique, even if soot is probed in the flame. This study was performed under different conditions and locations within the diffusion flames of a wick burner therefore cannot

be considered identical to the sampled soot described in 3.2 due secondary formations. Electron microscopy (EM) provides the detailed reading of a sample by applying a particle beam of electrons to illuminate the image and produce a magnified image of the sample particles. Conventional optical microscopes are limited by the wavelength of light, the de-Broglie wavelengths for an electron are 10^5 times smaller than light photons and this reveals the possible resolution of images at the atomic level by the electron microscope.



Agglomerates

Primary particles

Figure 3- 6 TEM images of agglomerates and primary particles adapted from (173, 174).

Agglomeration size can fluctuate from 10 to 1000 nm with a surface area of about $200 \text{ m}^2\text{g}^{-1}$. In contrast nanoparticles in the agglomerate are more or less spherical with typical diameters from 10 to 80 nm but most of them were between 15 to 30 nm (174).

In this work, the transmission electron microscopy employed achieves imaging with a resolution down to 1.1 \AA . In TEM, a high voltage electron beam emanating from the electron gun is transmitted through the sample partially transparent to the electron and scatters them partially. This transmitted electron beam that emerges from the sample carries the detailed properties of the sample like the structure, and this is subsequently magnified and focussed onto the imaging device and detected by the camera.

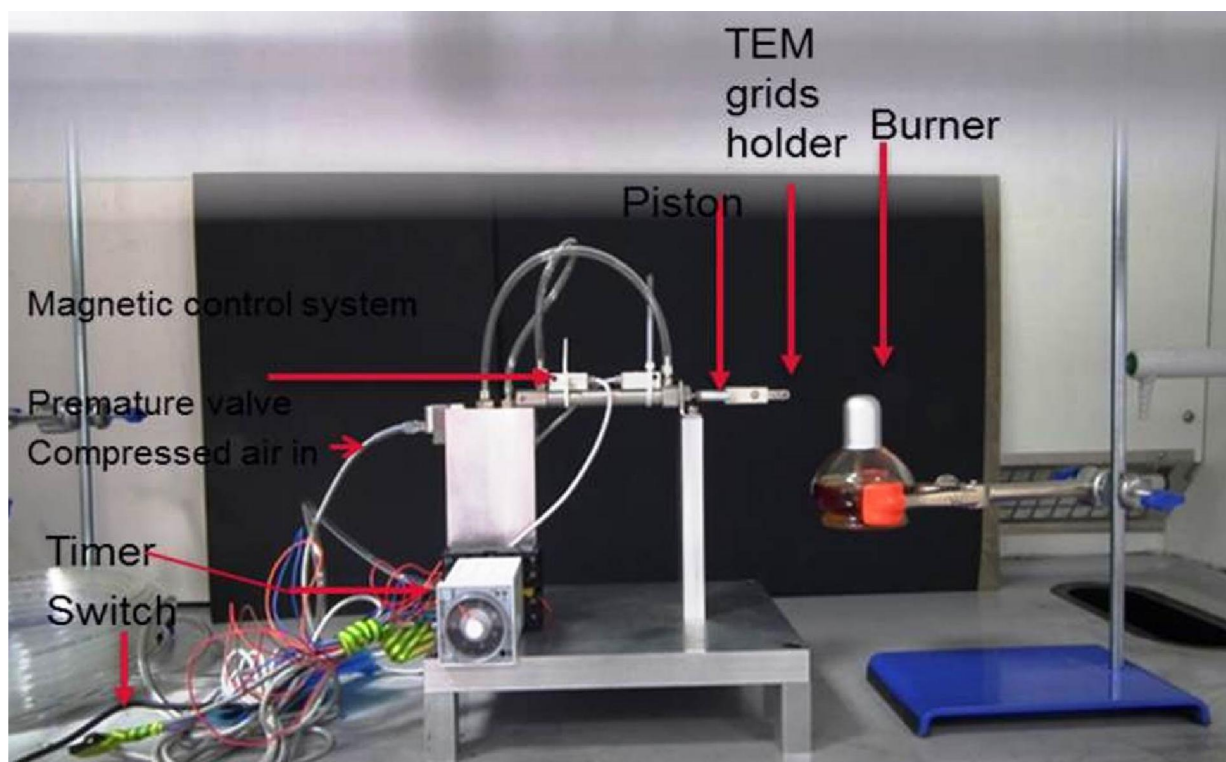


Figure 3- 7 Shows the thermophoretic soot sampling device for TEM analyses.

A high speed soot sampling system was developed in order to collect samples for Transmission Electron Microscopy (TEM), as shown in the above figure 3-7. The soot sampling system allows rapid and controlled collection of the soot at different flame heights. The set-up comprises of a wick burner as a source of flame and TEM grid holder. The grid holder is attached to a compressed air driven piston. A magnetic control system is used.

3.7 Scanning electron microscopy, SEM

Scanning electron microscopy, SEM, has been employed for soot morphological structure (175) In this present work, soot samples are generated on glass slides and on filter papers from a wick burner flame for all the investigated fuels soots were allowed to cool under an argon atmosphere for about 8 hours, then placed on an SEM holder and coated with a thin gold layer before analysis by scanning electron microscopy (SEM) on a Zeiss EVO MA 15 (Carl Zeiss Microscopy, Germany). This method was employed for morphological structure of the soot particles emanating from the diffusion flames (112).

3.8 Differential mobility spectrometry DMS and soot sampling

A differential mobility spectrometer DMS 500 series also known as a particle mobility spectrometer was developed and manufactured by Cambustion Limited. This instrument is a fast particle analyser which accounts for the measurement of particle size distributions in real time (176). The particles are sized according to their electrical mobility diameter to give the particle diameters. The analyser can determine particle diameters ranging from 5 to 1000 nm (177).

Soot aerosols were directly channelled from the burner top through the sample transfer line to the DMS 500 series unipolar corona charger by online sampling. The process description of the sample introduction system applied for these investigations has been provided [Cambustion 500series]. The measurement was performed using an ion mobility spectrometer and the operation of the instrument was conducted and equipped with an inlet membrane. The instrument operates with a bi-functional flow system. The operational parameters employed to obtain the spectral data of the particle size distribution were: Temperature of the inlet system: 800⁰C; carrier gas flow rate in front of inlet 417 mL/min; electric field: 245V/min; temperature of the drift tube: 50⁰C; pressure: atmospheric pressure. Compressed air at 2 bar was used as the carrier gas. A series of measurements with increasing soot concentrations were obtained for each sample and the data files were extrapolated using Matlab software.

3.8.1 DMS Instrumentation and its basic operations

The series 500 differential mobility spectrometer is one of the first commercially available real-time spectrometers as defined by Johnson et al 2004 (178). According to Mirme, et al, 1984 (179) at that time it was followed by the TSI EEPS, TSI fast mobility particle sizer (FMPS) and Cambustion MDS50. All the itemized instruments undergo the same basic working principles as developed by Tartu University, Estonia from the 1980's onwards in their electrical aerosol spectrometer (EAS) (180). A corona diffusion charger is present in all of the instruments which is mounted on a classification column. The column consists of a central rod held at high voltage

and a series of collection rings connected to the sensitive electrometers along the column and co-axial to the rod as shown in Figure 3-8 below. The classification column allows the passage of charged particles which are carried towards the bottom by the flow of a sheath of air. The electric field causes the particles to deflect from the central rod on to the collection rings, the particles with higher charge i.e. aerodynamic drag ratio, is collected at the top of the column. These charged particles produce signals on the electrometers which are subsequently processed resulting in a real- time size versus concentration spectrum.

The machine operates under a pressure of 250 (mb) which enable an increase of the possible size range between 5nm to 1 μ m (180).

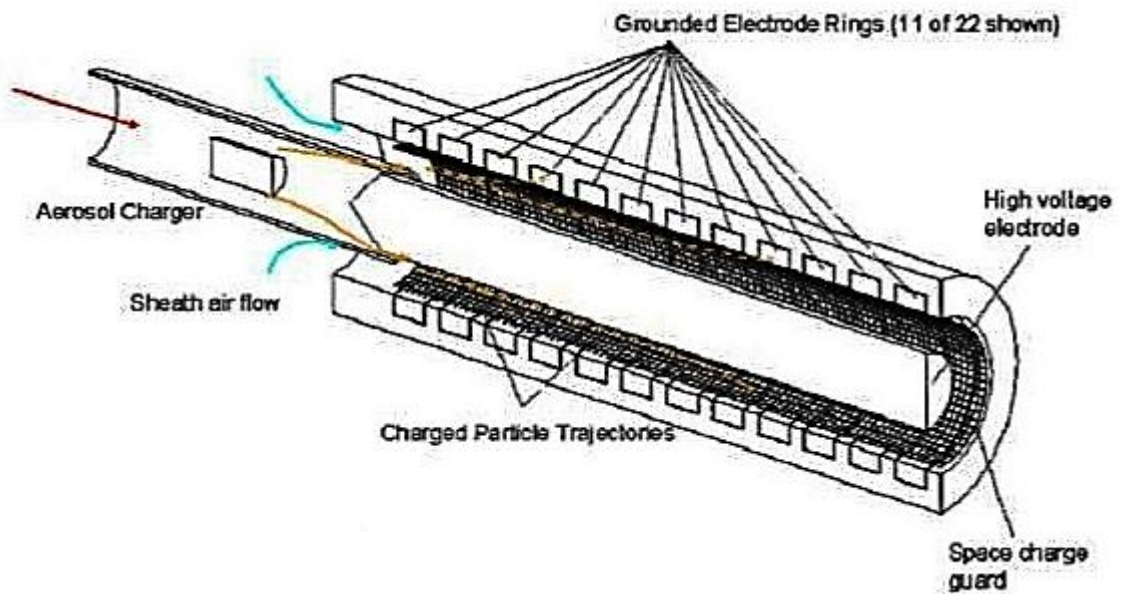


Figure 3- 8 Principle of operation for the DMS 500 Series

3.8.1.1 System dilution

The system is designed for engine applications and includes dilution. In order to improve the time response and also reduce the accumulation or agglomeration of the particles, as well as ensuring the sensitivity of the instrument system, dilution is required (primary dilution). This also ensures the combustors exhaust pressure instability is minimized (secondary dilution).

These instruments comprise a 2-stage-built-in dilution system and a heated line for absolute exhaust sampling and these are shown in Figure 3-9 below.

Firstly, it consists of up to 4:1 dilution by use of meter also shown in Figure 3-10. HEPA filtered pre-warmed air is needed near the sampling point in order to prevent the condensation of water vapour in the instrument. Then the diluted aerosol is dropped to 250 mbar via a sophisticated orifice which provides a concentration reduction equivalent to the primary dilution of the 16:1 orifice, which plays an important role during sampling in conjunction with the ejector diluter. The aerosol then passes through 5m of heated silicone tubing (55°C) in this work. This line length decreased the time response to about 300ms.

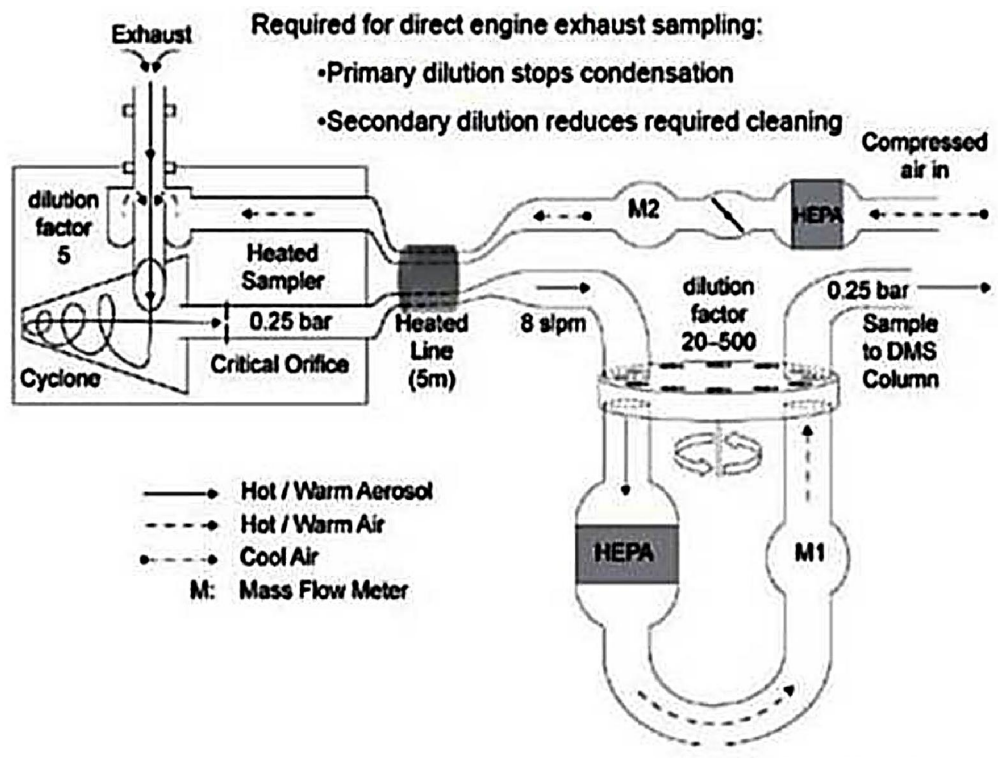


Figure 3- 9 Dilution system during sampling

The sample is further diluted by an integral mechanical rotating disc diluter in the instrument already designed for the DMS series. The 8 slpm of flow passes direct through one of the several holes in a disc, i.e. HEPA filtered and then passes on to a hole at 180°C. The disc now rotates and a small batch of aerosol is carried from the dirty stream in to the clean stream. The spectrum is corrected in real-time for primary dilution depending upon the flow of clean

dilution air and also the dominant air flow through the secondary diluter after HEPA filtration. At the same time, correction for the secondary diluter is made via the feed- back motor speed. Data interpretation is undertaken on the desktop computer controlling the instrument. The signal information from the 22 grounded electrode rings of the electrometers are processed to give a 38 channel spectrum by numerical solution by controlling the entire spectrum to be continuous, finite and always positive in concentration. The instrument is initially calibrated based upon a numerical model of the charging process and a Monte Carlo simulation [Johnson et al, 2004].

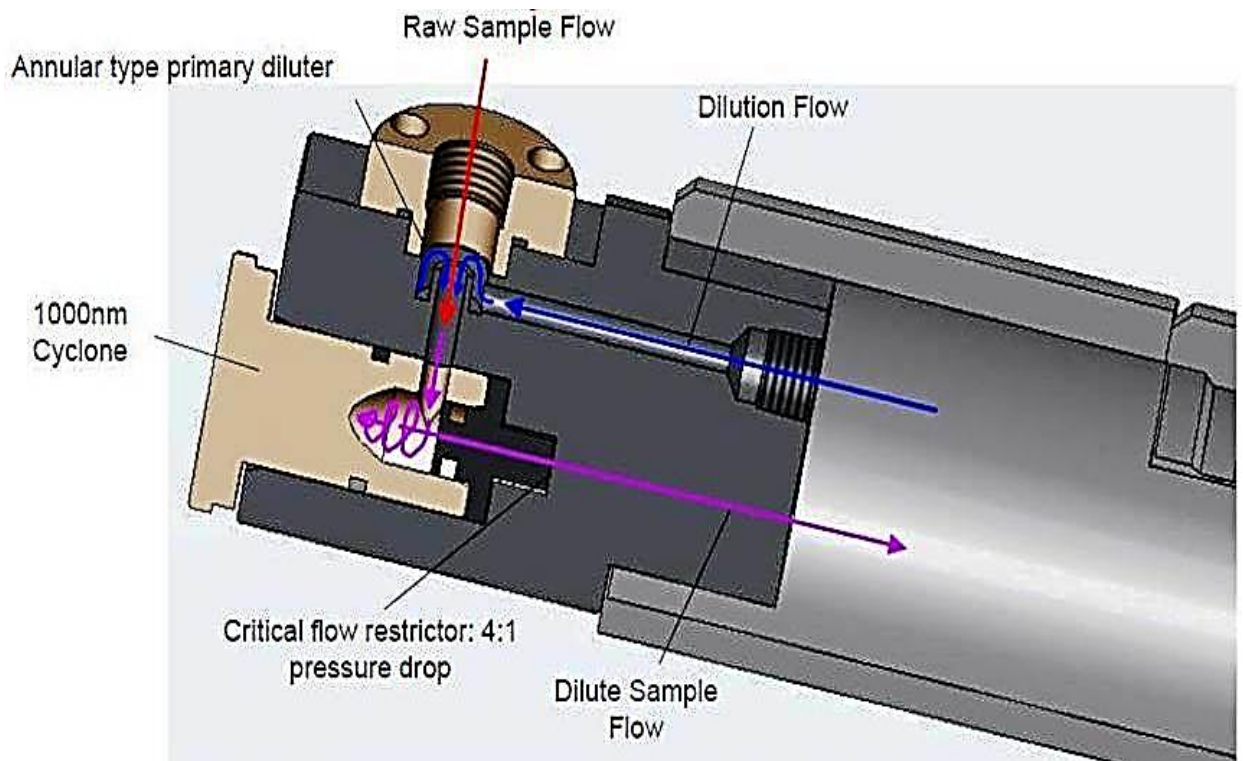


Figure 3- 10 DMS primary dilution system [Cambustion Ltd]

3.9 Laser induced incandescence (LII)

Laser induced incandescence has been used for decades, and this technique is based on the incandescence signal induced by laser excitation. Short laser pulses of a few nanoseconds duration heat up the particles of soot. The particle temperature changes significantly (400K) above the initial gas as well as the initial particle temperature (1600K). Research has shown that, the strong incandescence signal emitted by a soot particle corresponds to that of a grey-body emission band radiation governed by Plank's radiation law (Figure 3-11).

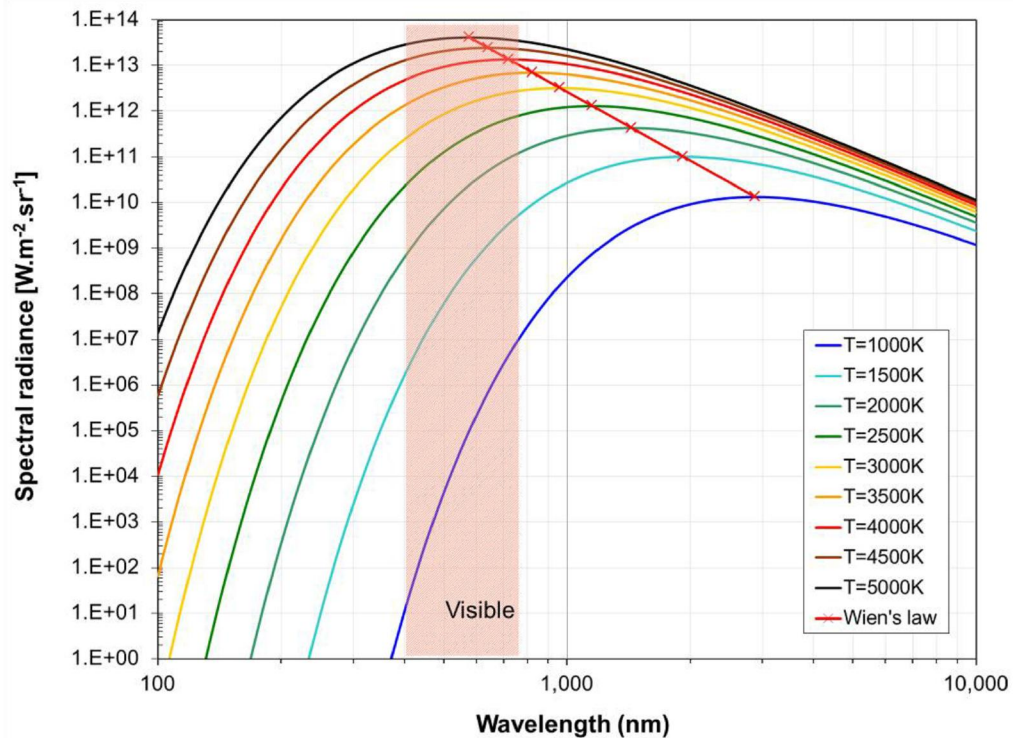


Figure 3- 11 Spectral radiance of a blackbody for different temperatures (181)

Research has shown that Eckbreth was the first scientist to recognise the interaction between laser light and carbon particles (182). However, the real developer of the laser-induced incandescence technique was Melton (183). In his findings he exploits the potential of lasers as a powerful diagnostic tool for soot concentration measurement and particle sizing, as well as being used for soot investigation (visualisation) in an optical diesel engine by (184). Particle sizing was achieved by two different research groups (185, 186). LII has advanced over the last two decades into a particularly attractive technique that offers the possibility of accurate and spatially resolved soot volume fraction and particle size measurements. This technique has been developed for in-situ spatially and temporally resolved measurements of soot concentration and had been applied into different conditions, from flame (Melton, 1984) (183) to vehicle engine (Bladh, 2006; Dec, 1991) (184, 187).

3.9.1 Time-resolved laser induced incandescence (T-R LII)

Time-resolved LII has also been used as a powerful tool to set apart the primary particle diameters of soot, black carbon or ashes. Equally, this can be applied to a non-carbonaceous

nanoparticle sizing as long as the matter does not sublime at high temperatures and can radiate like a black or grey body. Thus, studies have also been carried out on iron, silver, manganese oxide and titanium particles (188-190) or on carbon nanotubes and nanofibers (173, 190, 191).

The LII signal is highly dependent on gas temperature and pressure and the pressure effect on the LII signal had been experimentally studied by Hofmann et al., 2003 (192). Also optimal excitation and detection conditions have been reported in (193, 194).

This technique has been functional for different types of flame, atmospheric laminar diffusion flame (Boiarciuc et al., 2006), in a pressurized vessel (Pickett and Siebers, 2004), in engine (Kock et al., 2006, Bladh et al., 2006, Boiarciuc et al., 2006) or at exhaust conditions (Di Iorio et al., 2005). In an internal combustion chamber, the conditions are less favourable than in an atmospheric flame or a pressurized vessel. More attention must be given to the physical processes for laser-heated soot particles. The operating conditions in an internal combustion engine can vary over a large range of temperatures and pressures during the engine cycle, the uncertainties between the LII signal strength and these different parameters may introduce uncertainties in measurements. Many research groups are working on it, to improve the LII in terms of better quantitative and accurate diagnostic, especially in an internal combustion engine. The interest in the model has increased with the fact that particle sizing can be estimated by time decay of the time-resolved LII signal (Will et al., 1995). In addition, the comprehension of heat conduction has been improved. The heat conduction is the main cause of soot particle cooling after laser heating. The treatment of the heat conduction in various environments including those encountered in engine, has been reviewed by Liu et al. (Liu et al., 2006).

The particle sizing theory is based on the energy balance, and on the actuality that the smallest particles cool down faster than the largest ones, after heating up by the laser pulse. The two-colour time resolved LII is used to determine the soot temperature by pyrometry.

The experiment for the soot generated from the diffusion flames of a wick burner is shown in Figure 3-12. Optical investigations have been performed using laser induced incandescence in the Department of Mechanical Energy, Strathclyde University (Dr I Burns).

Laser-induced incandescence (LII) measurements were made by a pulsed Nd: YAG laser (Surelite Continuum) emitting at 1064 nm. Excitation was carried out using a beam with 1-mm

diameter and a top-hat spatial profile. The time-resolved LII signal was imaged onto a 1-mm diameter pin-hole and detected using a photomultiplier tube (Hamamatsu R636-10) with a narrow band-pass filter centred at 450 nm. Averages of 64 signal decays were recorded. Measurements were made 10 mm above the top of the wick at a range of radial locations. These measurements were performed in flames of n-decane, anisole, eugenol and furfural. The soot volume fraction was quantified by comparing peak signal levels to the measurements when the wick burner was replaced with a laminar flat-flame of premixed ethylene and air, in which the soot volume fraction was determined by extinction measurements. Temporal decay profiles allowed primary particle sizes to be estimated.

3.10 Pyrolysis Gas Chromatography Mass Spectrometry (Py-GCMS)

3.10.1 Pyrolysis GCMS Sample preparation

Soot samples from diffusion flames were prepared for analysis using the pyrolysis-GC-MS dry method. Soot was sandwiched between silica glass wool in a fire-polished quartz tube of 25mm length and 2mm internal diameter which had been previously heated in the flame of a Bunsen burner to remove all contaminants. A small piece of the cleaned silica glass wool was placed half way down the fire-polished quartz tube with the angle end downwards and it was then weighed.

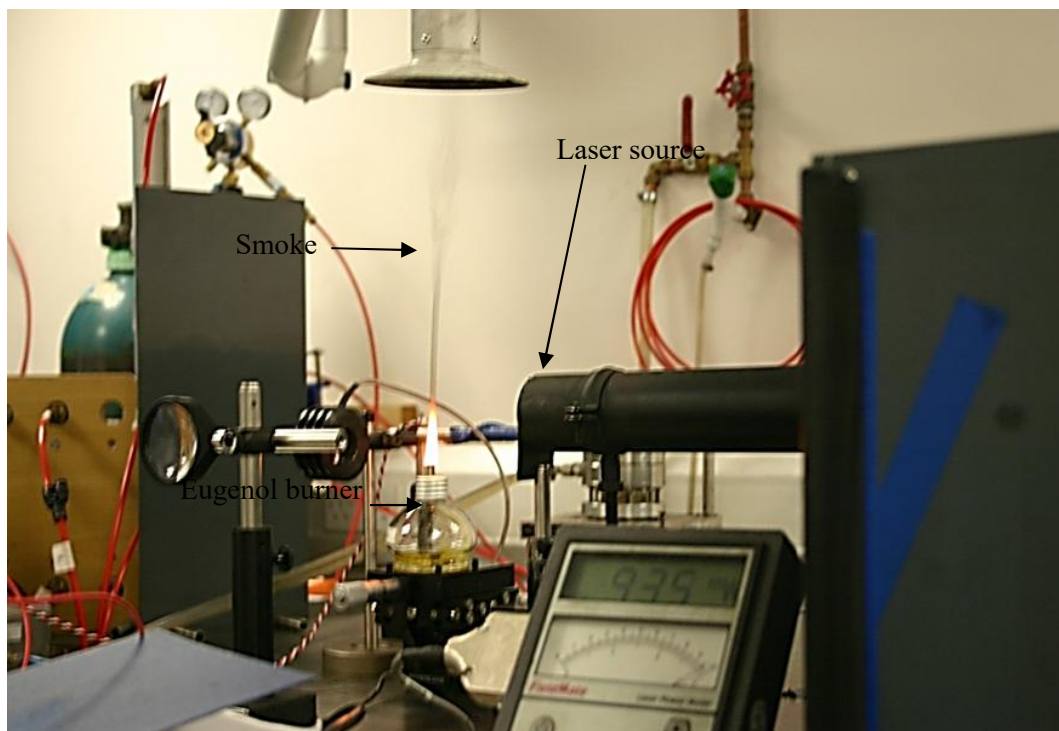


Figure 3- 12 Shows the LII set-up for sampling soot volume fraction in the laboratory.

This was then followed by a tiny proportion (2mg) of the sample placed inside the fire-polished quartz tube. Another piece of silica glass wool was used to cover the top of the tube. The overall weight measurement of the tube was carried out as follows: (1) tube +silica wool. (2) Tube, silica wool and sample. (3) Tube, silica wool, sample and silica wool. Finally, the tube was kept in a desiccator prior to analysis to avoid secondary reactions. The tube, silica wool, and pyrolysed sample residue were also weighed after analysis.

3.10.2 Pyrolysis method for soot sample

Pyrolysis-GC-MS analyses were carried out on the samples using a CDS 5000 series pyrolyser connected to a Shimadzu 2010 GC-MS. Prepared samples were placed gently into the coil of the pyroprobe. The helium flow at 273.69 kPa was checked. Pyrolysis products from the sample were transferred immediately to the GC using the pyroprobe attached to an HP 5890 series II gas chromatograph fitted with an Rtx 1701 60 m capillary column, 0.25 id and 0.25 μ m film thickness. Separation of products was achieved by using a temperature program of 40 $^{\circ}$ C, hold for 2 minutes, injection temperature was set to 280 $^{\circ}$ C at split injection mode and oven

temperature of 40⁰C. The helium carrier gas was set as follows; premium pressure of 725-130.5kPa, flow control mode: pressure was set to be 306.09kPa, total flow of 46.2 mL/min, column flow 2.06 mL/min, linear velocity 36.6 cm/sec, purge flow 3.0 mL/min, split ratio of 2.0 and a total program time of 67min respectively. The column oven temperature was programmed as follows: initial temperature of 40⁰C held for 2.0min and a rate of 6.00mL/min at a final temperature of 280⁰C held for 25min and a total programme time of 67min. This programme method was immediately loaded followed by data acquisition of the sample information and when the GC and MS turned ready then the CDS pyroprobe method was set up as follows; initial temperature of 50⁰C, ramp 20⁰C /ms and a final temp of 600⁰C at a dwell time of 20 seconds. The purge flow removes traces of oxygen prior to pyrolysis. Then finally the sample was pyrolysed and in the last 1 minute of the pyrolysis the GC was made to start running for 67minutes and then after 5minutes the tubes were removed from the probe and weighed to obtain the amount of volatiles. Mass spectroscopy ion source was programmed to 230⁰C and the interface to 280⁰C. For all GC-MS studies, the chromatograms were assigned on the basis of the NIST Mass Spectral Library Database, from previous literature and by known retention times, as described in (195). These analyses were done for all the soot samples generated from combusted fuels and at different pyrolysis temperature of 300⁰C, 400⁰C, 500⁰C and 600⁰C respectively, and in some cases up to 1200⁰C (in the case of some fuels such as Heavy fuel oil asphaltene, Shell marine asphaltene, Bio-oil, and Bio-oil asphaltene) with the view to study the effects of pyrolysis temperature on the samples.

3.10.3 Sequential Temperature Application (STA)

Sequential temperature was performed on the sample fuels by applying the pyrolysis lower temperature to higher temperature, keeping the sample on hold for all the rest of the temperature (from 300-600⁰C, or 300-1200⁰C in the cases of heavy oils samples). These temperature application patterns will help to study the reaction pathway of the volatile products, and devolatilization of the products with respect to temperature. Additionally, volatile rates can be determined.

3.11 Thermogravimetric analysis TGA

Thermogravimetric analyses was carry out on a Stanton Redcroft DTA or TA 50 instruments IR5000Q TGA from 40-900°C in 50ml/min N₂ at a heating rate of 10°C min⁻¹. The peak of the first derivative of the weight loss curve indicates the point of greatest rate of change and is called the inflection point. The corresponding first derivative of the TGA curves was obtained at various points to investigate the volatilisation rate in Wt.%/°C, and this is called the DTG curve or derivative mass loss, which also indicates the temperature of the highest volatilisation rate.

The TGA program was set up to reach 105°C at the rate of 10°C/min and held for 5 min, this provides a measurement of the water content of the soot by measuring the weight loss at 105 °C.

Also the TGA analysis was performed in a constant flow rate of nitrogen. This is followed by heating under N₂ to 900°C to obtain the ass of volatiles (organic carbon) and fixed carbon. This is followed by switching the gas flow to air at a particular program temperature (900°C), to burn out the soot and obtain the ash fraction.

Fixed carbon content or elemental carbon is calculated by taking the difference from the volatile fraction and ash as demonstrated in the following equations 3-2 to 3-5:

$$\text{Wt. \% Moisture} = \frac{\text{Mass}_{\text{initial}} - \text{Mass}_{105^{\circ}\text{C}}}{\text{Mass}_{\text{initial}}} \times 100 \quad \text{Equation 3- 2}$$

$$\text{Wt. \% Volatile} = \frac{\text{Mass}_{105^{\circ}\text{C}} - \text{Mass}_{900^{\circ}\text{C N}_2}}{\text{Mass}_{\text{initial}}} \times 100 \quad \text{Equation 3- 3}$$

$$\text{Wt. \% Ash} = \frac{\text{Mass}_{900^{\circ}\text{C Air}}}{\text{Mass}_{\text{initial}}} \times 100 \quad \text{Equation 3- 4}$$

$$\text{Wt. \% Fixed Carbon} = 100 - (\text{Wt. \% Ash} + \text{Wt. \% Volatile} + \text{Wt. \% Moisture}) \quad \text{Equation 3- 5}$$

Chapter 4 Combustion of model compounds

4.1 Introduction

Soot is formed from the incomplete combustion of biomass and conventional fossil fuels. Soot is known to consist of carbonaceous particles onto which volatile organic species are adsorbed. The carbonaceous core is Elemental Carbon (EC), and is commonly known as Black Carbon (BC) in accordance to its light absorbing properties, whereas the adsorbed volatile organic species are commonly termed Organic Carbon (OC). There are also lesser amounts of water and ash species such as metal oxides present. The ratio of BC/OC is of increasing interest in terms of the effect of soot particles on climate change. Particles with a higher ratio of BC will absorb heat to a greater degree rather than reflecting it, and cloud and snow albedo are significantly affected by deposition of BC, thus increasing the Global Warming Potential (GWP). Initial studies suggest that some biomass particles exhibit higher ratios of BC to OC in comparison with conventional fuels. The composition of the OC is also a key factor to consider when assessing the climate impact. This chapter presents an analysis of biomass soot using pyrolysis–GCMS techniques, Ultimate analysis was carried out on the samples under investigation for the elemental content for C, H, N, S, and O using a CE Instruments Flash EA 1112 series elemental analyser, the experimental details of this analysis were given in the previous **chapter 3** of this thesis. Furthermore, both particles size measurements and morphological structure investigations were performed on the fresh soot samples via online sampling of the soot directly from the flame and above the flame by DMS, SEM and TEM. The soot samples were generated from biomass model compounds such as eugenol, furfural and anisole, as well as soot from pine, and forecourt wood (wood from a petrol station forecourt) combustion. Additionally, pyrolysis of the raw biomass fuels such as the pine wood, forecourt wood and rape straw was conducted. These results are compared with analysis of soot from hydrocarbon fuels, and with soot collected from the flues of a wood burning stove and a multifuel stove. The pyrolysis GCMS results are used in conjunction with thermogravimetric

analysis linked to FTIR in order to give detailed characterisation of the BC/OC ratios, as well as the chemical composition of the OC, and the relative amounts of the other species present. The implications of the results in terms of climate change are considered.

4.2 Composition of black carbon /organic carbon and its effect

The Global Warming Potential (GWP) of combustion gases such as carbon dioxide and methane has been well researched. There is increasingly interest in the GWP associated with the particulate and aerosol fractions of combustion emissions. Soot formed by the incomplete combustion of fossil or bio-fuels consists of agglomerated chains of carbonaceous spherules of elemental carbon (EC) with condensed organic compounds (OC). OC is also known as the volatile fraction or solvent extractable fraction. The nature of the soot emitted depends on the fuel being burned, the conditions under which it is formed and surrounding atmosphere before being emitted into the atmosphere as this affects condensation, coagulation and agglomeration of the particles. Black Carbon (BC) consists of the whole light absorbing fraction of the carbonaceous aerosols which mainly consists of EC. The ratio of BC/OC is of interest in terms of the effect of soot particles on climate change (196). Particles with a higher ratio of BC absorb heat rather than reflecting it, affect cloud albedo, so affect reflectivity of snow and ice.

Exposure to soot leads to adverse health effects. Many of the health impacts are associated with the adsorbed volatile species in the soot OC fraction. In particular it is known that oxy-PAH species can cause damage to cell tissue (197, 198). Many studies have been made of the nature of smoke or soot emitted from the industrial utilisation of fossil fuels, however there is much less data available for biomass derived soots.

A number of analytical methods have been devised. Soots have been analysed by pyrolysis GC-MS, by analysis of the extracted organic compounds, and by optical means. The results are complicated by the fact that the organic material consists of the precursors to the formation of soot and by incompletely combusted fuel. This thesis considers some of these issues.

A number of studies have been made of the properties of soot produced by the combustion of biomass. Extensive studies have been made of the soot forming mechanism occurring during the combustion of pure organic compounds from a fundamental viewpoint and soot forming mechanisms have been postulated (16, 199-202). The mechanism of soot formation from biomass will involve the same basic mechanism but a key step is the way in which biomass pyrolysis determines the type of organic compounds formed. Recent models have been proposed for the formation of soot from wood combustion (199, 201) in which the aromatic lignin components are responsible for much of the soot formation. The issue is whether this influences the BO/OC ratio and how these compare with values in the literature. There are considerable differences between the values obtained for biomass combustion by the various groups. Schmidl et al (203) made measurements using chemical methods and also summarised earlier results. Ross et al (204) measured the solvent extractable organic fraction and concluded that a range of compounds were present which could be divided into three classes. The results suggest the presence of three different types of soot material: weakly bound PAH easily desorbed and easily extractable in solvents, more strongly bonded surface material that are probably large three-dimensional PAH or polyene compounds and highly developed ordered soot, i.e. elemental carbon. An aerosol time of flight mass spectrometer (ATOFMS) has also been used (113, 202, 203, 205). In view of the different results a number of researchers have discussed the meaning of BC and OC (206-208).

Small thermal capacity combustors may contribute significantly to ambient air pollution. Feedstock parameters significantly influence emissions of NO_x, CO and PM. The soots studied in this work are chimney samples from multi-fuel and wood burning domestic stoves. Previous work has identified the main pyrolysis products during the first stages of biomass combustion to include eugenol, furfural and anisole (200, 201) so these species are investigated as model compounds for detailed combustion analysis. The results are discussed in terms of soot forming models (209-212). A number of papers have considered the nature of BC (213, 214) and this research considers this aspect in the case of biomass combustion. Soot has been examined from combustion appliances and from diffusion flames.

4.2.1 Experimental Methods

4.2.1.1 Soot sampling

Soot samples were obtained from diffusion flames for biomass pyrolysis oils burning on a wick burner as described in chapter 3 and stored under argon prior to analysis to minimize secondary reactions.

Additionally, samples were obtained from the chimneys of multi-fuel and wood-burning domestic stoves, which have typical operating temperatures of 300-600⁰C. The multi-fuel stove had been used previously for the combustion of various fuels, including coal, peat, woods, straw and briquettes. The soot collected in this case is thus from a mixture of fossil and biomass sources. The soots had been allowed to cool in air before collection.

4.2.1.2 Thermogravimetric analysis TGA

Thermogravimetric analysis (TGA) was used to measure the OC, EC and ash fractions. The samples were stored in a desiccator prior to analysis to remove any moisture. The OC mass fraction was determined by heating the soot samples in nitrogen to 550⁰C, ensuring that a steady mass was achieved. During this heating period, continuous FTIR characterisation was conducted on the evolved material using a Thermo Scientific Nicolet iS10 model analyser. The gas was switched to air and the temperature was increased to 600⁰C and held until no further mass loss was observed, this represented the EC. The mass remaining after the OC and EC were measured represented the ash fraction.

4.2.1.3 Pyrolysis gas chromatography Py-GCMS

Py-GC-MS was used in conjunction with a sequential temperature pyrolysis for detailed analysis of the OC. The system used was a Shimadzu 2010 GCMS linked to a CDS 5200 series pyrolyser, operating in trap mode. In this, the sample was heated in temperature steps of 100⁰C

to a maximum of 600°C with each desorbed separately into the GC-MS in order that chromatograms could be obtained for each temperature. After sample pyrolysis, the resulting products (C₄-C₂₀) are trapped onto an adsorbent trap (Tenax TA) at 40°C by operating the CDS pyrolyser in adsorbent mode. The trap is then desorbed at 300°C in a flow of helium onto the chromatographic column. The gaseous products (H₂, CO, CO₂, CH₄ etc) are not trapped onto Tenax TA and are vented. The CDS 5200 pyrolysis unit was connected to a Shimadzu 2010 GC-MS. The products were separated on an Rtx 1701 60m capillary column, 0.25 mm id., 0.25 µm film thickness, using a temperature program of 40°C, static time 2 min, ramped to 250°C at a ramp rate of 4°C/min with a static time of 30 min; the column head pressure at 40°C was 2 bar. For all GC-MS studies, the chromatograms were assigned on the basis of the NIST Mass Spectral Library Database, from previous literature and by known retention times, as previously described (215).

EC/TC was also estimated from the Py-GC-MS studies at 600°C. The mass remaining after desorption at this temperature is assumed to be EC+ ash. Ash was determined as the mass remaining after combusting the residue in the pyroprobe tube over a Bunsen flame.

5.3 Experimental Results

4.3.1 TGA-FTIR Analysis

A TGA plot of chimney soot collected from a wood burning stove is shown in Figure 4.1 and the method was used to define EC, OC and ash content. The summary of the mass fractions obtained by TGA on the soots are given in Figure 4.2. These values were used to calculate the EC/TC Total carbon (TC) ratios as given later in Table 4.2.

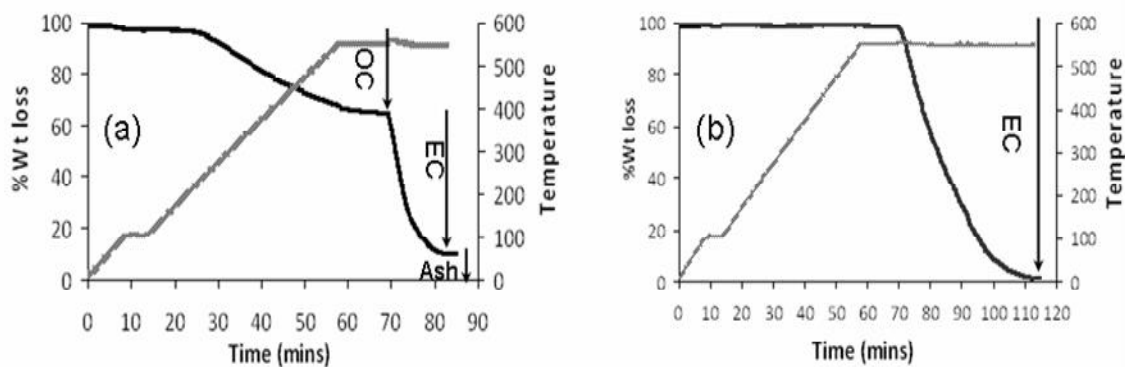


Figure 4- 1 TGA plot of analysis for: (a) wood stove soot, (b) eugenol soot.

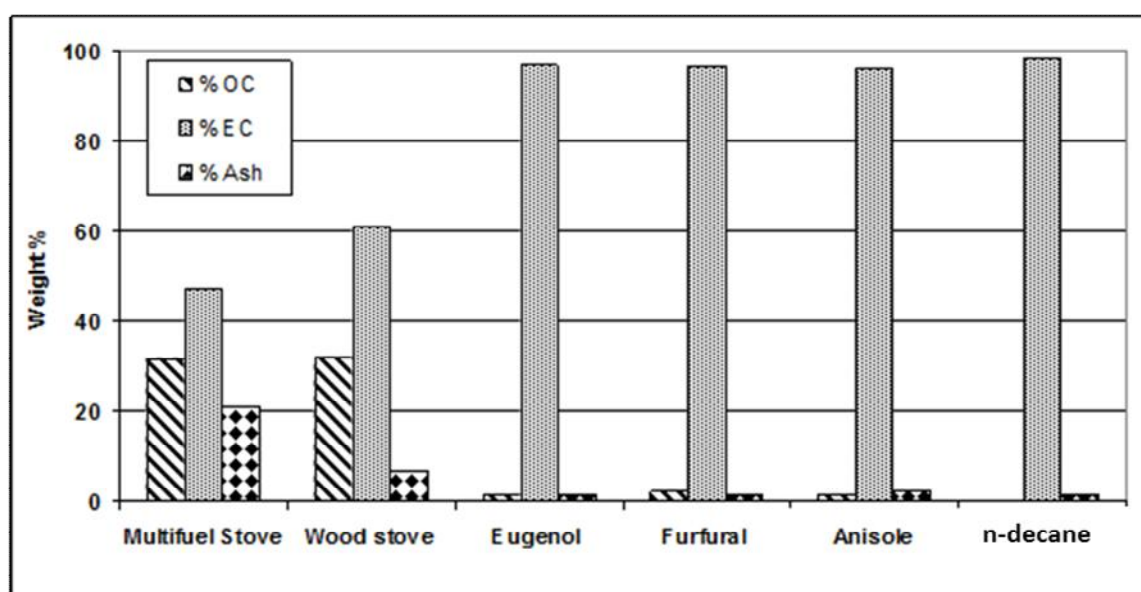


Figure 4- 2 Results of TGA, weight percentage of OC, EC and ash for the fuels studied.

The most notable difference between the wick burner samples and the stove samples is the very high levels of EC measured for the wick soots. Uncontrolled air/fuel mixing characteristics of domestic stoves could result in a higher level volatile components surviving combustion, hence adsorbing onto the EC cores as OC. It is also likely that the collection method is significant for these results, in that the domestic soots cooled naturally after combustion, allowing condensation of remaining unburned fuel onto the particle surface whereas the wick burner soots were collected under hot conditions and then stored under argon, hence minimising condensation. Trace ash measurements seen for the wick burner soots are within the accuracy limits of the technique so are considered to be negligible. However, considerable ash was

present in the particulate samples for both domestic stoves and was highest for the multi-fuel stove at 21% wt.

Analysis of the DTG for each sample showed that the most significant amount of mass loss was after 500°C for all the wick burner samples. In contrast, both the stove samples had significant mass loss from lower temperatures- ~250°C for the wood stove compared to ~180°C for the multi-fuel stove. The multi-fuel stove had two phases of mass loss: with most loss up to ~320°C then a slower rate of OC release up to the final temperature. These two phases may correlate with the phases of weakly bound and strongly bound material proposed by Ross et al (204), however none of the other samples showed a significant rate change during mass loss. This indicates that the biomass derived soots are behaving differently to the fossil fuel soot.

The organic components evolved during the TGA analysis were analysed by FTIR, however only very low levels of absorbance were seen. The most significant readings were for evolved CO and CO₂, which was seen for all samples. There was a small peak in the aromatic region at ~500°C for both stove soots and there was also a peak attributed to SO₂ for the multi-fuel soot indicating the use of fossil fuels in that stove. However, the technique did not show any significant aliphatic peaks or oxygenates, and it is considered that this system did not provide sufficient accuracy for the low levels of material under investigation.

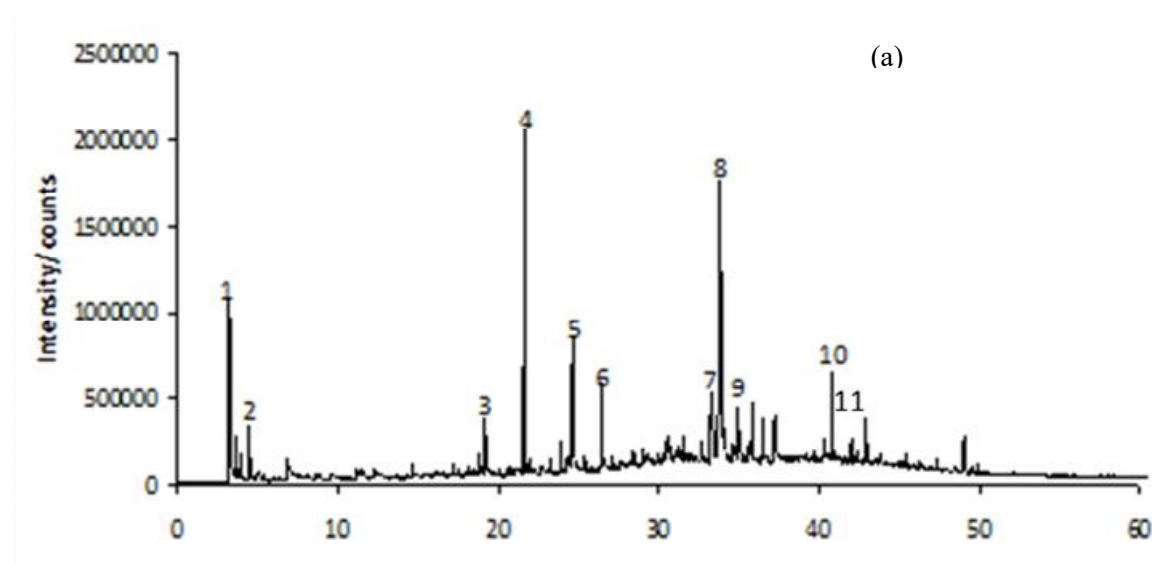
4.3.2 Pyrolysis-GC-MS

As found during TGA analysis, the soot collected from real stoves contained significantly more OC than soot collected from the wick burner experiments. A comparison of typical chromatograms is given in Figure 4.3, comparing wood stove soot with anisole soot at pyrolysis temperature of 400°C. The best matches given by the mass spectral library are provided. The temperatures used for the pyrolysis study are aimed at desorbing the OC from the particulate with minimal thermal degradation and correspond with temperatures analysed using FTIR. It was anticipated that evidence for weakly bound material would be given at the lower

temperatures and more strongly bound material would be given by analysis at the higher temperatures.

The soots derived from the wood burning stove contained high levels of methoxyphenols and dimethoxyphenols at a pyrolysis temperature of 400°C. These species are associated with the lignin part of the wood structure. These phenolic species were present at 500°C but by 600°C mainly aromatics were seen for the same sample. Song et al (212) used a pyrolysis temperature of 700°C to investigate soots and charcoals, finding that the products were dominated by aromatic compounds. Song also found oxygen containing pyrolytic products in all the samples analysed, but proposed that these arose from thermal decomposition of the carbonaceous solid particles.

Analyses of the soot from the multi-fuel stove are given in Figure 4.4. This showed desorption of mainly alkane species at the lower temperature of 400°C, giving a chromatogram that appears typical of other fossil fuel soots such as diesel particulates. Correlation with the TGA mass loss results shows that these alkanes are the main OC components for this soot and represent unburned fuel components that are weakly bound to the soot. Much less material was seen at 500°C and 600°C, but these are more strongly bound components including a variety of phenols, methyl phenols and aromatic species.



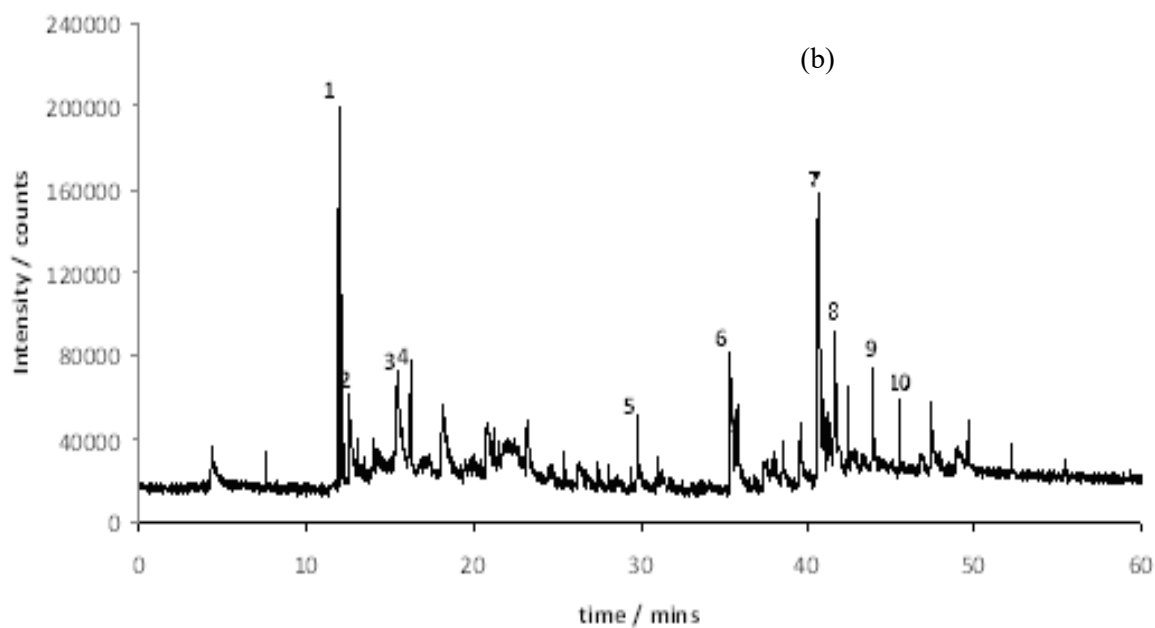


Figure 4- 3 Py-GCMS Chromatograms of; (a) wood stove soot and (b) anisole soot, both produced at 400°C

Key (a) **1:** 2,5-dimethylfuran , **2:** furan, 2-methyl-, **3:** phenol, 5 2-methoxy-, **4:** levoglucosenone, **5:** 2,4-dimethyl- phenol, **6:** phenol, 2,6-dimethoxy-, **7:** 3,4-altrosan, **8:** d-allose, **9:** alpha.-d-glucopyranose, 4-o-.beta.-d-galactopyranosyl-, **10:** 1,1'-biphenyl, 5-hydroxy-3,4'-dimethoxy-. **11:** retene

(b) **1:** siloxane attributed to column bleed-, **2:** alkane, **3:** alkane: **4:** siloxane attributed to column bleed **5:** unknown :m/z= 175: **6 :** phenanthrene;**7:** fluoranthene; **8:** pyrene, **9:** alkane **10 :** alkane

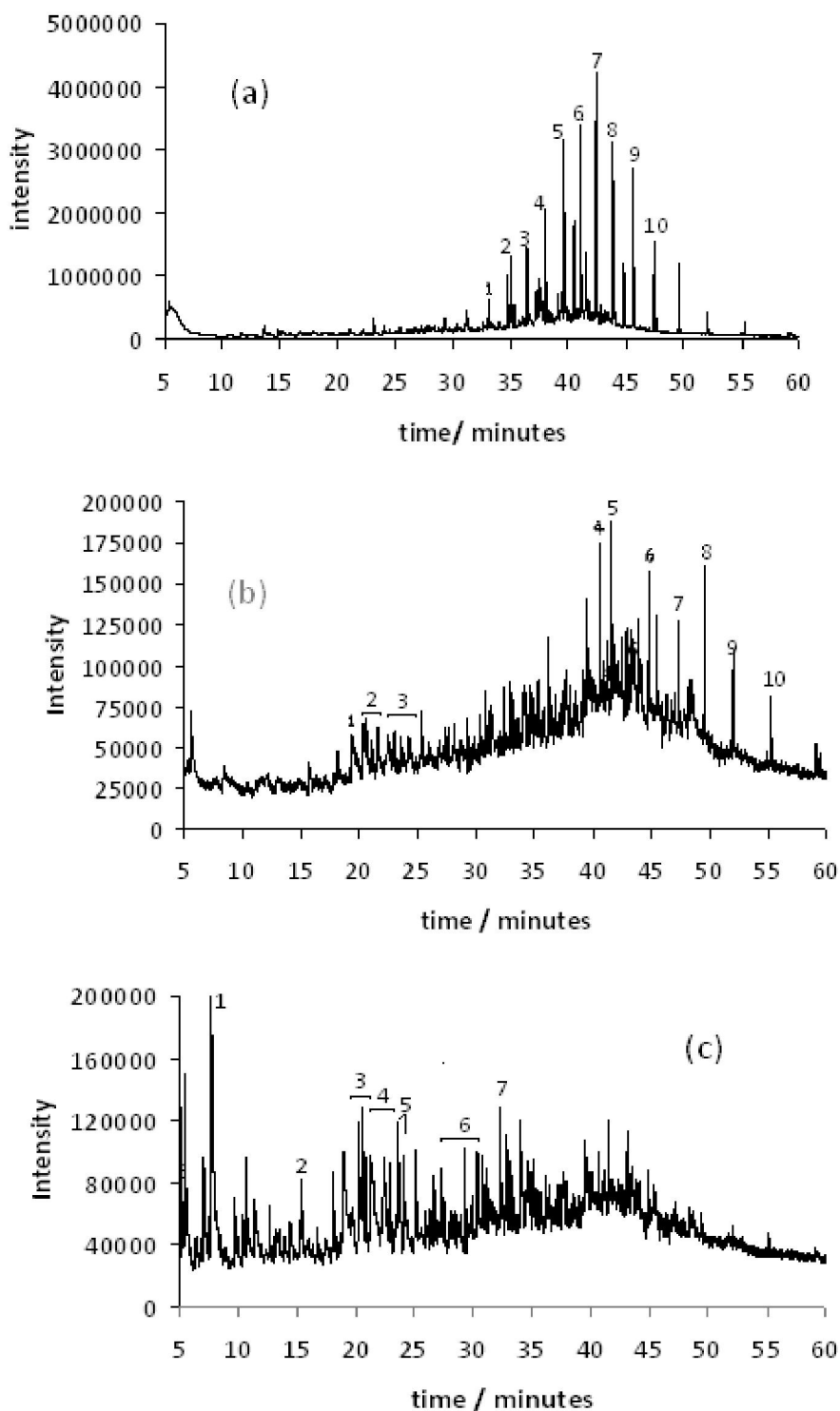


Figure 4- 4 Py-GCMS Chromatograms of multi-fuel soot at (a) 400°C, (b) 500°C and (c) 600°C
 Key (a) 1, 3-10 alkanes, 2: phenanthrene (b) 1: phenol, 2: methyl phenols, 3: di-methyl phenols, 4: fluoranthene, 5: pyrene, 6: unknown, 7-10: alkanes.

(c) 1: toluene, 2: Phenol, 3: methyl phenols, 4: di-methyl phenols, 5: methyl naphthalenes, 6: dimethyl naphthalenes, 7: naphthalenol

The major species types identified in the OC using Py-GCMS are shown in Table 4.1. Results for n-decane have been omitted from this table as no significant peaks were identified across the pyrolysis temperatures investigated. Further investigations were performed on raw biomass fuels such as forecourt wood and rape straw. Evidently, the decomposition products at 500°C were mainly phenols and complex phenols as well O-PAHs (Figure 4.5-6). However, the data interrogation shows the presence of PAHs.

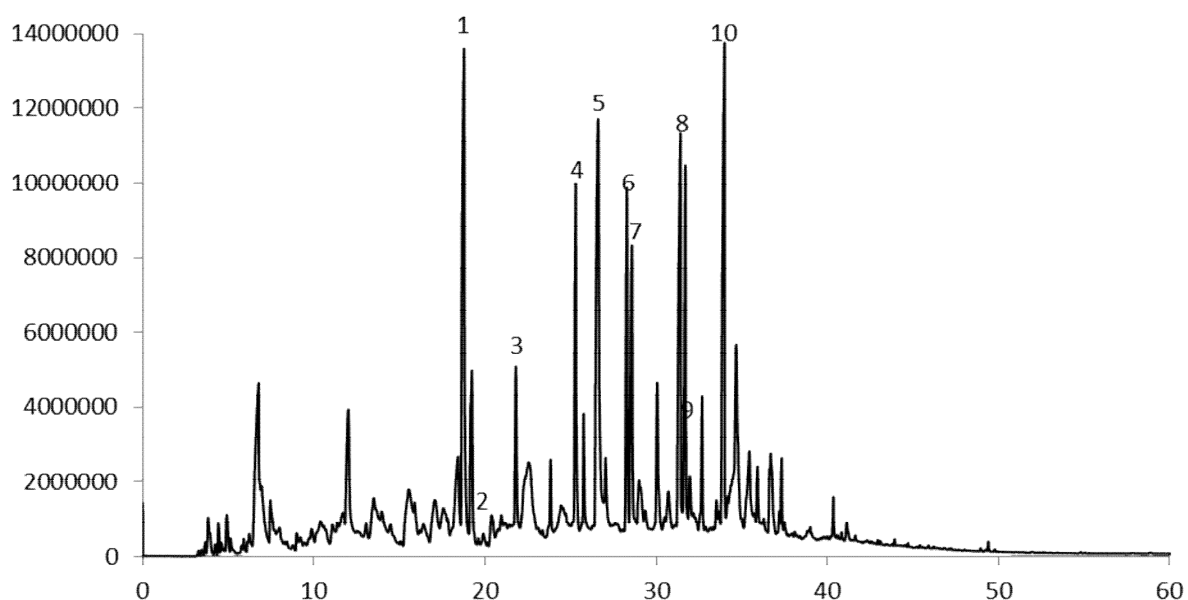


Figure 4- 5 Py GCMS Chromatogram of Forecourt wood at 500°C.

The volatile species generated are assigned as; 1: phenol, 2: mequinol, 3: phenol, 2-methoxy-4-methyl-, 4: phenol-4-ethenyl- 5: phenol, 2,6-dimethyl-, 6: acetophenol, 2-methoxy-4[2-propenyl-, 7: 1,2,4-trimethoxy benzene, 8: bicyclo[4.1.0] heptan-2-ol, 9: not identified 10: phenol, 2,6,-dimethoxy-4(2-propyl-

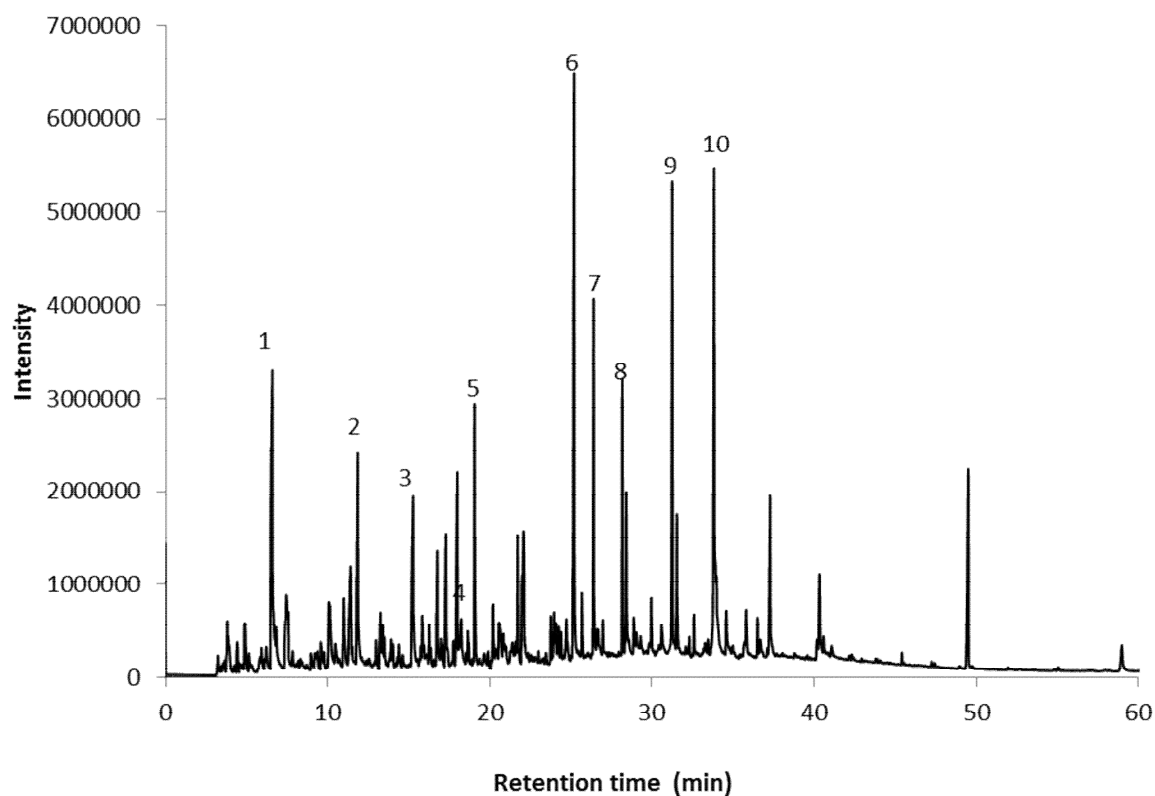


Figure 4- 6 Py GCMS Chromatogram of Rape straw at 500⁰C.

The volatile species generated are assigned as; 1: acetic acid, 2: 2-cyclopenten-1-one, 3: 6-oxa-bicyclo[3.1.0] hexan-3-one, 4: 1,2-cyclopentandione, 3 methyl-, 5: phenol, 2- methoxy-, 6: 2-methoxy-4-vinyl phenol, 7: phenol, 2,6-dimethoxy-, 8: not identified, 9: 6 methoxy coumaran-7-ol, 10: phenol, 2,6-dimethoxy -

Table 4- 1 Major Species types identified in the Soot Organic Carbon Fraction

Pyrolysis Temp °C	Multi-fuel Stove	Wood Stove	Eugenol	Furfural	Anisole
400°C	Alkanes	Methoxyphenols furans, levoglucosone, sugars	Oxygenates including carboxylic acids and esters	Alkanes	Aromatics Alkanes
500°C	Aromatics Phenols Methyl phenols	Phenols, furans, methoxyphenols dimethoxyphenols	Methoxyphenols, traces of carboxylic acids	No significant peaks	aromatics
600°C	Aromatics Phenols Methyl phenols	Traces of organic acids, aldehydes	No significant peaks	No significant peaks	No significant peaks

4.4 Discussion

4.4.1 Determination of EC/TC ratios by different methods.

The role of black carbon in atmospheric chemistry has been well documented, and an important parameter is the relative proportions of elemental carbon (EC) and co-emitted organic carbon (OC), together representing total carbon, TC. A number of methods have been proposed for the determination of EC/TC. In this work analysis of the mass lost during pyrolysis in conjunction with correction for ash enabled a calculation of EC/TC to be made as shown in Table 4-2. It is seen that the diffusion flames all have high values for EC/TC but they are in agreement with the TGA results.

Table 4- 2 Comparison of soot EC/TC determined by Py-GCMS with TGA

Soot sample	EC/TC by Pyrolysis GC-MS	EC/TC by TGA
Multifuel Stove	0.66	0.60
Wood stove	0.65	0.65
Eugenol	0.98	0.99
Furfural	0.95	0.98
Anisole	0.97	0.98
n-decane	0.98	1.00

Previous work has used an Aerosol Time-of-flight mass spectrometer (ATOFMS) for investigation of EC/TC ratio in both eugenol and n-decane soots. Using the method of Ferge et al (205) and the comparison with this work is shown in Table 4-3. In this method C_nH_y peaks with three or more carbon atoms and low hydrogen content are assigned to EC-like polymeric

carbonaceous fractions, while C_nH_y peaks with higher relative hydrogen content are assigned to fragmented organic compounds, or more “OC-like” polymeric fractions.

Table 4- 3 ET/TC Comparison of Py-GCMS with ATOFMS

Soot sample	EC/ TC by Pyrolysis	EC/TC by ATOFMS [7]
Pine wood	0.62	0.62
Eugenol	0.98	0.52+/-6
n-decane	0.98	0.88+/-5

The results presented by Ferge et al (205) are in good agreement with those presented here. For instance, diffusion flames have an EC/TC range between 0.8 and 0.94, whereas soot from a road tunnel had a value of 0.5 in the Ferge study as measured by aerosol mass spectrometry (205). EC/TC ratios of 0.52 and 0.88 were obtained for eugenol and n-decane soots, respectively as shown in Table4-3. Lower values for eugenol using this method reflect the influence of sample collection in terms of the way that OC can condense onto the particles. These values are comparable with those reported for soot produced from hydrocarbon combustion by Ferge et al.(205) using this same method (87-94%).

Another study by Schmidl et al (203) looked at the composition of soots from different types of woods using a closed stove system. The TC and EC were measured using combustion based methods and the OC calculated by difference. Very low EC/TC values were reported compared to this work, with values of 0.15-0.30 for the woods and 0.43 for the briquettes. The high OC fraction suggests poor combustion conditions. Levels of EC covered a wider range, with mean values of 9.8% for larch, 21% for spruce, 19% for beech and 15% for oak, and are subject to much greater variability for a given wood type. Results suggested that combustion environment is more important for EC formations but fuel type and form can also have an impact as discussed in next section.

4.4.2 Variation of EC/TC ratios with fuel, combustion conditions and sample collection method.

A wide spread of values are reported by Schmidl for TC and EC (203). In the case of briquettes, the higher EC levels of around 31% of the total PM₁₀ for beech as against around 20% average for spruce; there is a corresponding decrease in the level of OC, from around 52% to only 40%, which seem to indicate a significant influence of physical form of the fuel rather than of the wood type. Since briquettes are made of compressed wood chips, and disintegrate under the burning conditions, access of air to the fuel seems to be better. However, it is well established that these ratios would vary according to the combustion conditions and will depend on factors such as the fuel type, air flow patterns, and the quenching of the combustion products (low temperature post combustion conditions produce lower EC/TC ratios). The sampling method is also important since traditional sampling, methods where soot is collected at higher temperature, produces larger EC/TC ratios than the new methods, where sampling is done at temperatures close to atmospheric, to replicate the conditions when products from a furnace enter the atmosphere.

4.4.3 Chemical composition of soot pyrolysis products

In this work it was observed that the TGA graph of weight loss against time/temperature for the multifuel soot had three types of regions: an initial low-temperature region; a second, generally more extensive section; and a final rapid weight loss during oxidation in air. These correspond to the three types of material which were identified by Ross et al (216) as constituents of soot or BC: weakly-bound material, easily thermally desorbed, and extractable by solvents ; more strongly-bound material less easily desorbed; and finally highly developed soot which is burned in the final phase of the TGA.

As for hydrocarbon-fuels, the first type of material for biomass consists of lower MW PAH soot precursors which arise from the primary radical products of combustion and might include acetylene (the HACA route- hydrogen abstraction-C₂H₂ addition), or react through

cyclopentadienyl (CPDyl); devolatilisation products of the fuel may also be present and these, such as the resinous constituents of coniferous wood, may be converted into marker compounds including retene (1-methyl-7-isopropylphenanthrene) as detected here. Any differences between the soots lie in the relative amounts of different products. Further weight-loss regions then arise from the desorption of higher MW analogues and secondary derivatives of those responsible for the first, and together these represent the BC co-emissions which are vitally important in studies of climate transformation in that they can bring about either cooling or warming.

The situation in biomass combustion is complicated by the additional presence of large amounts of oxygenated compounds such as methoxy phenols resulting from the initial pyrolysis of the fuel; this is especially important in low temperature combustion of biomass, such as smouldering straw or when burning the model compounds studied here, where the OC consists mainly of oxygen-containing compounds. This contrasts with the products of high temperature biomass combustion such as wood burned in a fixed bed furnace as studied previously (216). Both groups of products originate by the same single route and the PAH are formed from the initial major oxygenated reaction products.

4.5 Conclusions

Values of the ratio EC/TC for a range of soot samples determined by Py-GC-MS were in good agreement with those derived from TGA measurements. However the method of soot collection and analysis affects the values of EC/TC ratio obtained.

The results of the TGA measurements were consistent with the presence of different types of material in BC.

A range of pyrolysis products and oxygenated species including PAH were observed. Phenolic fragments associated with lignin were also present. These results are complicated by the fact that the organic material consists of the precursors to the formation of soot and also incompletely combusted fuel

Differences were observed between stove soots, such as adsorbed SO₂ for soot from the multi-fuel stove and higher ash. However, this study did not find any significant differences between EC/TC for biomass components.

4.6 Particle size distributions and volatile composition of soot from diffusion flames

4.6.0 Introduction

Studies have been conducted into the combustion of biomass pyrolysis oil and fossil fuels, with particular emphasis on the influence of chemical structure on the sooting characteristics. This work investigated the sooting characteristics of heptane, decane, anisole and eugenol which have been studied experimentally. The experiments involved the combustion of the fuels in a Seta Smoke Point Lamp (ASTM D1322). Flame height was varied systematically ranging from shorter to longer height up to the end of the smoke point. Results showed that the n-heptane (13.5mm) flame height < n-decane (27mm) while eugenol gave the lowest value (6.5mm). This implies that eugenol produces more soot than the other fuels. Differential mobility spectrometry was used to measure the particle size distributions at different flame heights above a wick burner (0.2mm height and 0.7mm diameter wick). Interestingly, the results revealed that the total number of particles decreases with increasing height above the flame for all the fuels. At 5cm sampling height, anisole soot particles are up to 500nm diameter, while eugenol soot particles are over 1000nm. Additionally, as the number of carbon atoms increases in the molecules, the final mean soot particle diameter decreases. The more aromatic fuels (eugenol and anisole) have the larger mean size soot particles compared to normal paraffin soot with a similar or the same carbon number. However, the fuel with higher burning rate produces less smoke, as in the case of n-decane; while the ones that burn quiescently were found to have high sooting propensity and this was used to rank the fuel according to their sooting tendencies. Further test investigations were made for volatile organic compounds using pyrolysis gas

chromatography mass spectrometry. This current work provides an experimental data-set for both model and conventional fuels for predicting the burning profile and mechanisms of soot formation.

As noted earlier, biomass and fossil fuel combustion emissions enter into the atmospheric environment as numerous small carbon particles known as ‘soot’. Particles emanating from soot have attracted much attention from the scientific community as they are the evidence of low efficiency combustion and play a major role in global warming (217).

Soot emanating from natural sources, such as biomass pyrolysis oil and biomass combustion in forest fires, or from human activities, ends up in the atmosphere, with high concentrations found in urban areas. The particulate can be classified as particulate matter $10\mu\text{m}$ (PM_{10}) and the smallest particles are under $1\mu\text{m}$. This also exists as PM_1 (ultrafine particles) and $\text{PM}_{2.5}$. However, the lightness of the soot particles means they stay longer in suspension in the atmosphere since they have insignificant falling speeds (218).

The particle size determines how deeply the soot infiltrates the respiratory system. The smaller the particles size, the faster they penetrate the lungs and the more noxious they are for an individual’s health; particularly the ultrafine particles under $2.5\mu\text{m}$ which can be trapped in the alveoli (218). Although the modern combustion scenario successfully reduces the overall particulate matter emission, they conversely result in the production of a higher fraction of ultrafine particles. The consequence of these particles is well-known; they increase the risk of cancers (lung cancer, cancer of mouth and skin), respiratory illness (asthma, bronchitis and gasping) and cardiovascular diseases (hypertension and strokes), and reduce pulmonary capabilities of humans (114). The toxicity of the soot particles does not come from the carbon, but rather from the hydrocarbon compounds, sulphur containing compounds and metallic ashes trapped inside the particles(219).

This current work demonstrates the particles size distribution using an DMS 500 series fast particle analyser at different flame heights (5cm, 10cm, and 15cm) above the flame of a wick burner, and the pyrolysis gas chromatography mass spectroscopy was used to explore the

volatile products of the soot particle from each components with the view to study the processes involved in particulate soot formation.

4.6.1 Experimental methods

The particle size distribution experiments in this chapter were performed using DMS 500series instruments as described in **Chapter 3**. The model and hydrocarbon fuels used were obtained from a commercial source, Sigma Aldrich. Sample work up and analysis methods were described in **Chapter 3**.

4.6.1.1 Pyrolysis gas chromatography mass spectrometry (Py-GC-MS)

Py-GCMS experiments were carried out using a Shimadzu 2010 GCMS linked to a CDS 5200 series pyrolyser as described in **Chapter 3**. All sample work up details and analysis methods were also covered in Chapter 3.

4.6.1.2 Differential mobility spectrometry and soot sampling

Differential mobility spectrometer DMS 500series, also called a particle mobility spectrometer was developed and manufactured by Cambustion Limited. This instrument is a fast particle analyser which measures particle size distributions in real-time (176). The particles are sized according to their electrical mobility diameter, which is called the particle diameter. The analyser can determine particle diameters ranging from 5 to 1000nm (177).

Soot aerosols were directly channelled from the burner top through the sample transfer line to the DMS 500 series unipolar corona charger for online sampling. The process description of the sample introduction system applied for these investigations has been provided [Cambustion 500series]. The measurement was carried out using an ion mobility spectrometer and the operation of the instrument was conducted and equipped with an inlet membrane, using the following parameters which operate with a bi-functional flow system. The operational

parameters employed to obtain the spectral data of the particle size distribution were: temperature of the inlet system: 80°C; carrier gas flow rate in front of inlet 417 mL/min; electric field: 245V/min; temperature of the drift tube: 50 °C; pressure: atmospheric pressure, compressed air at 2 bars was used as the carrier gas. A series of measurements with increasing concentration were obtained for each sample and the data files were extrapolated using excel as shown in the figs4-7-10 below.

4.6.2 Results and discussion

The results of the particle size distribution obtained from the DMS and the pyrolysis gas chromatography mass spectroscopy for all the fuels are shown in the following figures.

4.6.2.1 Particle size distribution of soot (PSDS)

The results of the particle size distribution obtained from the DMS for soot from n-decane, n-heptane, anisole, and eugenol are shown in Figures 4-7 to 4-10. Table 4-4 summarises the mean particle diameters and size ranges.

Table 4- 4 Summery of mean diameters and sizes

Sampling height	Dp (nm) from DMS		
	5cm	10cm	15cm
n-decane	100	190	210
n-heptane	100	100	220
anisole	250	180	220
eugenol	220	280	250

Each soot was also studied for OC by Py-GC-MS and results are given in Figs 4-11 to 4-22.

The predicted particle sizes (D_p) nm) of soot BC generated from n-decane flames ranges from 100 to 400nm with a mean diameter of between 100 – 200 nm. It is clear from Table 4-4 that the black carbon particle diameter increases with increase in flame height, i.e. (from 5cm to 15cm sampling position). A similar results is observed for soot from n-heptane combustion, where mean particle diameter increases from 100 – 220 nm sampling height. Unlike decane soot which has a particle size distribution in the range of 400nm and shows limited evolution of VOCs, the black carbon soot heptane demonstrate a particle size distribution (PSD) ranging from 100nm up to 1000nm (Fig. 4-8a-c) and present large amounts organovolatiles fragments.

This means that soot particles tend agglomerate. Since the fuel is burned at high temperatures, the volatile species present are not large in the soot as a result of the complete burning of the fuel. This is apparent in the Py-GC-MS results (Figure 4-17 to 4-19). The emission of the species became higher with increasing sampling position from 10-15cm as indicated in soot from the heptane flames (Figs.4-20 to 4-22). It is proposed that, the higher yield of the organic species are associated with slow fuel flow during the fuel combustion compared to the fuel n-decane.

The Cambustion DMS500 data file was used to predict the particle sizes distribution (PSD) of particulates emanating from the combustion of the biomass pyrolysis model compounds anisole, and eugenol. A comparison was made with the PSD and VOCs of the particulate soot of the hydrocarbon fuel during combustion. The results showed that the PSD fall over a large range of 100-600nm (anisole) and 100 – 1000nm for eugenol soot. The Py-GC-MS results are given in Figure 4-11 to 4-16 and show a well constituted volatile composition of different proportions such as oxygen containing polycyclic aromatic hydrocarbon (O-PAH), phenols, alkanes, and alkyl-PAH and polycyclic aromatic hydrocarbon PAHs.

Soot from eugenol presents a particle size range of 1000, 800, and 600nm for the 5, 10, and 15cm particulate soot sampling heights from the top of a wick burner respectively. The results show that for this fuel the agglomerate sizes decrease with increase in sampling height. This

might suggest that the agglomerates are burning out with flame height. There is low fuel flow rate during combustion of the eugenol leading to a shorter flame height, resulting in large emission compared to the hydrocarbon fuels. This indicates that the low flame height is also the genesis of soot formation and subsequent large soot particle inception as well as rapid particulate agglomeration. Closed to the wick the DMS results give information on the size of the agglomerates present forming soot in the flames. TEM will yield information on the different primary particle sizes and this is discussed later in section 4.8.4.

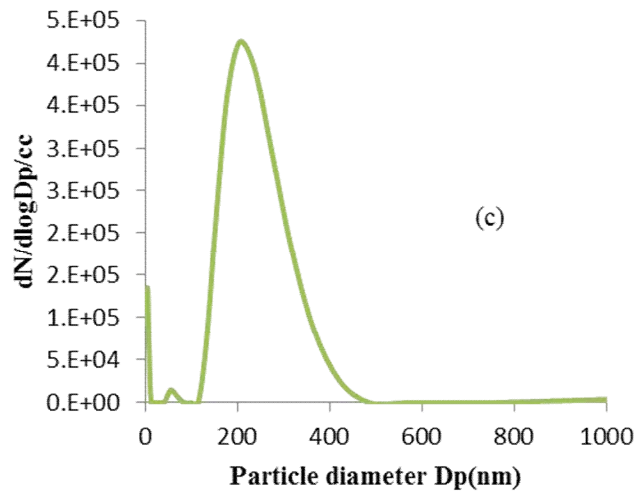
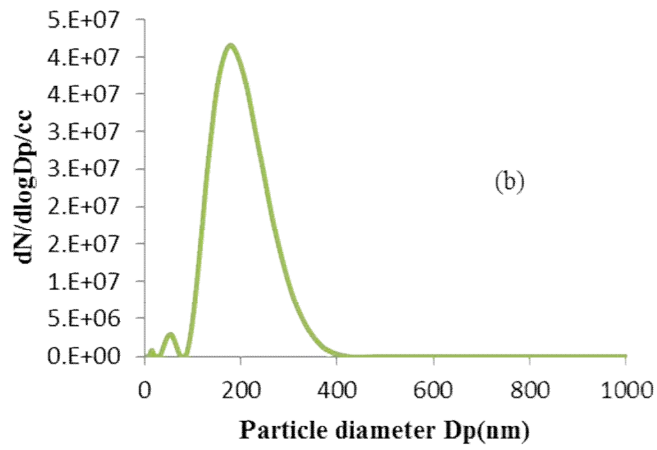
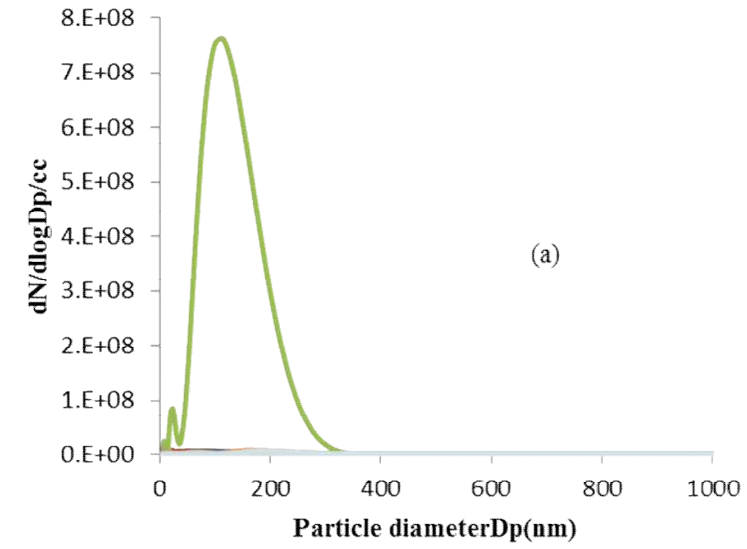


Figure 4- 7 The particle size distributions for soot from n-decane combustion sampled at (a) 5cm, (b) 10cm and (c) 15 cm above the flame

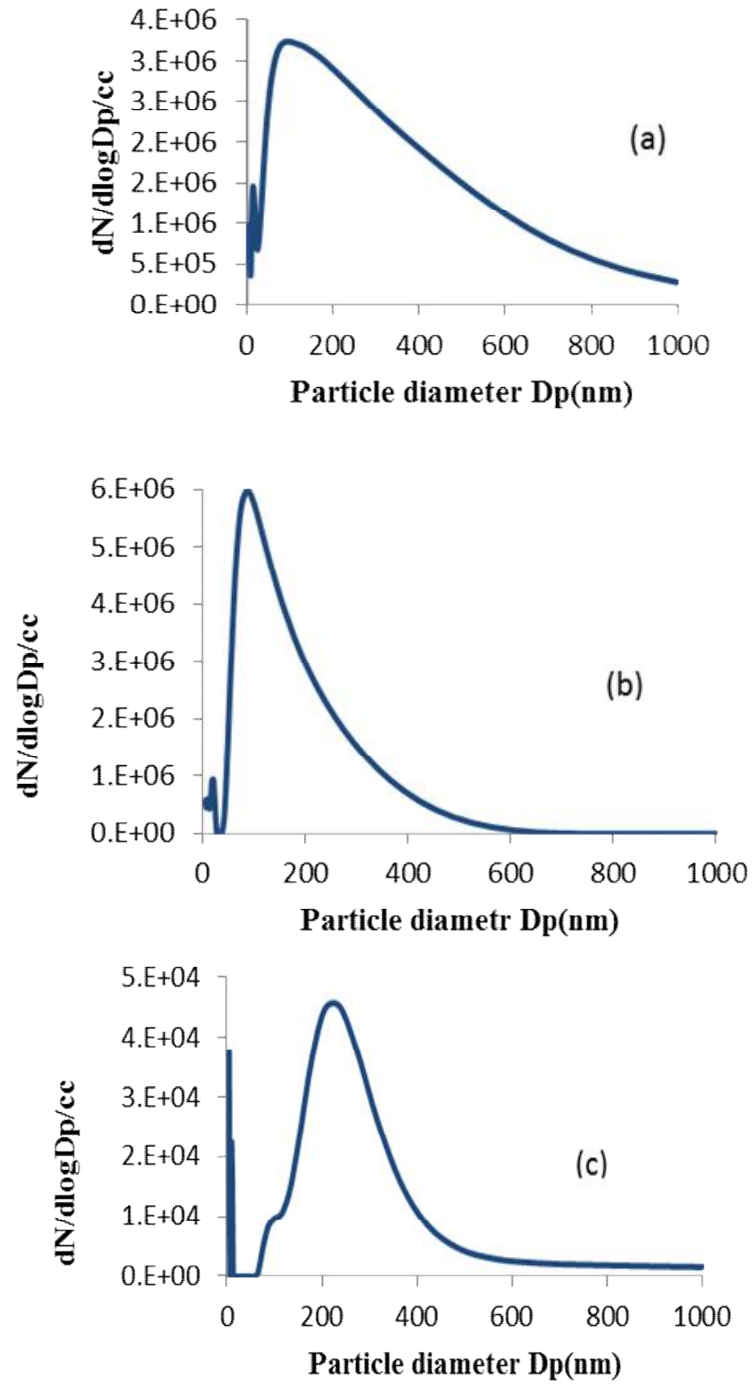


Figure 4- 8 The particle size distributions for soot from n-heptane combustion sampled at (a) 5cm, (b) 10cm and (c) 15cm above the flame.

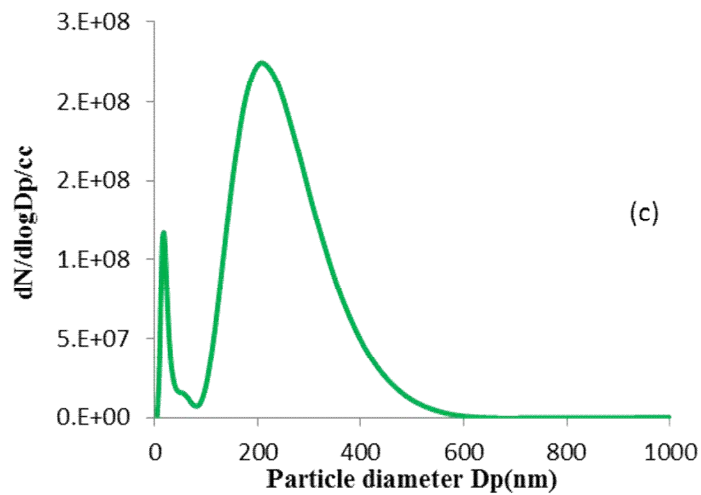
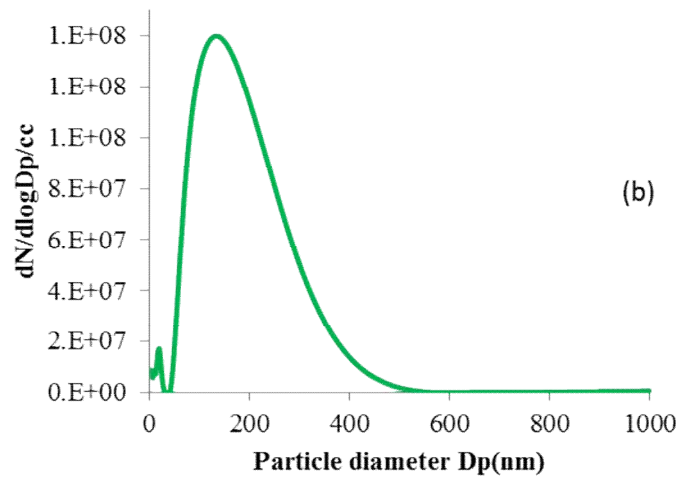
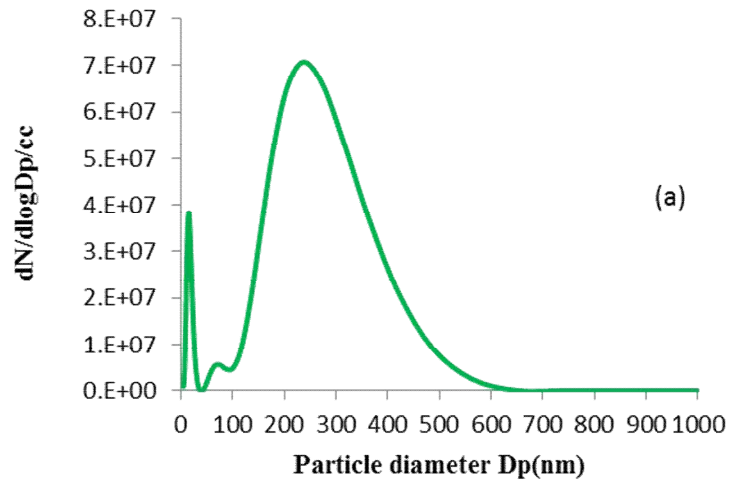


Figure 4- 9 The particle size distributions for soot from anisole combustion sampled at (a) 5cm, (b) 10cm and (c) 15 cm above the flame

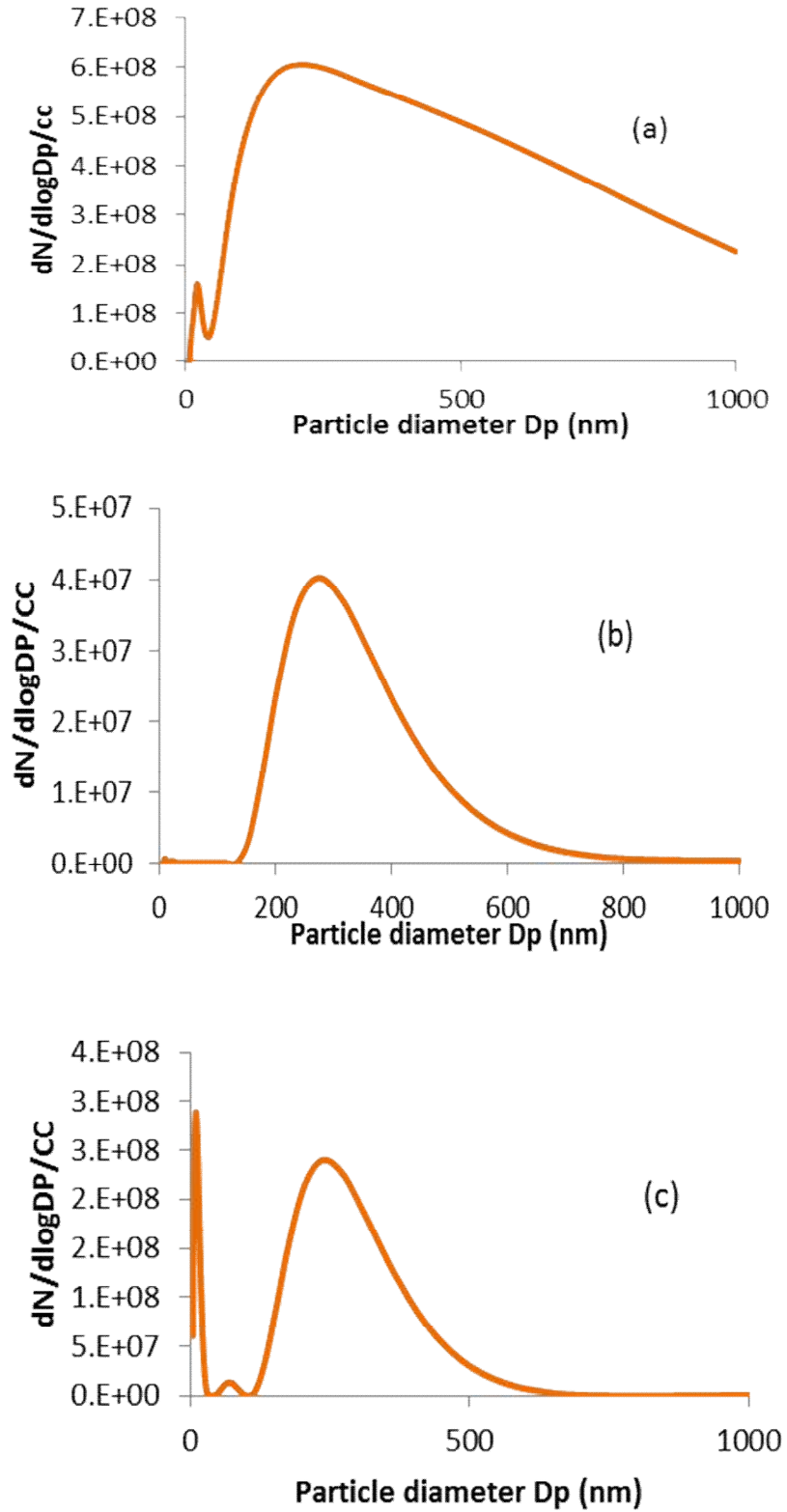


Figure 4- 10 The particle size distributions of soot from eugenol combustion sampled at (a) 5cm, (b) 10cm and (c) 15cm above the flame

4.6.2.2 Pyrolysis- Gas Chromatography Mass Spectrometry (Py-gcms)

The Py-GCMS technique was employed to determine different volatile organic species released. The details of the analysis have been previously explained (199). Carbonaceous particle (BC) emanating from pyrolysis of the model fuels (eugenol and anisole), biomass (pine wood etc.), and conventional fuels (decane and heptane) are produced in a similar way with a slight difference in volatile fragments (220, 221). The analysis revealed the compositional and structural difference of the soot particles generated.

Py-gcms chromatograms of the black carbon from the model fuels eugenol and anisole (with assignment reference to the main peaks) are demonstrated in Figs. 4-11 to 4-13 and 4-14 to 4-16, and comparisons were observed from the Py-gcms chromatogram for hydrocarbon fuels (decane and heptane) which are also presented in Figures 4-17 to 4-22 unfortunately there is some contamination but the major peaks could be assigned from the mass spectral detection NIST05A MS library and previous work (199, 200). A wide variety of pyrolytic ligninocellosic product as well as decomposition products of oil from the fuel (eugenol and anisole) were observed from the chromatogram, including phenols and chains of substituted phenols. These products among others are the only abundantly available (lignocellulosic materials) and also a promising raw material for production of bio-fuels. Qualitative comparisons of the pyrolysis products from both eugenol and anisole soot samples showed a clear difference significantly. The dominant pyrolysis products derived from eugenol soot are oxygenated compounds and this is due the high lignin content of the pyrolysis oil. Additionally, this work has been extended to consider high temperatures (400, 500, and 600°C and above) and still some of these species are present (222). However, pyrolysis of soot anisole is dominated by the formation of aromatics and saturated hydrocarbons. Decane soot, on the other side, presented a limited number of peaks corresponding to phenols, alkanes and amides. Perhaps, the presence of the nitrogen containing compound was due to a secondary reaction which occurred within the flame or afterwards. Further investigation of the sample above 300°C shows no significant peaks. Unlike decane, heptane soot showed significant peaks. Obviously, low temperature combustion promotes

understanding of the mechanism of soot formation in the diffusion flames of both biomass pyrolysis oil and some hydrocarbon fuels.

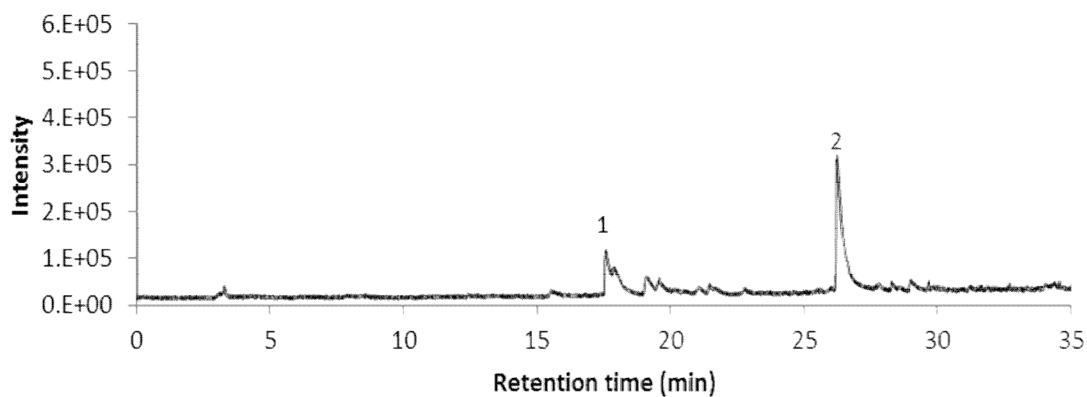


Figure 4- 11 Py-GCMS chromatogram of eugenol soot (5cm) adsorbed at 300°C

The key markers are 1: phenol, 2: pentadecanoic acid,

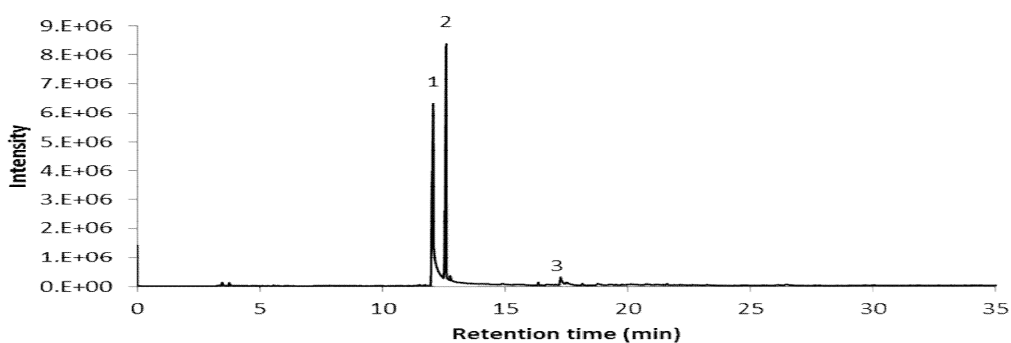


Figure 4- 12 Py-GCMS chromatogram of eugenol soot (10cm) adsorbed at 300°C

Key 1: furfural, 2: benzene methoxy-, 3: 1-ethenyl-3-methyl styrene, this is for only the three prominent peaks but there are traces of complex phenols.

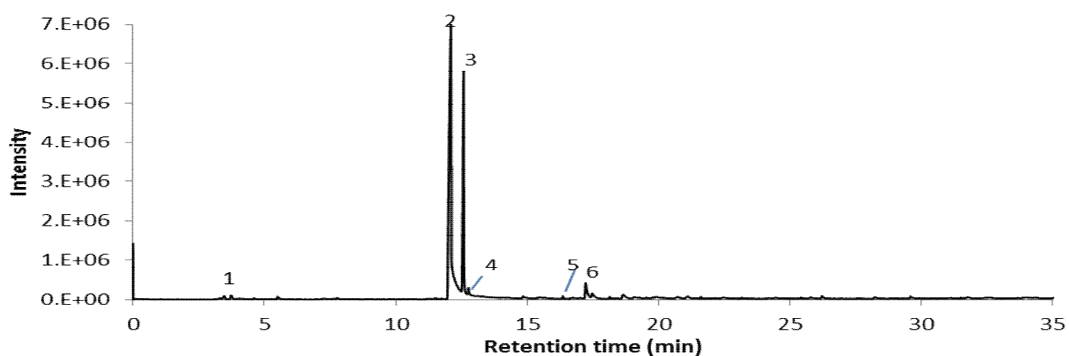


Figure 4- 13 Py-GCMS chromatogram of eugenol soot (15cm) adsorbed at 300°C

The volatile fragments generated are 1: not identified, 2: furan carboxaldehyde, 3: Phenol, 4-, 6 – dimethyl, 4: benzene methoxy-, 5: benzene, 6: 1-methyl, phenol-

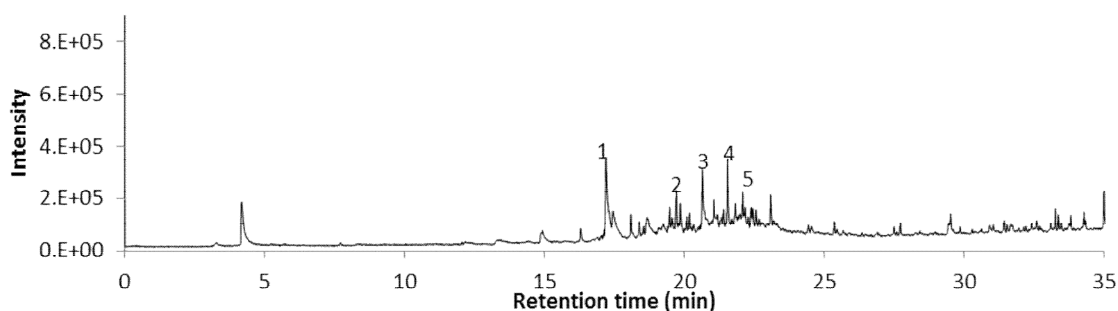


Figure 4- 14 Py-GCMS chromatogram of anisole soot (5cm) adsorbed at 300°C

The key markers are 1: benzene, 2: 2,3-dimethylbenzene-1 4-diol 3: naphthalene, 4: 2, 3-di methyl, naphthalene, 5: 2-phenyl naphthalene, other peaks are mainly complex phenols

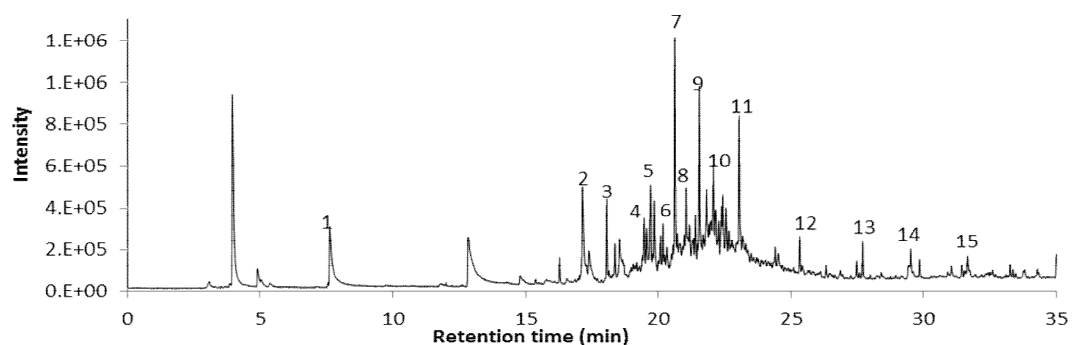


Figure 4- 15 Py-GCMS chromatogram of anisole soot (10cm) adsorbed at 300°C

The volatile moieties includes 1:L-proline, 5-oxo-methyl ester, 1:1-ethenyl-3-ethyl styrene, 3: dodecane, 4: decane-5- propyl, 5: tridecane -3-methyl, 6: dodecane 2, 6, 11, trimethyl, 7: n-hexadecane, 8: pentadecane 2, 6, 10 trimethyl, 9: hexadecane-3-methyl, 10: nonane 3 methyl-5 propyl, 11: decane 3, 8-dimethyl, 12: Octacosane, 13: Heptadecanal 2, 6, 10, 15,-tetramethyl, 14: octadecanol, 15: tetradecane, 15: phenanthrene, 14: pyrene, 15: fluoranthrene,

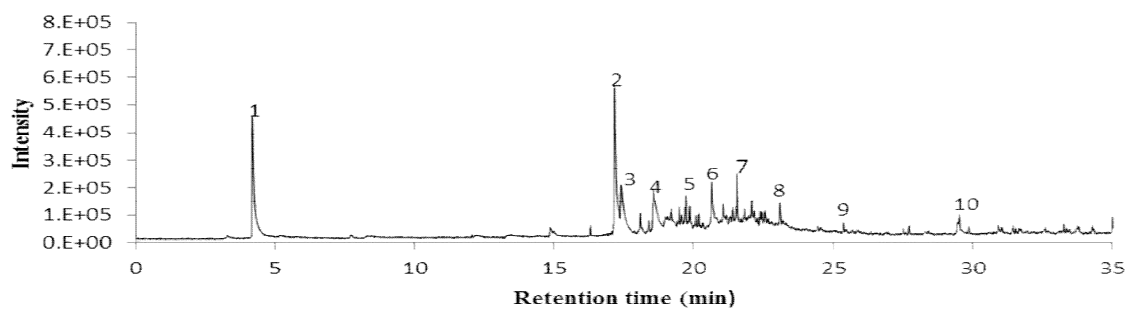


Figure 4- 16 Py-GCMS chromatogram of anisole soot (15cm) adsorbed at 300°C

The volatile species detected are 1: L-proline, 5-oxo-methyl ester, 2: 1-phenyl-1-butene, 3: dodecane 2, 6, 10 trimethyl, 4: tridecanol, 5: nonadecane, 6: diphenyl ethyne, 7: tetradecanol, 8: tritetracontane, 9: naphthalene, 10: pyrene,

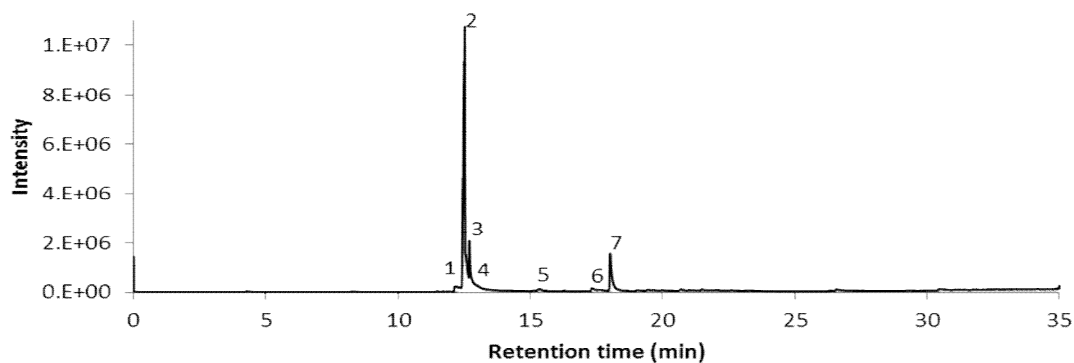


Figure 4- 17 Py-GCMS chromatogram of n-decane soot (5cm) adsorbed at 300°C

Adsorbed volatiles are 1: furfural, 2: octane 3, 5 -dimethyl-, 3: Benzene, methoxy-, 5, 6, 6-trimethyl-heptane-3-yne-2,5-diol, 5: tridecane , 6: methyl, benzene, 3-ethyl-, 7: dodecane.

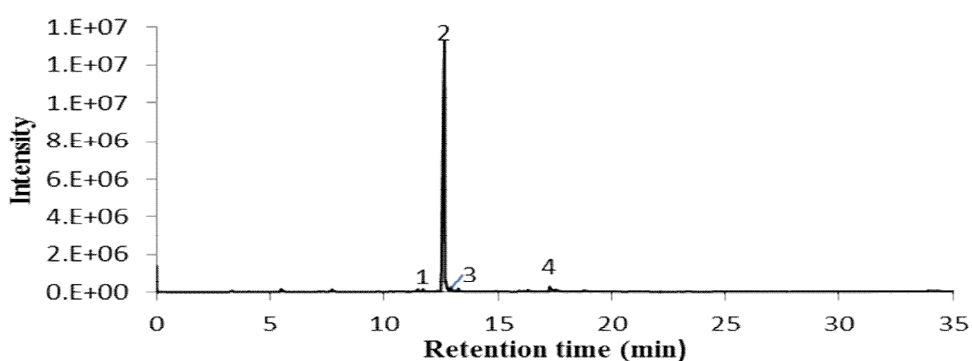


Figure 4- 18 Py-GCMS chromatogram of n-decane soot (10cm) adsorbed at 300°C

1. Phenyl hydrazine, 2: octane 3, 5-dimethyl-, 3: trans -3-decene. 4. Not known. The tiny peaks indicate complex phenols and acids

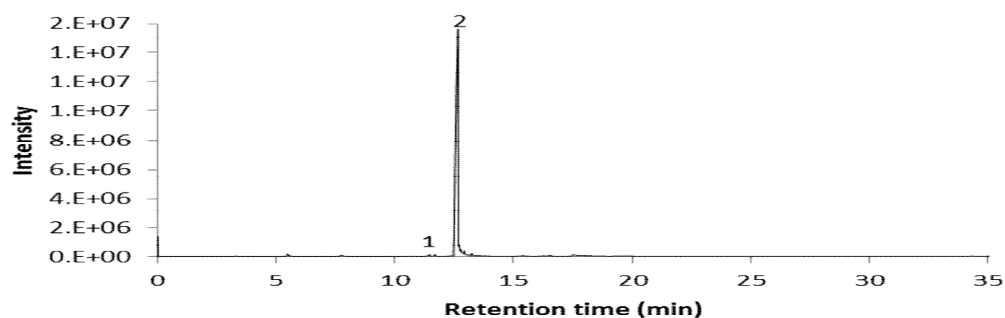


Figure 4- 19 Py-GCMS chromatogram of n-decane soot (15cm) adsorbed at 300°C

1: tetracontane, 3, 5, 24-trimethyl- 2: pentanol, 4-methyl-2-propyl, 3: squalene.

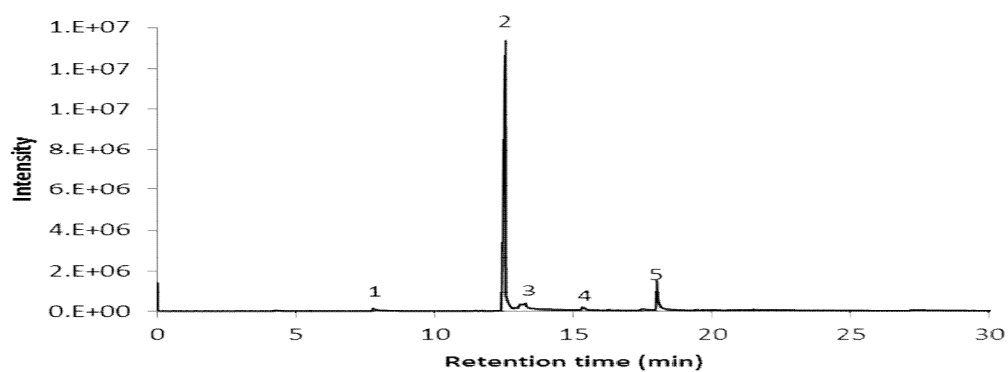


Figure 4- 20 (a) Py-GCMS chromatogram of n-heptane soot (5cm) adsorbed at 300°C

1. benzene, hydroxyl-, 2. Dodecane, 3. anisole, 4: decane, 2,3,5,8-tetramethyl-, 5. Benzene, 1-ethenyl-3-ethyl-styrene.

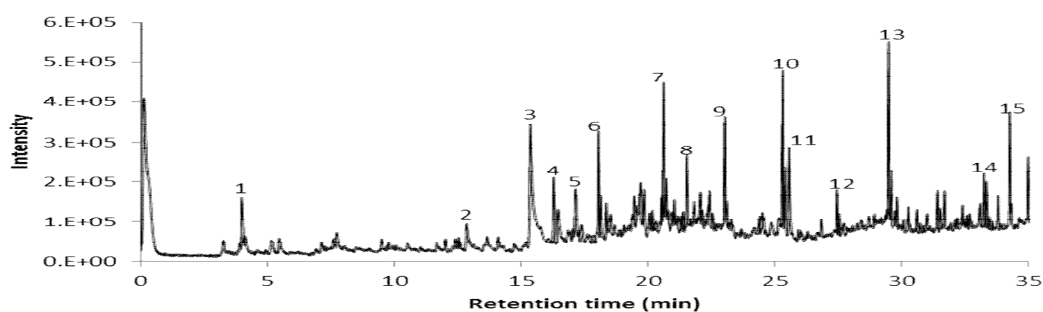


Figure 4- 21 Py-GCMS chromatogram of n-heptane soot (10cm) adsorbed at 300°C

1. cyclopropane acetic acid, 2. 1-heptanol, 2-propyl-, 3. hexadecane, 4. 3-octadecane, 5. undecanone, 6,10-dimethyl-, 6. tetradecanol, 7. Spiro[androst-5-ene-17, 1-cyclo-butan-2-one-3-hydroxy, 8. 7-hexadecanal [z], 9. ascorbic acid, 10. tetratriacontane. Others are complex oxygenated compounds.

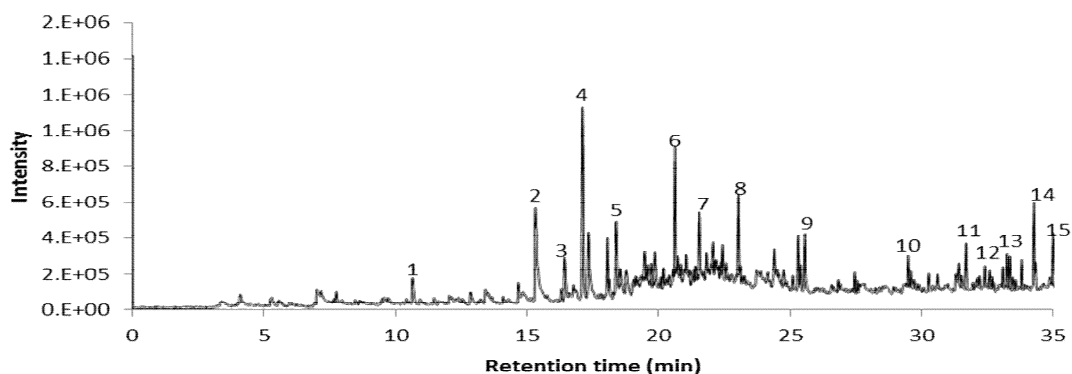


Figure 4- 22 (c) Py-GCMS chromatogram of n-heptane soot (15cm) adsorbed at 300°C

1. benzene-1-ethnlyl-, 2. 1-heptanol, 2-propyl-, 3. 1- octanol, 4. ethyl-iso-allochololate, 5. 7-hexadecyn-1-ol, 6. Pyrole, 8. 9-octadecanamide[z], 9. 2-pentacosanone, 10. 1-hexadecyne.

4.6.3 Discussion

The mechanism of formation of soot from the pyrolysis model fuels from wood and the hydrocarbon fuels, n-decane and n-heptane were studied. It was observed in these findings that model fuels, eugenol and anisole soot Py-GC-MS are very similar. This highlights the key important role of lignin decomposition products in the formation of soot in diffusion flames. However, further investigations have been conducted where real samples of wood (pine wood soot) and other pyrolysis fuel such as furfural are burned under controlled conditions in which the black carbon produced was analysed in the same way and the results show that furfural soot is more related to anisole during combustion and soot formation. Additionally, the higher VOCs and O-PAC content of soot at the 5cm sampling position in eugenol soot compares to the decane soot and this is due to surface oxidation observed in the eugenol flame (223). This indicated the oxygenated species of pyrolysis oil has a significant important role to play in the black carbon particle formation process and in the end products of generated soot particulates.

Generally, emissions, such as polycyclic aromatic compounds (PAC) from combustion of the fuel samples under investigation are very important to the health and environmental effects (223-225). It was found that biomass pyrolysis oil is an important source of polycyclic aromatics compounds (PAC), which is related to the environmental and health effects. However, in order to complete the data bank of emissions from the burning of the model and hydrocarbon fuels more experimental data from other model fuels is needed to make stronger conclusions.

4.6.4 Conclusions

Offline analysis of the soot particles generated from a wick burner was carried out using pyrolysis-gas chromatography mass-spectroscopy for VOCs, PAC and O-PAC investigations. Soot from n-heptane and n-decane produce simple chromatograms and species such as

hydrocarbons and simple aromatics were detected upon desorption at 300°C. There was more OC on the n-heptane soot particles sampled at 10 and 15cm.

Soot from model lignin decomposition products, eugenol and anisole, had adsorbed benzene and phenol derivatives. This indicates that the importance of these species in the soot production mechanisms derive biomass combustion. DMS results showed some differences between the soots from the four fuels, sampled at different flame heights above the flame. The hydrocarbon fuels soot agglomerates are generally smaller than those from anisole and eugenol. Eugenol, in particular, gave a wide distribution of agglomerates close to the flame and this distribution became narrower as sampling height above the flame increased. The results can be interpreted in terms of soot agglomeration vs oxidation rates.

4.7 Elemental analysis of soot fuel properties and burning characteristics

Ultimate analysis was determined by the C, H, N, S content of the samples using a CE Instruments Flash EA 1112 series elemental analyser. The results from the proximate analysis were used to calculate the elemental composition on a dry ash free basis. The details of the sample preparation and sample running as well as the basic principles governing the instrument have been described in the chapter 3.

4.7.1 Results and discussion

The CHNO analysis are presented in Table 4-5 and the HC vs OC molar ratios displayed in Figure 4-23

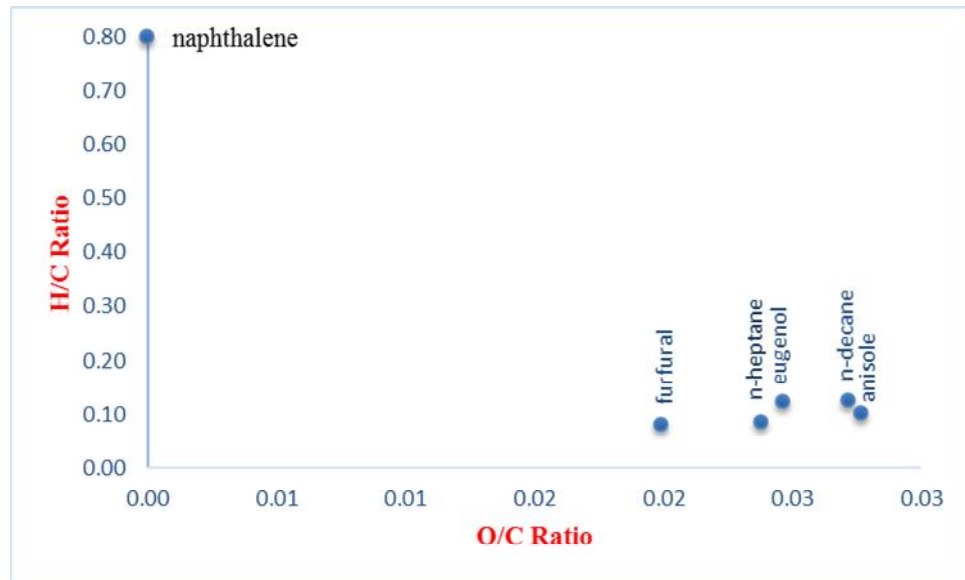


Figure 4- 23 Van Krevelen analysis of soots showing hydrogen /carbon to oxygen carbon ratio generated from the model fuels

Table 4- 5 shows the elemental analysis of the model fuels pyrolysis products (soot) generated from a wick burner : The HHV was calculated using the *Dulong formula* [105].

S/N	Fuel	Nitrogen (%)	Carbon (%)	Hydrogen (%)	Oxygen (%)	H/C Ratio (mass)	O/C Ratio(mass)	GCV (MJ/Kg)	NCV (MJ/Kg)	H/C Ratio(mole)	O/C Ratio (mole)
1	Naphthalene 1	0	93.7	6.29	0	0.067	0	0	0	0.800	0
2	Naphthalene 2	0	93.7	6.29	0	0.067	0	0	0	0.800	0
3	soot eugenol 1	1.44	94.3	0.9	3.37	0.010	0.036	8002	7954	0.114	0.027
4	soot eugenol 2	1.46	94.7	1.06	2.83	0.011	0.030	8078	8021	0.133	0.022
5	soot furfural 1	1.56	95.0	0.65	2.82	0.007	0.030	7983	7948	0.082	0.022
6	soot furfural 2	1.39	95.7	0.65	2.23	0.007	0.023	8046	8011	0.081	0.017
7	soot n-decane 1	1.5	94.2	0.8	3.47	0.008	0.037	7968	7925	0.101	0.028
8	soot n-heptane 2	1.51	94.8	0.69	3	0.007	0.032	7979	7943	0.087	0.024
9	soot anisole 1	1.55	94.5	0.9	3.01	0.010	0.032	8023	7975	0.113	0.024
10	soot anisole 2	1.42	93.7	1.1	3.79	0.012	0.040	8012	7953	0.140	0.030

Figure 4-23 shows the Van Krevelen analysis of the soot samples based on the elemental analysis. Surprisingly, all the soots (a part from that from naphthalene standard) fall in similar range (H/C 0.08-0.13, O/C 0.017 – 0.03). However, it was noted in Section 4-4 that all the soots from the wick burner were > 95% EC. Thus, the H/C: OC ratios are dominated by the EC content.

4.8 Model fuel burning rate, emission factors and morphological structure of soot and its formation mechanisms

4.8.1 Introduction

Wood is a widely used fuel and the formation of smoke from its combustion in small scale domestic, commercial and industrial heating units presents a major health hazard (196). Together with the effects of wild fires it is also a global environmental problem (226). The emission of black carbon (BC) and organic carbon (OC) and the ratio of BC/OC is important.

The general mechanism of biomass combustion has been extensively studied for a number of years. The cellulose and lignin components can be considered separately (116, 201) and the cellulose decomposes readily at high temperatures to CO and H₂ together with some small molecules; the lignin element decomposes to give much more complex products. We have recently proposed that the cellulose products can eventually form smoke largely via the HACA route and the lignin decomposition products form smoke via an aromatic species mechanism (116, 199).

Both hard and soft woods give similar devolatilization products although the distribution of the products is different, this resulting from the differences in the hemicellulose and lignin content. GC-MS analysis shows that the principal initial volatile decomposition products of pine, soft wood, include carbohydrate-derived material such as levoglucosan. At higher temperatures the guaiacols, syringols and furans begin to decrease and complex thermally stable cyclic oxygenates are formed and polycyclic aromatic compounds (PAC) become significant species. Some of the

dominant primary products are now furfuryl alcohol, furfural, and levoglucosan from the cellulose, and eugenol, isoeugenol, vanillin and guaiacols from the lignin. Furfural (furan-2-carbaldehyde) has been taken to be a typical product associated with cellulose pyrolysis and eugenol (4-allyl-2-methoxyphenol) to be associated with lignin. Previous studies have been made of the formation of smoke and PAH arising from the combustion of these compounds using an atmospheric time of flight mass spectrometry (ATOFMS) (202, 203). In the present study we have extended earlier work (202-204) to consider the processes leading to the formation of particulate soot.

This Section is primarily concerned with an investigation of the formation of soot from the combustion of some of the primary pyrolysis products formed during pine wood combustion. Comparisons are made between the combustion products of model compounds (furfural for cellulose, eugenol and anisole to represent lignin; and n-decane for comparison) with the smoke emissions from the previously studied combustion of pine wood. These compounds were burned in a wick burner and the appearance and composition of the resulting particulate were studied by TEM. The adsorbed PAH precursors were studied by mass spectrometry and Py-GC-MS as discussed earlier. It is concluded here that wood soot formation proceeded via pyrolytic breakdown followed by a mechanism based on HACA reactions with the participation of cyclopentadienyl intermediates, while eugenol soot originated predominantly through the CPDyl route. The formation of furfural soot is mainly via HACA.

4.8.2 Material and methods

The analytical methods employed in this section have been previously described in the previous chapter 3.

4.8.3 Analytical technique

4.8.3. Design of thermophoretic soot sampling device and testing

A high speed soot sampling system was developed in order to collect samples for Transmission Electron Microscopy (TEM), as shown in Figure 4-24.

The soot sampling system allows rapid and controlled collection of soot at different flame heights. The set-up comprises of a wick burner as a source of flame and TEM grid holder. The grid holder is attached to a compressed air driven piston.

A magnetic control system is used.

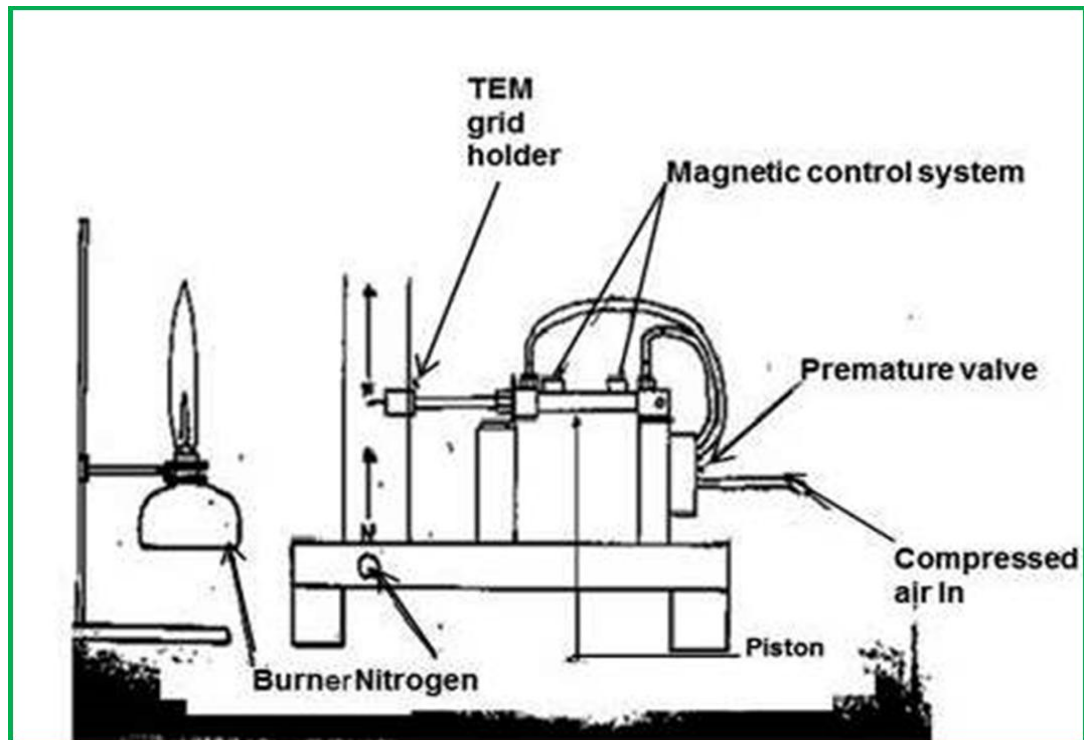


Figure 4- 24 Schematic diagram of soot sampling device

4.8.4 Results and discussion

4.8.4.1 Scanning electron microscopy

Soot samples were obtained by deposition on a plate placed 5cm above the flame using the method previously used before for ethylene flames (227) and was also described in chapter 3 of this thesis. It was clear that there were two significantly different classes of deposits. The hydrocarbons, n-heptane and n-decane, gave dense sooty deposits similar to that found previously from ethylene flames, as did the furfural flame. The anisole and the eugenol flames produced greater yields of fluffy cotton-like soot aggregates typical of soot from benzene pyrolysis or flames (228). These samples were examined by SEM and the first group consisted of spherical samples of about 20-40 nm diameter. The second group which overall was cotton-like actually consisted of clusters of chains of spherical particles with diameters of individual soot particles of about 40-60 nm. These clusters are fragile and an example of such a deposit is shown in Fig 4-25.

SEM images of biomass pyrolysis oil soot (Figure 4-25a, c and d) have similar topography to hydrocarbon soot, the soot particles in decane soot appear to be smaller than the other soots. Analysis of the Figures 4-25 by electron microscopy showed particle sizes typically in the range of 10nm- 60nm. These particles had agglomerated to form chains, consistent with the larger particle sizes observed by DMS analysis.

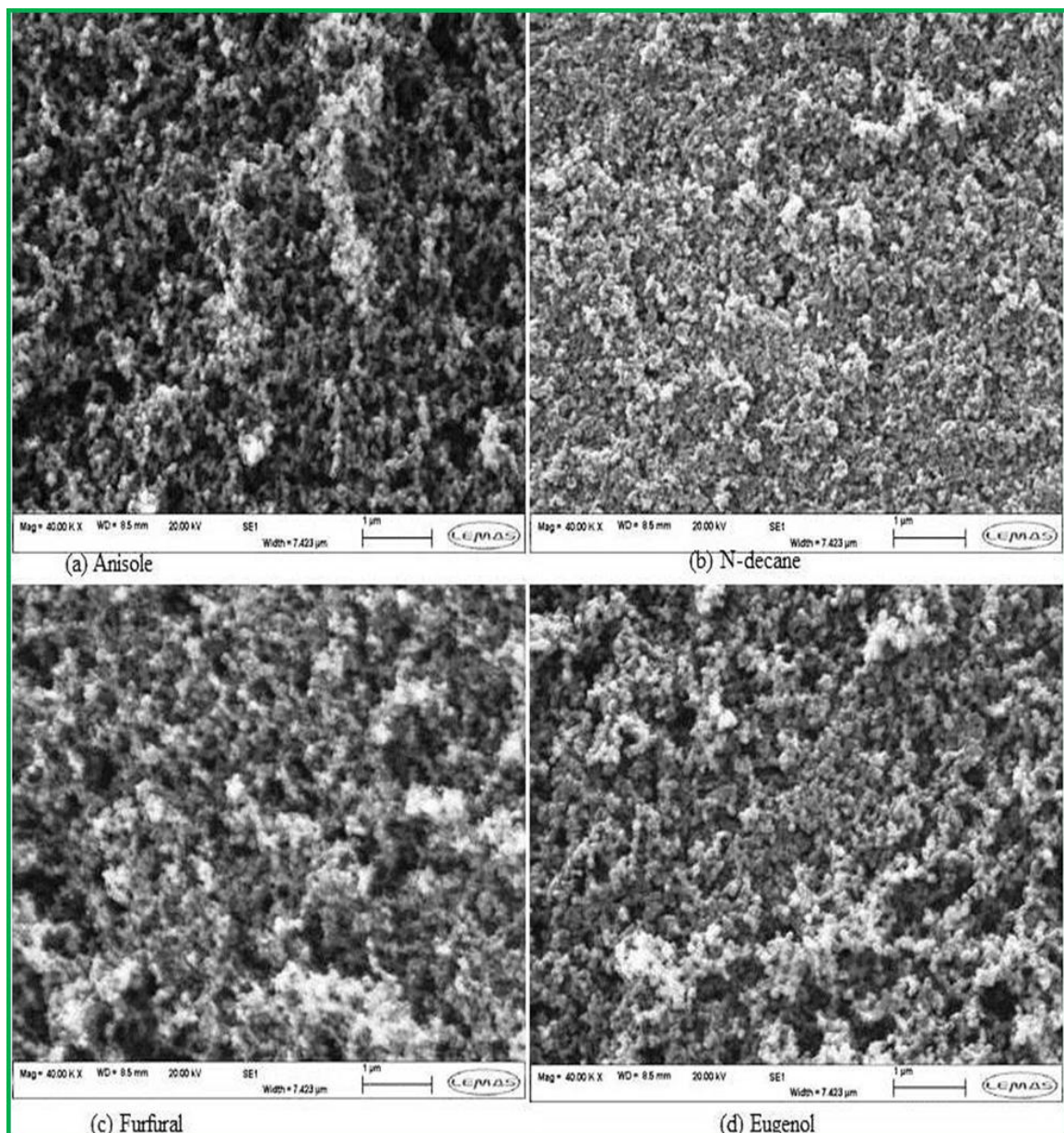


Figure 4- 25 Scanning electron microscopy (SEM) images of soots deposited on glass slides of diffusion flames for (a) anisole (b) n-decane (c) furfural and (d) eugenol.

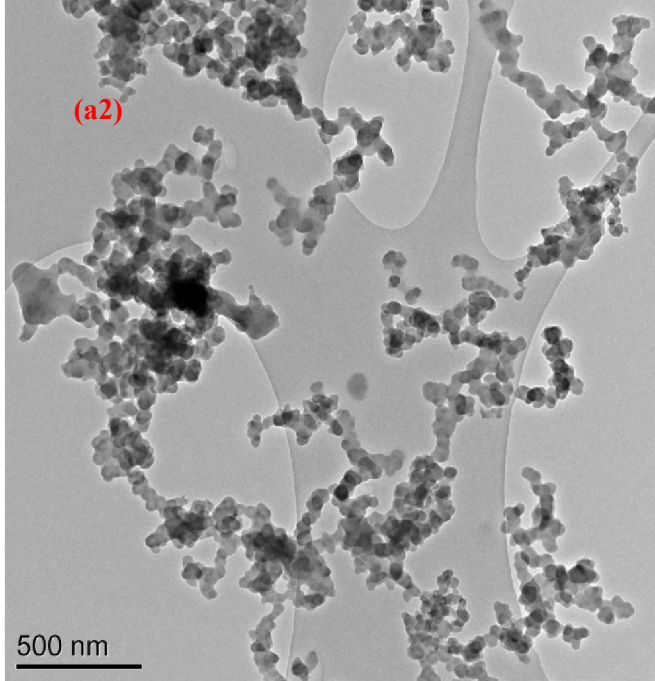
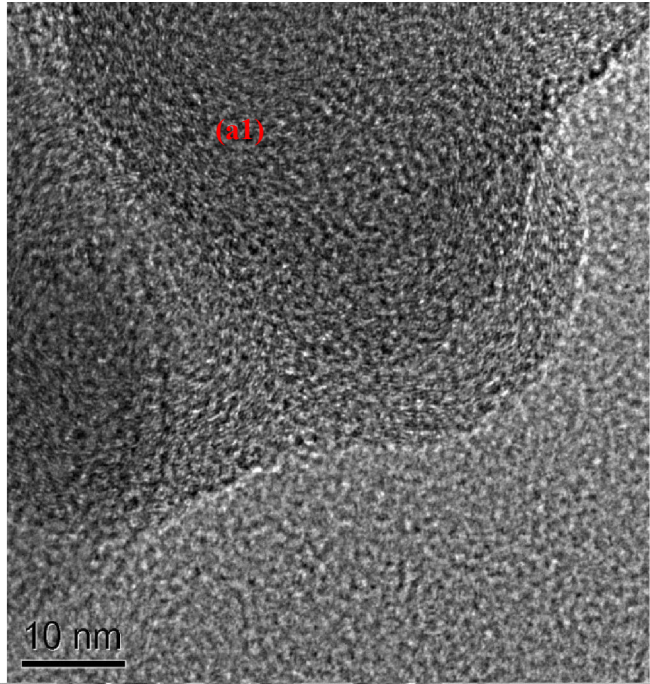
4.8.4.2 Transmission electron microscopy

Samples of newly formed soot particles were withdrawn by an electron microscope grid from inside the flame (10 mm above the wick) and examined via transmission electron microscopy TEM. Table 4-6 shows the measured average particle diameters as measured for the different soots from analysis of the TEM micrographs.

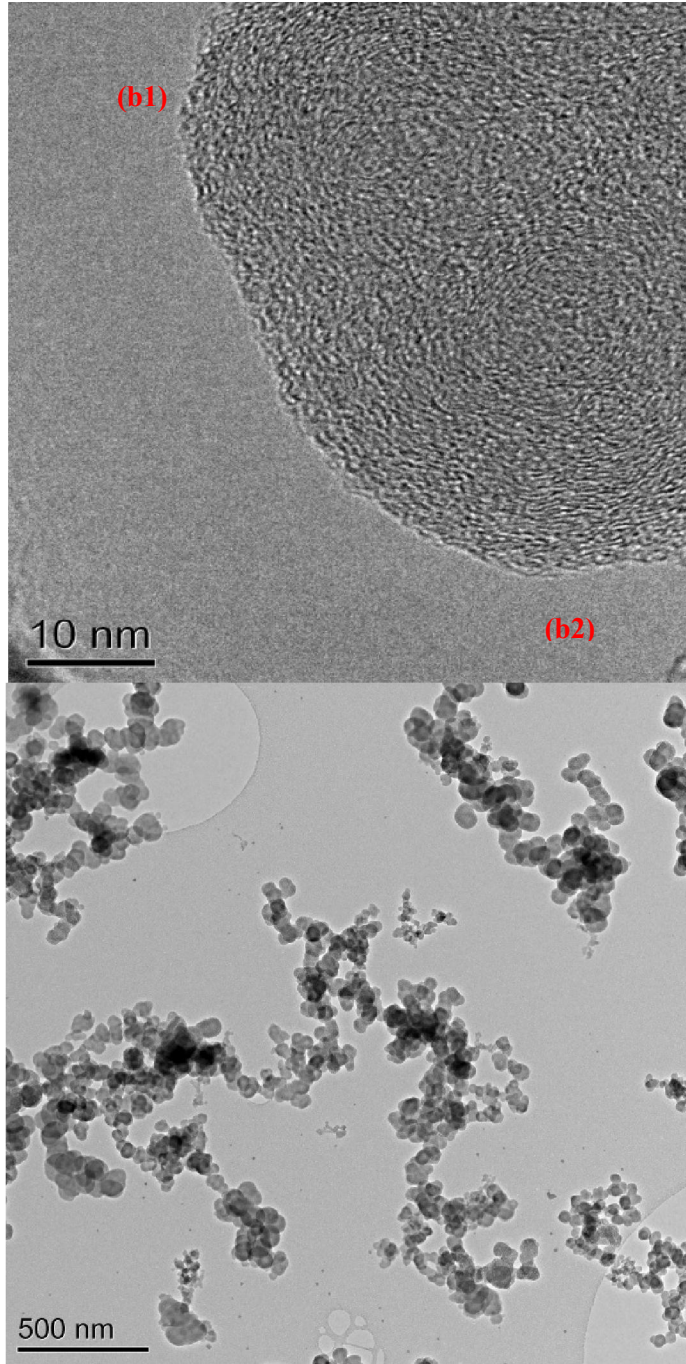
Table 4- 6 Average particle size (Dp) from TEM images using ImageJ

Samples	Average particle size (μm)	Particle size range (nm)
n-decane soot	0.0202	10-25
n-heptane soot	0.01	10-35
anisole soot	0.025	20-25
eugenol soot	0.03	20-30
furfural soot	0.019	15-20

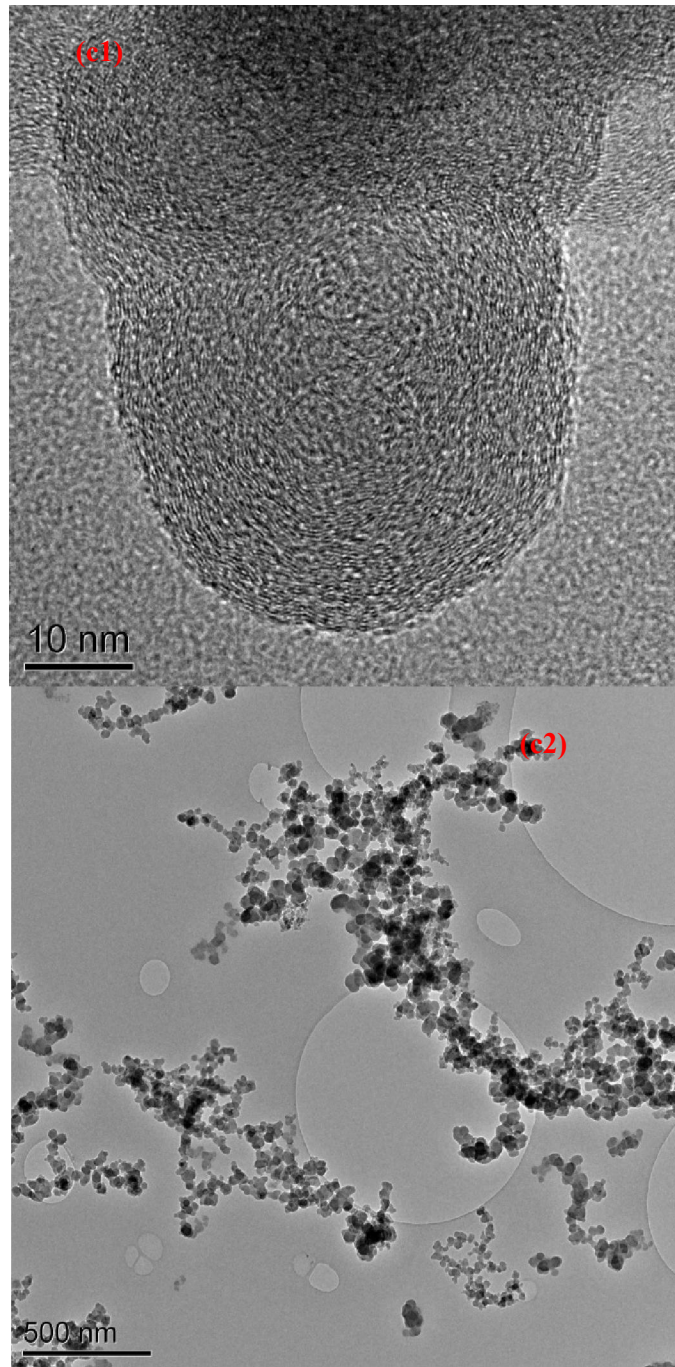
At the base of the flame the particle diameters were about 10-15 nm in diameter for the eugenol flame, increasing in size with reaction time to the exit particle size stated above of 40-60 nm. An example is shown in Fig. 4-26(a) for a sample withdrawn in a mid-position in the flame. Particles from furfural were similar but soot particles from pine smoke tended to be larger.



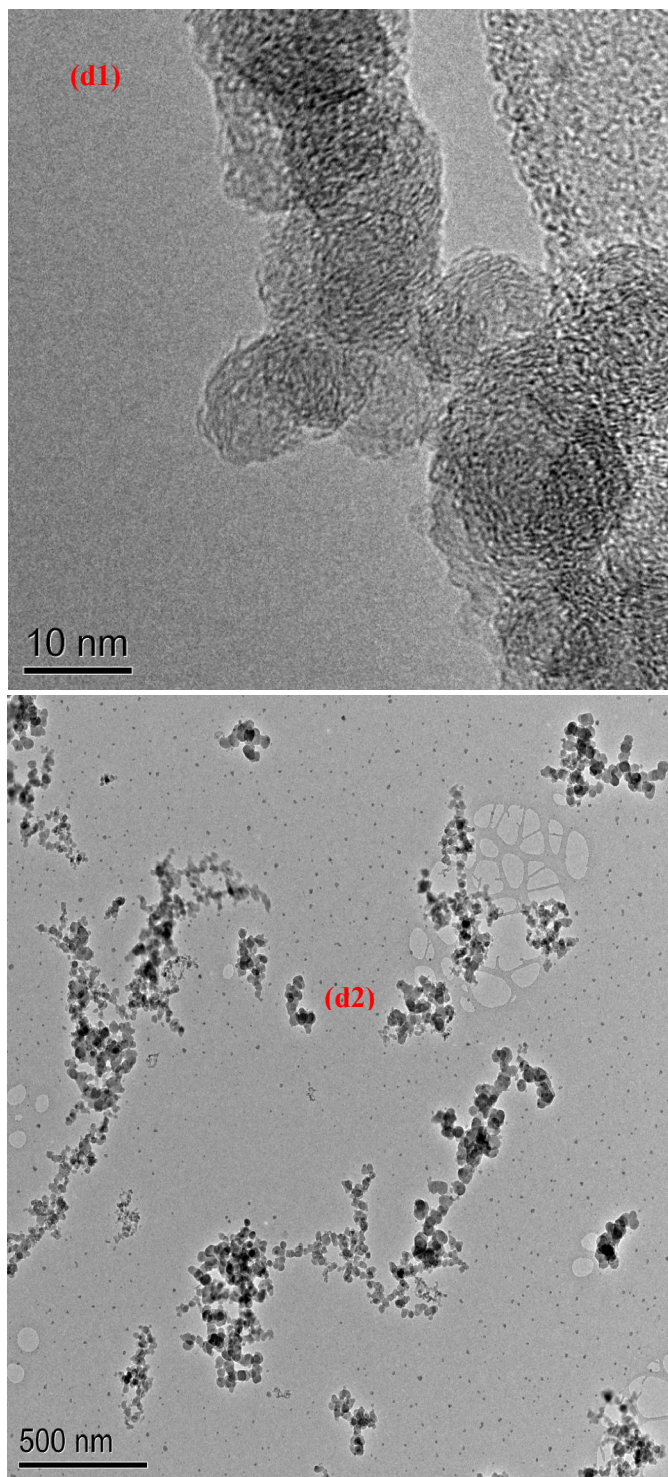
Anisole



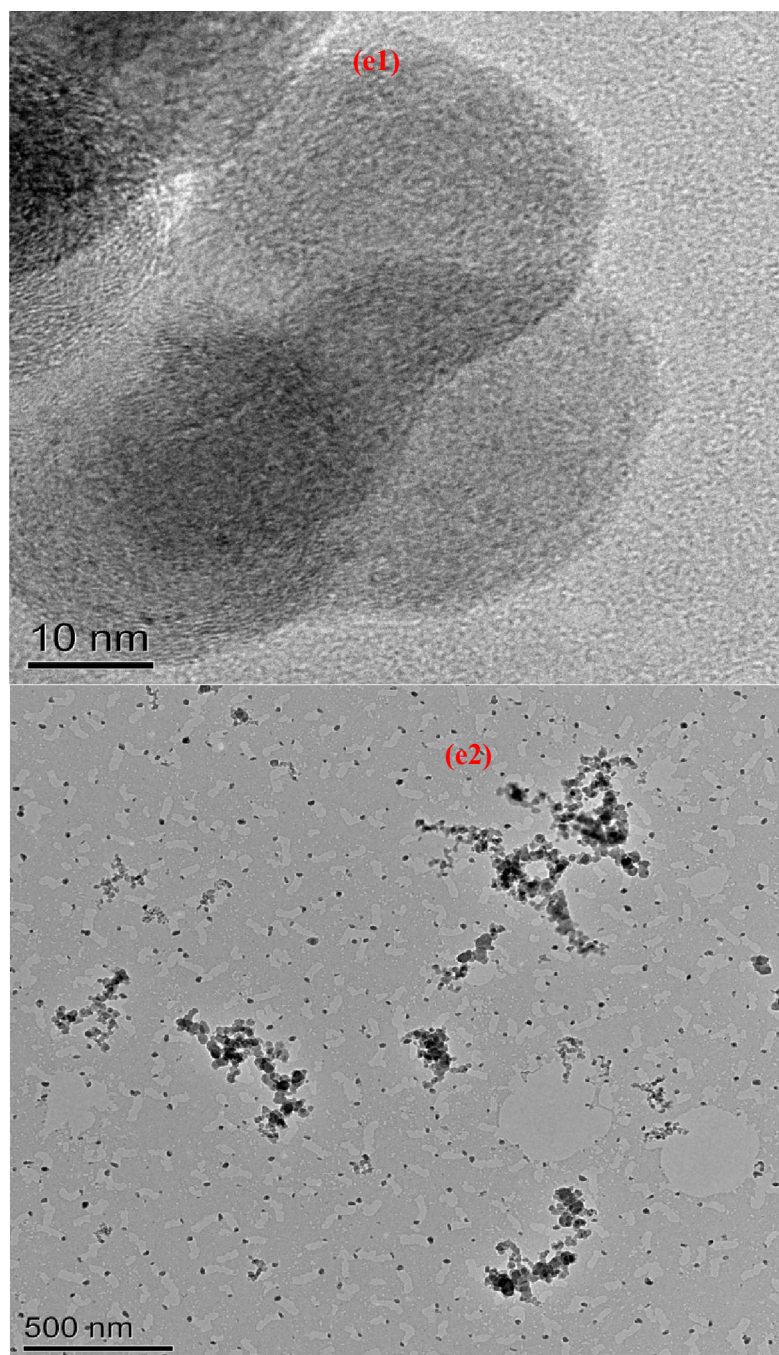
eugenol



furfural



n-decane



n-heptane

Figure 4- 26 TEM micrographs of (a1-2) anisole, (b1-2) eugenol, (c1-2) furfural, (d1-2) decane and (e1-2) heptane

TEM images of soot (Figure 4-26) from the diffusion flames of the biomass pyrolysis oil (anisole, eugenol and furfural) were compared with the hydrocarbon fuels (decane and heptane). Additionally, preliminary work showed the degree of disorder within the soot. Nano structural composition becomes more disordered with increase in oxygen content of the parent fuel. This is consistent with the results found by Vander Waal and Mueller (2006). The hydrocarbon fuel

soot has discernible lamella which forms onion like concentric rings (Figs 4-26 c & d) at the same time biomass pyrolysis oil such as eugenol and anisole (Figs 4-26 a & b) have more disordered sections of lamella; the concentric rings are less visible. Interestingly, furfural soot shows a well-developed onion-like soot structure.

Image analysis using ImageJ software of the TEM micrographs for agglomerates revealed the characteristics particle properties of soot agglomerates for the model fuel as indicated in the Figures 4-27 – 31. Also Table 4-7 present these properties for all the fuel.

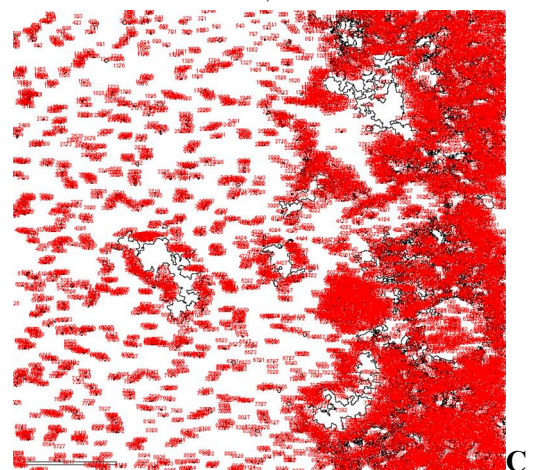
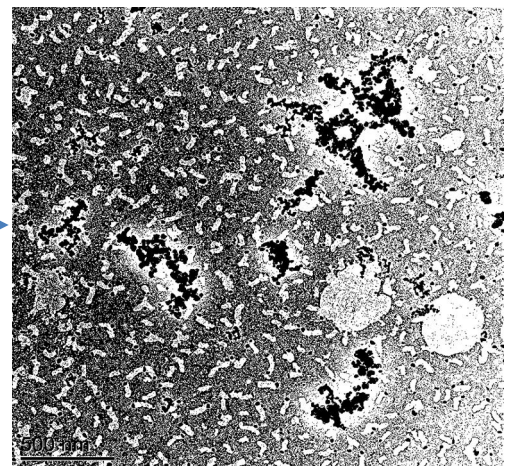
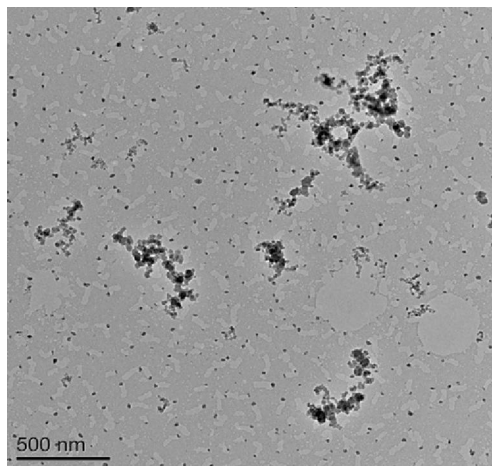
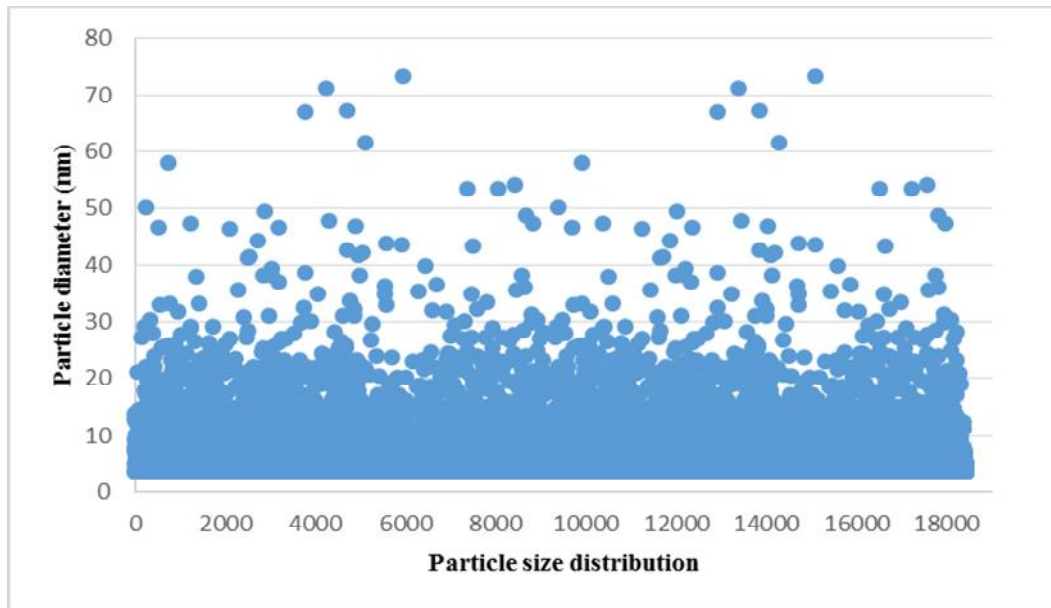


Figure 4- 27 Image analysis of Heptane soot TEM micrographs using ImageJ

(a) TEM of image of the agglomerates average particle size distribution, (b&c) are before and after analysis respectively.

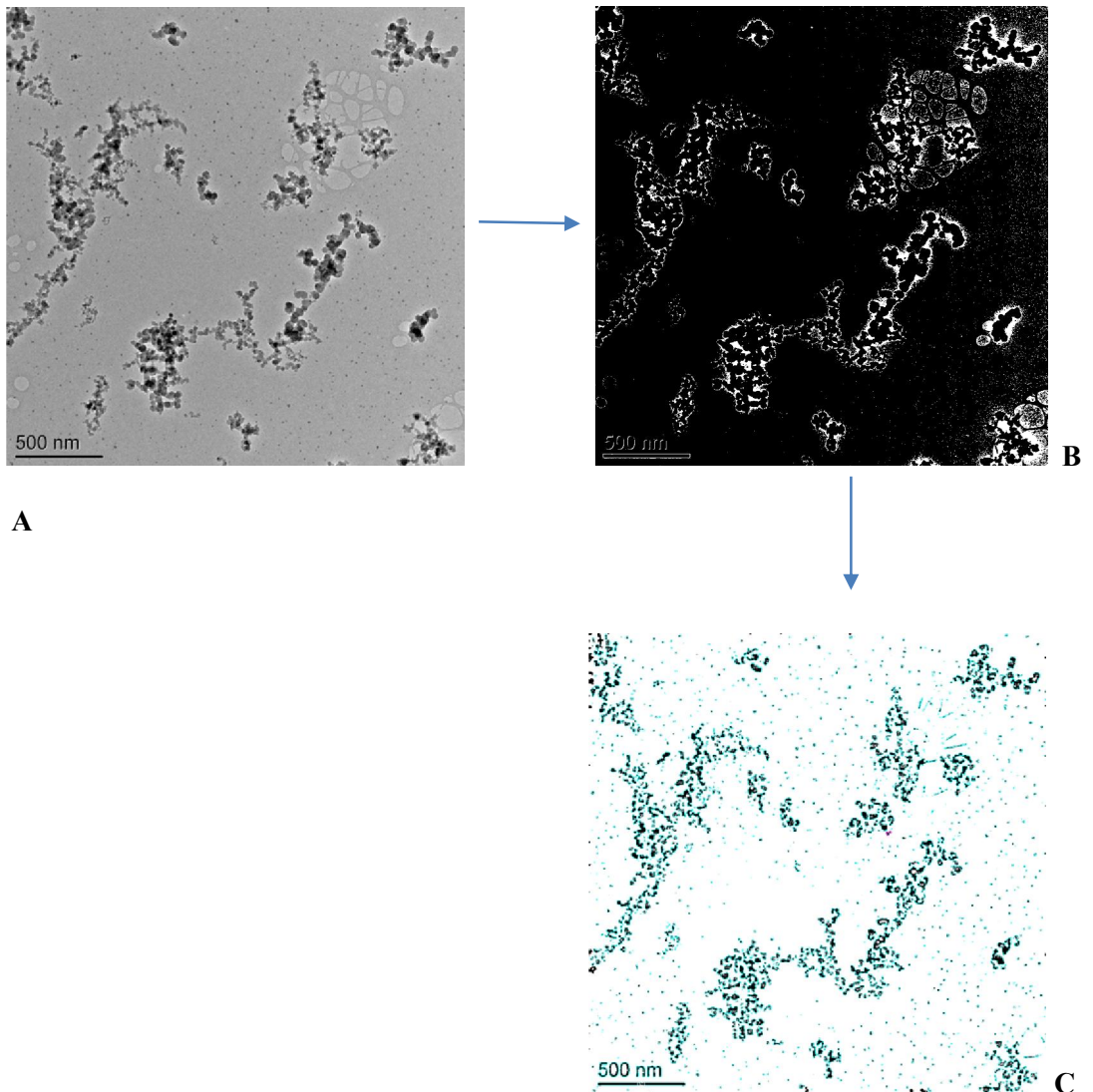
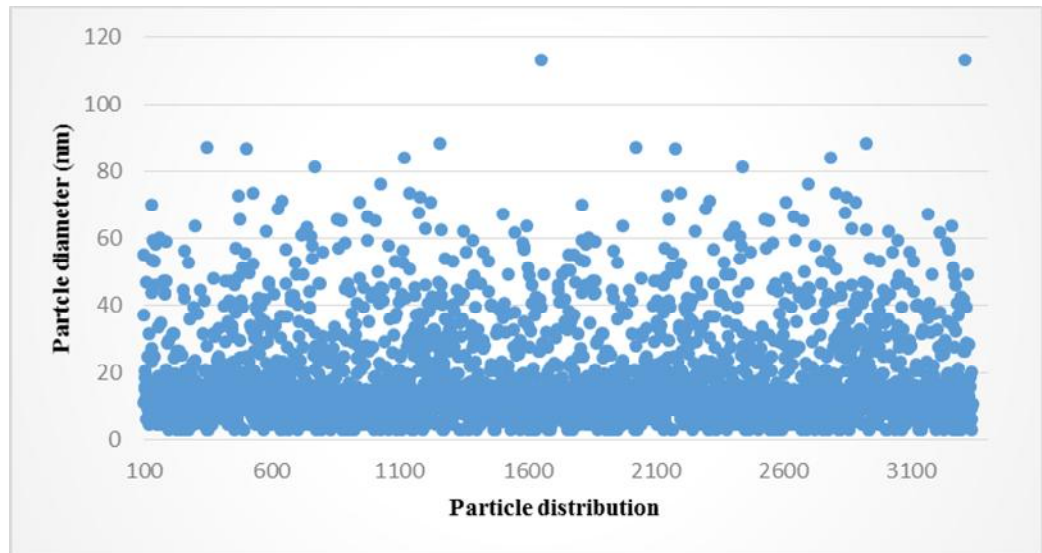
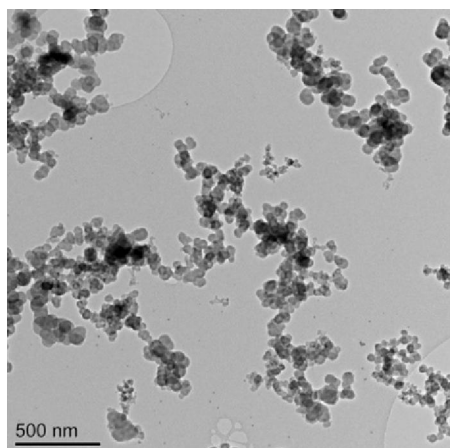
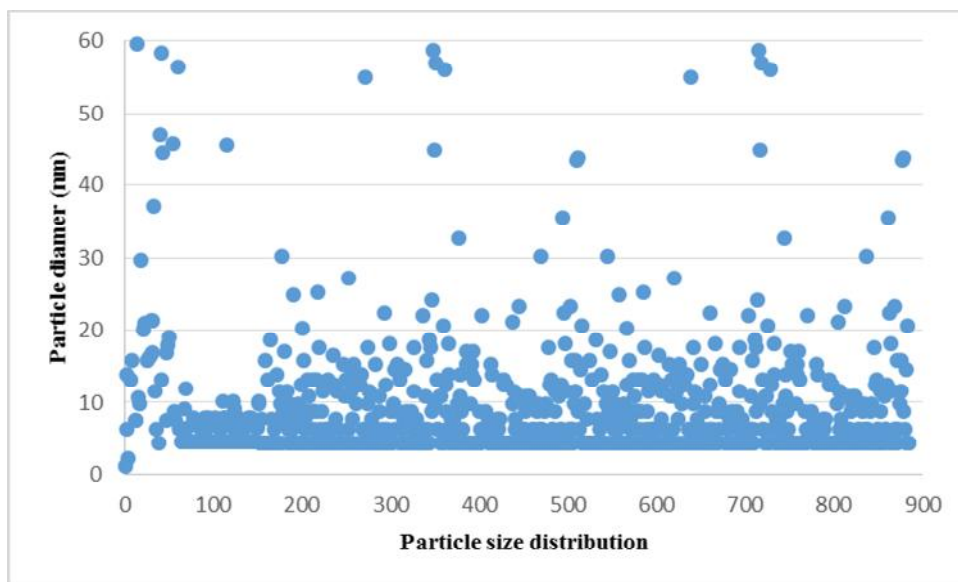
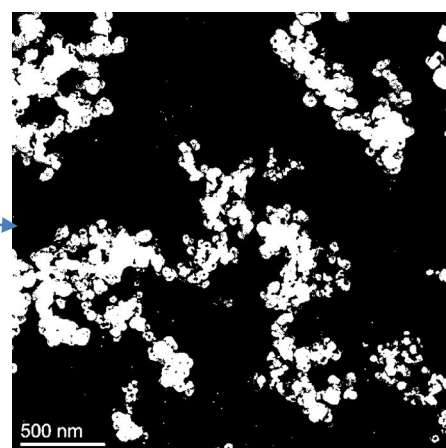


Figure 4- 28 Image analysis of Decane soot TEM micrographs using ImageJ

(a) TEM of image of the agglomerates average particle size distribution, (b&c) are before and after analysis respectively.



A



B

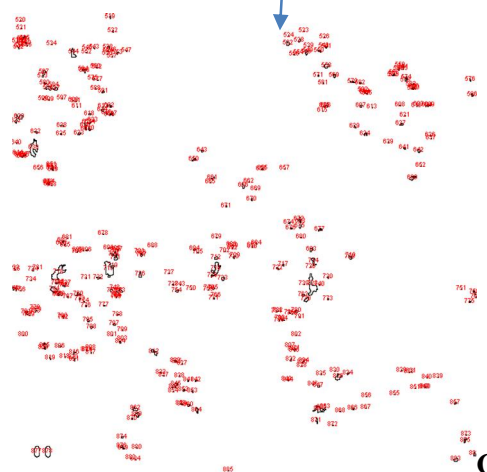


Figure 4- 29 Image analysis of Eugenol soot TEM micrographs using ImageJ

(a)-TEM of image of the agglomerates average particle size distribution, (b&c) are before and after analysis respectively.

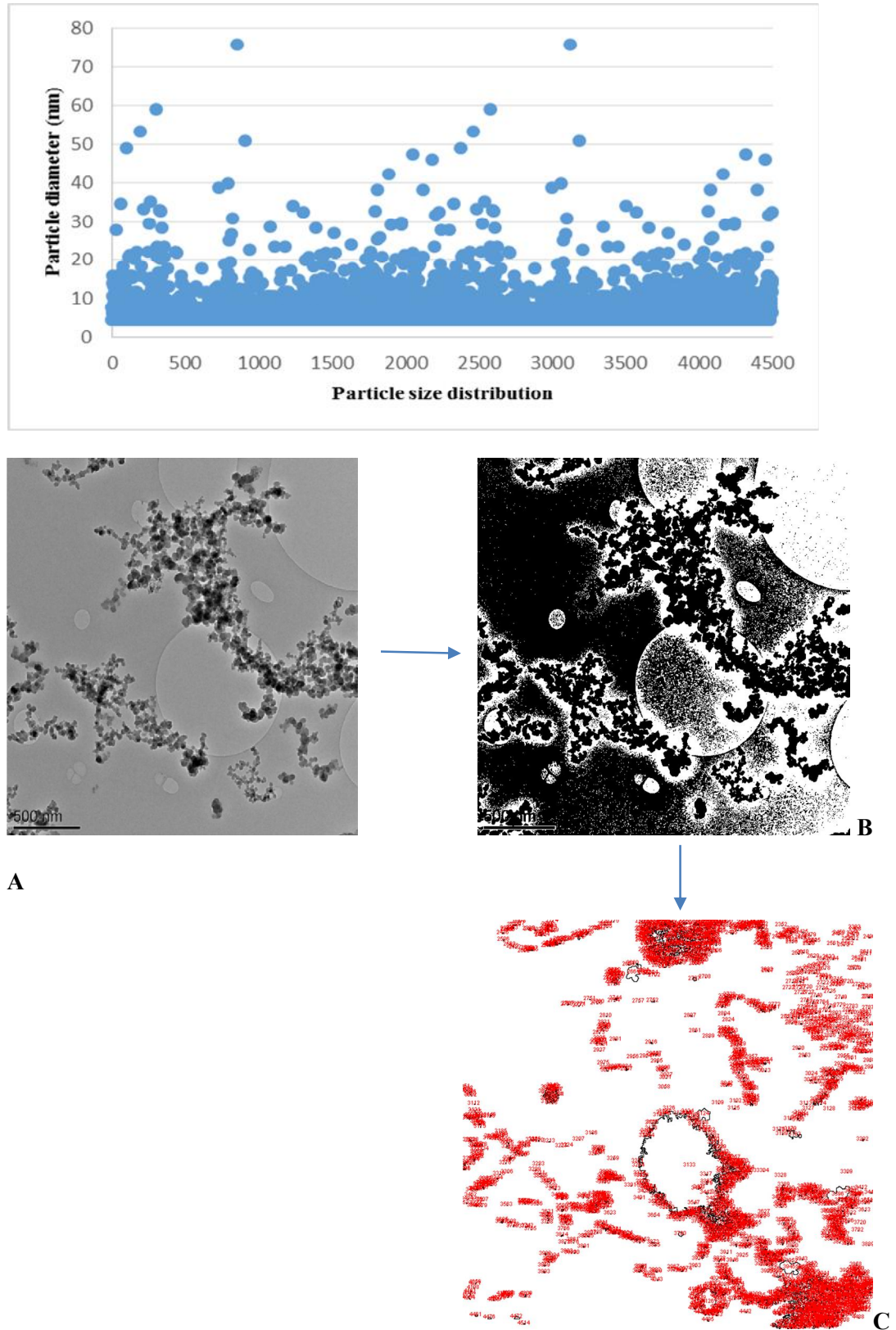
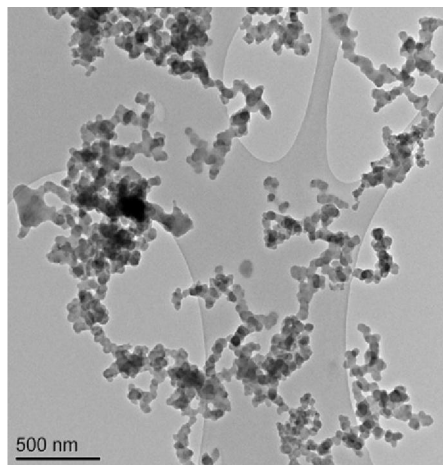
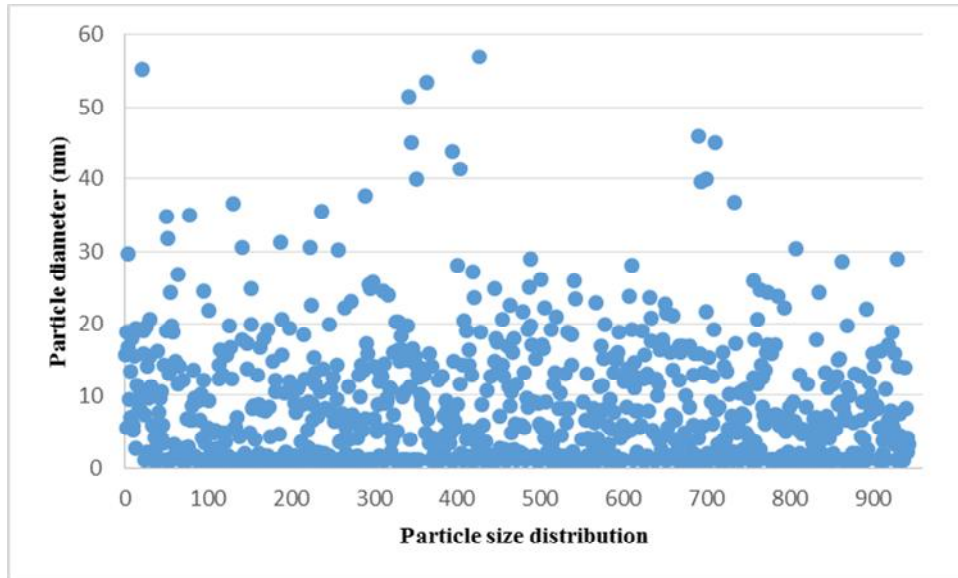
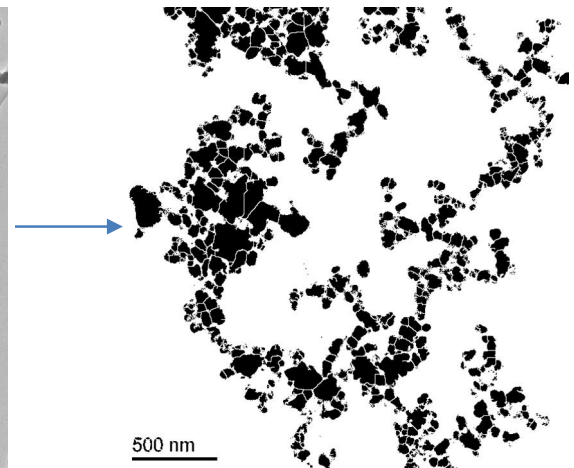


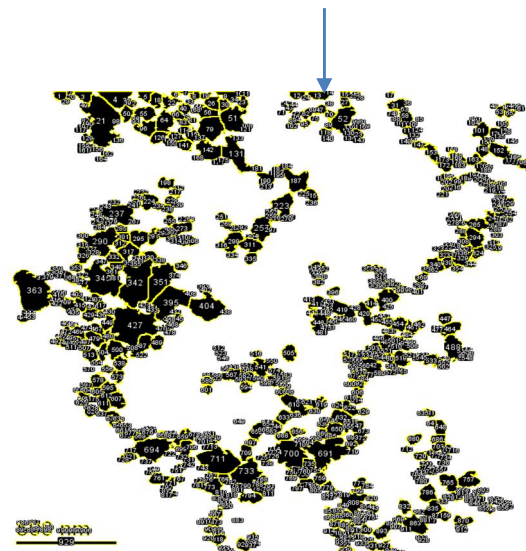
Figure 4- 30 Image analysis of furfural soot TEM micrographs using ImageJ
 (a)-TEM of image of the agglomerates average particle size distribution, (b&c) are before and after analysis respectively.



A



B



C

Figure 4- 31 Image analysis of anisole soot TEM micrographs using ImageJ

(a)-TEM of image of the agglomerates average particle size distribution, (b&c) are before and after analysis respectively.

Table 4- 7 Characteristic properties of soot particle agglomerates generated using ImageJ

Sample	Parameters	Avg. Particle size μm	Avg. Particle size range nm	Average particle size distribution nm
Heptane soot		0.01 \pm 0.01	10-35	2000 to 18000
Decane soot		0.0202 \pm 0.01	11-25	100 to 3400
Eugenol		0.03 \pm 0.01	20 – 30	100 to 900
Furfural soot		0.019 \pm 0.01	15-20	500 to 4500
Anisole soot		0.025 \pm 0.01	20-25	100 to 960

4.8.5 Flame photography of the combusted fuels

The flames were photographed by direct photography or using a 430 nm optical filter to give an indication of the CH* species [10], a marker of the main reaction zone, or with an optical filter at 520 nm to observe C2* emission.

4.8.5.1 Direct photography

Direct photography of the flames of the model fuels are shown in Figure 4-27. The yellow emission show soot particle formation zones of the flames

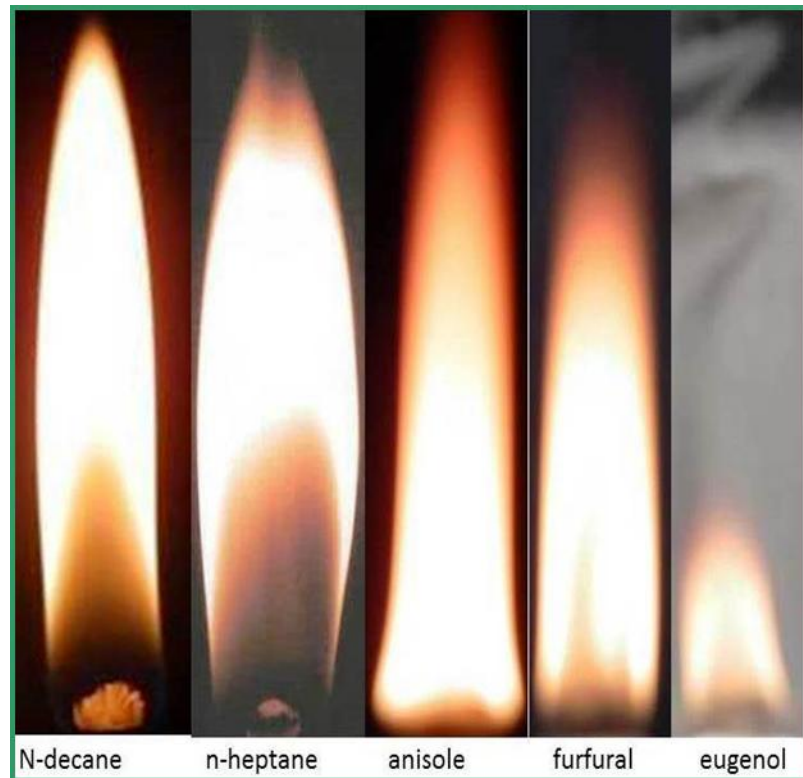


Figure 4- 32 Direct photography of flames for the model fuels

4.8.5.2 CH* emission from flames

Figure 4-28 show the CH* emission from the model fuel combustion flames. The CH* emission is considered to be the result of the $C_2H + O$ reaction and an indicator of the main reaction zone.

The position of the CH* is on the lean side of the combustion zone.

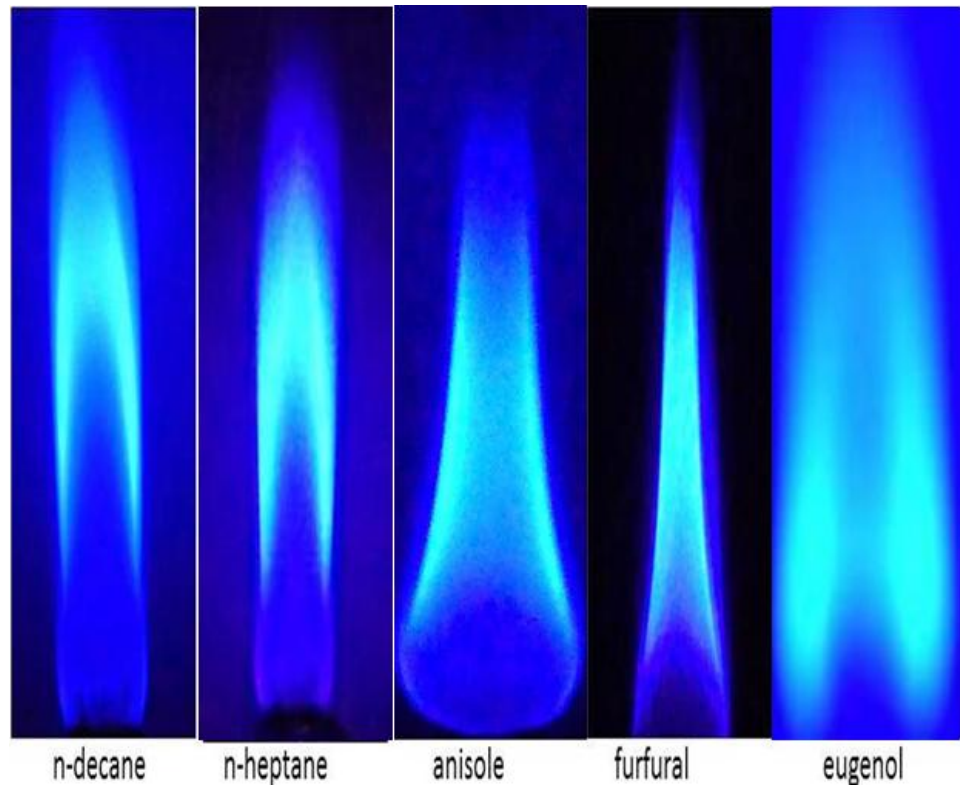


Figure 4- 33 CH* filtered flames for different oils using a 430 nm optical filter

4.8.5.3 C₂* emission from flames

C₂* emissions are an indication of the soot formation zone. A comparison of these flames show the relationship between the different reaction zones. The C₂* is on the lee rich side of the reaction zone as showed in Figure 4-29. This images also show the position of black carbon enveloped as indicated in the hydrocarbon flames.

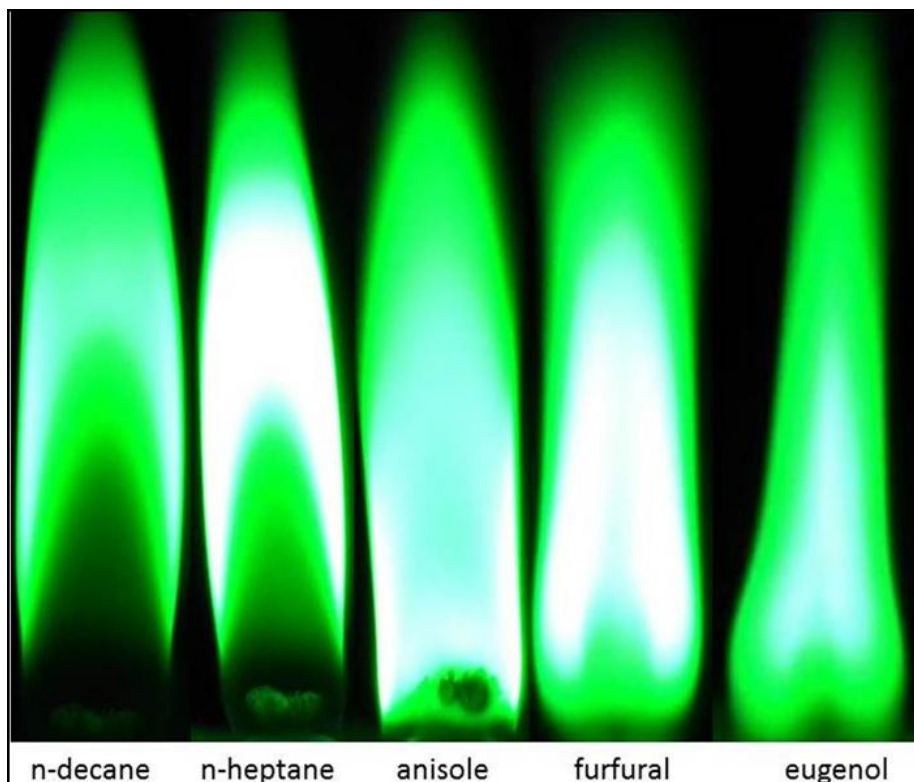


Figure 4- 34 C_2^* analysis of the soots of the pyrolysis oils using 520nm optical filter

4.8.5.4 Smoke point, mass burning rate and soot emission factor

Table 1 demonstrates the boiling point, smoke point, mass burning rate, carbon to hydrogen ratio and soot emission factor for all the fuels upon combustion.

It can be seen that, eugenol produces least smoke point value of 6.5 while n-decane has the highest value up to 27, indicating that n-decane produces less soot than the eugenol which was the highest soot producer.

Table 4- 8: Fuel properties and burning characteristics

Fuel	B pt °C	Smoke Point (mm)	Mass burning rate, mg/s	C/H ratio	Emission factor mg soot/ gfuel
n-heptane	98.4	13.5	4.6	0.44	0.25
n-decane	174.1	27.0	5.4	0.45	0.18
furfural	161.7	16.0	4.8	1.25	27.0
anisole	154	11.0	4.7	0.875	17.1
Eugenol	254	6.5	1.4	0.83	132.2
furfural/eugenol 50/50	-	12	3.1	-	52.2

Measurement using the laser induced incandescence showed extent in n-decane, anisole, and furfural flames particle sizes were in the range of 35-50nm across the flame. The soot volume fraction was about 1×10^{-6} except for anisole which was 0.2×10^{-6} . There are considerable errors have due to flame movement particularly for eugenol which is not induced.

4.8.6 Discussion

The flames were photographed both by direct photography and through filters to have an indication of the C_2^* and CH^* species, a marker of the reaction zone. Clear differences are observed between the hydrocarbon fuels and the oxygenated bio-oils, of which eugenol was observed to be highly sooting. Other analysis showed that eugenol produces least smoke point value of 6.5 while n-decane has the highest value up to 27, indicating that n-decane produces less soot than the eugenol which was the highest soot producer.

The order of sooting propensity is heptane<decane<anisole=furfural<eugenol

4.8.7 Conclusion

- ❖ Model species of wood pyrolysis products are furfural for cellulose and eugenol for lignin. Smoke from their diffusion flames is initially similar and the initial soot particles grow to larger spherical particles.
- ❖ The particle sizes are approximately 30 nm and the particles agglomerate to form chains. There is a significant difference between the final soot product from furfural and eugenol because of the aromatic nature and concentration of soot particles. This aromatic nature is not seen in biomass soot.
- ❖ Furfural tends to follow HACA because of initial decomposition to suitable molecules to follow the HACA route. Eugenol undergoes side-chain cracking, followed by conventional phenol decomposition reactions, and also decomposition and reaction via cyclopentadiene.
- ❖ Comparison has been made to pine soots which contain both organic carbon and black carbon. The decomposition products suggest an important PAH route via cyclopentadiene, which is derived after cracking of lignin monomer fragments.

Chapter 5 Heavy Fuel Oil Combustion

5.0 Introduction

Heavy fuel oils, such as Bunker C and vacuum residue, are commonly used as fuels for industrial boilers, power generation, and as transport fuels, for example in large marine engines. Bio- and algal oils, are nowadays promising fuels which can potentially play the same role. The combustion of these oils can give rise to carbonaceous particulate emissions ('black carbon') which, along with associated polynuclear aromatic hydrocarbon (PAH) soot precursors (229), are associated with major health hazards, especially respiratory diseases such as asthma (230, 231). Moreover, it has recently been estimated (196) that 'black carbon' is the second most important human emission in terms of climate-changing: only carbon dioxide is estimated to have a greater effect.

Soot and char formation during the combustion of heavy oils is associated with their content of asphaltenes which are operationally defined as the oil fraction insoluble in an n-alkane solvent such as n-heptane but soluble in an aromatic solvent such as toluene; attempts have been made (232) to characterise asphaltenes in general from their number-average molecular weight, M_n , their content of heteroatoms (such as nitrogen, oxygen, as well as sulphur) and their degree of aromatic condensation. Therefore, such approaches are consistent with the differences between the 'average structures' for asphaltenes which have recently been suggested and which can have a strong influence on how asphaltenes affect heavy oil combustion and its environmental impact. Thus, two markedly different structural types (233) have been suggested: 'island' (or 'continental') in which a single aromatic core containing approximately seven rings is substituted with pendant groups, especially long-chain alkyl groups (234); and 'archipelago' structures in which small naphthenic and aromatic groups ranging from monocycles upwards are joined together by alkyl and heteroatomic links (235). A single asphaltene may, however, contain mainly one structural type but may also contain another. The overriding importance of 'archipelago' structures has been concluded by Karimi et

al. (235) on the basis of pyrolysis of thin films of asphaltene which yielded the constituent molecular ‘building blocks’ whereas the ‘island’ structures might be expected to produce more condensed molecules.

5.1 Background

The influence of asphaltenes on the combustion of heavy oils has been investigated (236) by burning oil droplets with different asphaltene content either suspended singly or by passage through a drop tube, and by spray combustion. It was observed that asphaltenes reduced ignition delay because of the volatiles generated by pyrolysis, but did not affect the droplet burning time; the stack solids collected during spray combustion depended in a second-order fashion on the asphaltene content of the oil. The emitted smoke is made up of residual fuel, soot particles as well as cenospheres.

This chapter presents experimental studies of the rates of combustion of droplets, and hence sprays, of these fuels, the combustion mechanism and the way in which fine particulate soot and cenospheres are produced. The environmental consequences of this information in relation to oil-fired boilers and to slow-speed diesel engines are described and the influence of the chemical composition of the fuels, especially the asphaltenes of the heavy fuel. An extended preliminary pyrolysis-gas chromatography-mass spectrometry (Py-GC-MS) experiment suggested by Bartle, et al. 2012 (6) gave results consistent with the thin-film pyrolysis results of Karimi et al. (235). Complementary atomic emission (AED) previously found in Ross, et al 2001(237) was used as a versatile highly selective detector for fossil-fuel derived materials analysed by GC (Py-GC-AED). AED is an element-selective detector with a wide range, allowing the detection of all the elements except helium; GC-AED has found particular use as a selective detector for sulphur (238), nitrogen (238, 239) and oxygen-containing (240) constituents of fuels.

5.2 Experiments conducted

5.2.1 Extraction of asphaltenes and their characterisation

Heavy oils have an asphaltene content of up to 16%. N-Heptane asphaltenes were separated from Marine Bunker C fuel oil, obtained from Shell Oil Ltd., and from Heavy Fuel oil supplied from Innospec Ltd, UK. These oil samples were used for the extraction of heavy asphaltene by a method (ASTM D6560 IP-143) consistent with ASTM method D2007-80. ASTM D6560, IP143 is a well-known standard asphaltene extraction procedure with a significant number of asphaltene fractions having high Bureau of Mine Correlative Index (BMCI). Details of the oil and asphaltene compositions are given in Table 5-1. The vanadium content of the heavy fuel oils and of the collected combustion residues was determined by atomic absorption spectrophotometry at 318.5nm on hydrochloric acid digests of ashed materials (6) and by inductively coupled plasma.

5.2.2 Ultimate analysis

Ultimate analyses were carried out on a CE Instruments Flash EA 1112 Series analyser. The details of this procedure have been explained in detail in chapter three of this thesis. The results of these compositions are shown in the table below.

Table 5- 1 Elemental composition of the fuels (wt. %).

Fuel oil	C	H	S	N	% asph	O	H/C	N/C	O/C
SMO	83.34	7.1	3.03	1.45	16	4.09	1.00	0.01	0.04
HFO	81.39	7.3	1.73	1.24	16	8.34	1.07	0.01	0.08
Pyrolysis oil	76.58	6.40	0.18	0.52	-	16.32	1.00	0.01	0.16

Key: SMO –Shell marine oil, HFO- Heavy fuel oil. Elemental compositions are on dry basis calculation.

5.2.3 Size exclusion chromatography

Size exclusion chromatography was used on the Bunker C asphaltene samples for molecular weight determinations which were made on that portion of each asphaltene sample soluble in tetrahydrofuran (THF). (By size-exclusion chromatography with polystyrene standards). This procedure was explained in the methodology chapter of this thesis. An example result is shown in Figure 5-1. Figure 5-3 show the highest proportion of molecular organics in heavy fuel oil asphaltene than the Shell Marine asphaltene.

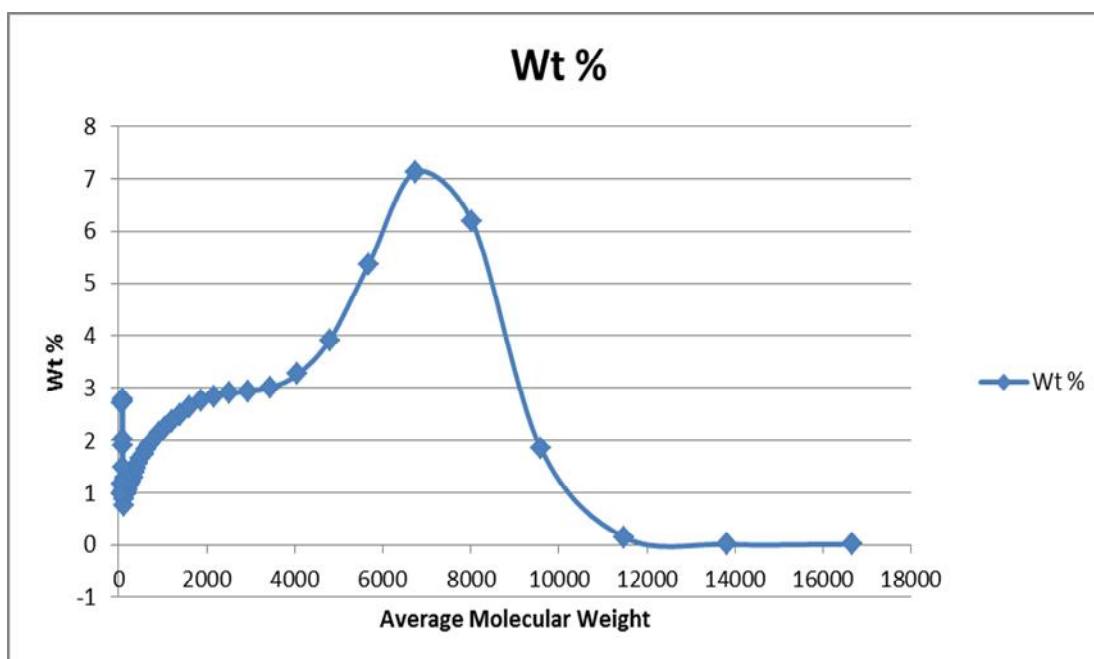


Figure 5- 1 Size exclusion chromatogram showing the molecular weight distribution in the asphaltene fraction of Shell Marine oil

The above Figure 5-1 indicates high proportions of heavy aromatic hydrocarbons in asphaltene derived Shell marine oil as shown in the size exclusion chromatogram (Figure 5-2) compared to bio-oil asphaltene.

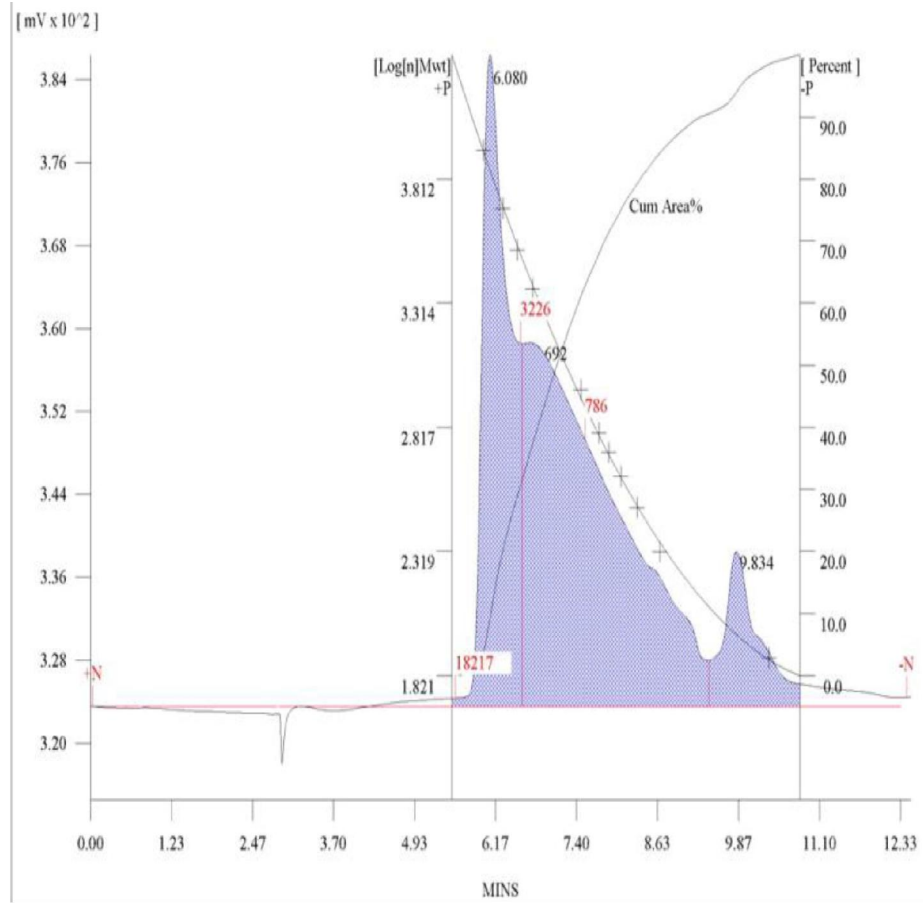


Figure 5- 2 Size exclusion chromatogram showing heavy molecular weight of organic fraction of SMO asphaltene

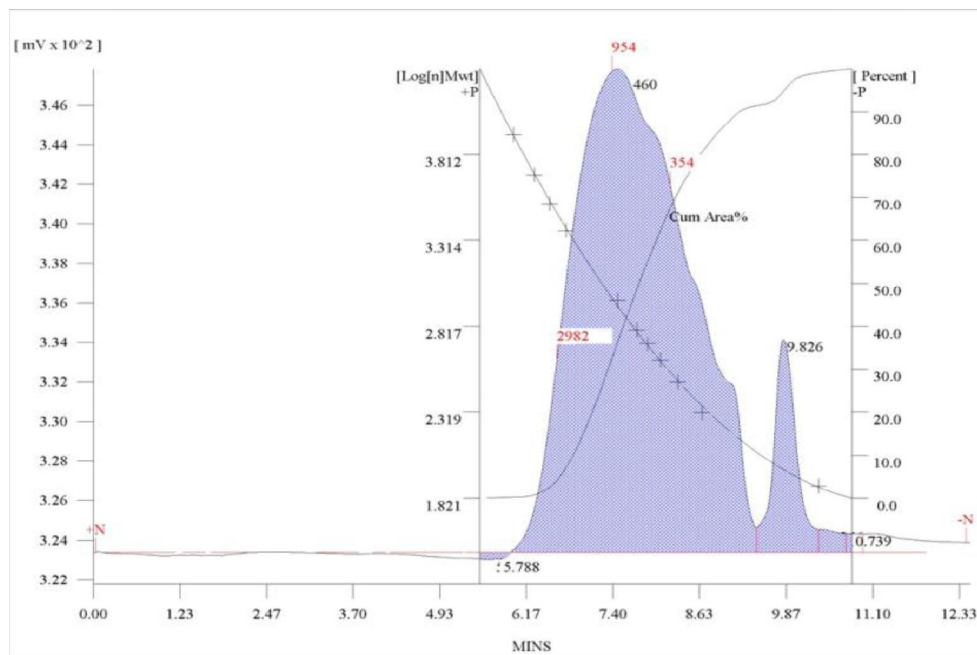


Figure 5- 3 Size exclusion chromatogram showing heavy molecular weight of organic fraction of HFO asphaltene

5.2.4 Thermogravimetric analysis (TGA)

Thermogravimetric analysis (TGA) was carried out on the asphaltenes at a number of heating rates; kinetic data for processes involving heat losses were derived as described by the method of Senum and Yang (241).

5.2.5 Pyrolysis - GC of asphaltenes

Py-GC-MS was carried out as described elsewhere in chapter 3 (6) at 300-1000°C in a flow-cell hyphenated pyrolysis system (242) which allowed on-line trapping and subsequent transfer of products to the GC-MS. The GC peaks were identified from the NIST library, from the retention times of standard chromatographs under the same conditions, and where appropriate from complementary element-specific Atomic Emission Detection chromatograms. For Py-GC-AED the transfer line, heated at 320°C, was connected to a JAS AED plus G2350A instrument with helium make-up gas at 40 mL/min. The AED utilised a high-purity (99.99%, Air Products, UK) helium microwave induced plasma (MIP) contained within a polyimide-coated silica tube. The MIP was water cooled (63°C) and doped with reagent gases (Table 5-2) to reduce chemical interference, carbon deposition and the formation of refractory oxides. The spectrometer was purged with oxygen free nitrogen at 2 L min⁻¹. Emission lines for the elements studied are listed in Table 5-2.

Table 5- 2 Atomic emission detection monitoring wavelengths and reagent gases.

Element	Wavelength/nm	Reagent gas
C	193	H ₂ / O ₂
N	174	H ₂ / O ₂
O	777	H ₂ / 10% CH ₄ in N ₂
S	181	H ₂ / O ₂
V	292	H ₂ / O ₂

5.3 Experimental results and discussion

5.3.1 Pyrolysis of asphaltenes.

TGA analysis of the asphaltenes (e.g. Bunker C, (Figure 5-3) and Heavy Fuel Oil (Figure 5-3) showed a small weight loss between 150°C and 300°C corresponding to moisture and light organics.

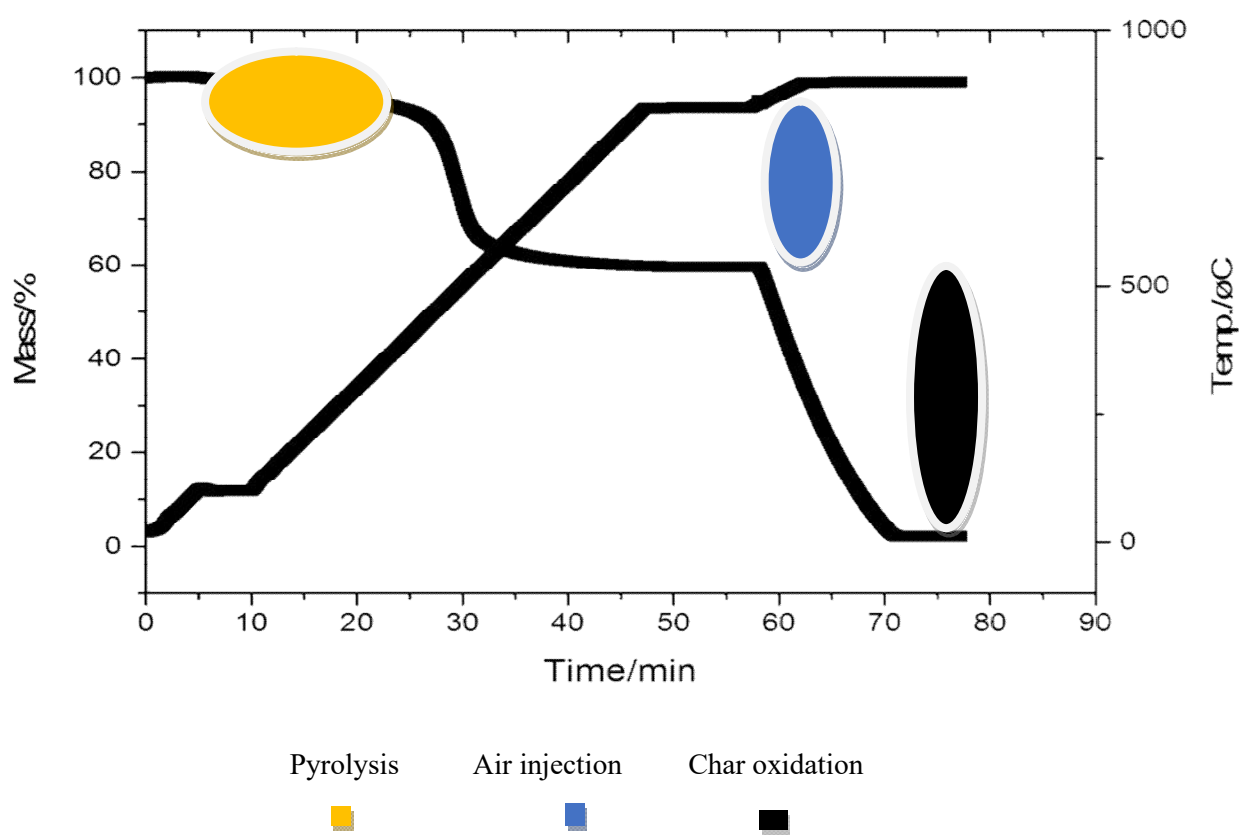


Figure 5- 4 TGA of Bunker C fuel oil asphaltene

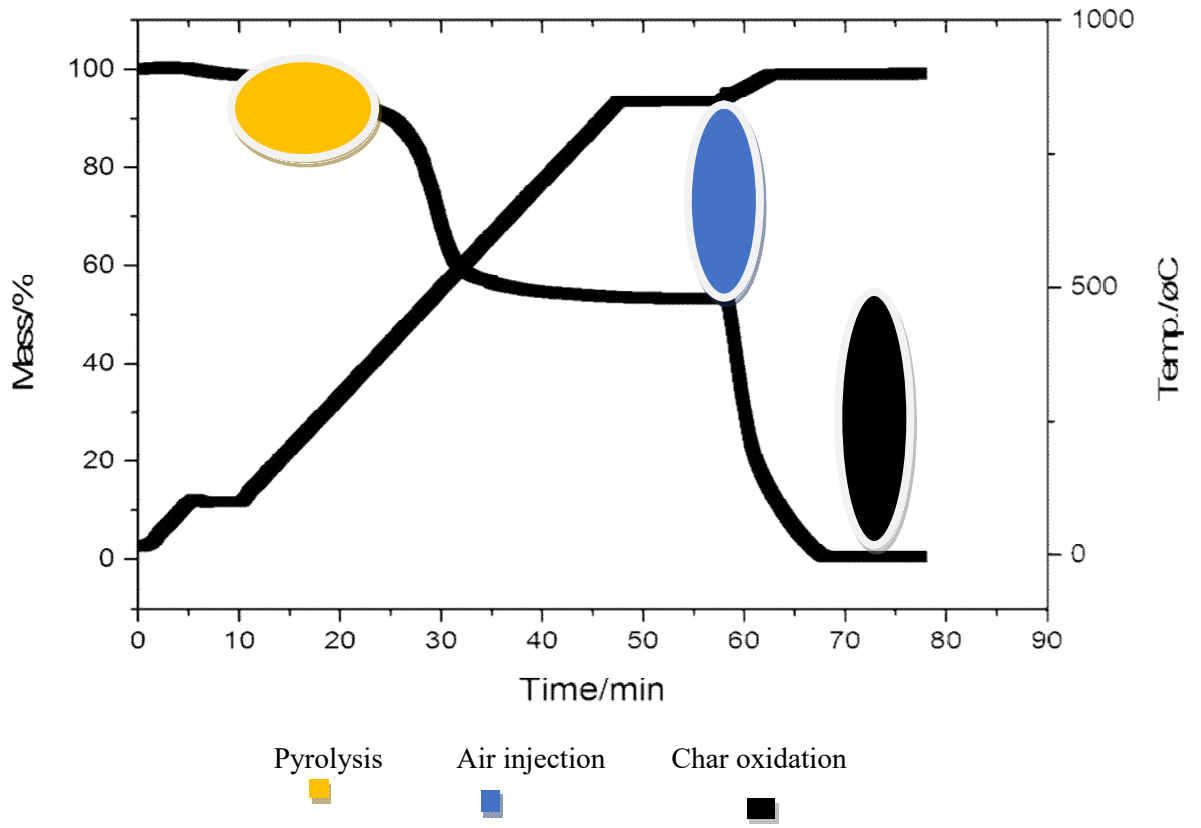


Figure 5- 5 TGA of Heavy fuel oil asphaltene

By comparison of these two graphs, it is seen that the pyrolysis process in both fuels is similar, but the char oxidation is different.

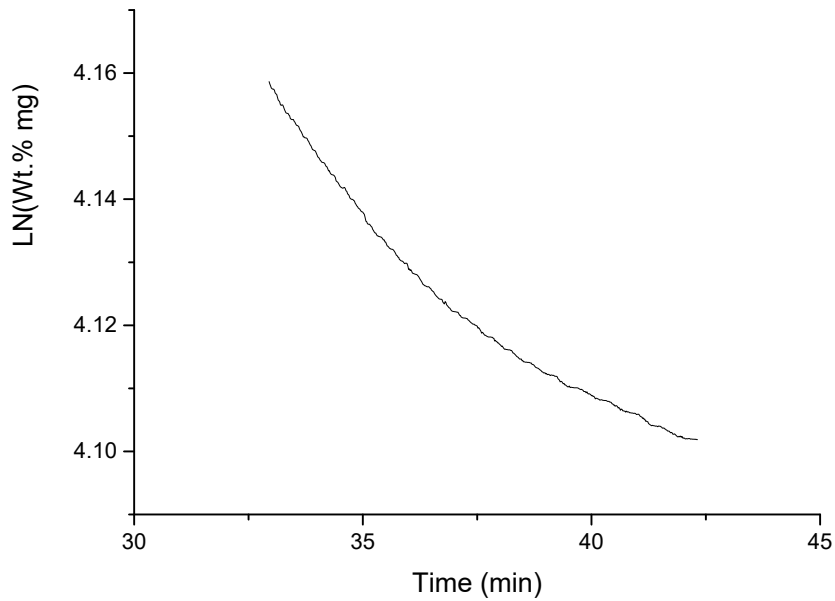


Figure 5- 6 Derivative weight loss for H F O asphaltene

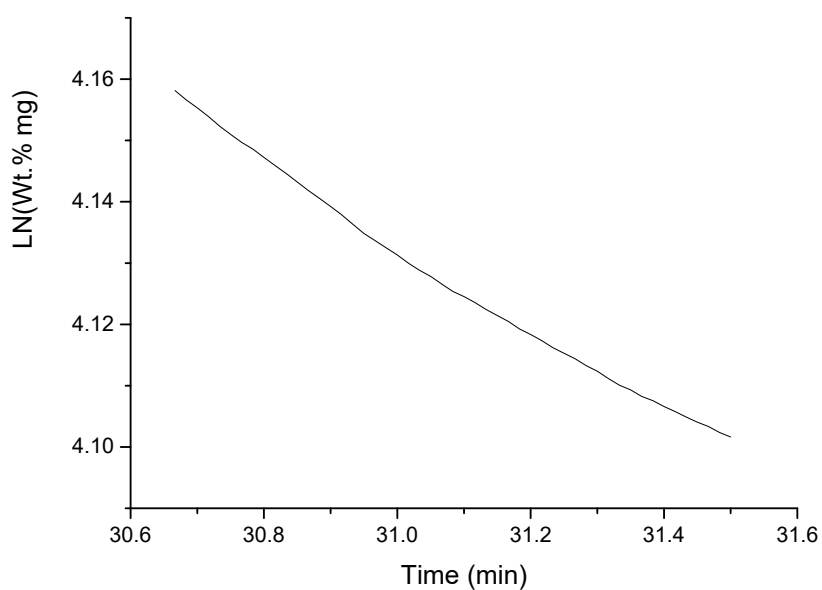


Figure 5- 7 Derivative weight loss for Bunker C fuel oil asphaltene

The pyrolysis rates for both fuels are similar as shown the dw/dt plots. But the char rates are different. This is probably due to the Vanadium contents of the oils.

The pyrolysis in this range was also investigated by Py-GC-MS of the asphaltene at 300⁰C. The resulting chromatogram led to the evolution of a range of volatile n-alkanes and monocyclic aromatic hydrocarbons.

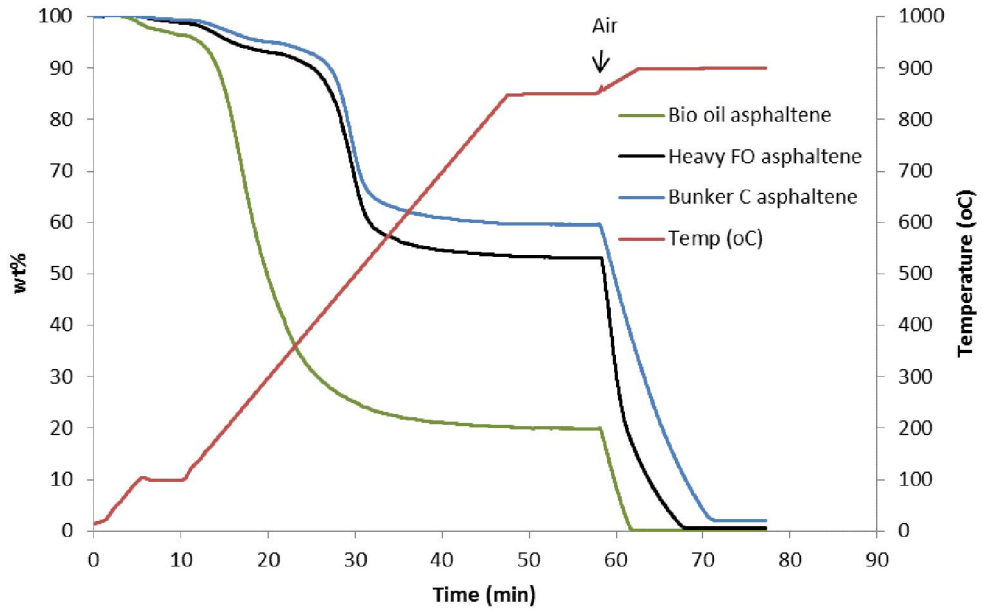


Figure 5- 8 TGA profiles comparing the three asphaltene fractions in temperature programmed pyrolysis under nitrogen, followed by combustion in air.

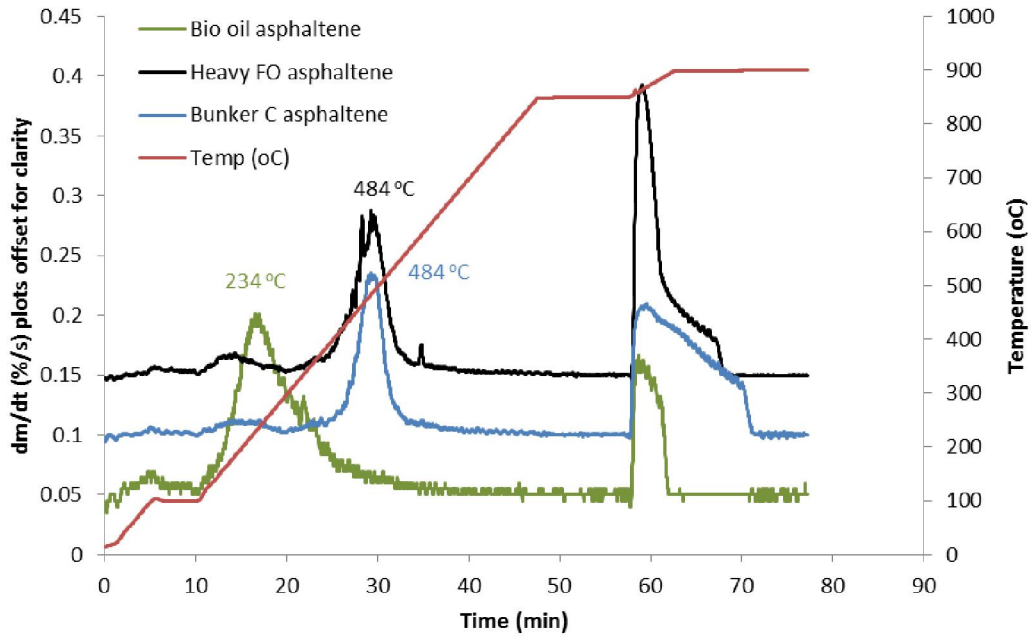
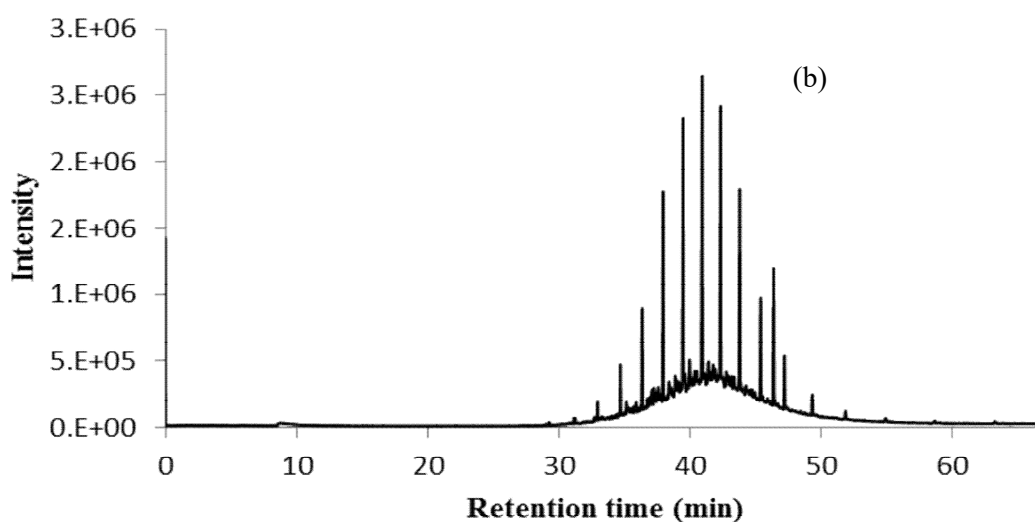
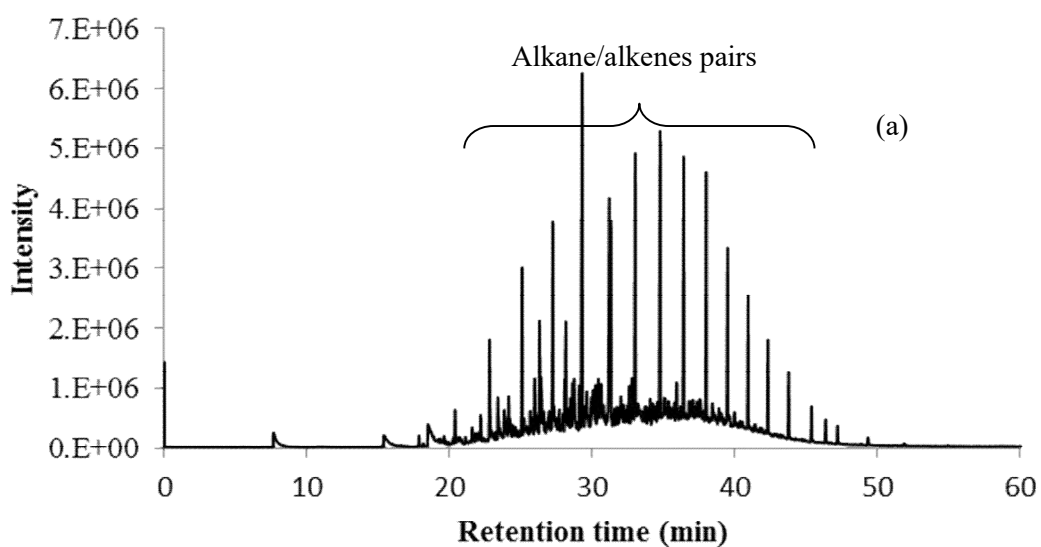


Figure 5- 9 Derivative weight loss time plots comparing the three asphaltene fractions.

Plots are offset for clarity and the peak maximum temperatures during pyrolysis are indicated.

TGA of the asphaltene indicated the commencement of major weight loss at 400°C, while a temperature near 500°C was employed in analytical pyrolysis experiments by Karimi et al (235) and 600°C by Sarmah et al. 2010 (243). At both 400 and 500°C our Py-GC-MS chromatograms (Figure 5-6) contained prominent peaks attributed, as in the previous work (234), to alkane/alkene pairs extending at 400°C from C13 to C26. At 500°C, small quantities of lower MW alkanes/alkenes were observed, indicating the commencement of secondary pyrolysis.



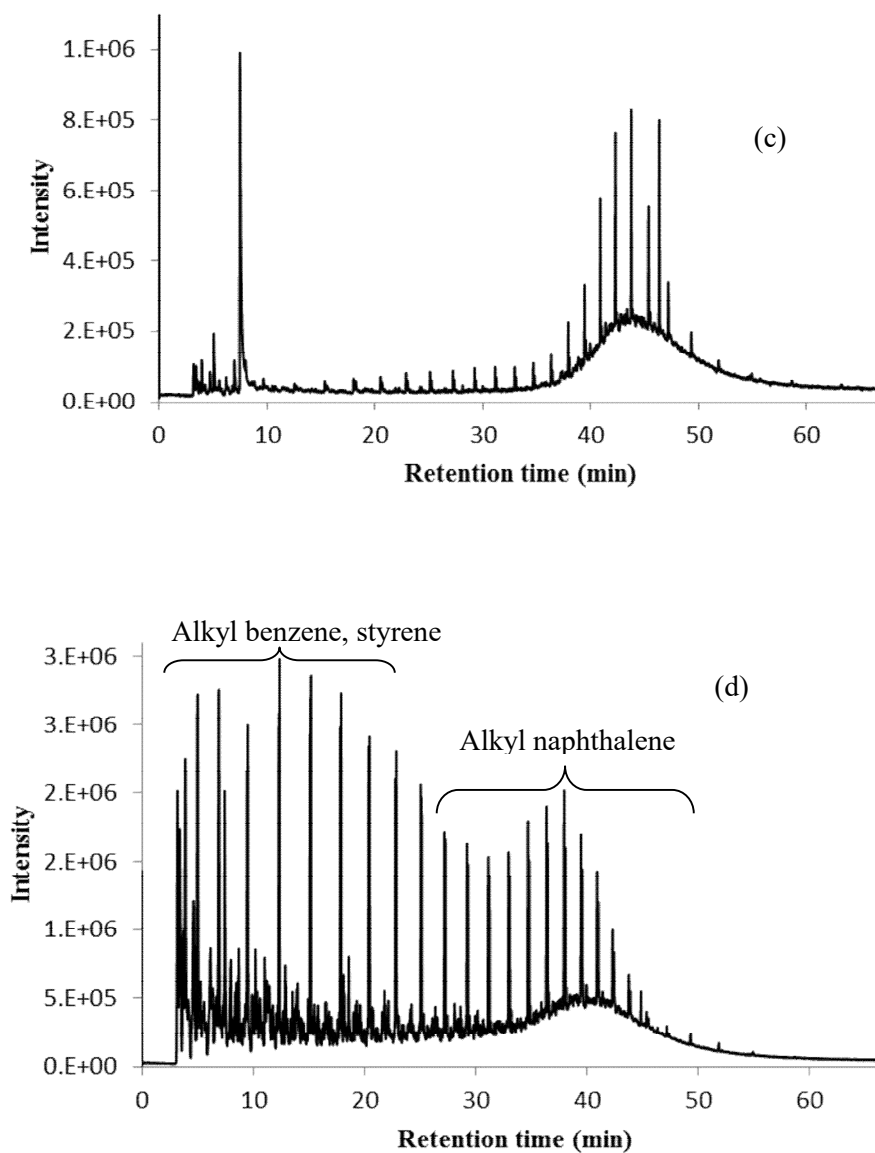


Figure 5- 10 Typical Py –GC-MS of asphaltenes at (a) 300, (b) 400 and (c) 500C (d) 600C.

Extended to lower carbon numbers with increasing pyrolysis temperature (Figure 5-7).

In addition to the alkanes and alkenes, the primary pyrolysis products of all of the asphaltenes detected by Py- GC –MS were C1-C4 alkyl substituted aromatic hydrocarbons, especially: benzenes; styrenes: methyl styrenes; naphthalenes and hydrogenated naphthalenes (dihydroindenes, dihydromethanonaphthalene and tetrahydronaphthalenes); phenanthrenes and

anthracenes; pyrenes and isomers (fluoranthene and acephenanthrylene); and at high temperatures, traces of chrysenes. Some of the compounds identified are listed in Table 5-3, along with positions of methyl substitution when these could be identified. Naphthalenes and phenanthrenes with up to and including C4 alkyl substitution were particularly prominent from 400°C.

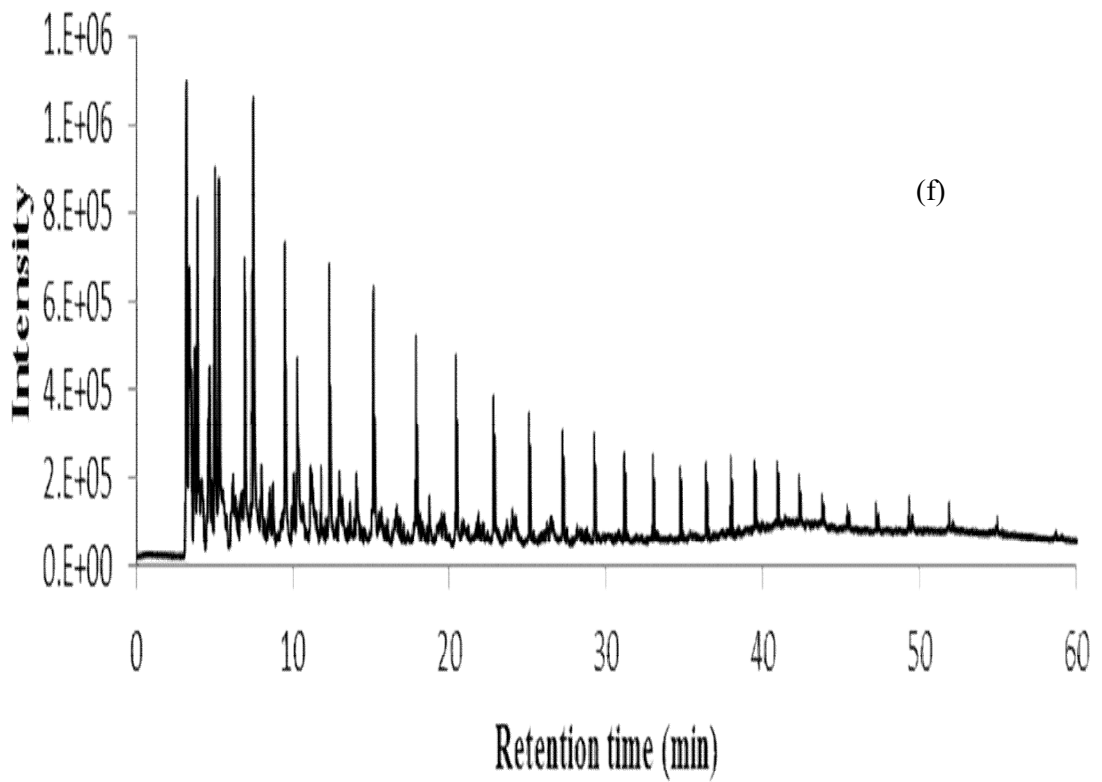
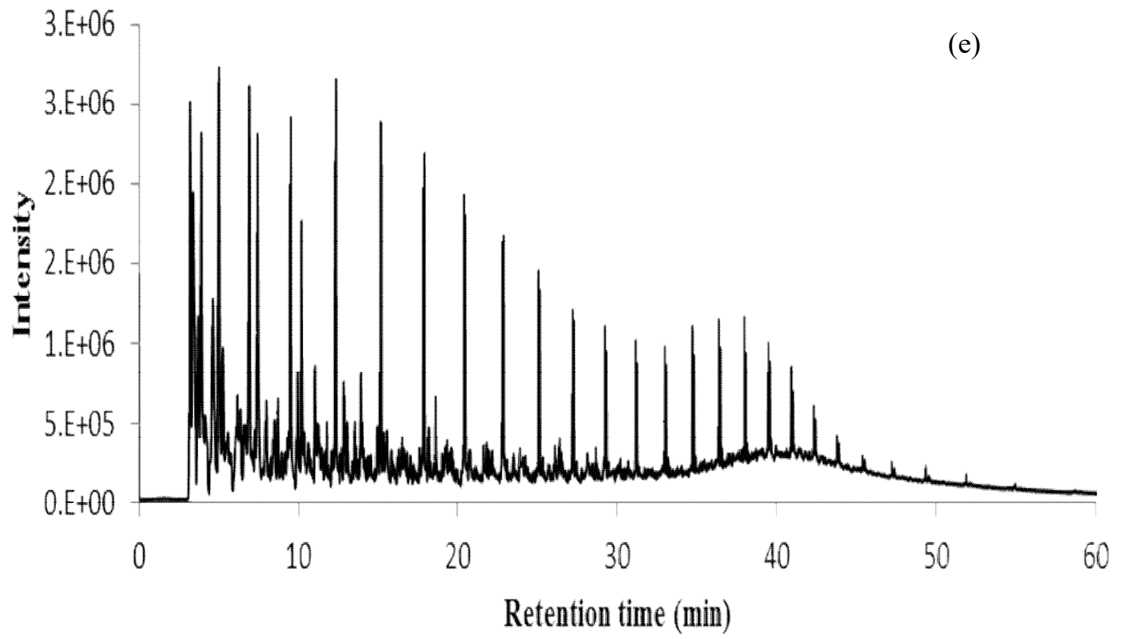
Table 5- 3 Aromatic hydrocarbons identified in pyrolysis products of asphaltenes (HFO and SMO)

Benzenes	Et. 1,2- Me2. 1,3-Me2. 1,4-Me2 (106) 1,3,5-Me3 1-Me-3-Et 1-Me-4-Et 1-Me-2-Et 1,2,4-Me3 1,2,3-Me3 (120) C4 (134) See appendix B
Styrenes	Parent (104) C 1 (118) See appendix B C2 (132)
Naphthalenes	Parent (128) 1-Me 2-Me (142) 1,3- Me2 1,6-Me2 1,7-Me2 (156) C3 (170) See appendix A
Phenanthrenes	Parent (178) 1-Me 2-Me 3-Me 9-Me C2 C3 C 4 See appendix A
Anthracene	Parent (178) See appendix A
Fluoranthene	Parent (202) See appendix A
Acephenanthrylene	Parent (202) See appendix A
Pyrenes	Parent (202) 1-Me 2-Me 4-Me (216)* See appendix A
Chrysenes	Parent (228) 1-Me 2-Me 3-Me 6-Me (242) See appendix A

*Also includes methylfluoranthenes

Single-ion monitoring (SIM) was performed in order to enhance detection of the particular classes of compounds, and the M/Z was used for this are listed in the Table 5-3. For example, SIM at M/Z 178 enabled identification of substituted anthracenes and phenanthrenes.

No systematic change of composition within isomer groups with temperature was detected, although as the pyrolysis temperature rose there was evidence of de-methylation: For example, the ratio of monomethylphenanthrenes to dimethylphenanthrenes increased, while the degree of alkylation of naphthalenes was much less at the higher temperatures; at 600C C3>C1 and at 900C C1>C2>C3 (Figure 5-7(g)).



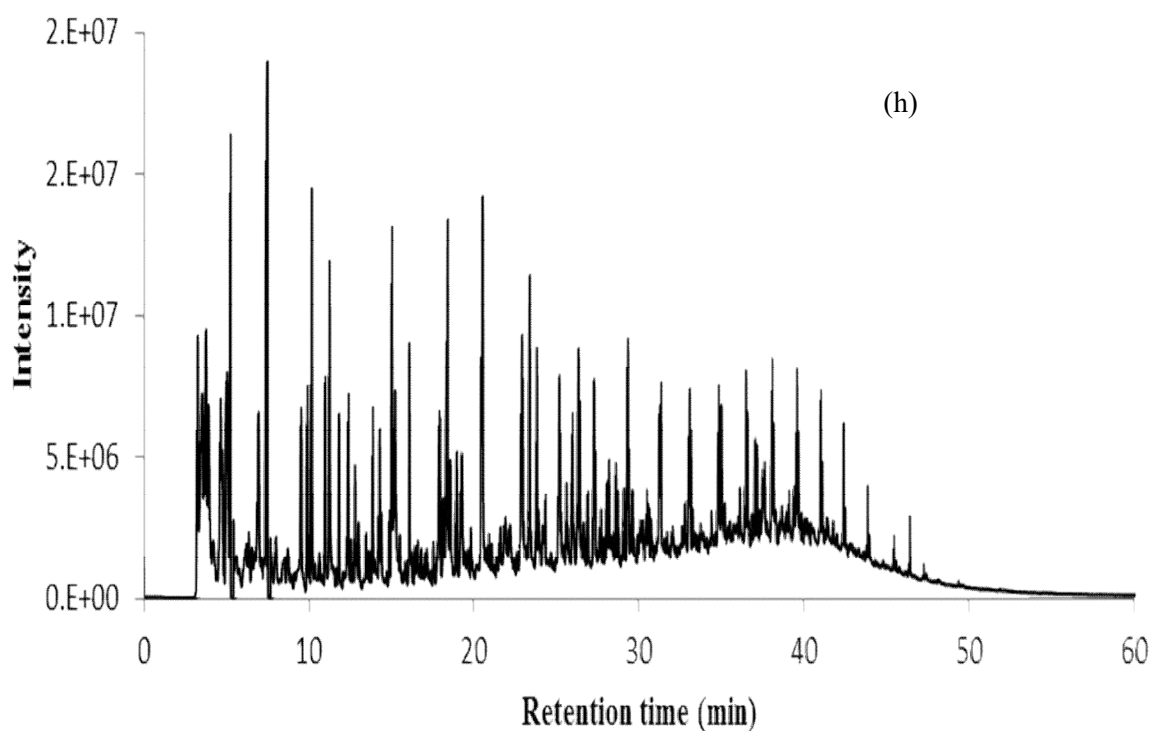
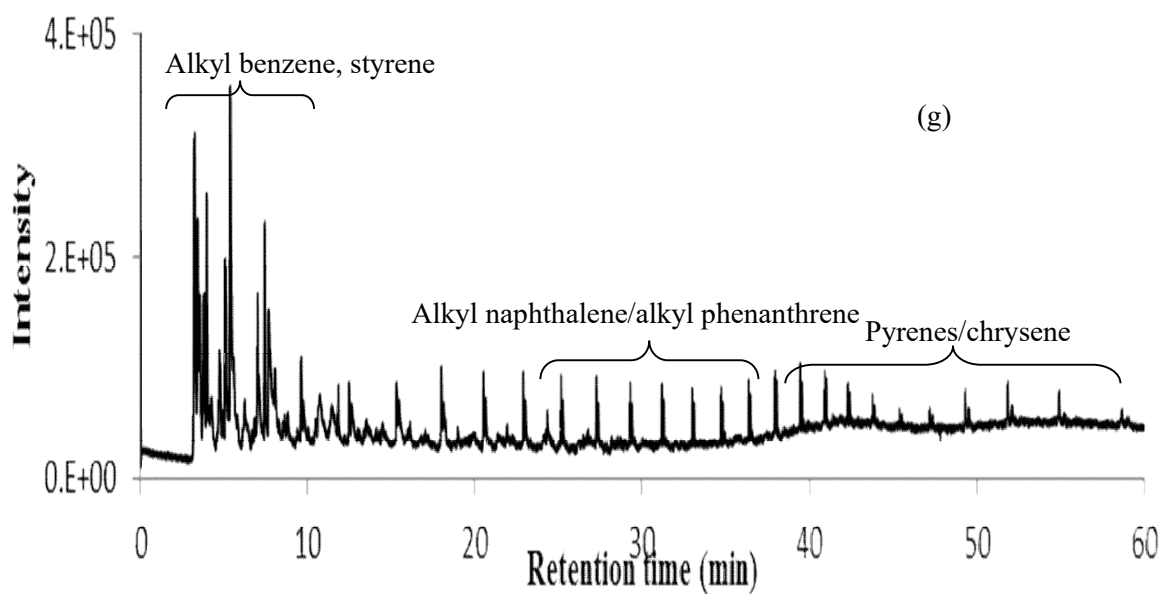


Figure 5- 11 Typical Py –GC-MS of asphaltenes at (e) 700, (f) 800 and (g) 900C (h) 1000C

The evolution of alkyl benzenes was significant from 500°C, and then released increasing quantities of, at first, in particular C4 benzenes, followed by C3 and C2 benzenes as demethylation became important. Alkyl substitution in the dimethynaphthalenes from

asphaltene pyrolysis favoured the 1-position. A well-known group of carcinogens which originate during heavy oil combustion are the PAH. Among the seven such compounds specified among the EPA 16 as having activity, only two, benz[a]anthracene and chrysene, were identified in the mixture of two-to-four- ring PAH identified in the pyrolysis experiments described here. However, these are also representative of a range of other PAH also produced, such as a number of methylchrysenes/methylbenz[a]anthracenes, some of which, e.g. 5-methylchrysene, are potent carcinogens, while 3- and 6-methylchrysenes are strong tumour initiators (244-246).

Examination of the pyrolysis products by sulphur-specific AED detection revealed (Figure 5-8) the presence of numerous polycyclic aromatic sulphur compounds (PASH), especially benzothiophenes and dibenzothiophenes, the latter dominated.

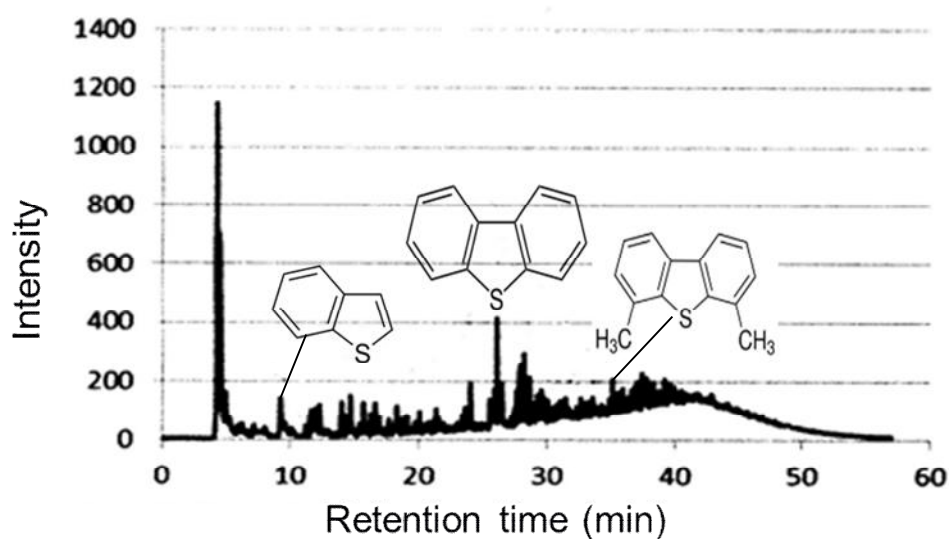


Figure 5- 12 Py-GC-AED of Bunker C Oil Asphaltene with sulphur detection at 181nm.

The pattern of alkyl group substitution on the benzothiophenes and dibenzothiophenes (Figure 5-8) liberated from the asphaltene during Py-GC-AED, at least as far as C_3 , derivatives involved mainly methyl groups, although this may be a partial consequence of the greater availability of standard compounds with methyl substituents. The prominence of compounds with methyl in the sterically hindered 4- and 6- positions is noticeable, however, and the same range of

compounds identified by MS and literature retention data (239) were shown by AED to be produced by pyrolysis at 450, 500 and 600°C.

The relative proportions of alkyl benzothiophens and dibenzothiophens in the asphaltene Py-GC-AED products was determined from the corresponding AED peak areas using response factors per unit mass of sulphur determined for standard PASH (benzo[*b*]thiophen, dibenzothiophen, diphenylsulphide and diphenyldisulphide (247); in agreement with literature (246), these were always near unity. Alkylated DBT were present in the concentration sequence C₂>C₁>C₃. The toxicity of PASH is often greater than that of PAH isosteres (248) although the mutagenic activity of PASH and their alkylated derivatives is generally weak (249).

Because of poor selectivity arising from interference by lines in the carbon emission spectrum (238), the results of the Py-GC-AED with nitrogen detection (174 nm) experiments reported here were consistent only with the liberation of a poorly resolved 'background' of low-concentration nitrogen compounds. Speight similarly observed that nitrogen compounds were not released during the pyrolysis of asphaltenes (84).

5.3.2 Thermal reactions of asphaltenes

The peaks from volatiles evolved at 300°C were attributed by Gray et al., (2011) (250) to the evaporation of compounds occluded in the asphaltene pore structure (either macroporous with >200 nm pores, or microporous with pores < 1.5 nm). A second series of higher alkanes liberated in low concentration at 300°C originate from the larger pores. Previous experiments in which alkanes were extracted at different temperatures from fossil fuels suggested (6) slight thermolysis below 350C. .

The alkane/alkene pairs of peaks in the chromatogram of the pyrolysis products are thought (233) to arise from alkyl radicals generated by beta-bond scission of long-chain alkyl aromatics and proposed as the most important reaction route for a range of fuels (251, 252). Hence the pyrolysis of n-pentadecylbenzene yielded toluene and alkane/alkenes, and dodecylbenzene gave rise to undecene/undecane, toluene and ethylbenzene (253). Experiments in which

asphaltenes separated from coal-derived oils were reprecipitated showed that n-alkanes below C₄₀ were retained in the alkane solvent during the separation procedure and that asphaltenes do not contain significant quantities of alkanes; the long alkyl chains are directly bonded to aromatic groups (254). Alkyl chains are well-characterised contributors to the structure of petroleum constituents, for example, the aromatic fraction of Diesel fuel contains alkyl benzenes across the whole volatility range (255).

The aromatic products of pyrolysis of asphaltenes are indicative of an 'archipelago' structure made up of linked aromatic clusters, termed 'building blocks' by Karimi et al. (235); these are the conjoined small (1 – 4) ring systems in Table 5-3 substituted with the lipophilic long chain alkyl groups discussed above, and with (mainly methyl) shorter chain alkyls, some of which are the remnants of the loss of the long chains on pyrolysis which leave methyl groups substituted on the aromatic ring. That the PAH originate from the cross-linked aromatic structure at 500°C and not by pyrosynthesis from the long alkyl chains first liberated is shown by previous research work in (242) with the same pyrolyser in which temperatures in the region of 800°C were required to produce PAH from n-hexadecane.

It must also be emphasised, however, that the larger aromatic ring systems with six or more rings would not be eluted under the gas chromatographic GC conditions employed here, so that the presence of 'island' asphaltene structures is not excluded. Five -ring picenes and benzopyrenes were not detected, although these compounds are sufficiently volatile to be eluted from the GC column and pentaaromatics have previously been found in the pyrolysis product of the Maya asphaltene (256). Slight material was evident in the chromatogram beyond the elution time of methylchrysenes. It is conceivable that at least some of the pyrolysis- liberated arise by fission of large condensed aromatic 'island' structures, but also in related work (242) we have found that temperatures above 800°C were necessary to bring about even a limited degree of ring break-up.

At temperatures above 600°C a range of alkyl benzenes was produced indicating an origin from the cross-linked asphaltene rather than from the alkanes for which higher temperatures (242) were required. It seems that monocyclic aromatics produced at high temperatures originate in

part from the pyrolysis of the aliphatic hydrocarbons (6, 237). The observed pattern of methyl group substitution in naphthalenes and phenanthrenes is similar to that in volatile petroleum oil fractions. Similarly, the predominance of 1-substituted dimethylnaphthalenes resembles that in crude oils and geochemical sediments (243).

Indications of the nature of the structures linking the aromatic ring systems are provided by the identification of unsaturated naphthenic and hydroaromatic compounds in the asphaltene pyrolysis products. Furthermore, the high degree of methyl substitution of the naphthalenes and other aromatic units points to the breaking of alkyl bridges between building blocks to leave methyls as well as an origin for these groups from the beta-bond scission of long alkyl chains.

X-ray absorption spectroscopy has previously been used to show that sulphur occurs in petroleum asphaltenes in both thiophenic and sulphidic forms (257), but only these thiophenic derivatives survive heating in our pyrolysis experiments and appear in the products. Researches have shown that sulphide bonds are broken during pyrolysis along with other groups linking the aromatic/heterocyclic building blocks, as is suggested by the loss of hydrogen sulphide. An important contribution by PASH structures to that of asphaltene is suggested by the resemblance between alkyl substitution in asphaltene pyrolysates and low MW petroleum oils.

Knowledge of the identity of nitrogen-containing compounds liberated from asphaltenes during pyrolysis is important in understanding the formation of gaseous pollutants such as NO_2 , NH_3 and HCN during HFO combustion. A combination of XPS, Fourier transform infra-red and chemical analysis has previously shown that the low (258) concentrations of nitrogen compounds in petroleum asphaltenes has functionality dominated by five- and six-membered ring structures of the carbazole and quinoline types.

In other related work we have observed (259) that during thermal processing of petroleum residues, the nitrogen compounds, which are predominantly non-basic, accumulate in the high molecular weight residue which would correspond in the current work to the cenospheres - here the combustion residue, so that only small amounts of nitrogen are predicted to be transferred to the vapour phase. Py-GC-AED with detection at 777 nm was also consistent with the liberation

of only minor amounts of oxygen compounds, although traces of alkanolic acids were detected by Py-GC-MS (6).

5.3.3 Structure of asphaltenes: affinities with lower MW petroleum fractions.

The distribution of alkyl groups in monoaromatics, dimethylnaphthalenes (e.g. Figure 5-8) and methylphenanthrenes, together with the observed similarity between the PASH and those present in crude oil, middle distillates (e.g. light gas oil)] and decant oil (83), taken with the occurrence of long alkyl chains bonded to aromatics in both Diesel fuel and asphaltenes, are all consistent with the importance of thermodynamic stability as a factor in asphaltene structure, and the suggestion that asphaltenes are structural analogues of other constituents of petroleum. Sarmah et al., 2010 (243) found that the pyrolysis of petroleum asphaltenes gave dimethyl phenanthrenes with a distribution similar to those in the parent oil. A complementary view of the origin of the pattern of alkyl substitution lies, however, in cyclisation and aromatisation of linear carbon chains (260).

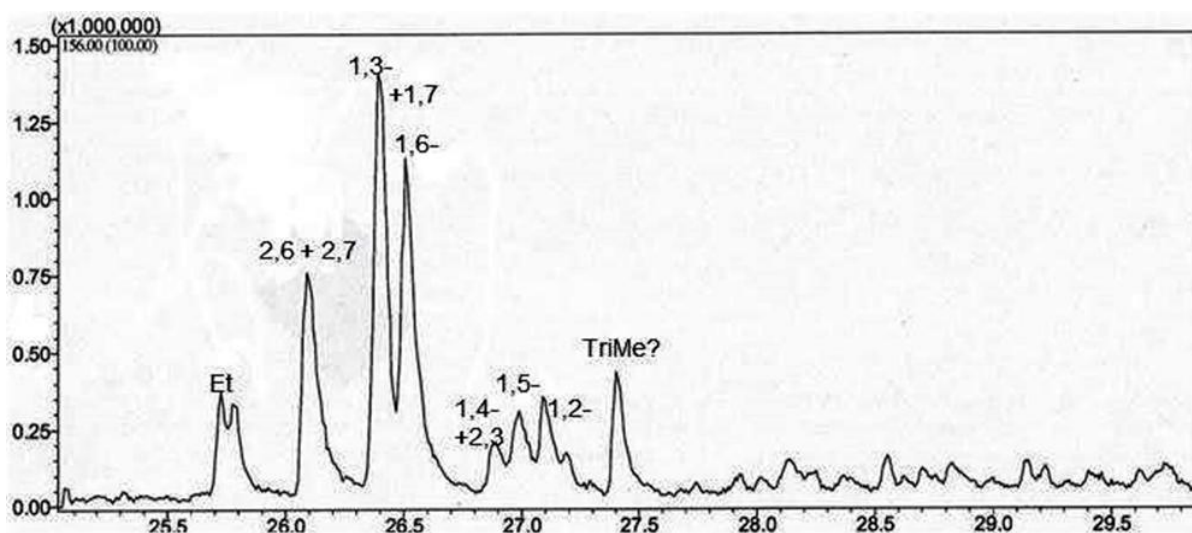


Figure 5- 13 Dimethylnaphthalene region (m/z 156) of pyrolysis product of Bunker C asphaltene at 600°C

The above Figure 5-9 is a SIM chromatogram at M/Z 156 (the dimethylnaphthalene species) showing the dimethyl naphthalenes peaks from pyrolysis at 600C with selected peak identifications, Et-ethyl naphthalene, 2,6 naphthalene etc. The result shows that observed the

pattern of methyl substitution in the naphthalenes and phenanthrenes resulting from asphaltene pyrolysis are similar to that of petroleum oil fractions. Additionally, the predominance of 1-substituted dimethylnaphthalenes resembles that of crude oil and geochemical sediments (239).

The distribution of structural types and individual molecules in the mixture may have properties different from other asphaltene constituents since asphaltenes are necessarily heterogeneous as a consequence of their definition (232); chromatographic separation by partitioning/ adsorption is well known (261). It follows that the small aromatic building blocks detected in our experiments and those of Karimi et al. (235) provide evidence in support of ‘archipelago’ structures, but do not exclude the concurrent presence of ‘islands’

A proposed reaction scheme for the asphaltenes during the early stages of the combustion of heavy fuel oils is shown in Figure 5-10 and is consistent with the simultaneous generation of soot and cenospheres.

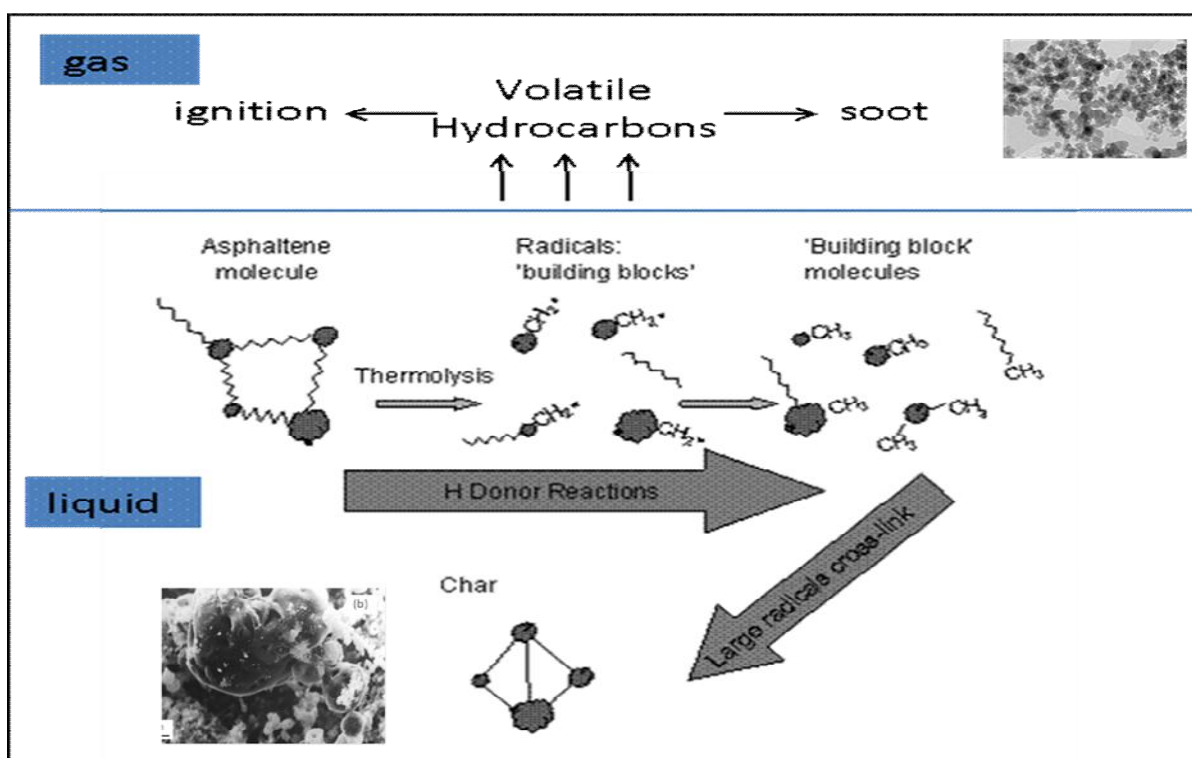


Figure 5- 14 General reaction scheme for the pyrolysis of asphaltenes showing the effect on ignition, soot and cenosphere formation.

The mechanism, indicated in Figure 5-10, then involves the loss of parent oil species which are largely combusted, but some of the higher molecular weight species crack and form smoke and PAH. The asphaltene also undergoes thermal decomposition leading to condensed aromatic coke precursors by carbon rejection processes: de-alkylation and aromatisation (of respectively aromatic and hydroaromatic species), for which there is NMR evidence, as well as IR indications of oxidation. The large PAH species form more rapidly near the droplet surface because it is hotter and because of droplet surface regression. Consequently a flexible carbonaceous skin is initially observed to be formed on the surface which then forms a solid carbon shell, a cenosphere, which also contains inorganic species and which later graphitizes (37). For lighter fuels (such as the model compounds discussed in chapter 4) the vapour phase reaction to soot is more important than the heterogeneous cenosphere reaction.

5.3.4 Thermogravimetric analysis

TGA results (Figure 5-2 and 5-3) show significant weight loss from the liberation of volatiles from 400°C resulting from breaking of the bonds linking the ‘archipelago’ sub-units in the parent asphaltene. Activation energies determined from TGA curves are reported to be considerably smaller (91-105 kJmol⁻¹ depending on the weight loss region (6)) than typical bond-dissociation energies. The results of Py-GC with MS and AED detection of the thermolysis products are consistent (Figure 5-9) with the capping of the resultant radicals by hydrogen donation from the more thermally stable asphaltene molecules which may have ‘island’ structures; the large-molecule radical products then cross link to form a char in the form of cenospheres. The volatile small-molecule ‘building blocks’ are available for the ignition of the fuel oil and also to act as PAH soot pre-cursors (6).

A key issue is the formation of soot and carbon. Emission factors have been determined for HFO containing 0.46, 2.5 and 5.0%wt of asphaltene using a spray combustion system. This percentage stack solids is given in Table 5-4.

Table 5- 4 Percentage total stack solids produced by combustion of heavy oils containing different amounts of asphaltenes as a function of flue gas oxygen content.

Flue gas O ₂ mol %	0.36% wt asphaltene	2.5% wt asphaltene	5.0% wt asphaltene
2	1.55		
3	1.2	2.2	
4	1.05	1.8	
5	0.9	1.3	2.4
6	0.8	1.05	2.0
7	0.75	0.85	1.6
8	0.6	0.7	1.24
9	0.95	0.65	1.15
10	0.4	0.6	0.95
12			0.8

If 5% oxygen is taken as typical value for the excess air level in a furnace, then by extrapolation to 0% asphaltene content then the contribution to the smoke formation is 0.7wt%. Therefore at higher levels of asphaltene it may be deduced that the conversion efficiency of asphaltene to solids emission/smoke is about 25%. Consequently it is possible to estimate stack solids emission for any asphaltene content.

Another means of reducing the ignition delay and smoke formation is by disruptive burning which causes secondary atomisation. This is observed when water is emulsified with HFO but it also is observed during the combustion of bio-oils. Whilst these may undergo secondary atomisation they share a problem with high asphaltene oils in they agglomerate/associate in an analogous way and have high boiling point species present, namely the lignin-derived species. An extreme case of this is observed during the combustion of carbon black-water slurries, which has many similarities to the combustion of a high-asphaltene containing heavy fuel oil.

The vanadium content of heavy oils increases with asphaltene content (6) and vanadium – containing structures in HFO are believed to be incorporated in the chemical structure of asphaltenes and to give rise to toxic emissions during HFO combustion. However, the metal within the cenosphere residue might give accelerated catalytic burnout. In agreement, on a weight basis, the vanadium concentration on total suspended atmospheric particulates was greater than that in PM₁₀ for samples collected from contaminated atmospheres (262). The vanadium contents for petroleum asphaltene and bio-oil asphaltene is indicated in Figure 5-15.

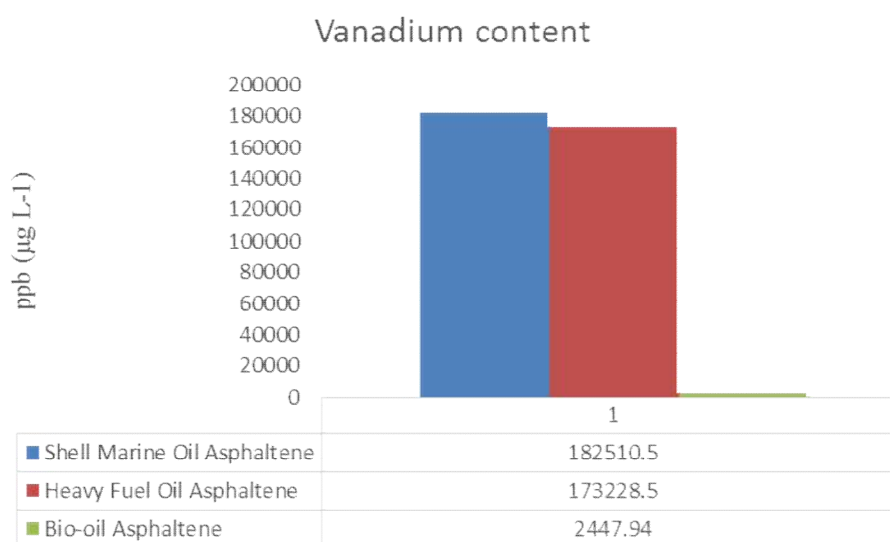


Figure 5- 15 Vanadium content for Shell marine asphaltene, Heavy fuel oil asphaltene, and Bio-oil asphaltene

5.5.5 Routes to smoke formation during the combustion of heavy oils.

Smoke consists of both gas-phase produced soot and cenospheres and these, together classified by WHO (263) as hazards, are both increased by increasing the asphaltene content of the oil. Smoke formation during the combustion of asphaltene-rich fuel oils can be described by the general reaction in Fig.5-10, for the thermolysis of the asphaltene macromolecule. The fuels studied in this work produced total smoke emission concentrations of between 1 and 12 mgm⁻³, as measured as stack solids (6). Over 90% of the cenospheres had diameters between 5 and 15 μm, whereas the soot particles were sub-micron in size. The properties of the gas phase soot are

alike whether formed at atmospheric pressure or at high pressure in an engine. The burn-out rates of the soot and the cenospheres determine the stack solids and these can be calculated using intrinsic reaction rates as shown in Figure 5-11(39).

The overall thermal mechanism then involves the loss of parent oil species which are largely combusted, but some of the higher molecular weight species crack and form smoke and PAH (6). The asphaltene also undergoes thermal decomposition leading to condensed aromatic coke precursors by carbon rejection processes: de-alkylation and aromatisation (of respectively aromatic and hydroaromatic species), for which there is nuclear magnetic resonance as well as infra-red spectroscopic indications of oxidation. These large PAH species form the flexible carbonaceous skin initially formed on the surface-described earlier- which then forms the cenosphere shell.

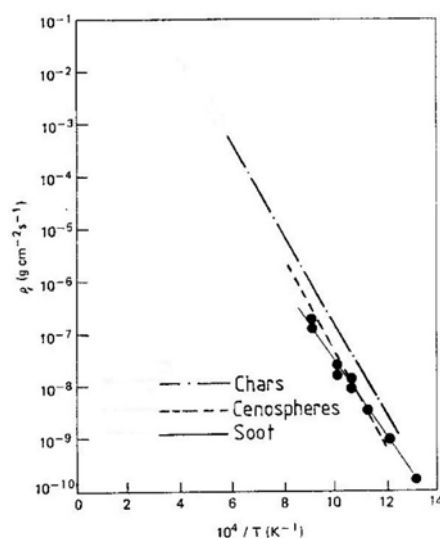


Figure 5- 16 intrinsic oxidation rate of soot, HFO cenospheres and cokes based on (39)

5.3.6 Environmental significance of heavy oil asphaltene structure

Emissions from the stacks of furnaces burning heavy oils e.g. bunker fuel, in both mobile and stationary sources pose significant threats to the environment in a number of ways since, as it was observed in previous work (6), collected stack solids (the sum of soot and cenospheres)

increased linearly with the square of the asphaltene content of the oil. Emissions from shipping make a particularly important contribution to atmospheric pollution and comparisons among different real-world operations have been made (264).

A comparison of the emission factors from stationary industrial boilers and boilers with different fuels revealed that the burning of heavy oil produced the most pollutants, by a factor of over four in comparison with Diesel (265). Similarly, the emissions from heavy-oil fired plant were the highest among a variety of sources.

The hazardous emissions are principally carbonaceous particles, generally with adsorbed organic compounds, which are primarily produced by burning heavy oil, are termed particulate matter (PM) or so-called black carbon (BC); this impacts directly on climate change by absorbing heat from the atmosphere and also affecting the albedo of snow and ice on which it is deposited thus increasing the Global Warming Potential (GWP). Indeed it has been estimated that BC aerosols are the second most important contribution to GWP after carbon dioxide (196). BC also contribute to respiratory and cardiac disease since cenosphere size distribution depends on the asphaltene content of the oil; for an oil containing 9% asphaltenes over 90% of the cenospheres had diameter <20 μm so that they can penetrate deep into the lungs. The World Health Organisation has recently designated atmospheric PM as a group 1 carcinogen (245, 248).

Figure 5-10 shows how some of the PAH liberated during asphaltene pyrolysis are potential soot precursors. A variety of routes are available from the early stages of combustion, including hydrogen abstraction/carbon addition (HACA), through cyclopentadienyl, or by pyrosynthesis. Any of the 2-4 ring parent PAH found here (see Table 5-3) can act as the starting compound for the synthesis of dense, planar 'protographite' soot; reaction with CPDyl can lead to soot molecules with a more open structure; and PAH with curved structures from PAH with a five-membered ring can lead to 'protofullerenes' in which the sheets curl over. In contrast with the indications of the concentration of vanadium with cenospheres discussed above, Jang et al. found (266) that vanadium was enriched in the fine particles (<0.1 μm diameter), i.e. soot, from the combustion of heavy oils. These observations point to two different mechanisms for

vanadium concentration consequent on the presence of both thermally stable vanadium alkyl porphyrins and vanadium bound by hetero atoms within the asphaltene structure. Gas chromatography –AED (267) with selective detection of vanadium at 292 nm, shows that the vanadium porphyrins may be transferred to the gas phase along with the soot precursors at temperatures between 350 and 400°C. Compounds derived from the (tetrapyrrole) alkyl porphyrins are hence likely to accumulate in the combustion soot, but at higher temperatures (> 400°C) the alkyl vanadium porphyrins are transformed (47) into multiaryl vanadium porphyrins which collect, along with the bound vanadium, in the char which forms the cenospheres. The bound vanadium also affords the possibility of involvement in bridges between the ‘building blocks’ of the parent asphaltene, in addition to the bonds through alkyl and sulphide groups discussed above.

5.4 Conclusions

Based on the preceded experimental investigations the following conclusions are summarised. Petroleum asphaltenes were pyrolysed in a hyphenated Py-GC system. Mass spectrometry detection revealed the presence in the products of mono and hydroaromatic compounds and alkylated PAH in addition to long-chain alkanes and alkenes. The patterns of alkyl substitution and the contribution of long alkyl chains suggest affinities between the structures of petroleum asphaltenes and lower MW constituents of petroleum. However, these results are consistent with an ‘archipelago’ structure for asphaltenes in which alkyl substituted small (1 to 4 ring) aromatic ring systems are linked by bridging groups. A general reaction scheme for thermal reactions of asphaltenes accounts for ignition and soot formation in the gas phase and cenosphere formation in the solid phase, all via formation and reaction of ‘building block’ radicals in the liquid phase.

Chapter 6 Bio-oil combustion and its derived asphaltenes

6.1 Introduction

There is interest in the use of bio-oil as an alternative to petroleum fuel oils and studies have been made into their handling and combustion properties. Units of ‘‘asphaltene-like’’ material which are about 35 to 40Å in size form aggregates with themselves, although remaining dispersed in the oil. However, the actual nature of the chemical bonding (such as polar interactions, acid-based interactions between the basic nitrogen and acidic carbonyl groups) that exist between the monomer of asphaltene molecules of these aggregates is not fully understood. Hence this problem has attracted research attention (6, 268).

Nowadays, the utilization of renewable energy resources carriers as replaceable sources of energy for conventional fuels have been improving. Energy from biomass combustion is a promising, clean, and renewable energy, although there is difficulty in utilising due to the low energy density. Bio-oil provides one way of improving the energy density of biomass.

Fast pyrolysis technologies have been extensively applied, and the energy content of fast pyrolysis oil (bio-oil) is approximately ten times that of the original biomass by volume (12, 140). In the case of a centralised pyrolysis process, the cost of biomass feedstock collection is reduced significantly. Bio-oil has a low calorific value (on a mass basis) and poor thermal stability due to its high oxygen content which limits its extensive application and replacement of fossil-based fuels. Thus, bio-oil upgrading and also related technologies for bio-oil utilisation, including combustion characteristics studies, became necessary as an answer to this problem.

Several researches have been undertaken towards characterizing and upgrading crude bio-oil (152, 153). Additionally, the nature and the structure of the composition of these oils during combustion, as well as new bio-refinery technologies which reduced oxygenates in bio-oils have been investigated by many research authors. Separation and fractionation into different fractions such as aliphatic, aromatic, polar fractions, and ‘‘asphaltene’’ became interesting areas for many researches (269, 270). All fractions that have been widely studied were analyzed by GC-MS

except for the ‘‘asphaltene’’ fraction [12-14]. Currently, in order to determine the nature and structure of bio-oil ‘‘asphaltene’’, we employed both raw bio-oil (upgraded or fast pyrolysis bio-oil) and its extracted asphaltene fraction for investigation.

In petroleum chemistry the asphaltenes are defined as the fraction of a heavy hydrocarbon oil insoluble in an alkane but soluble in an aromatic hydrocarbon solvent. The asphaltene content of bio-oils has a significant effect on their combustion behaviour and consequent environmental impact, so that knowledge of the composition and mode of action of these asphaltenes is increasingly important. Because of the use of bio-oils in thermal power plant and boiler facilities and as transport fuels the study of these equivalent asphaltenes (or ‘bio-asphaltenes’) is of significant interest. During these applications there are emissions of carbonaceous particles ('black carbon', BC) along with carcinogenic polycyclic aromatic hydrocarbon (PAH) soot precursors, both of which are major health hazards, especially for the respiratory and cardiac systems; it is also thought that BC comes second only to CO₂ in terms of climate -forcing.

Firstly, in this work, bio-oil (upgraded bio-oil) was studied for its physical and chemical parameters such as density, viscosity, kinematic viscosity, (at two different temperatures), and heating values (146, 271).

Secondly, the composition and chemical structure of asphaltenes separated from bio-oils has been investigated by novel pyrolysis-gas chromatography-mass spectrometric (Py-GC-MS) and thermogravimetry- infra red spectroscopic (TGA-IR) techniques. Comparisons were made with the properties of corresponding petroleum-derived asphaltenes. Emphasis was placed on both compositional structure, (although particulate compositions such as cenosphere and small diameter soot may be present, including BC components) and the vapour phase products of bio-oil and bio-asphaltene (heavy aromatics fractions) pyrolysis and combustion so as to determine the origin and mechanism of the effect on the environment of the use of bio-oils.

6.2 Background

- ❖ Asphaltene has been originally defined by many authors as a distillation residue of bitumen, insoluble in alcohol and soluble in turpentine (268, 272). Asphaltene is termed as the heaviest compound of petroleum fluids that are insoluble in light hydrocarbons such as n-pentane (nC₅) or n-heptane (nC₇) but soluble in aromatic solvents such as toluene (273).
- ❖ It's believed that crude petroleum consist of thousands of components of different classes (SARA based on their solubility in organic solvents). Asphaltene happens to be an extremely complex and variable mixture of crude oil (274, 275).
- ❖ PAHs are termed as persistent organic compounds and priority pollutants. They are produced during the combustion process and also due to pyrolysis reactions in cooler, fuel rich zones of the internal combustion engine reported by Lea-Langton., *et al* (2013) (6). Additionally, they are hydrophobic and exhibit a high accumulation in the living system. Unlike in living systems, asphaltene causes serious complex problems in the petroleum industry because of its low dissolving power. Its accumulation in the production system may cause the obstruction of wells and transport lines(276, 277).
- ❖ Petroleum asphaltene is mainly aliphatic and polycyclic aromatic hydrocarbons. However, there exists a small portion of heterocyclic compounds containing oxygen, nitrogen and sulphur components as well as organometallic compounds (such as porphyrins) which are due to the heavy metals (nickel, vanadium etc.) that are present in small proportion.
- ❖ Its concentration largely affects the burning properties of heavy fuel oil and its analyses are becoming more significant now as it has a distortion on the global environment. In fact, this study is not restricted to only the oil industry but also to use by thermal power plants, boiler facilities, ship-building industries, oceans vessels port and harbour authorities.

6.2 Aim and objectives

The aim and objectives of this chapter six are described below in this section

6.2.1 Research aims

The aim of this research is to examine the nature and structure of the bio-oil and its heavy fractions, and evaluate the constitutional properties such as the combustion properties of both bio-oil (Fast pyrolysis bio-oil) and its heavy aromatics fractions derived from the oil known as asphaltene under variable temperatures with controlled conditions.

6.3 Experimental techniques

6.3.1 Preparation and extraction of bio-asphaltene

The method for measuring asphaltene from bio-oil using ASTM D6560 was described in **Chapter 3**. All sample work up details and analysis methods were also covered in Chapter 3, and this procedure is shown in the Figure 6-1.

6.3.2 Ultimate analysis and some physical parameters

The N C, H, and S values of the asphaltene fraction were determined by flash combustion using a Thermo- Instruments Flash EA 1112 Series Analyser. Measurements were done as a weight percentage. All measurements were done in duplicates and corrected for moisture, and a mean value was reported. The viscosity, density and kinematic viscosity measurements were conducted using ASTM D 445 method.

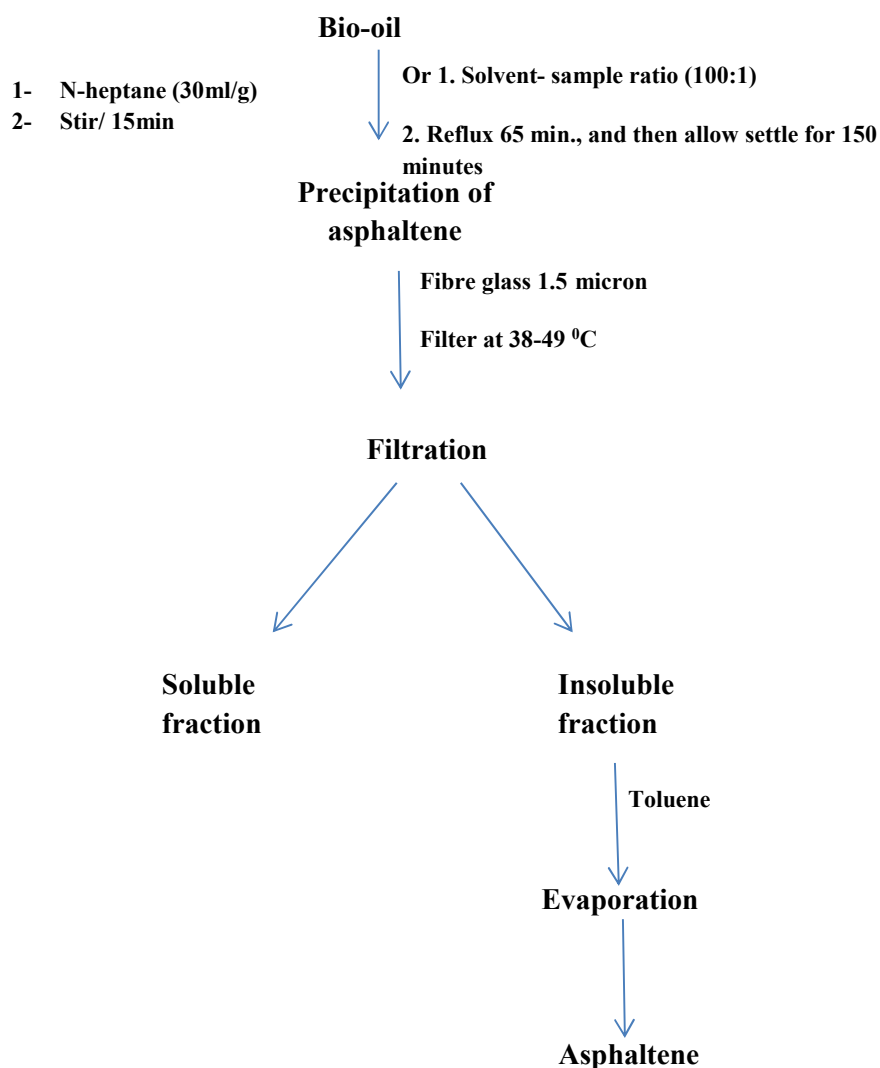


Figure 6- 1 Extraction of Bio-oil-asphaltene (ASTM D6560-IP-143)(171)

6.3.3 Thermogravimetric analysis

The bio-asphaltene combustion investigations were conducted to explore the sample decomposition and combustion behaviour using a Netzsch STA (Simultaneous Thermal analysis) 449C Jupiter®. The STA consist of the simultaneous application of thermogravimetry (TG) (which measures sample mass loss in a stately temperature program) and differential thermal analysis (DTA) (which monitors the temperature difference between the sample and an inert reference material). The heating rate was set to be 10°C/min in 12.5% O₂/He.

10 mg of the sample (< 600 µm) was placed in a microbalance and heated to 900°C at heating rates of 100°C/min and 48 20°C/min under helium flowing at 50 ml min⁻¹. Mass loss curves and

Differential Thermogravimetric (DTG) curves were obtained for each sample and are plotted Figure 6-2 to 4.

6.3.4 Pyrolysis of the bio-oil asphaltene via Py-GC-MS

Pyrolysis of asphaltene generated from bio-oil was studied using a CDS 5000series pyrolyser attached to a Shimadzu 2010 gas chromatograph with mass spectrometric detector. The pyrolyzed products of the sample were separated on an Rtx 1701 60 m capillary column, 0.25 mm i.d., 0.25 μ m film thickness, having a temperature programme of 40°C, which was held for 2 min followed by ramped to 250°C, held time 30 min at a ramp rate 4°C/min, as well as, the column head pressure at 40°C of 30 psi. Identification of the products were made via matching the mass spectrum of each product component with the mass spectrum of a species in the National Institute of Standards and Technology (NIST 2007) spectral library database, and also by matching the product retention time with the reference standards compositional fragments of the compound. These methods are described in detail in **chapter three** of this thesis.

6.4 Results and discussion

6.4.1 Properties of fast pyrolysis bio-oil from pine wood

Bio-oil may replace fossil fuel oils in many applications such as boilers, furnaces, heavy duty engines and turbines in energy generation in the next generation. However, physical fuel properties such as density, viscosity, surface tension, pour point, significantly play important roles in combustion as they for instance, affect flow performances like pump and pipelines design. In addition, they affect the average droplets sizes and hence atomization quality and this in turn affect the efficiency of the combustion and emissions subsequently (270, 278). During spray combustion these parameters determine the droplet sizes as well as the spray penetration and also the cone angle. In this work the viscosity, density at 40 and 20°C have been

investigated for oil from lignocellulosic material (pine wood) and are consistent with the results identified in Lehto, et al 2014 (270) and shown in Table 6-1.

Also in this Table 6-1 carbon, hydrogen, and oxygen content of the bio-oil have been presented. Asphaltene extraction reduces oxygenates in the bio-asphaltene samples compared to the parent oil with increases in carbon and hydrogen contents as shown in Table 6-2; similar results was also detected in Zhang, et al 2014. The NCV is low in the fast pyrolysis oil because of the high water content (typically 20%). Note that the oxygen content is still significant (36.7%).

Table 6- 1 Physical and chemical properties of pyrolysis bio-oil

Parameters	Density (g/cm ⁻³)	Kinematic viscosity Mm ² /s	Dynamic viscosity mPa.s	Carbon content	Hydrogen content	Oxygen content
40°C	1.2037	60.010	72.236	41.04	6.01	52.95
20°C	1.2.172	130.59	158.94			

*Note oxygen calculated by difference. Based on dry basis

Table 6- 2 Elemental composition for Bio-crude asphaltene from fast pyrolysis bio-oil

Carbon%	Hydrogen%	Oxygen %	H/C Ratio	O/C Ratio	NCV kJ/kg	GCV KJ/kg
56.9	6.4	36.7	0.74	0.48	6583	23.27

6.4.2 Thermogravimetric analysis results

The results of TGA analysis of the extracted bio-asphaltene are shown in Figures 6-2 to 6-4.

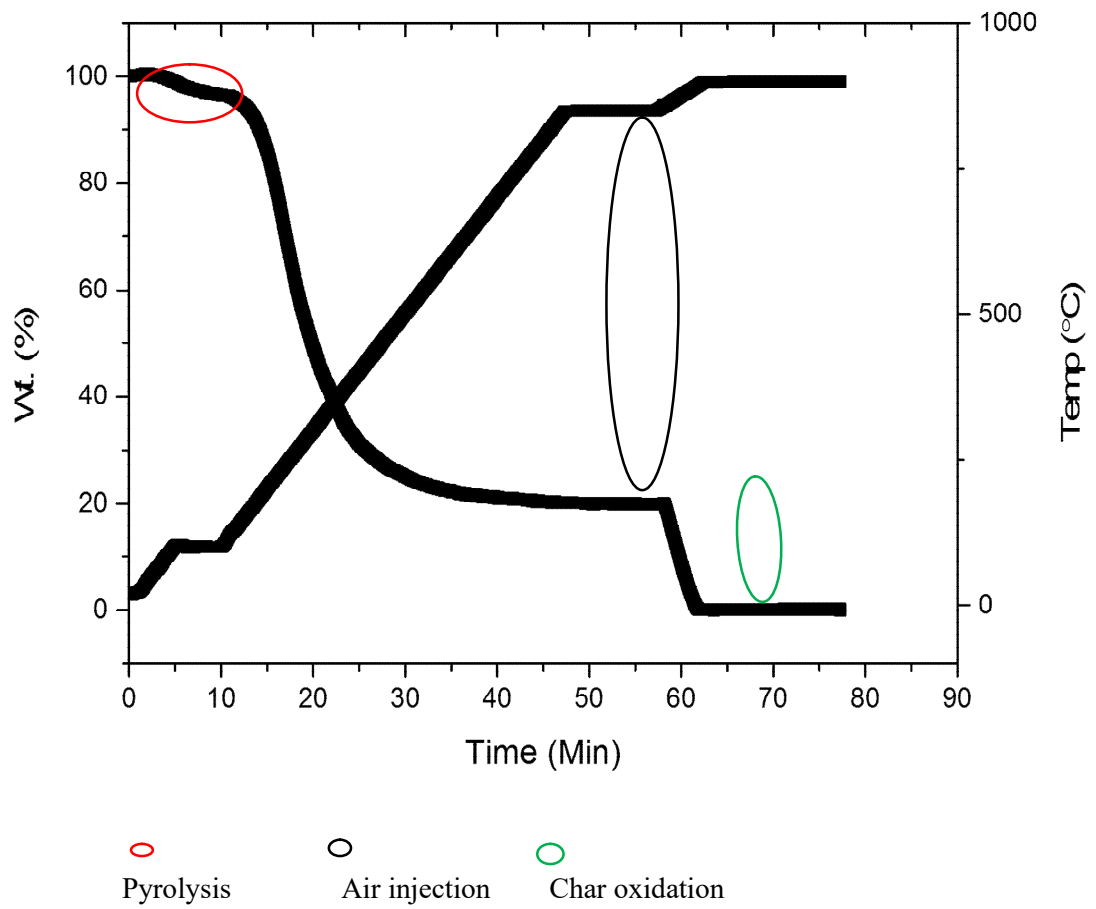


Figure 6- 2 TGA for Bio-oil Asphaltene fraction

Figure 6-2 indicated that the pyrolysis process are more related to the previous samples but less char is observed here. Therefore less cenospheres, and expect more soot traces of cenospheres.

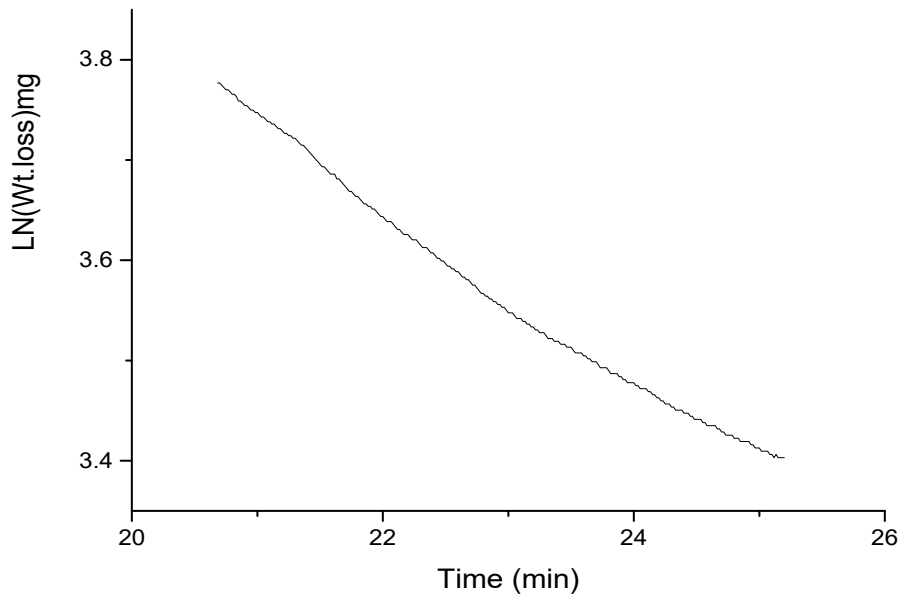


Figure 6- 3 Derivative weight loss for Bio-oil Asphaltene

The above figure indicated that the pyrolysis rates looks the same faster or slower

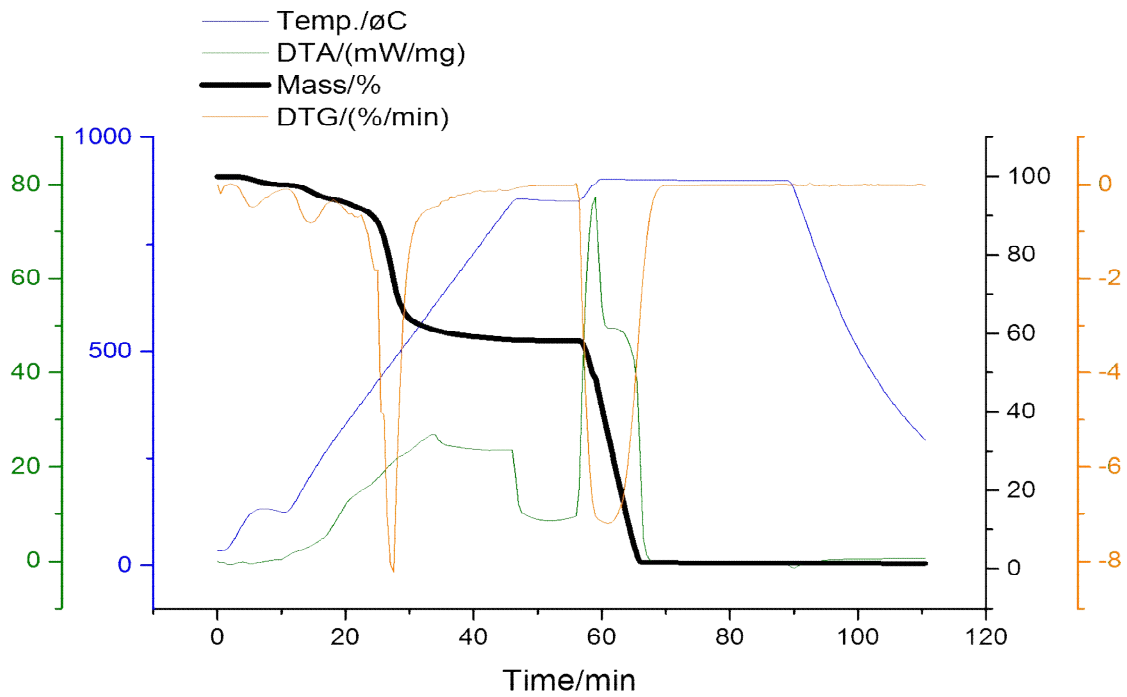


Figure 6- 4 Mass loss curves, derivative of mass loss (DTG) curves and temperature against time for the bio-oil asphaltene sample from TGA pyrolysis using STA

The starting lower heating rate is in order to be able to clearly separate the different processes occurring. Distinctively, two regions of mass loss are seen; an initial mass loss at temperature

<110°C which is due to moisture evaporation and a larger mass loss at $T > 200^{\circ}\text{C}$ due to the release of volatile species. The residue that remains at 850°C is the elemental carbon comprising of a chars. It is observed from Figure 6-2 that there is higher volatile matter content compared to petroleum asphaltene (Figs 5-2 & 5-3) which is an indication that the ratio of organic carbon OC will be higher in comparison to elemental carbon EC, and also gives higher mass loss in pyrolysis region.

Figure 6-3 displays the DTG curve, which also show how these heavy fractions behave under pyrolysis conditions. A distinct peak between 250°C and 500°C can be attributed to evaporation/decomposition of the fractions in this case of fast pyrolysis bio-oil, the most likely oils are the biomass decomposition products, particularly those from lignin-namely substituted phenols. There may also be small amount of oils (such as fatty acids) which have high boiling points (270). This is discussed further in Section 6.4.3 where pyrolysis GC-MS was carried out at lower temperature (300°C-1200°C) for the sources of these fractions under investigation. Note that the bio-oil is derived from hemicellulose (decomposition occurs 220-315°C), cellulose decomposition (occurs 315-400°C), and lignin decomposition (Darvell et al., 2010, Giuntoli et al., 2009, Mansaray and Ghaly, 1998)(279-281) to produce monomers and oligomers which are the asphaltene fraction.

6.4.3 Pyrolysis gas chromatography mass spectrometry Py-GCMS

6.4.3.1 Pyrolysis of Bio-oil

The chromatograms for the bio-oil pyrolysed at 300°C – 1200°C are shown in above **Figures 6-4 to 14** respectively. The corresponding peak identities of the components are listed in **Tables 6-3 to 6-12** respectively. The peak identities have been determined from the NIST 05A MS library and by comparison with previous work (93, 222, 240, 270, 282). Pyrolysis at low temperature (Figure 6-5 & 6-6) results in evolution of lignocellulosic decomposition products, including acetic acid, alkyl phenols, methoxy phenols, furanone, and furfural.

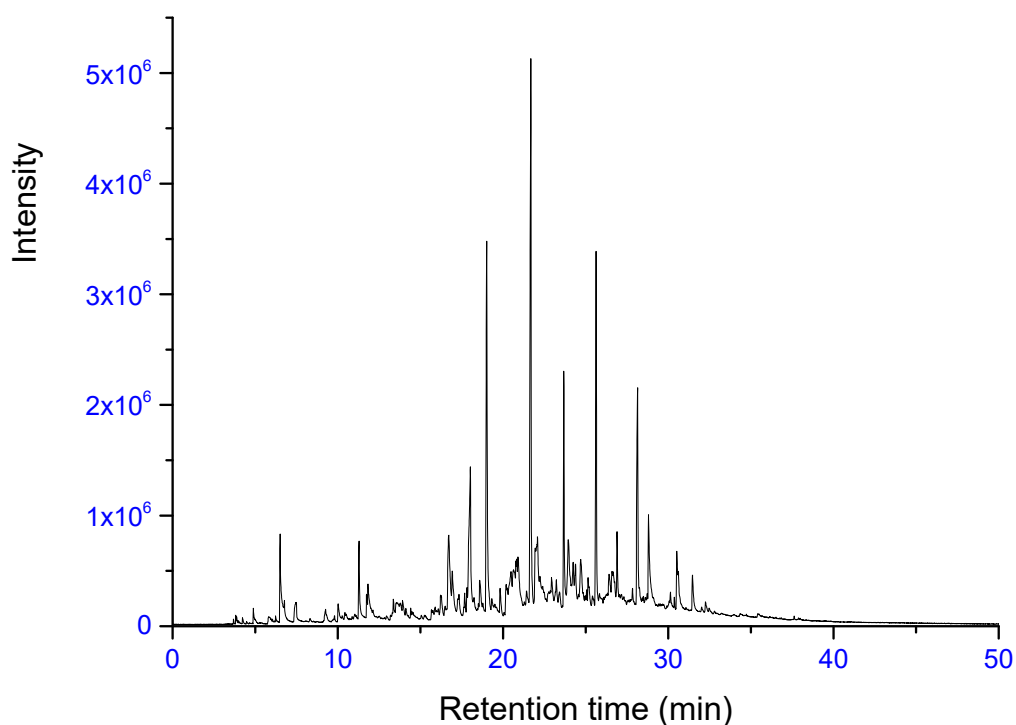


Figure 6- 5 Py-GCMS Chromatogram of Bio-oil with marker compounds indicated at 300°C pyrolysis temperature.

The compounds identified are shown below.

Table 6- 3 Compound identification for bio-oil at 300°C pyrolysis temperature

Peak#	Ret.Time	Area%	Name
1	6.508	2.83	Acetic acid
2	11.282	2.44	Unknown
3	11.733	0.47	Phenol, 2,6-dimethoxy-
4	16.713	4.61	2(5H)-Furanone
5	17.667	0.33	Ethanone, 1-(4-hydroxy-3,5-dimethoxyphenyl)
6	17.808	0.65	Phenol, 4-ethyl-
7	18.022	8.66	1,2-Cyclopentanedione, 3-methyl-
8	19.013	15.44	Phenol, 2-methoxy-
9	20.826	0.58	Phenol, 2-methoxy-3-methyl-
10	21.683	21.09	Phenol, 2-methoxy-4-methyl-
11	22.086	5.22	1-Isobutoxy-2-ethylhexane
12	23.676	6.26	Phenol, 4-ethyl-2-methoxy-
13	23.944	2.31	Trimethaneacetic acid, decyl ester
14	25.63	11.69	Phenol, 2-methoxy-4-(2-propenyl)-, acetate
15	26.4	0.77	Phenol, 2,6-dimethoxy-
16	26.898	1.75	Phenol, 2-methoxy-4-(2-propenyl)-, acetate
17	28.139	8.5	3,4-Anhydro-d-galactosan
18	28.803	3.48	Vanillin
19	30.515	2.12	Ethanone, 1-(4-hydroxy-3-methoxyphenyl)-
20	30.625	0.77	Octadecanoic acid (Z)-, methyl ester

Table 6- 4 Compound identification for bio-oil at 400°C pyrolysis temperature

Peak#	Ret. Time	Area%	Name
1	6.546	4.48	Acetic acid
2	11.307	2.17	Unknown
3	11.785	1.3	Furfural
4	18.034	7.83	1,2-Cyclopentanedione, 3-methyl-
5	19.022	13.85	Phenol, 2-methoxy-
6	20.818	0.67	Phenol, 3-methyl-
7	21.721	18.12	Phenol, 2-methoxy-4-methyl-
8	21.933	1.73	Phenol, 2,4-dimethyl-
9	22.138	2	Unknown
10	23.698	6.3	Phenol, 4-ethyl-2-methoxy-
11	24.08	4.2	Unknown
12	25.124	2.57	2-Methoxy-4-vinylphenol
13	25.664	12.35	Phenol, 2-methoxy-4-(2-propenyl)-, acetate
14	26.899	2.25	Phenol, 2-methoxy-4-(2-propenyl)-, acetate
15	28.113	7.99	Phenol, 2-methoxy-4-(1-propenyl)-
16	28.158	4.64	1-Butoxy-2-methyl-2-butene (E)-
17	28.823	3.37	Vanillin
18	30.514	2.2	Ethanone, 1-(4-hydroxy-3-methoxyphenyl)-
19	30.625	0.66	Guanosine, 2-deoxy-N-trimethyl acetate
20	31.452	1.3	2-Propanone, 1-(4-hydroxy-3-methoxyphenyl)-

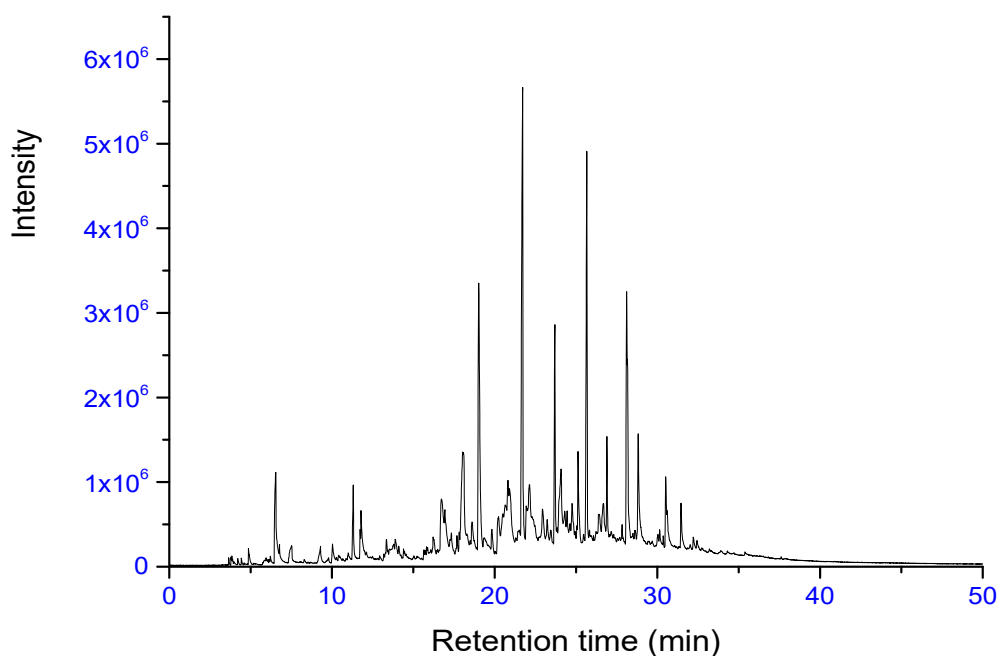


Figure 6- 6 Py-GCMS Chromatogram of Bio-oil with marker compounds indicated at 400°C pyrolysis temperature.

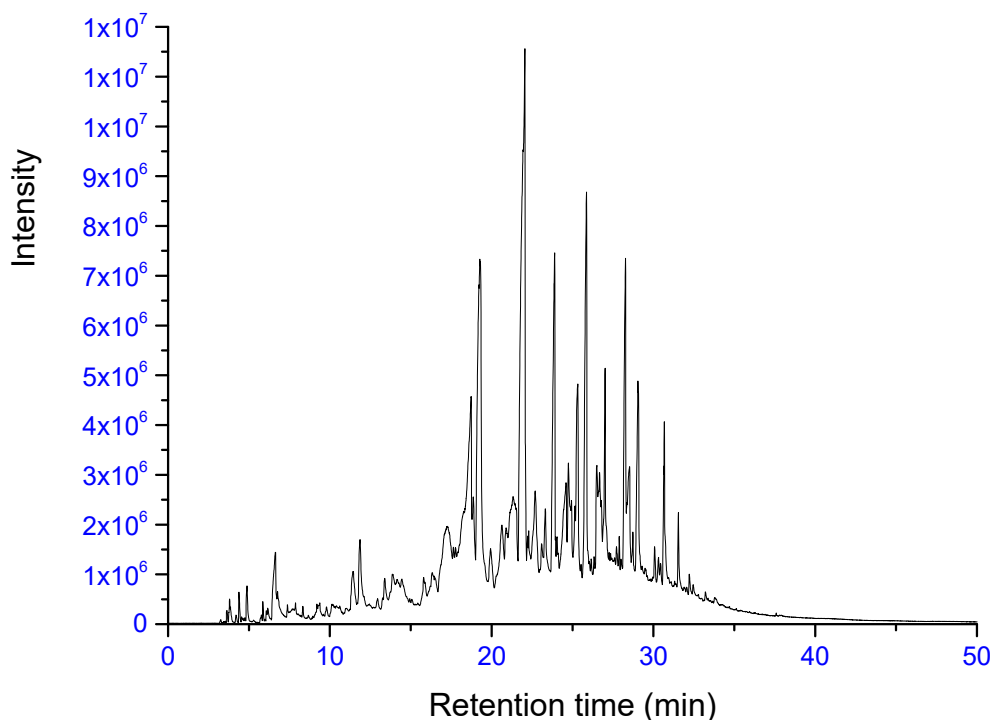


Figure 6- 7 Py-GCMS Chromatogram of Bio-oil with marker compounds indicated at 500°C pyrolysis temperature.

Table 6- 5 Identification of compound for bio-oil at 500°C pyrolysis temperature

Peak#	Ret. Time	Area%	Name of compound
1	6.644	1.71	Unknown
2	11.865	1.36	3,5-Dimethylpyrazole-1-methanol
3	18.6	1.26	2-Cyclopenten-1-one, 2-hydroxy-3-methyl-
4	18.738	1.69	1,2-Cyclopentanedione, 3-methyl-
5	19.267	14.59	Phenol, 2-methoxy-
6	22.055	25.56	Phenol, 2-methoxy-4-methyl-
7	22.695	1.34	2-Octenoic acid, (E)-
8	23.319	1.08	Benzene, 1,4-dimethoxy-2-methyl-
9	23.895	8.38	Phenol, 4-ethyl-2-methoxy-
10	24.743	1.68	Benzene, 1,4-dimethoxy-2-methyl-
11	24.942	1.03	Anhydro-d-mannosan
12	25.325	4.56	2-Methoxy-4-vinylphenol
13	25.864	9.2	Phenol, 2-methoxy-3-(2-propenyl)-
14	26.505	2.13	1,2-Benzenediol
15	26.683	2.6	3-Penten-2-one, 4-(2,2,6-trimethyl-7-oxabicyclo[4.1.0]hept-1-yl)-, (E)-
16	27.014	3.64	Phenol, 2-methoxy-3-(2-propenyl)-
17	28.274	6.75	Phenol, 2-methoxy-4-(1-propenyl)-, (Z)-
18	28.529	3.68	1-Butene, 3-butoxy-2-methyl-
19	29.044	4.84	Vanillin
20	30.675	2.93	Ethanone, 1-(4-hydroxy-3-methoxyphenyl)-

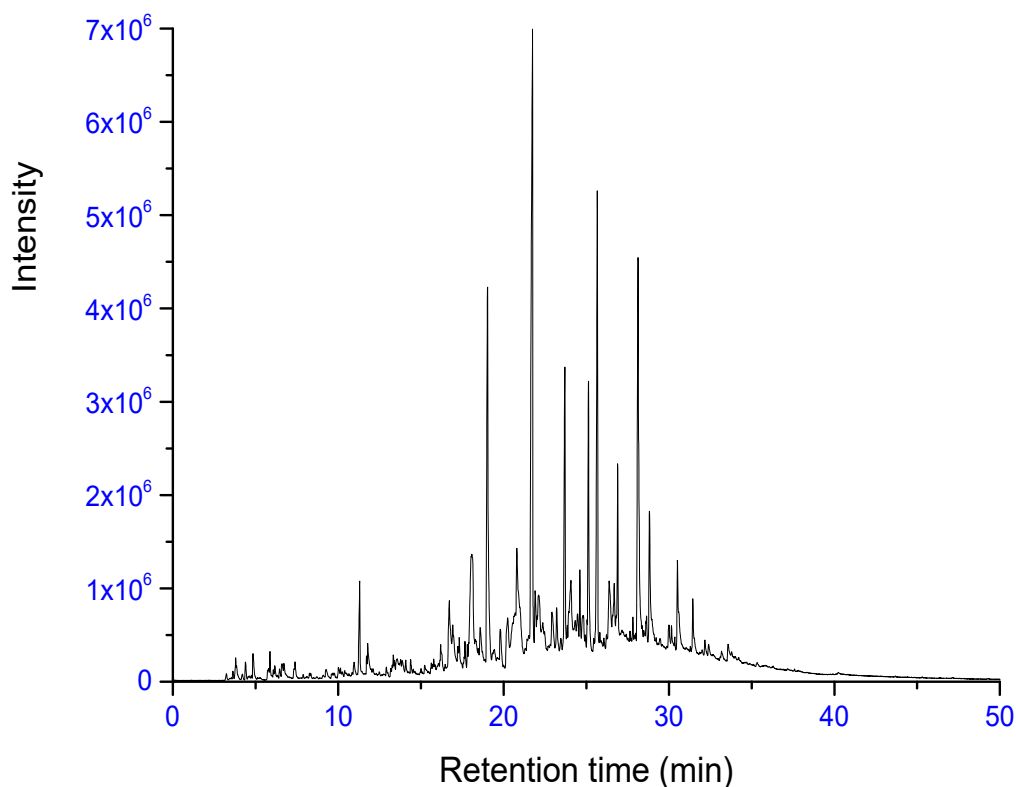


Figure 6- 8 Py-GCMS Chromatogram of Bio-oil with marker compounds indicated at 600°C pyrolysis temperature.

Table 6- 6 Compound identification for bio-oil at 600°C pyrolysis temperature

Peak#	Ret. Time	Area%	Name of compound
1	11.297	2.03	Unknown
2	16.717	2.16	2(5H)-Furanone
3	17.8	0.53	2(5H)-Furanone, 3-methyl-
4	18.078	6.93	1,2-Cyclopentanedione, 3-methyl-
5	19.029	12.67	Phenol, 2-methoxy-
6	20.798	1.42	Phenol, 3-methyl-
7	21.748	21.92	Phenol, 2-methoxy-4-methyl-
8	21.905	1.36	Phenol, 2,5-dimethyl-
9	22.11	2.15	Unknown
10	23.204	0.78	3-Isopropylidene-5-methyl-hex-4-en-2-one
11	23.704	6.69	Phenol, 4-ethyl-2-methoxy-
12	24.067	2.66	Unknown
13	24.607	1.13	Benzeneethanol, 2-methoxy-
14	25.13	6.36	2-Methoxy-4-vinylphenol
15	25.665	11.12	Eugenol
16	26.895	2.51	Phenol, 2-methoxy-4-(2-propenyl)-, acetate
17	28.127	12.43	Phenol, 2-methoxy-4-(1-propenyl)-
18	28.817	3.07	Vanillin
19	30.509	1.27	Ethanone, 1-(4-hydroxy-3-methoxyphenyl)-
20	31.438	0.79	2-Propanone, 1-(4-hydroxy-3-methoxyphenyl)-

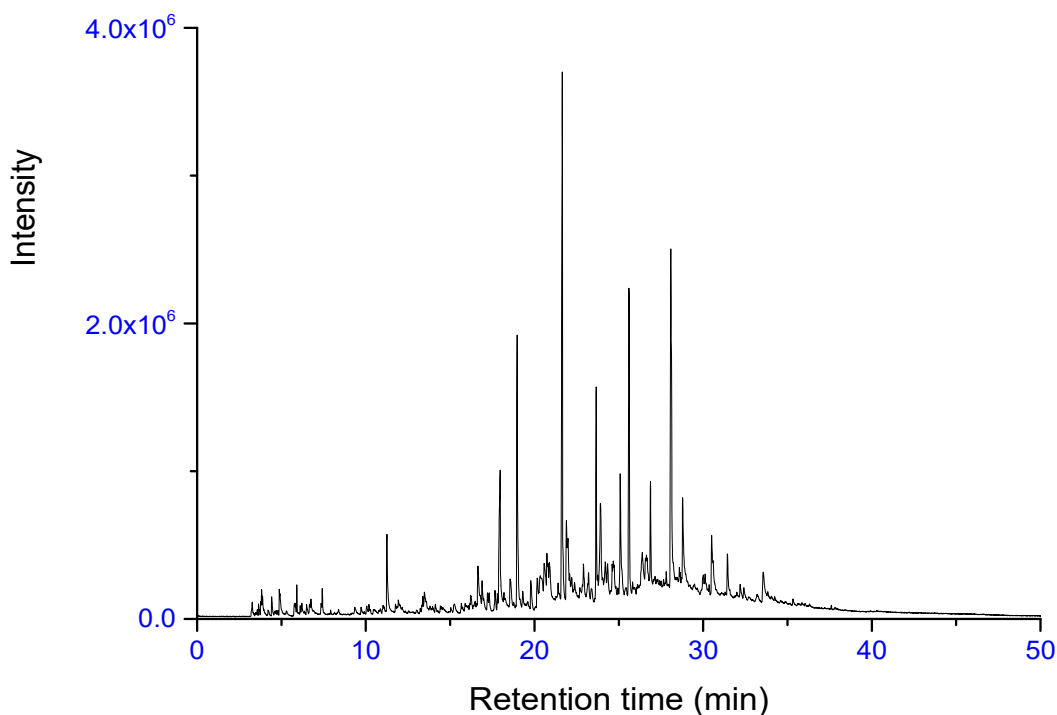


Figure 6- 9 Py-GCMS Chromatogram of Bio-oil with marker compounds indicated at 700°C pyrolysis temperature.

Table 6- 7 Compound identification for bio-oil at 700°C pyrolysis temperature

Peak#	Ret.Time	Area%	Name of compound
1	3.828	0.54	1-Methylcyclopropanemethanol
2	11.25	2.44	Unknown
3	16.642	1.81	Unknown
4	17.963	5.95	2-Cyclopenten-1-one, 2-hydroxy-3-methyl-
5	18.971	8.54	Phenol, 2-methoxy-
6	20.158	1.39	2-Cyclohexen-1-one, 3-(hydroxymethyl)-6-(1-methylethyl)-
7	20.317	2.09	Unknown
8	20.567	1.35	Unknown
9	20.736	0.64	Phenol, 3-methyl-
10	21.649	17.04	Phenol, 2-methoxy-4-methyl-
11	21.892	2.61	Phenol, 2,4-dimethyl-
12	22	2	Unknown
13	22.903	0.82	Phenol, 2-ethyl-
14	23.657	5.13	Phenol, 4-ethyl-2-methoxy-
15	23.911	4.7	Cyclohexanol, 4-methyl-, cis-
16	24.674	2.13	4,5-Octanediol, 2,7-dimethyl-
17	25.085	3.28	2-Methoxy-4-vinylphenol
18	25.603	10.19	Phenol, 2-methoxy-4-(2-propenyl)-, acetate
19	26.383	2.39	1,3-Benzodioxole, 2-methoxy-
20	26.64	2.21	2-Hydroxy-3-methylsuccinic acid
21	26.875	3.12	Phenol, 2-methoxy-4-(2-propenyl)-, acetate
22	28.083	14.1	Phenol, 2-methoxy-4-(1-propenyl)-
23	28.785	2.88	Benzaldehyde, 3-hydroxy-4-methoxy-
24	30.505	1.33	Ethanone, 1-(4-hydroxy-3-methoxyphenyl)-
25	31.439	1.32	2-Propanone, 1-(4-hydroxy-3-methoxyphenyl)-

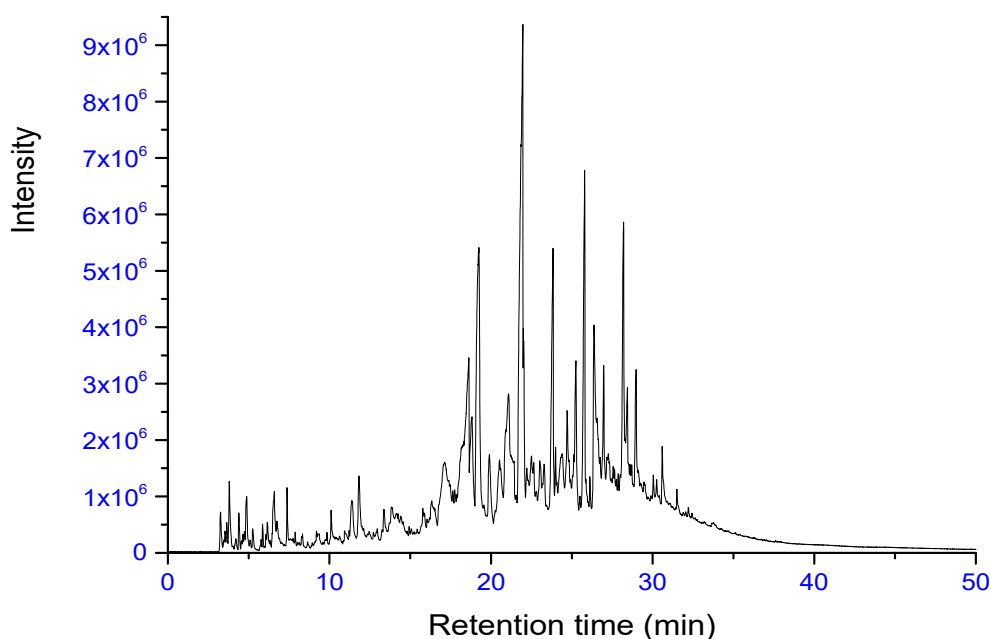


Figure 6- 10 Py-GCMS Chromatogram of Bio-oil with marker compounds indicated at 800°C pyrolysis temperature.

Table 6- 8 Compound identification for bio-oil at 800°C pyrolysis temperature

Peak#	Ret. Time	Area%	Name of compound
1	3.26	0.7	Bicyclo[1.1.0]butane
2	3.801	1.49	3-Buten-1-ol, 2-methyl-
3	4.876	1.02	Cyclobuta[1,2-d:3,4-d']bis[1,3]dioxole-2,5-dione, tetrahydro-
4	6.591	1.23	Unknown
5	7.376	0.68	Toluene
6	11.831	1.33	Unknown
7	18.625	2.59	2-Cyclopenten-1-one, 2-hydroxy-3-methyl-
8	18.816	2.96	Phenol
9	19.249	14	Phenol, 2-methoxy-
10	19.893	2.54	Phenol, 2-methyl-
11	21.08	4.52	Phenol, 4-methyl-
12	21.85	12.41	Phenol, 2-methoxy-4-methyl-
13	21.963	11.24	Phenol, 2-methoxy-4-methyl-
14	22.001	2.95	Butanoic acid, 3-methyl-, 1-ethenyl-1,5-dimethyl-4-hexenyl ester
15	23.835	7.72	Phenol, 4-ethyl-2-methoxy-
16	24.71	1.13	2,4-Dimethylanisole
17	25.251	3.42	2-Methoxy-4-vinylphenol
18	25.791	8.72	Phenol, 2-methoxy-3-(2-propenyl)-
19	26.369	3.87	1,2-Benzenediol
20	26.971	1.79	Phenol, 2-methoxy-3-(2-propenyl)-
21	27.256	0.95	Unknown
22	28.2	6.91	Phenol, 2-methoxy-4-(1-propenyl)-
23	28.438	2.67	1-Butene, 3-butoxy-2-methyl-
24	28.595	0.84	Phenol, 2-methyl-6-(2-propenyl)-
25	28.976	2.33	Vanillin

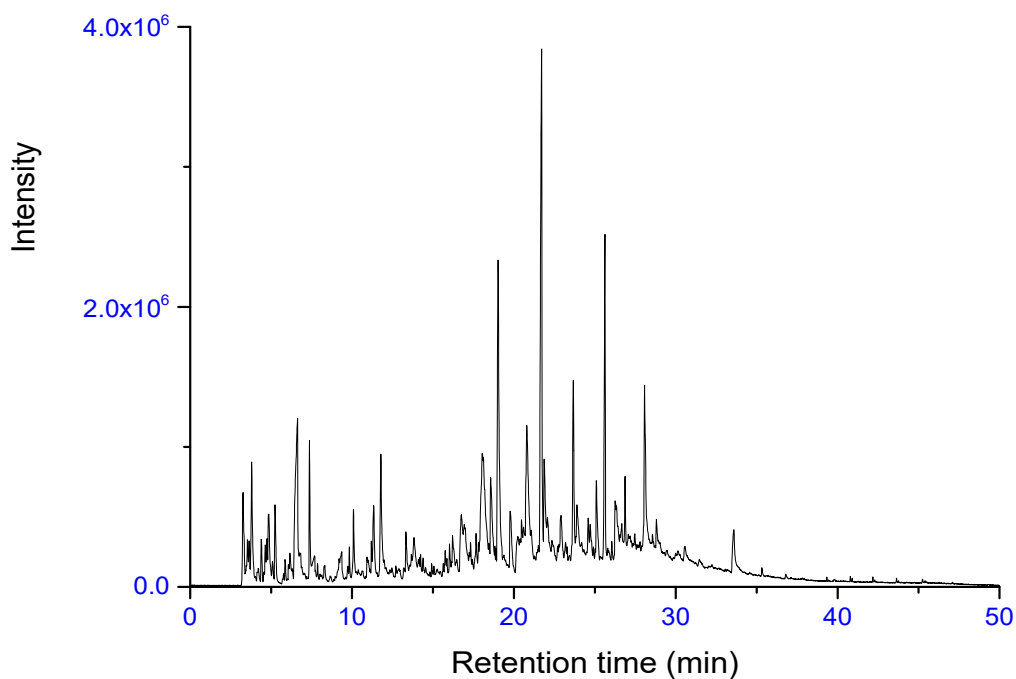


Figure 6- 11 Py-GCMS Chromatogram of Bio-oil with marker compounds indicated at 900°C pyrolysis temperature.

Table 6- 9 Compound identification for bio-oil at 900°C pyrolysis temperature

Peak#	Ret. Time	Name of compound
1	3.263	1,3-Butadiene
2	3.537	1,3-Pentadiene, (Z)-
3	3.797	Bicyclo[2.2.1]non-2-ene, 5-(aminomethyl)-, exo- or endo-
4	4.392	Furan, 2-methyl-
5	4.743	Unknown
6	4.849	Butanedioic acid, cyclic hydrazide
7	5.239	Benzene
8	6.638	Unknown
9	7.367	Toluene
10	10.087	p-Xylene
11	11.336	Unknown
12	11.779	Unknown
13	18.041	1,2-Cyclopentanedione, 3-methyl-
14	18.561	Phenol
15	19.024	Phenol, 2-methoxy-
16	19.762	Phenol, 2-methyl-
17	20.796	Phenol, 3-methyl-
18	21.711	Phenol, 2-methoxy-4-methyl-
19	21.87	Phenol, 2,4-dimethyl-
20	23.669	Phenol, 4-ethyl-2-methoxy-
21	25.093	2-Methoxy-4-vinylphenol
22	25.621	Phenol, 2-methoxy-4-(2-propenyl)-, acetate
23	26.865	Phenol, 2-methoxy-4-(2-propenyl)-, acetate
24	28.07	Phenol, 2-methoxy-4-(2-propenyl)-, acetate
25	33.588	D-Allose

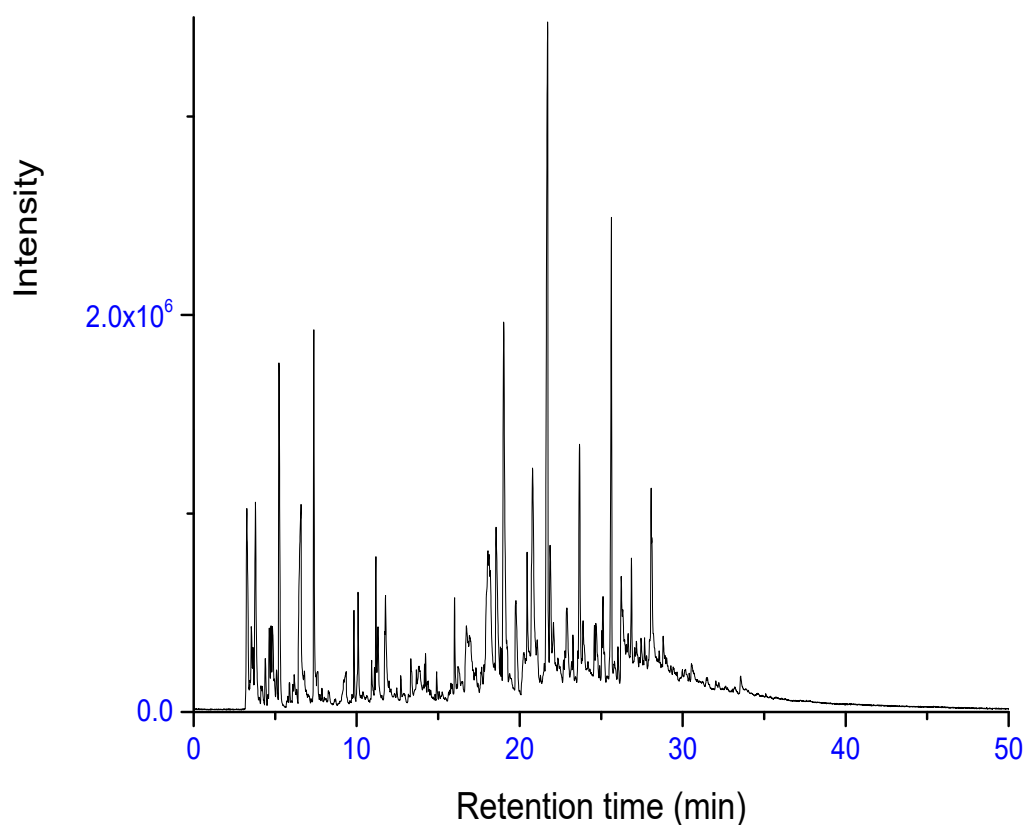


Figure 6- 12 Py-GCMS Chromatogram of Bio-oil with marker compounds indicated at 1000°C pyrolysis Temp.

At higher temperatures (500-700°C) most of the products detected are from lignocelluloses and include methoxyphenols and eugenol, furfural derivatives, and some possible heterocyclic aromatics like indole, imidazole and pyrrole are also detected (Figure 6-6 to 7); these types of compounds are also detected during vapour-phase cracking of eugenol (283).

Table 6- 10 Compound identification for bio-oil at 1000°C pyrolysis temperature

Peak#	Ret. Time	Area%	Name of compound
1	3.26	5.08	1,3-Butadiene
2	3.525	2.32	1,3-Pentadiene, (Z)-
3	3.789	5.04	Unknown
4	4.383	0.72	Furan, 2-methyl-
5	4.633	0.9	-
6	5.236	7.51	Benzene
7	6.586	7.02	Unknown
8	7.369	5.27	Toluene
9	9.83	1.09	2,4,6-Tri-O-benzyl-.alpha.-d-glucose
10	10.086	1.11	o-Xylene
11	11.176	1.47	Bicyclo[4.2.0]octa-1,3,5-triene
12	11.717	0.67	-
13	11.765	1.76	3-Furaldehyde
14	16.005	1.23	Unknown
15	19.02	11.14	Phenol, 2-methoxy-
16	20.454	1.44	Naphthalene
17	20.793	6.63	Phenol, 3-methyl-
18	21.716	18.31	Phenol, 2-methoxy-4-methyl-
19	21.866	2.83	Phenol, 2,4-dimethyl-
20	23.671	4.91	Phenol, 4-ethyl-2-methoxy-
21	25.113	1.11	2-Methoxy-4-vinylphenol
22	25.625	8.28	Phenol, 2-methoxy-4-(2-propenyl)-, acetate
23	26.859	0.97	Phenol, 2-methoxy-4-(2-propenyl)-, acetate
24	28.063	1.94	Phenol, 2-methoxy-4-(2-propenyl)-, acetate
25	28.117	1.23	1-Butene, 3-butoxy-2-methyl-

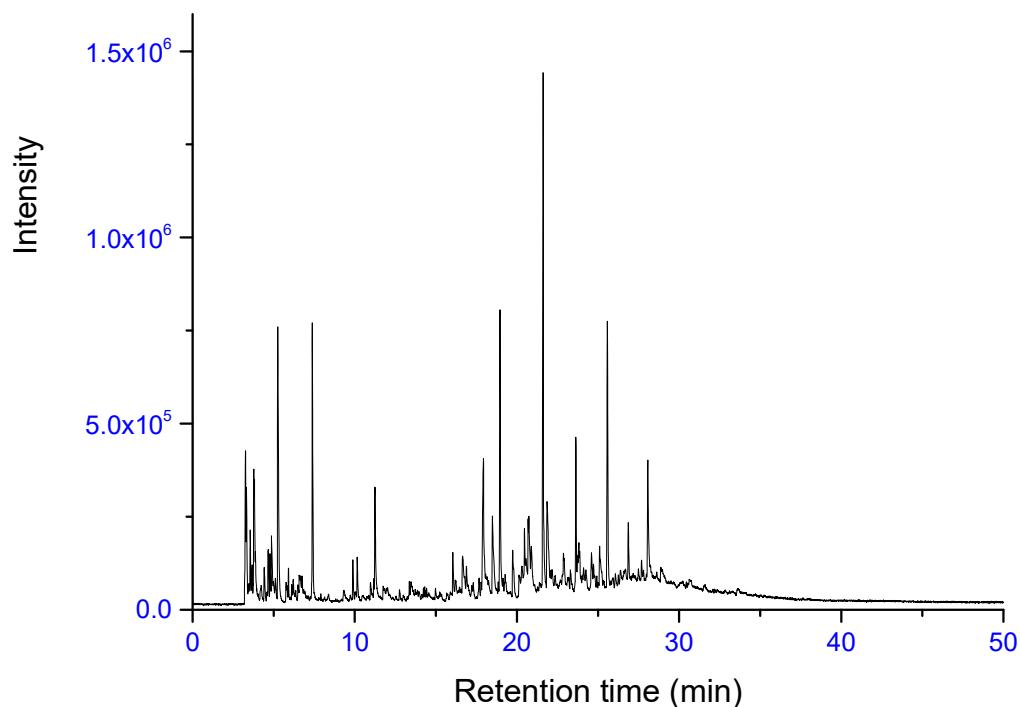
**Figure 6- 13 Py-GCMS Chromatogram of Bio-oil with marker compounds indicated at 1100°C pyrolysis temperature.**

Table 6- 11 Compound identification for bio-oil at 1100°C pyrolysis temperature

Peak#	Ret. Time	Area%	Name
1	3.262	4.51	1,3-Butadiene
2	3.32	2.8	1-Buten-3-yne
3	3.552	2.14	2-ethenyl cyclohexane
4	3.773	2.65	1,3-Cyclopentadiene
5	3.817	2.63	3-Buten-1-ol, 2-methyl-
6	4.663	1.82	2-Methoxy-4-vinylphenol
7	4.769	1.41	1,5-cyclooctadiene
8	4.867	2.28	Unknown
9	5.1	1.31	Xylene
10	5.251	9.57	Benzene
11	7.382	7.0	Toluene
12	11.244	3.45	Styrene
13	16.642	1.92	Undetermined--
14	17.933	5.77	2-Cyclopenten-1-one, 2-hydroxy-3-methyl-
15	18.487	3.63	Phenol
16	18.956	7.92	Phenol, 2-methoxy-
17	20.735	2.16	Phenol, 3-methyl-
18	20.885	1.28	2,7-Unknown
19	21.617	13.24	Phenol, 2-methoxy-4-methyl-
20	21.861	4.51	Phenol, 2,6-dimethyl-
21	23.635	3.13	Phenol, 4-ethyl-2-methoxy-
22	24.592	1.28	4,7-Methano-1H-indene-1,8-dione, 3a,4,7,7a-tetrahydro-
23	25.575	8.41	Phenol, 2-methoxy-4-(2-propenyl)-, acetate
24	26.868	1.53	Phenol, 2-methoxy-4-(2-propenyl)-, acetate
25	28.068	3.67	Phenol, 2-methoxy-4-(2-propenyl)-, acetate

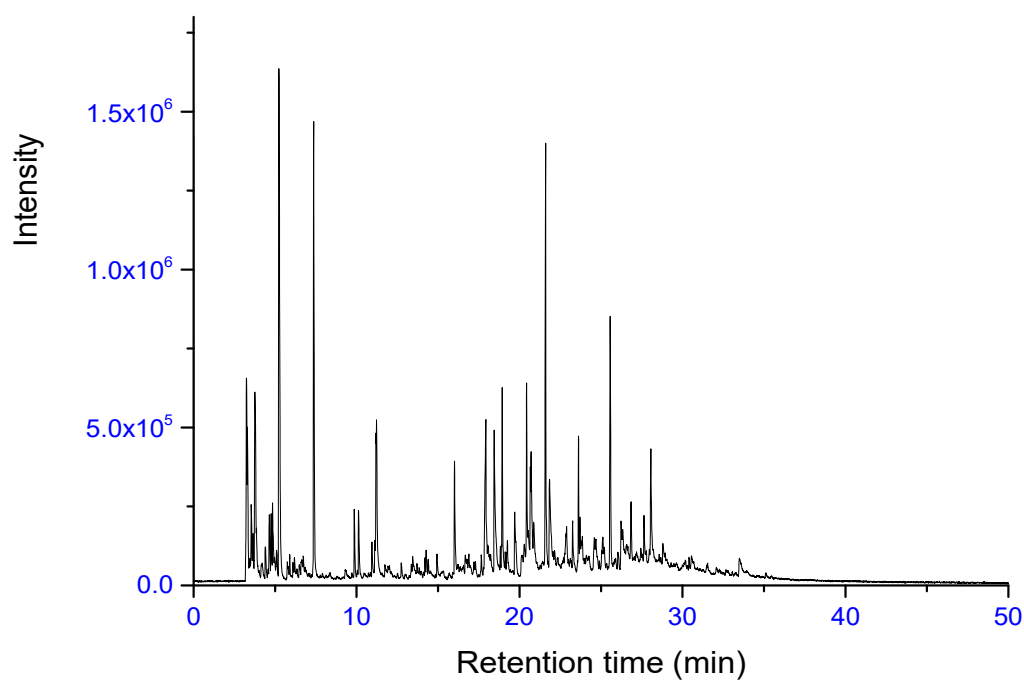
**Figure 6- 14 Py-GCMS Chromatogram of Bio-oil with marker compounds indicated at 1200°C pyrolysis temperature.**

Table 6- 12 Compound identification for bio-oil at 1200°C pyrolysis temperature

Peak no.	Ret. Time	Area%	Name of compound	Marker
1	3.245	5.26	1,3-butadiene	
2	3.302	3.28	1-buten-3-yne	
3	3.535	2.09	1,3-pentadiene, (Z)-	
4	3.76	5.25	1,3-cyclopentadiene	
5	4.648	1.48	1,3,5-hexatriene, (Z)-	
6	4.76	1.28	cyclopentanedione	
7	4.842	1.37	Unknown	
8	5.233	16.87	Benzene	
9	7.365	10.01	Toluene	
10	9.859	1.36	Ethylbenzene	
11	10.12	1.47	o-Xylene	
12	11.183	1.88	Styrene	
13	11.223	3.44	Unknown	
14	16.008	2.38	Indene	
15	17.93	4.99	1,2-Cyclopentanedione, 3-methyl-	
16	18.444	4.77	Phenol	
17	18.938	3.57	Phenol, 2-methoxy-	
18	20.432	3.35	Azulene	
19	20.658	1.91	Phenol, 3-methyl-	
20	20.709	2.62	Phenol, 2-methyl-	
21	21.6	8.89	Phenol, 2-methoxy-4-methyl-	
22	23.62	2.05	Phenol, 4-ethyl-2-methoxy-	
23	25.563	6.21	Phenol, 2-methoxy-4-(2-propenyl)-, acetate	
24	26.842	1.39	Phenol, 2-methoxy-4-(2-propenyl)-, acetate	
25	28.057	2.81	3,4-Anhydro-d-galactosan	

For pyrolysis between 700 and 1000°C most of the products are aromatics such as benzenes, phenols, but now secondary products begin to form including naphthalenes, indenenes as well as, some PAHs precursors. These cracking products are associated with lignin decomposition products of pine wood and also consistent with the pyrolysis products during combustion of pine wood detected by Fitzpatrick, et al., 2007 (201). In general, data interrogation of these high temperatures demonstrates small quantities of PAHs, O-PAH, and trace amount of hetero atoms (PANH such as carbazole, and benzocarbazole). However, these results revealed that there is no PASH detected at the pyrolysis level and this is consistent with the elemental analyses which indicate a level of sulphur content below the detection limits. Table 6-1. Some of the peaks detected could not be reliably identified from the NIST05A library and they are suspected to be nitrogen containing compounds.

6.4.3.2 Pyrolysis of asphaltene derived from pyrolysis bio-oil

Pyrolysis for the asphaltene fraction derived from bio-oil was conducted for comparison with results for petroleum based asphaltene using pyrolysis gas chromatography mass spectrometry.

The analysed results for these experiments were shown in Figs 6-15-23.

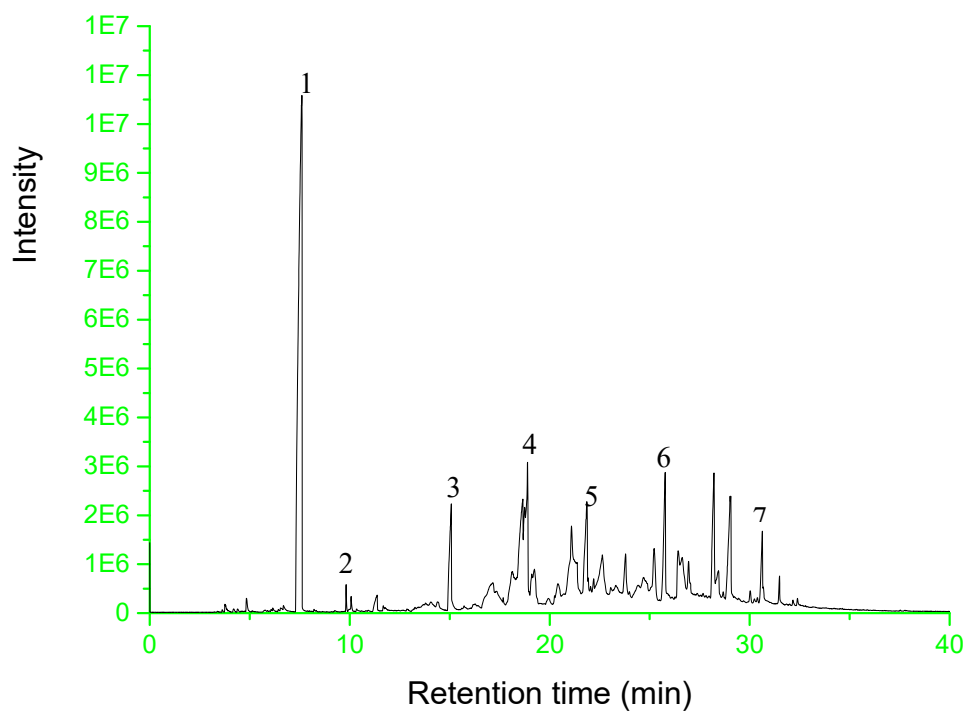


Figure 6- 15 Py-GCMS chromatogram of asphaltene extract from Pyrolysis bio-oil at 300°C

The key makers are: 1. Toluene, 2: 2-Deoxy ribitol, 3: Benzaldehyde, 4: Benzyl alcohol, 5:

Phenol, 2-methoxy-4-methyl-, 6: Phenol, 2-methoxy-3-(2-propenyl)-, 7: Cyclohexanone, 2-(2-methyl propylidene

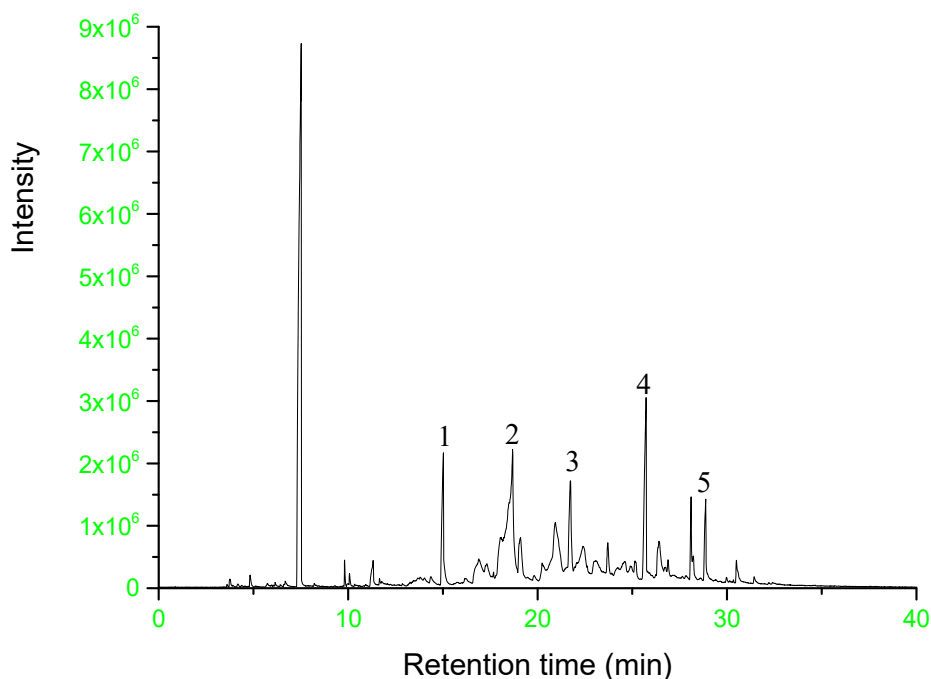


Figure 6- 16 Py-GCMS chromatogram of asphaltene extract from Pyrolysis bio-oil at 400°C

The key makers are: 1: Toluene, 2: Benzaldehyde, 3: Phenol, 2-methoxy-4-(2-propenyl)-, acetate, 4: Phenol, 2-methoxy-3-(2-propenyl)-, 5: Vanillin

Table 6- 13 Interrogation of the GCMS data for bio-oil asphaltene from Bio-oil at 300C

Number	Molecular weight (m/z)	Retention time	Class of ompounds	Comments
1	92	7.467	Alkyl benzene	BM
2	106	14.933	Alkyl benzene	BM
3	120	24.033	Alkyl benzene	BM
4	128	27.633	Naphthalene	BM
5	134	23.158	1,4-Methanonaphthalene, 1,4-dihydro-	PBM
6	142	24.458	2,7-Naphthalenediol, decahydro-	BM
7	156	ND	Naphthalene	-
	152	ND	Naphthalene	-
	164	ND	Alkyl naphthalene	-
8	170	ND	Naphthalene	-
9	178	ND	Phenanthrene	-
10	184	ND	Naphthalene	-
11	192	ND	1-H-Indene, 2-butyl-5-hexalocahydro-	-
12	206	ND	Alkyl Phenanthrene	-
13	220	ND	Alkyl Phenanthrene	-
14	234	ND	Alkyl Phenanthrene	-
15	252	ND	ND	-
16	216	ND	Pyrene	-
17	202	ND	Pyrene	-

Note: PBM-perfect best match 96-99%, BM-best match 80-90%

Table 6- 14 Interrogation of the GCMS data for bio-oil asphaltene from Bio-oil at 400°C

Number	Molecular weight (m/z)	Retention time	Class of ompounds	Comments
1	92	7.608	Benzene	PBM
2	106	15.050	Xylene	PBM
3	120	ND	Alkyl benzene	-
4	128	19.383	Naphthalene	PBM
5	134	27.675	Naphthalene	BM
6	142	23.325	2,7-Naphthalenediol, decahydro-	
7	156	26.725	Naphthalene	-
	152	28.992	Naphthalene	
	164	25.742	Alkyl naphthalene	BM
8	170	ND	Naphthalene	-
9	178	ND	Phenanthrene	-
10	184	ND	Naphthalene	-
11	192	ND	1-H-Indene, 2-butyl-5-hexalocahydro-	-
12	206	ND	Alkyl Phenanthrene	-
13	220	ND	Alkyl Phenanthrene	-
14	234	ND	Alkyl Phenanthrene	-
15	252	ND	ND	-
16	216	ND	Pyrene	-
17	202	ND	Pyrene	-
18	228	ND	Chrysene	-
18	242	ND	Chrysene	-
19	276	ND	Picene	-
20	278	ND	Picene	-

Note: PBM-perfect best match 96-99%, BM-best match 80-90%

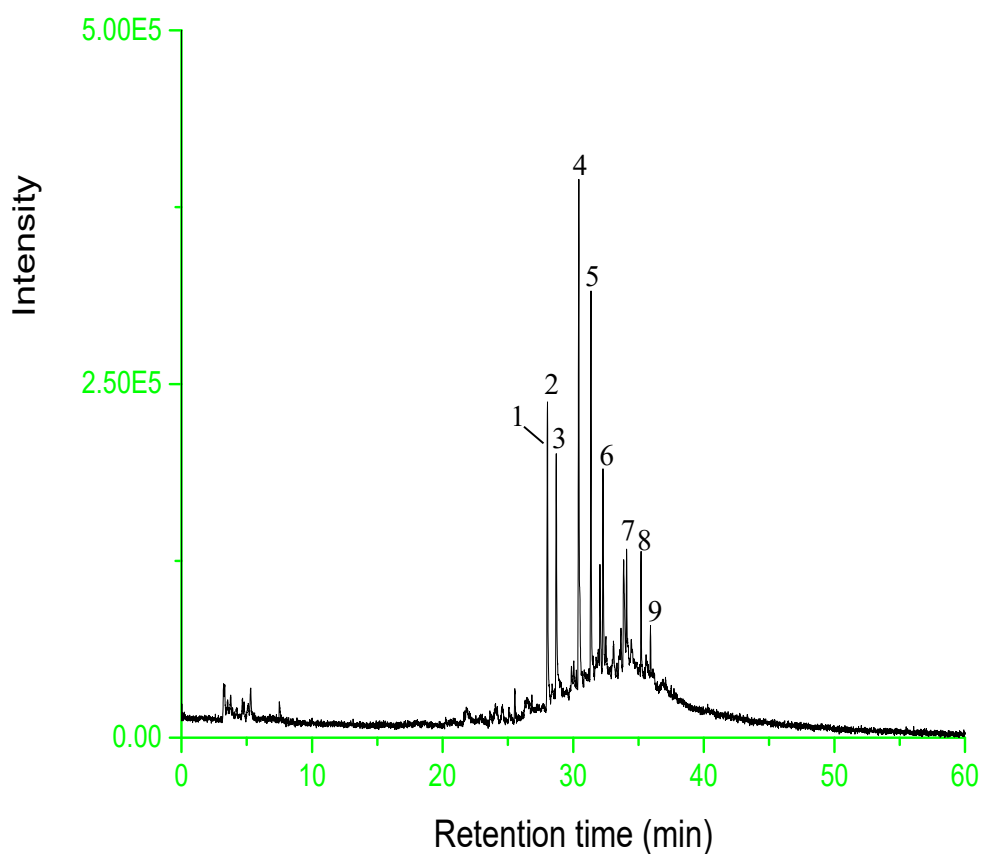


Figure 6- 17 Py-GCMS chromatogram of asphaltene extract from Pyrolysis bio-oil at 500°C

Key markers are: 1: 7,7a-Dimethyl-3a,4,5,7a-tetrahydro-3H-benzofuran-2-one, 2: Cyclooctene, 1,2-dimethyl-, 3: Cyclohexanone, 3-vinyl-3-methyl-, 4: Pentanoic acid, 2-isopropoxyphenyl ester, :5 2H-Pyran, tetrahydro-2-(2-propynyloxy)-, 6: Phenol, 2-methoxy-4-(1-propenyl)-, 7: Benzaldehyde, 3-hydroxy-4-methoxy-, 8: 4-Hydroxy-2-methoxybenzaldehyde, 9: 2-Propanone, 1-(4-hydroxy-3-methoxyphenyl)-

Table 6- 15 Interrogation of the GCMS data for bio-oil asphaltene from Bio-oil at 500°C

S/N	Molecular weight (m/z)	Retention time	Class of ompounds	Comments
1	92	7.392	Alkyl benzene	PBM
2	106	16.108	Alkyl benzene	PBM
3	120	16.447	Alkyl benzene	PBM
4	128	21.392	Naphthalene	PBM
5	134	18.702	1,4-Methanonaphthalene, 1,4-dihydro-	-
6	142	23.801	2,7-Naphthalenediol, decahydro-	
7	156	ND	Naphthalene	-
	152	ND	Naphthalene	-
	164	ND	Alkyl naphthalene	
8	170	28.800	Naphthalene	BM
9	178	35.300	Phenanthrene	BM
10	184	ND	Naphthalene	
11	192	37.316	1-H-Indene, 2-butyl-5-hexalocahydro-	BM
12	206	39.194	Alkyl Phenanthrene	
13	220	ND	Alkyl Phenanthrene	
14	234	ND	Alkyl Phenanthrene	
15	252	ND	ND	
16	216	44.107	Pyrene	BM
17	202	41.632	Pyrene	BM
18	228	ND	ND	
18	242	ND	ND	
19	276	ND	ND	
20	278	ND	ND	

Note: PBM-perfect best match 96-99%, BM-best match 80-90%

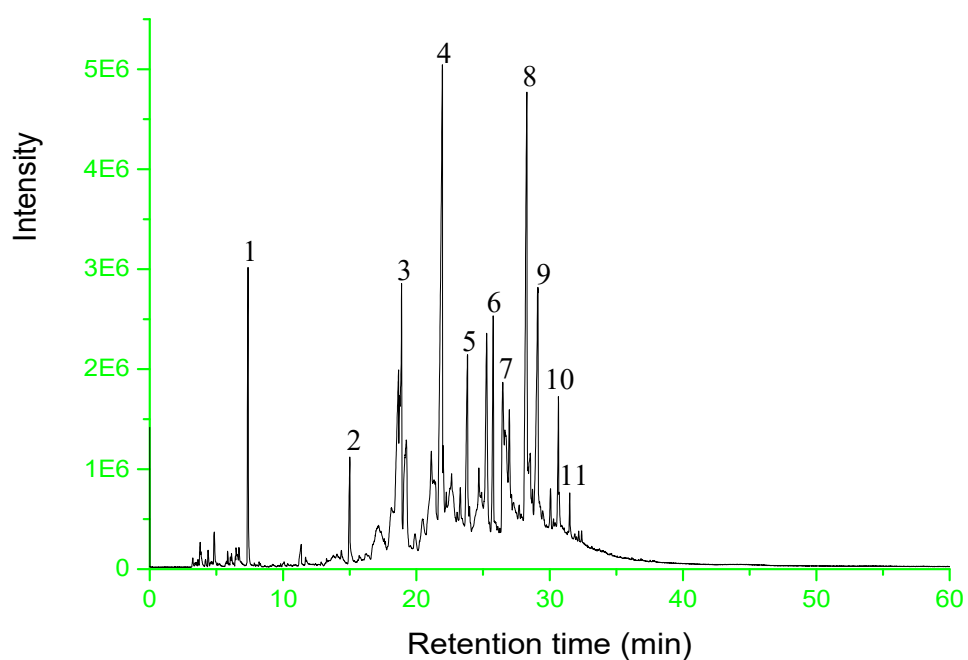


Figure 6- 18 Py-GCMS chromatogram of asphaltene extract from Pyrolysis bio-oil at 600°C

Key markers are: 1. Toluene, 2: Benzaldehyde, 3: 1-Cyclohexene-1-methanol, 4: p-Cresol, 2-methoxy-, 5: 2-Isopropylidene-5-methylhex-4-enal, 6: 8-Methylenecyclooctene-3,4-diol, 7: 1,3-Benzodioxole, 2-methoxy-, 8: 2(3H)-Benzofuranone, hexahydro-3-methylene-, 9: Benzaldehyde, 4-(acetyloxy)-3-methoxy-, 10: Ethanone, 1-(4-hydroxy-3-methoxyphenyl)-, 11: 2-Propanone, 1-(4-hydroxy-3-methoxyphenyl)-

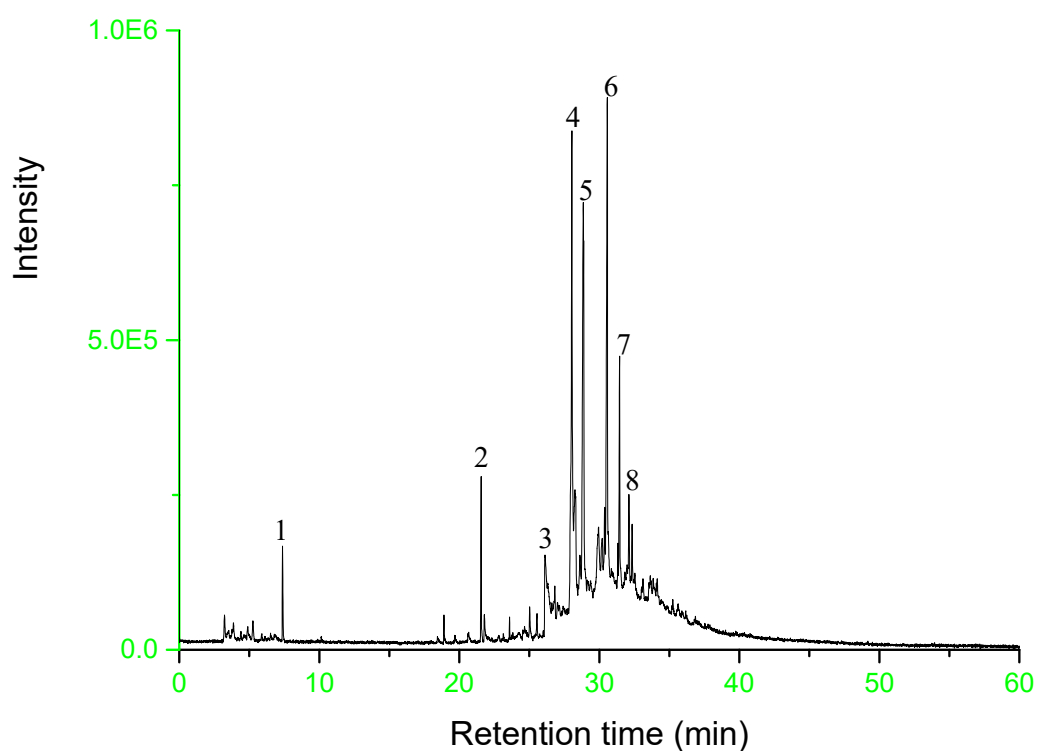


Figure 6- 19 Py-GCMS chromatogram of asphaltene extract from Pyrolysis bio-oil at 700°C

The markers are: 1. Benzaldehyde-2-benzyloxy-3, 5-dimethyl-, 2: Isocarpesterol, 3: 1,3-Benzodioxole, 2-methoxy-, 4: Phenol, 2-methoxy-4-(2-propenyl)-, acetate, 5: 2(3H)-Naphthalenone, 4,4a,5,6,7,8-hexahydro-1-methoxy-, 6: Ethanone, 1-(2-hydroxy-6-methoxyphenyl)-, 7: Phenol, 4-(3-hydroxy-1-propenyl)-2-methoxy-, 8: 2(3H)-Naphthalenone, 4,4a,5,6,7,8-hexahydro-1-methoxy-

Table 6- 16 Interrogation of the GCMS data for bio-oil asphaltene from Bio-oil at 600°C

S/N	Molecular weight (m/z)	Retention time	Class of ompounds	Comments
1	92	7.325	Alkyl benzene	BM
2	106	10.367	Alkyl benzene	BM
3	120	18.717	Alkyl benzene	PBM
4	128	ND	Naphthalene	Showed peaks
5	134	ND	1.4-Methanonaphthalene, 1,4-dihydro-	Showed peaks
6	142	23.542	2,7-Naphthalenediol, decahydro-	-
7	156	ND	Naphthalene	-
	152	29.200	Naphthalene	
	164	28.242	Alkyl naphthalene	
8	170	ND	Naphthalene	-
9	178	ND	Phenanthrene	-
10	184	ND	Naphthalene	-
11	192	ND	1-H-Indene, 2-butyl-5-hexalocahydro-	-
12	206	ND	Alkyl Phenanthrene	-
13	220	ND	Alkyl Phenanthrene	-
14	234	ND	Alkyl Phenanthrene	-
15	252	ND	ND	-
16	216	ND	Pyrene	-
17	202	ND	Pyrene	-
18	228	ND	Chrysene	-
18	242	ND	Chrysene	-
19	276	ND	Picene	-
20	278	ND	Picene	-

Note: PBM-perfect best match 96-99%, BM-best match 80-90%

Table 6- 17 Interrogation of the GCMS data for bio-oil asphaltene from Bio-oil at 700C

Number	Molecular weight (m/z)	Retention time	Class of ompounds	Comments
1	92	7.392	Ethyl benzene	BM
2	106	10.125	Alkyl benzene	BM
3	120	ND	Alkyl benzene	Peaks present
4	128	20.525	Naphthalene	BM
5	134	25.983	1,4-Methanonaphthalene, 1,4-dihydro-	-
6	142	23.383	2,7-Naphthalenediol, decahydro-	-
7	156	ND	Naphthalene	-
	152	ND	Naphthalene	-
	164	28.242	Alkyl naphthalene	-
8	170	29.192	Naphthalene	-
9	178	29.942	Phenanthrene	BM
10	184	ND	Naphthalene	-
11	192	37.707	1-H-Indene, 2-butyl-5-hexalocahydro-	BM
12	206	39.933	Alkyl Phenanthrene	BM
13	220	ND	Alkyl Phenanthrene	-
14	234	ND	Alkyl Phenanthrene	-
15	252	ND	ND	-
16	216	ND	Pyrene	-
17	202	41.850	Pyrene	BM
18	228	ND	ND	-
18	242	ND	ND	-
19	276	ND	ND	-
20	278	ND	ND	-

Note: PBM-perfect best match 96-99%, BM-best match 80-90%

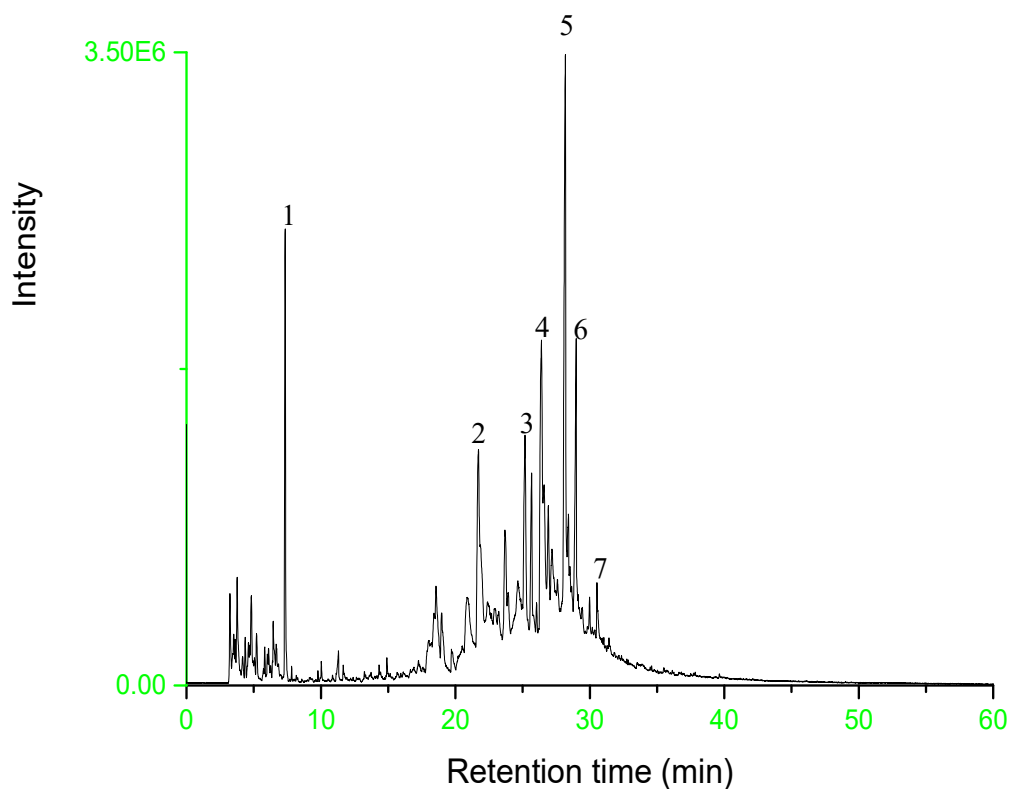


Figure 6- 20 Py-GCMS chromatogram of asphaltene extract from Pyrolysis bio-oil at 800°C

The key markers are: 1. Benzene, methyl/1-Deoxy-2,4:3,5-dimethylene-d-xylitol, 2: Phenol, 2-methoxy-4-methyl-, 3: 2-Methoxy-4-vinylphenol, 4: 1,3-Benzodioxole, 2-methoxy-, 5: Phenol, 2-methoxy-4-(2-propenyl)-, acetate, 6: Benzaldehyde, 4-(acetyloxy)-3-methoxy-, 7: 1,4-Benzenediol, 2-(1,1-dimethylethyl)-

Table 6- 18 Interrogation of the GCMS data for bio-oil asphaltene from Bio-oil at 800°C

S/N	Molecular weight (m/z)	Retention time	Class of ompounds	Comments
1	92	7.292	Alkyl benzene	BM
2	106	10.667	Alkyl benzene	BM
3	120	13.733	Alkyl benzene	BM
4	128	20.408	Naphthalene	BM
5	134	23.992	Alkyl naphthalene	
6	142	24.283	2,7-Naphthalenediol, decahydro-	PBM
7	156	ND	ND	Showed peaks
	152	29.200	Naphthalene	PBM
	164	28.242	Alkyl naphthalene	
8	170	29.192	Naphthalene	BM
9	178	35.683	Phenanthrene	BM
10	184	ND	ND	Showed peaks
11	192	ND	ND	Showed peaks
12	206	39.817	Alkyl Phenanthrene	PBM
13	220	41.800	Alkyl Phenanthrene	
14	234	46.750	Alkyl Phenanthrene	
15	252	ND	ND	No peaks
16	216	44.183	Pyrene	BM
17	202	ND	ND	
18	228	ND	ND	
18	242	ND	ND	
19	276	ND	ND	
20	278	ND	ND	

Note: PBM-perfect best match 96-99%, BM-best match 80-90%

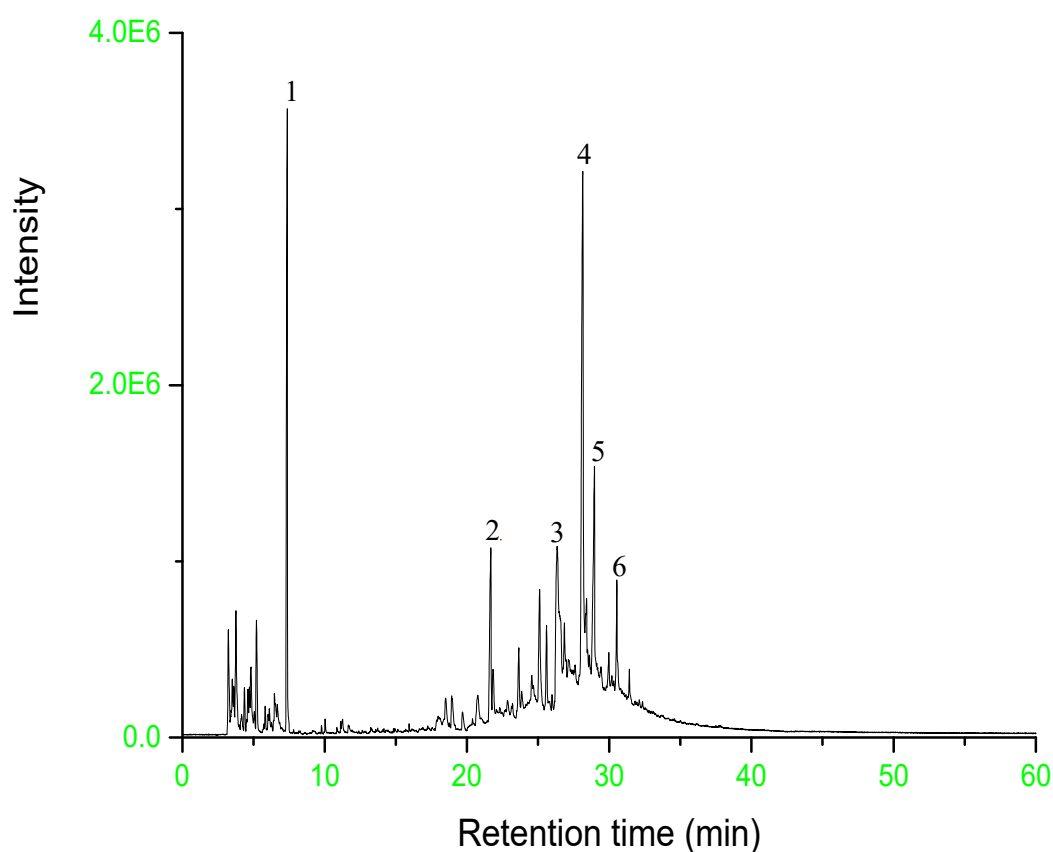


Figure 6- 21 Py-GCMS chromatogram of asphaltene extract from Pyrolysis bio-oil at 900°C
 The key markers are: 1: Bicyclo[1.1.0]butane, 2: Digitoxose, 3: Phenol, 2-methoxy-4-methyl-, 4: Phenol, 2-methoxy-4-(2-propenyl)-, acetate, 5: 2,5-Cyclohexadiene-1,4-dione, 3-hydroxy-5-methyl-2-(1-methylethyl)-, 6: 2(3H)-Naphthalenone, 4,4a,5,6,7,8-hexahydro-1-methoxy-, 7: 1,3-Benzodioxole, 2-methoxy-, 8: Ethanone, 1-(1-hydroxy-2,6,6-trimethyl-2,4-cyclohexadien-1-yl)-, 9: 2(3H)-Naphthalenone, 4,4a,5,6,7,8-hexahydro-1-methoxy-

Table 6- 19 Interrogation of the GCMS data for bio-oil asphaltene from Bio-oil at 900°C

S/N	Molecular weight (m/z)	Retention time	Class of ompounds	Comments
1	92	7.675	Alkyl benzene	PBM
2	106	10.667	Alkyl benzene	PBM
3	120	13.558	Alkyl benzene	PBM
4	128	21.392	Naphthalene	PBM
5	134	22.117	1,4-Methanonaphthalene, 1,4-dihydro-	
6	142	24.283	2,7-Naphthalenediol, decahydro-	
7	156	26.725	Naphthalene	PBM
	152	29.200	Naphthalene	PBM
	164	28.242	Alkyl naphthalene	
8	170	29.192	Naphthalene	
9	178	35.683	Phenanthrene	
10	184	34.917	Naphthalene	
11	192	38.000	1-H-Indene, 2-butyl-5-hexalocahydro-	
12	206	39.817	Alkyl Phenanthrene	PBM
13	220	41.800	Alkyl Phenanthrene	PBM
14	234	46.750	Alkyl Phenanthrene	
15	252	ND	ND	
16	216	44.183	Pyrene	BM
17	202	41.850	Pyrene	BM
18	228	ND	ND	
18	242	ND	ND	
19	276	ND	ND	
20	278	ND	ND	

Note: PBM-perfect best match 96-99%, BM-best match 80-90%

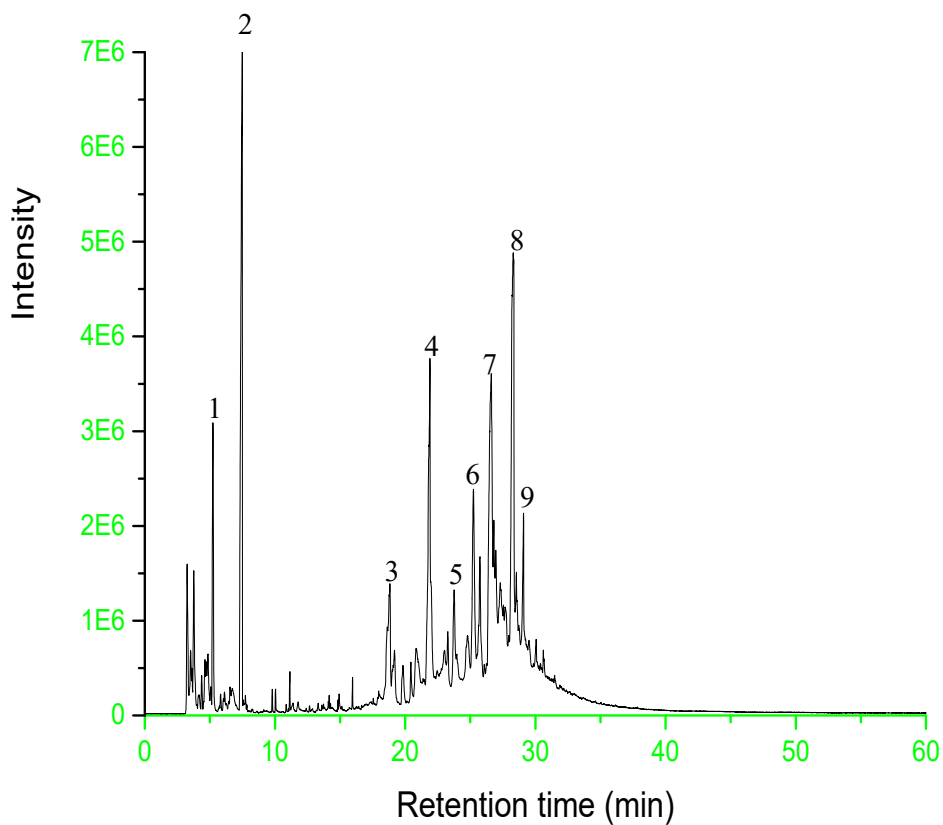


Figure 6- 22 Py-GCMS chromatogram of asphaltene extract from Pyrolysis bio-oil at 1000°C

The key markers are: 1. Coal naphtha, 2: 1,3,5-Cycloheptatriene, 3: cis-1,2-Dihydrocatechol, 4: Phenol, 2-methoxy-4-methyl-, 5: Benzeneethanol, 2-methoxy-, 6: 2-Methoxy-4-vinylphenol, 7: 1,3-Benzodioxole, 2-methoxy-, 8: Acenaphthene, 9: 2(3H)-Naphthalenone, 4,4a,5,6,7,8-hexahydro-1-methoxy-

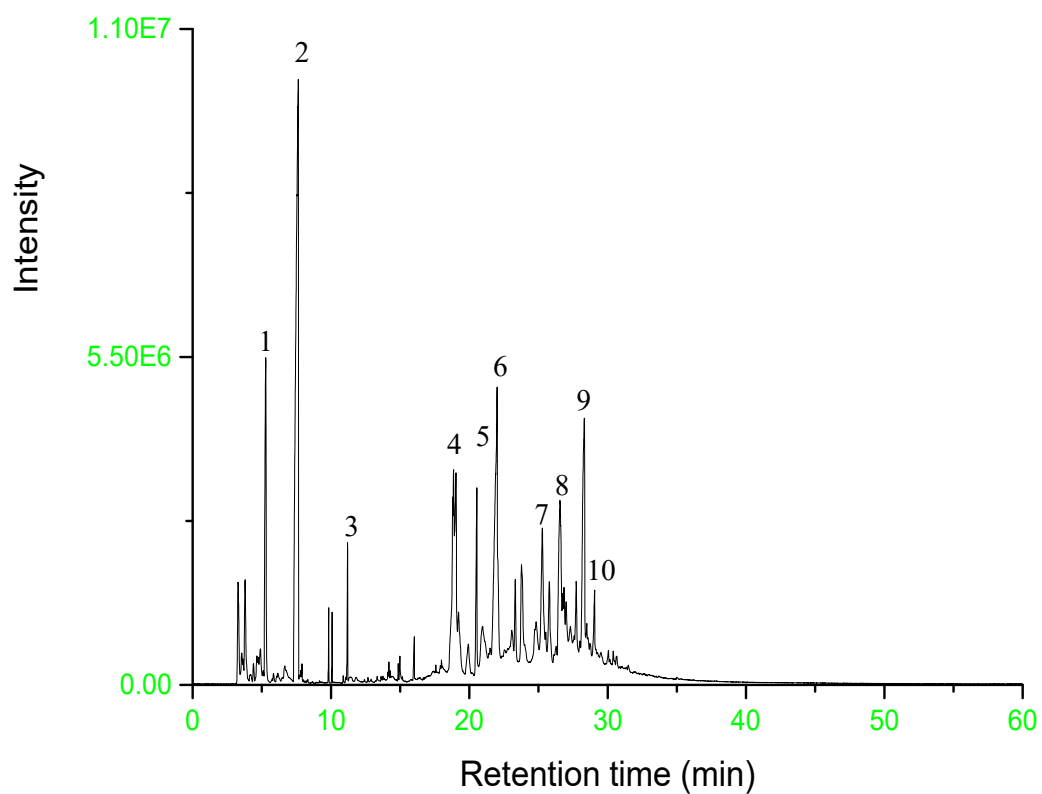


Figure 6- 23 Py-GCMS chromatogram of asphaltene extract from Pyrolysis bio-oil at 1100°C

The key markers are: 1. Benzene, 1-methyl-1, 2-propadienyl-, 2: Toluene, 3: Naphthalene, 4: Phenol, 2-methoxy-4-methyl-, 5: Naphthalene, 1-methyl-, 6: 2-Methoxy-4-vinylphenol, 7: 1,2-Benzenediol, 8: Phenol, 2-methoxy-4-(1-propenyl)-, 9: Phenol, 2-methoxy-4-(1-propenyl)-, 9: Benzaldehyde, 3-hydroxy-4-methoxy-

6.4.4. Nature and pyrolysis bio-oil asphaltene structure

Xu et al, (2014) (284) proposed average structures for bio-asphaltenes on the basis of methods employing NMR and IR spectroscopy originally developed for application to fossil-fuel asphaltene. They put forward structures for bio-asphaltene made of up small number of approximately two ring polycyclic aromatic nuclei and oxygen-substituted saturated rings such as furans, ketones, linked together by 1-3 carbon alkyl groups. Nearly, all of the rings and linking groups carried substituent aldehyde, alcohol, carboxylic acid, and phenolic hydroxyls and methoxyl groups. These structures differ from heavy fuel oil asphaltenes principally, in that they contain fewer aromatic groups, and many more oxygen-containing substituents; the characteristic long chain alkyl groups and methyls are absent, as sulphur-containing aromatic groups. While such structures are useful indicators of the types of functional groups linked together, they do not take into account the distribution of structures about a mean.

Pyrolysis of bio-oil asphaltene with the Xu structures might be expected to produce small alicyclic and aromatic molecules by, first, bond breaking to yield radicals, followed by hydrogen donation to yield a multiplicity of oxygen-containing low molecular weight alicyclic compounds as are identified in bio-oil according to Stas, et al (2014) (285). Some small aromatics are also expected. As they enter the gas phase, many of these compounds are expected to influence ignition. Two-rings and higher aromatic PAH can lead to soot via HACA, while a carbonaceous residue forms from crosslinking, especially of the hydrogen-donor bio-asphaltenes.

In this study the results of the aforementioned pyrolysis experiments showed significant variation among the pyrolysis temperatures ranging from 300°C to 1100°C while there are similar chromatographic trends and that some very heavy molecular weight compounds present in petroleum asphaltene are not present within the bio-oil asphaltene samples. In addition, these experimental results indicated a clear difference between the bio-oil asphaltene and petroleum based asphaltene both in term of elemental composition and heavy aromatic fractions. Overall there would be differences in environmental effects of the emissions emanating from the combustion of heavy fuels in combustors and heavy duty engines for power generation.

Data interrogation of these results (Figures 6-15 to 6-23) illustrates the presence of lower molecular weights fractions such as alkyl benzene, (with molecular weights; 92, 106, 120) and naphthalene (128MW) between all pyrolysis temperatures within the bio-oil asphaltene samples, and this is consistent with the ones detected in the petroleum based asphaltene; the same results were reported by (6, 286). However, there is no indication for very heavy fractions such as chrysene (228, 242 MWt) and Picene (276, and 278 MWt) (Table 6-13 to 19) in all temperatures run for bio-oil asphaltene. These compounds are detected in the previous pyrolysis GC-MS of the petroleum based asphaltene, and in the vacuum residual fuel oil.

Bio-oil asphaltene contain less oxygenates in comparison to bio-oil as indicated in the pyrolysis gas chromatography mass spectrometric results as, well as the Ultimate analysis. Thus the oxygen to carbon ratio is lower and the carbon to hydrogen ratio is higher in bio-oil asphaltene compared to the raw bio-oil. Additionally, sulphur is completely absent in asphaltene from bio-oil, but very significant in petroleum-based asphaltene where it results in the potential for adverse health and environmental effects. It is expected there is less probability of cenospheres formation from the combustion of bio-asphaltene because it is lower MW and higher oxygen than petroleum asphaltenes. This has been shown in the previous research by (287). Bio-oil with a high lignin components has been shown to form cenospheres Zhao et al, 2011(61)

Crude bio-oil obtain from lignocellulosic material have higher amount of oxygenated/hydroxyl compounds as evidenced by the occurrence of strong peaks of alcohols, phenols and esters. In addition the heavy fraction of this oil showed a higher fraction of fused poly aromatic rings with less oxygen content as indicated in Py-GCMS results i.e. this upgrades the quality of bio-oil.

In generally, the emission emanating from crude bio-oil combustion totally depends on the natural composition of the solids, nitrogen, and water in the oil under combustion. Hence, the emission levels are based on light and heavy volatiles fractions in the oils, as well as particulates. However, it has been experimentally found that there are no SO_x emission in the bio-oil and heavy bio-oil fraction (asphaltene) combustion. NO_x emission, woody oil contains trace nitrogen, but this is reduced further during the extraction of the bio-asphaltene fractions. The evidence suggests that the bio-asphaltene is less aromatic than that from petroleum and consequently much less cenospheres formation will take place during combustion of bio-oil.

Table 6- 20 Summary and comparison of petroleum and bio-asphaltene fraction

Property	HFO Asphaltene	Shell Marine Asphaltene Bunker C	Bio-asphaltene
Wt.% C	81.4	83.3	56.9
Wt.% O	8.3	4.1	36.7
Wt.% H	7.3	7.1	6.4
Wt.% S	1.73	3.03	Not detected
Wt.% N	1.24	1.45	Not detected
H/C ratio	1.02	1.08	0.74
O/C ratio	0.077	0.37	0.48
Main pyrolysis products 300 – 400°C	C13 – C24 alkanes/alkenes pairs. Substituted benzenes and styrenes	C13 – C24 alkanes/alkenes pairs. Substituted benzenes and styrenes	Methoxyl/ Phenolic groups, Aldehydes, ketones, carboxylic acids Benzenes and substituted benzenes; BTX
Main pyrolysis products 500 – 700°C	<ul style="list-style-type: none"> - As above plus alkylnaphthalenes Phenanthrenes, anthracenes, Pyrenes, & isomers. - Increased alkyl benzenes. - Evidence of some de-alkylation reaction in PAH. - Benzothiophenes and dibenzothiophenes. 		As above plus Naphthalenes, Phenanthrenes and alkyl phenantrenes
Main pyrolysis products >700°C	<ul style="list-style-type: none"> - As above plus traces of chrysene - Evidence of de-alkylation in the PAH 		More complex aromatics formation such as pyrenes, increase of alkoxy and Alkoxylation
Thermal decomposition	45 Wt.% evolved 200-700°C;	-35Wt. % evolved 200-700°C; 58Wt. fixed carbon; 2% ash;	- 75Wt. % evolved 200-700°C; 20% fixed carbon; zero

characterization	48 Wt.% fixed; carbon; 2Wt.% ash; 5% moisture	5% moisture.	ash; 5% moisture
Conclusion regarding structure	Archipelago of 1-4 rings PAH and SPAH linked by alkyl chain	Archipelago of 1-4 rings PAH and SPAH linked by alkyl chain	Resembles petroleum asphaltenes but very low in heteroatoms, N,&S, and some oxygenated PAH
Conclusion the soot routes	Cracking of side chains via HACA route + PAH growth mechanisms. Significant cenospheres from high MW in parallel	Cracking of side chains via HACA route + PAH growth mechanisms. Significant cenospheres formation from high MW in parallel	Cracking of alkyl phenols to CPD is an important route. HACA from cracked volatiles. Possibly some contribution from PAH growth. Low cenospheres formation since FC is low

Note that lower fixed carbon FC in bio-oil asphaltenes is predicted to results in lower cenosphere formation. Higher volatile matter VM might be expected to results in higher soot (compared to petroleum asphaltenes) and results from the model compounds in chapter 4 would predict this to be the case (Table 4-5). However, the high oxygen content is an important consideration because it results in competition for PAH growth vs oxidation.

6.5 Conclusions

- ❖ This work presented the experimental investigations on both bio-oil and the bio-asphaltene generated from the oil for volatile comparisons between raw bio-oil and extracted asphaltene using a pyrolysis gas chromatography mass spec and thermogravimetric techniques, and comparisons made with the properties of corresponding petroleum-derived asphaltenes.
- ❖ Emphasis was placed on both the tendency to form particulate cenospheres and small diameter soot (BC) components from the vapour phase products of heavy bio-oil and bio-asphaltene pyrolysis and combustion so as to determine the origin and mechanism

of the effect on the environment of the use of heavy bio-oil fuels. The low aromatic content and high oxygen content of bio-oil tends to reduce the tendency for the formation of carbonaceous products.

- ❖ A thorough data interrogation of the chromatograms has been made to determine the best match for aromatic, oxygenated compounds and other species at different pyrolysis temperatures (300-1200°C) based on a NIST search. Molecular weight, retention time and literature values and compared them to crude petroleum pyrolysis products. The results showed the presence of lower molecular weight alkenes/ alkanes. Additionally, polyhydroaromatics and alkyl PAH similar to that of crude petroleum suggesting characteristics features of asphaltene structure for fossil fuel. It did not show any PASH constituents in its fractions. Hence this indicates the mechanisms of the cracking products leading to PAHs formation and soot precursors.
- ❖ It was shown that overall crude bio-oil obtained from lignocellulosic material have higher amount of oxygenated/hydroxyl compounds as evidenced by the occurrence of strong peaks of alcohols, phenols and esters. The heavy fraction of this oil showed a higher fraction of fused poly aromatic rings with less oxygen content as indicated in Py-GCMS results i.e. this upgrades the quality of bio-oil.
- ❖ Generally, the emission emanating from bio-oil combustion totally depends on the natural composition of the solids, nitrogen, and water in the oil under combustion. Hence, the emission levels are based on light and heavy volatiles fractions in the oils. It has been experimentally found that there are no SO_x emission in the bio-oil and heavy bio-oil fraction (asphaltene) combustion.
- ❖ For NO_x emission, woody oil contains trace nitrogen, but this is reduced further during the extraction of the bio-asphaltene fractions.
- ❖ The evidence suggests that the bio-asphaltene is less aromatic than that from petroleum and consequently much less cenosphere formation will take place during combustion of bio-oil.

Chapter 7 Conclusion and future work

7.1 Introduction

The introduction of this thesis considers the use of oil from conventional sources and from bio-oil as a way of reducing the emission of carbon dioxide. This thesis has covered numerous objectives that were aimed at examining the fundamentals of combustion and its environmental impacts. Liquid fuel combustion and characterisation of pyrolysis biomass oil (bio-oil), and hydrocarbon fuels, including heavy fuel oil studied in detail. The combustion mechanisms for the investigated fuels were determined. This thesis also looked into the influence of the nature and molecular structure of the different fuels on combustion and emissions, as well as comparing experimental results with those predicted. This thesis also provides an investigation on the nature and behaviour of soot resulting from biomass fuels during combustion and their potential impact. The environmental impact of model biomass pyrolysis fuels was studied. Hence several areas of interest were considered such as model fuel combustion, processes involved in the flames and the emissions detected, as well as in the reaction zone, the products of pyrolysis and combustion and hence their environmental fate. Finally, at the end of this chapter the potential areas that require attention for further work have been addressed.

7.2 Combustion of model compounds

Combustion of five model compounds, furfural, eugenol, anisole, n-decane, n-heptane, has been studied. The first three represents models for bio-oil, and the latter two for HFOs.

To get a better insight of the chemistry of pyrolysis of model fuels and biomass, especially the nature of soot and volatile products during combustion of these fuels their physicochemical characterisations were first investigated. The standard fuel analysis showed that there were significant differences in these fuels, with respect to the structure and composition of volatiles emissions. Based on this investigation conclusions were obtained relating to the C/H ratio and the aromaticity.

7.2.1 Composition of black carbon /organic carbon and its effect

- ❖ Values of the ratio EC/TC for a range of soot samples determined by Py-GC-MS were in good agreement with those derived from TGA measurements. However the method of soot collection and analysis affects the values of EC/TC ratio obtained. For example, soot burner (i.e. hot) was almost exclusively EC for all fuels, in comparison, soot from a wood stove (cooler sampling) had a ratio of 0.6 – 0.7.
- ❖ The results of the TGA measurements were consistent with the presence of different types of material in the BC. The TGA and pyrolytic analyses show that a range of pyrolysis products and oxygenated species including PAH were present. Phenolic fragments associated with lignin were also present. These results are complicated by the fact that the organic material consists of the precursors to the formation of soot and by incompletely combusted fuel
- ❖ Differences were observed between laboratory produced soot and stove soot such as adsorbed SO₂ for multifuel stove and higher ash. However, this study did not find any significant differences between EC/TC for biomass model compounds in their wick combustion.

7.2.2 Particle size distribution and volatile composition of soot

In these findings the soot (black carbon, BC) generated during combustion of eugenol, anisole, decane and heptane from the diffusion flame of a wick burner have been analysed online by DMS, Soot from model lignin decomposition products, eugenol and anisole, had adsorbed benzene and phenol derivatives. This indicates that the importance of these species in the soot production mechanisms derive biomass combustion. DMS results showed some differences between the soots from the four fuels, sampled at different flame heights above the flame. The hydrocarbon fuels soot agglomerates are generally smaller than those from anisole and eugenol.

Eugenol, in particular, gave a wide distribution of agglomerates close to the flame and this distribution became narrower as sampling height above the flame increased. The results can be interpreted in terms of soot agglomeration vs oxidation rates.

Offline analysis of the same sample was carried out using a Pyrolysis gas chromatography-mass spectroscopy for VOCs, PAC and O-PAC investigations. These low temperature pyrolysis studies significantly play an important role in understanding the mechanisms of black carbon particle formation and the volatile component fragmentation process for the burning fuels. Organic carbon concentration were low, but some VOC and PAH were detected, consistent with CPD and HACA mechanisms of soot growth.

This current work provides an experimental data-set for both model and conventional fuels for predicting the burning profile and mechanisms of soot formation.

7.2.3 Structure of the soot from bio-oil model compounds

- ❖ Model species of wood pyrolysis products are furfural for cellulose and eugenol for lignin. Smoke from their diffusion flames is initially similar and the initial soot particles grow to larger spherical particles.
- ❖ The average particle sizes measured are approximately in range of 30 nm and the particles agglomerate to form chains of 10 to 30nm. There is a significant difference between the final soot product from furfural and eugenol because of the aromatic nature and concentration of soot particles. This aromatic nature is not seen in biomass soot.
- ❖ Furfural tends to follow the HACA soot formation mechanism because of initial decomposition to suitable molecules to follow the HACA route. Eugenol on the other hand undergoes side-chain cracking, followed by conventional phenol decomposition reactions, and also decomposition and reaction via cyclopentadiene to form PAH and ultimately soot.
- ❖ Comparison has been made to pine soots which contain both organic carbon and black carbon. The decomposition products suggest an important PAH route via

cyclopentadiene, which is derived after cracking of lignin monomer fragments as demonstrated by results from eugenol combustion.

7.3 Heavy fuel oil combustion

These experiments are on the basis of two applications which are as follows; firstly, to evaluate the development of toxic gases during the combustion of heavy fuel, and secondly to study the structure and nature of the products during pyrolysis of these heavy fuels (Asphaltene) from a lower to higher temperature. Results are relevant to combustion in large combustors, such as power plants, marine engines, furnaces and boiler for heating and energy generation.

Petroleum asphaltenes were pyrolysed in a hyphenated Py-GC system. Mass spectrometry detection revealed the presence in the products of mono and hydroaromatic compounds and alkylated PAH in addition to long-chain alkanes and alkenes. Py-GC with AED showed that alkylated (up to and beyond C₃) PASH benzothiophenes and dibenzothiophenes were also produced. The patterns of alkyl substitution and the contribution of long alkyl chains suggest affinities between the structures of petroleum asphaltenes and lower Mw constituents of petroleum. These results are consistent with an 'archipelago' structure for asphaltenes in which alkyl substituted small (1 to 4 ring) aromatic and sulphur heterocyclic ring systems are linked by bridging groups. However, only low concentrations of nitrogen and oxygen compounds were released by pyrolysis of asphaltene; most of the nitrogen is thought to remain in the char residue. A general reaction scheme for thermal reactions of asphaltenes accounts for ignition and soot formation in the gas phase and cenospheres formation in the solid phase, all via a formation and reaction route of 'building block' radicals in the liquid phase. At pyrolysis temperatures below 400C the vanadium compounds in the asphaltene are transferred to the gas phase and hence to the combustion soot. At higher temperatures involatile vanadium porphyrins accumulate in the cenospheres.

7.4 Bio-oil combustion

In an analogous way to asphaltenes in petroleum oil, bio-asphaltenes in fast pyrolysis bio-oil were also studied. In particular, the nature and structure of the oil and its heavy fractions, was evaluated and pyrolysis characteristics were assessed. Some of the key findings are illustrated below.

- ❖ The experimental investigations on both bio-oil and the bio-asphaltene generated using pyrolysis gas chromatography mass spectrometric and thermogravimetric techniques, enabled comparisons to be made with the properties of corresponding petroleum-derived asphaltenes.
- ❖ Emphasis was placed on the potential to form both the particulate (cenosphere) and small diameter soot components, the former from the high MW components, and the latter from the vapour phase products of bio-oil and bio-asphaltene pyrolysis and combustion.
- ❖ Based on the chromatograms a thorough data interrogation has been made to determine the best match polycyclic aromatic compounds at different pyrolysis temperatures (300-1200°C) using the NIST database together with retention time and literature data and to compare them with crude petroleum pyrolysis products. The results showed the presence of lower molecular weight alkenes/ alkanes. Additionally, polyhydroaromatics and alkyl PAH similar to that of crude petroleum suggesting characteristics features of asphaltene structure for fossil fuel. Because bio-oil is low in sulphur it did not show any PASH constituents in its fractions. Hence this indicates the mechanisms of the cracking products leading to PAHs formation and soot precursors.
- ❖ It was shown that overall bio-oil obtained from lignocellulosic material have higher amount of oxygenated/hydroxyl compounds as evidenced by the occurrence of strong peaks of alcohols, phenols and esters. In addition the heavy fraction of this oil showed higher fractions of fused poly aromatic rings with less oxygen content compared to the

raw bio-oil as indicated in Py-GCMS results and thus, this approach could upgrade the quality of bio-oil.

- ❖ Generally, the emission emanating from bio-oil combustion depends on the natural composition of the oil, the solids content, nitrogen content, and water in the oil under combustion. Hence, the emission levels are based on light and heavy volatiles fractions in the oils, as well as particulates. It has been experimentally found that there are no SO_x emission in the crude bio-oil and heavy bio-oil fraction (Asphaltene) combustion.
- ❖ For NO_x emission, woody oil contains trace nitrogen but this is reduced further during extraction of the bio-asphaltene fractions.

7.5 Future work

Based on the work in this thesis, it is clear that several lines of research investigation on the combustion of the liquid fuels should be made. The combustion of single droplets is important as these are the fundamental units of any spray. Hence the proposed work would at the beginning elucidate further the combustion of individual droplets of heavy fuel oil and bio-oils and also of the individual model fuels studied in this thesis. Detailed investigation of the structure of flames surrounding the liquid droplets and reaction zone would be conducted simultaneously. Liquid droplets could also be obtained using the wetted sphere technique in order to provide a steady state combustion system. In this case the key features to be investigated are the temperature, velocity, and compositional variations which occur between the liquid surface and the surrounding atmosphere. Comparisons could also be made with similar flames that are supported by cylindrical fuel surfaces.

Extensive investigations on suspended asphaltene particles for three samples (Shell marine oil asphaltene, vacuum residual oil asphaltene, and bio-oil asphaltene) and some liquids droplet burning rate investigations need to be conducted using a video technique to obtain details on the burning/evaporation rates of the droplet components.

In the case of the volatile model fuels (n-decane and n-heptane) the effect of fuel feed rate on flame sizes and evaporation rates would also be investigated using a porous sphere method. Additionally, the combustion characteristic which has assumed the most attention from both a theoretical and experimental standpoint is the burning rates of these heavy oils. Other parameters including flame temperature, size and shape would also be the subject investigations. The research conducted in this thesis has used several analytical methods of the fuels and the combustion or pyrolysis products. The most important analytical technique used is GC-MS and it has proved to be adequate in producing experimental results. However, more powerful analytical techniques are available giving better confidence in compound discovery, identification and quantitation. This performance is achieved through the superior resolving power, mass accuracy and sensitivity that more modern equipment can deliver and should be used for future work.

References

1. BP-STATISTICAL-REVIEW-OF-WORLD-ENERGY-. 2015.
2. ENERGY, B.S.R.O.W. *BP Statistical Review of World Energy-2015*. London, UK, 2015.
3. AGENCY, I.I.E. *World Energy Outlook*. Circular distributed OECD, Paris, 2015.
4. BERTINE, K. and E.D. GOLDBERG. Fossil fuel combustion and the major sedimentary cycle. *Science*, 1971, **173**(3993), pp.233-235.
5. BARTLE, K., E. FITZPATRICK, J. JONES, M. KUBACKI, R. PLANT, M. POURKASHANIAN, A. ROSS and A. WILLIAMS. The combustion of droplets of liquid fuels and biomass particles. *Fuel*, 2011, **90**(3), pp.1113-1119.
6. BARTLE, K., J. JONES, A. LEA-LANGTON, M. POURKASHANIAN, A. ROSS, J. THILLAIMUTHU, P. WALLER and A. WILLIAMS. The combustion of droplets of high-asphaltene heavy oils. *Fuel*, 2013, **103**, pp.835-842.
7. RAYMOND, P.A. Carbon cycle: The age of the Amazon's breath. *Nature*, 2005, **436**(7050), pp.469-470.
8. BRIDGWATER, A.V., PEACOCKE, G. V. C.,. Fast pyrolysis processes for biomass. *Renewable and Sustainable Energy Reviews*, 2000 **4**, pp. 1 - 73.
9. WILLIAMS, P.T. *Waste Treatment and Disposal*, [online]. Second edition ed. John Wiley& Sons, Ltd. , 2005.
10. BASU, P. *Biomass Gasification and Pyrolysis Practical Design* [online]. Elsevier Inc, 2010
11. BALAT, M.B., M.; KIRTAY, E.; BALAT, H. . Main routes for the thermo-conversion of biomass into fuels and chemicals. Part 1: Pyrolysis systems. *Energy Convers. Manag.*, 2009, **50** pp.3147–3157.
12. DEMIRBAS, F.M. Biorefineries for biofuel upgrading: A critical review. *Appl. Energy*, 2009 **86**, pp.S151–S161.

13. THEODORE, D.A.J.S. Catalytic Fast Pyrolysis: A Review,. *Energies* 2013, 2013, **6** pp.514-538.
14. BRIDGEWATER, A. Review of fast Pyrolysis of biomass and product upgrading. *Biomass & Bioenergy*, 2012 **38**, pp. 68-94.
15. YAMAN, S. Pyrolysis of biomass to produce fuels and chemical feedstock. *Energy Conver. Manag* 2004, **45**, pp. 651–671.
16. MOHAN, D.P., C U. JR., AND STEELE, P. H. . Pyrolysis of Wood/Biomass for Bio-oil: A Critical Review. *Energy & Fuels*, 2006, **20**, pp.848-889.
17. IPCC, I.P.O.C.C. *Special Report on Carbon Dioxide Capture and 39 Storage*. Cambridge University Press: Cambridge University, 2005.
18. ---. *The Physical Science Basis. Contribution of Working Group I to the Fourth Assessment, Report of the Intergovernmental Panel on Climate Change*. Cambridge University Press: Cambridge, 2007.
19. MUCKENHUBER H, G.H. The heterogeneous reaction between soot and NO₂ at elevated temperature. *Carbon*, 2006, **44**, pp.546-559.
20. CHAMEIDES WL, B.M. Soot takes center stage. *Science*, 2002, **297**(5590), pp.2214-2215.
21. MENON S, H.J., NAZARENKO L, LUO Y Climate effects of black carbon aerosols in China and India. *Science*, 2002, **297**(5590), pp.2250–2253.
22. GUSTAFSSON, Ö., M. KRUSÁ, Z. ZENCAK, R.J. SHEESLEY, L. GRANAT, E. ENGSTRÖM, P. PRAVEEN, P. RAO, C. LECK and H. RODHE. Brown clouds over South Asia: biomass or fossil fuel combustion? *Science*, 2009, **323**(5913), pp.495-498.
23. SYDBOM A, E.A. Health effects of diesel exhaust emissions. *Eur Respir J*, 2001, **17**(4), pp.733– 746.
24. WEITKAMP, E.A., SAGE, A. M, PIERCE, J. R, DONAHUE, N. M, ROBINSON A. L. Organic aerosol formation from photochemical oxidation of diesel exhaust in a smog chamber. *Environ Sci Technol*, 2007, **41**(20), pp.6969–6975.
25. VIONE D, M.V., MINERO C, ET AL. . Photochemical reactions in the tropospheric aqueous phase and on particulate matter. *Chem Soc Rev*, 2006, **35**(5), pp.441–453.

26. STADLER D, R.M.J. The reactivity of NO₂ and HONO on flame soot at ambient temperature: The influence of combustion conditions. *Phys Chem*, 2000, **2**, pp.5420–5429.
27. HAMILTON, J.G., ZANGERL, A.R., BERENBAUM, M.R., PIPPEN, J., ALDEA, M. AND DELUCIA, E.H. . Insect herbivory in an intact forest understory under experimental CO₂ enrichment. *Oecologia*, 2004, **138**(10.1007/s00442-003), pp.1463-5.
28. JACCARD, M.K. *Sustainable fossil fuels: the unusual suspect in the quest for clean and enduring energy*. Cambridge: Cambridge University Press, 2005.
29. JOHNSON, J., D. REICOSKY, R. ALLMARAS, T. SAUER, R. VENTEREA and C. DELL. Greenhouse gas contributions and mitigation potential of agriculture in the central USA. *Soil and Tillage Research*, 2005, **83**(1), pp.73-94.
30. MEINSHAUSEN, M., N. MEINSHAUSEN, W. HARE, S.C. RAPER, K. FRIELER, R. KNUTTI, D.J. FRAME and M.R. ALLEN. Greenhouse-gas emission targets for limiting global warming to 2 C. *Nature*, 2009, **458**(7242), pp.1158-1162.
31. JACOBSON, M.Z. Climate response of fossil fuel and biofuel soot, accounting for soot's feedback to snow and sea ice albedo and emissivity. *Journal of Geophysical Research: Atmospheres (1984–2012)*, 2004, **109**(D21).
32. CHANGE, I.P.O.C. *IPCC, 2014: Climate Change 2014: Synthesis Report. Contribution of Working Groups I, II and III to the Fifth Assessment Report of the* ISBN 978-92-9169-143-2. 2015.
33. SEARCHINGER, T.D., S.P. HAMBURG, J. MELILLO, W. CHAMEIDES, P. HAVLIK, D.M. KAMMEN, G.E. LIKENS, R.N. LUBOWSKI, M. OBERSTEINER and M. OPPENHEIMER. Fixing a critical climate accounting error. *Science*, 2009, **326**(5952), p.527.
34. PACHAURI, R.K., M. ALLEN, V. BARROS, J. BROOME, W. CRAMER, R. CHRIST, J. CHURCH, L. CLARKE, Q. DAHE and P. DASGUPTA. *Climate Change 2014: Synthesis Report. Contribution of Working Groups I, II and III to the Fifth Assessment Report of the Intergovernmental Panel on Climate Change*. 2014.

35. RAUPACH, M.R., S.J. DAVIS, G.P. PETERS, R.M. ANDREW, J.G. CANADELL, P. CIAIS, P. FRIEDLINGSTEIN, F. JOTZO, D.P. VAN VUUREN and C. LE QUÉRÉ. Sharing a quota on cumulative carbon emissions. *Nature Climate Change*, 2014, **4**(10), pp.873-879.
36. MCGLADE, C. and P. EKINS. The geographical distribution of fossil fuels unused when limiting global warming to 2 [deg] C. *Nature*, 2015, **517**(7533), pp.187-190.
37. ALLEN, M.R., D.J. FRAME, C. HUNTINGFORD, C.D. JONES, J.A. LOWE, M. MEINSHAUSEN and N. MEINSHAUSEN. Warming caused by cumulative carbon emissions towards the trillionth tonne. *Nature*, 2009, **458**(7242), pp.1163-1166.
38. MATTHEWS, H.D., N.P. GILLETT, P.A. STOTT and K. ZICKFELD. The proportionality of global warming to cumulative carbon emissions. *Nature*, 2009, **459**(7248), pp.829-832.
39. MCGLADE, C. and P. EKINS. The geographical distribution of fossil fuels unused when limiting global warming to 2 [deg]C. *Nature*, 2015, **517**(7533), pp.187-190.
40. ---. Un-burnable oil: An examination of oil resource utilisation in a decarbonised energy system. *Energy Policy*, 2014, **64**, pp.102-112.
41. YERGIN, D. It's still the one. *Foreign Policy*, 2009, **19**, pp.89-95.
42. KLASS, D.L. *Biomass for renewable energy, fuels, and chemicals*. Academic press, 1998.
43. RAMAGE, J., AND J. SCURLOCK. "Biomass." In *Renewable Energy: Power for Sustainable Future*., Oxford, England:: Oxford University Press., 1996.
44. PAPER., G.E.W. "Our Energy Future-creating a low carbon economy". Vesion 11., 2003.
45. DEMIRBAS, A. Biomass resources facilities and biomass conversion processing for fuels and chemicals. *Energy Conversion and Management*, 2001, **42**(11), pp. 1357-1378
46. BRAIDE, K.M., ISLES, G.L., JORDAN, J.B, WILLIAMS, A. . The combustion of single droplets of some fuel oils and alternative liquid fuel combinations. *J Inst Energy*, 1979, **52**, pp.115–124.

47. HOTTEL, H.C., WILLIAMS, G. C., SIMPSON H.C. Combustion of droplets of heavy liquid fuels. *Proc Combust Inst*; , 1955, **5**, pp. 101–29.
48. JACQUES M.T., J.J.B., WILLIAMS, A., HADLEY-COATES, L : The combustion of water-in-oil emulsions and the influence of asphaltene content. *Proc Combust Inst*, (1977), **16**, pp.307–19.
49. MICHAEL M. I, E.W.M.M. On the self-ignition of hydrocarbon mixtures. *Proc Combust Inst*, 1967, **11**, pp.1027–35.
50. WALLER, P.R., WILLIAMS, A., BARTLE, K.D. The structural nature and solubility of residual fuel oil fractions. *Fuel*, 1989, **68**, pp.520–6.
51. GROENZIN, H., MULLINS, O.C. Molecular size and structure of asphaltenes from various sources. . *Energy Fuels*, 2000, **14**, pp. 677–84.
52. LI, D.D., GREENFIELD, M.L. . High internal energies of proposed asphaltene structures. . *Energy Fuels*, 2011, **25**, pp.3698–705.
53. MORGAN T.J, G., A., ALVAREZ-RODRIGUEZ A.P., MILLAN, M., HEROD, A.A., AND KANDIYOTI, R. . Estimating molecular masses of petroleum-derived fractions: High mass (>2000l) materials in maltenes and asphaltenes from Maya crude oil. *J Chromatogram*, 2010, **1217**, pp.3804–18.
54. KARIMI, A., QIAN, K., OLMSTEAD, W.N., FREUND, H., YUNG, C., AND GRAY, M.R. . Quantitative evidence for bridged structures in asphaltenes by thin film pyrolysis. . *Energy & Fuels*, 2011, **25**, pp. 3581–9.
55. BARTLE, K.D., FITZPATRICK, E.M, JONES, J.M, KUBACKI, M.L, PLANT, R., & POURKASHANIAN, M. The combustion of droplets of liquid fuels and biomass particles. *Fuel*, 2011, **90**, pp.1113–9.
56. MOSZKOWICZ, P., WITZEL L, CLAUS G. Modelling of very fast pyrolysis of heavy fuel oil droplets. . *Chem Eng Sci*, 1996, **51**, pp. 4075–86.
57. AMBALAE, A., MAHINPEY, N., FREITAG, N. Thermogravimetric studies on pyrolysis and combustion behaviour of a heavy oil and its asphaltenes. . *Energy& Fuels*, 2006, **20**, pp. 560–5.

58. URBAN, D.L., HUEYT, S.P.C., DRYER, F.L. . Evaluation of the coke formation potential of residual fuel oils. . *Proc Combust Inst*, 1992, **24**, pp. 1357–64.
59. VILLASENOR, R., GARCIA, F. An experimental study of the effects of asphaltenes on heavy fuel oil droplet combustion. . *Fuel*, 1999, **78**, pp. 933–44.
60. WILK, R. The thermal decomposition of the liquid phase during the combustion of heavy oil droplets. *Fuel*, 1989, **69**, pp.371–4.
61. ZHAO, Y., YU, Y. . Kinetics of asphaltene thermal cracking and catalytic hydrocracking. *Fuel Process Technol*, 2011, **92**, pp.977–82.
62. MARY J. WORNAT, B.G.P., NANCY Y. C. YANG. single Droplet Combustion of Biomass Pyrolysis Oils. *Energy and Fuels* 1994, **8** (5), pp.1143–1148.
63. WESTLEY, F. *Chemical kinetics of the gas phase combustion of fuels: a bibliography on the rates and mechanisms of oxidation of aliphatic C1 to C10 hydrocarbons and of their oxygenated derivatives*. US Dept. of Commerce, National Bureau of Standards: for sale by the Supt. of Docs. US Govt. Print. Off., 1976.
64. LIDDY. J. P. AND NEWAY, D.C. Use of water-continuous emulsions of heavy oils as a means of reducing pollutant emissions from combustion'. *In: Joint Meeting of the British and French Sections of the Combustion Institute'*.
. 1989, p. 243.
65. MARCANO, N., M. POURKASHANIAN and A. WILLIAMS. The combustion of bitumen-in-water emulsions. *Fuel*, 1991, **70**(8), pp.917-923.
66. DAVIES, I.L.R., M.& WILLIAMS, P.T.& ANDREWS, G.E.& BARTLE, K.D. "Application of automated on-line microbore high-performance liquid chromatography/capillary gas chromatography to Diesel exhaust particulates". *Anal. Chem.*, 1987, **59**, pp.2579- 2585.
67. HIDALGO, R.O., JIMENEZ, E., AND RODRIGUEZ, D. . Coal and Slurry Technology *In: 14th International Conference on Coal and Slurry Technology*,, Pittsburgh Energy Technology Center. Washington, D.C., 1989.
68. LAW, C. Recent advances in droplet vaporization and combustion. *Progress in Energy and Combustion Science*, 1982, **8**(3), pp.171-201.

69. DRYER, F.L. Water addition to practical combustion systems—Concepts and applications. *Symposium (International) on Combustion*, 1977, **16**(1), pp.279-295.
70. MURDOCH, P.L., M. POURKASHANIAN and A. WILLIAMS. The mechanism of combustion of coal-water slurries. *In: Symposium (International) on Combustion*: Elsevier, 1985, pp.1409-1418.
71. MARCANO, N., POURKASHANIAN, M. AND WILLIAMS, A. The combustion of emulsions bitumen-in-water. *fuels*, 1991, **70**, pp. 917- 923.
72. CHIGIER, N.A. The atomization and burning of liquid fuel sprays. *Progress in Energy and Combustion Science*, 1976, **2**(2), pp.97-114.
73. WILLIAMS, A. *Combustion of liquid fuel sprays*. Butterworth-Heinemann, 2013.
74. N.A. CHIGIER, M.F.R. Twin-fluid atomizer spray combustion. *ASME Winter Annual Meeting, Paper No. 79-WA/HT-25, New York, (1972)*.
75. ONUMA, Y. and M. OGASAWARA. Fifteenth Symposium (International) on Combustion Studies on the structure of a spray combustion flame. *Symposium (International) on Combustion*, 1975, **15**(1), pp.453-465.
76. NAKAMURA, M., F. AKAMATSU, R. KUROSE and M. KATSUKI. Combustion mechanism of liquid fuel spray in a gaseous flame. *Physics of Fluids*, 2005, **17**(12), p.123301.
77. AGGARWAL, S.K. A review of spray ignition phenomena: present status and future research. *Progress in Energy and Combustion Science*, 1998, **24**(6), pp.565-600.
78. SIRIGNANO, W.A. Fuel droplet vaporization and spray combustion theory. *Progress in Energy and Combustion Science*, 1983, **9**(4), pp.291-322.
79. GOSMAN, A. and E. LOANNIDES. Aspects of computer simulation of liquid-fueled combustors. *Journal of Energy*, 1983, **7**(6), pp.482-490.
80. EDWARDS, J.D. Crude oil and alternate energy production forecasts for the twenty-first century: The end of the hydrocarbon era. *AAPG bulletin*, 1997, **81**(8), pp.1292-1305.
81. MASTERS, C.D., E.D. ATTANASI, W.D. DIETZMAN, R.F. MEYER, R.W. MITCHELL and D.H. ROOT. [25] WORLD RESOURCES OF CRUDE OIL,

- NATURAL GAS, NATURAL BITUMEN, AND SHALE OIL. *In: 12th world petroleum Congress: World Petroleum Congress, 1987.*
82. MASTERS, C.D., D. ROOT and E. ATTANASI. World oil and gas resources-Future production realities. *Annual Review of Energy*, 1990, **15**(1), pp.23-51.
83. ANCHEYTA, J. and J.G. SPEIGHT. *Hydroprocessing of heavy oils and residua*. CRC Press, 2007.
84. SPEIGHT, J.G. and B. OZUM. *Petroleum refining processes*. CRC Press, 2001.
85. FENTON, D.M., H. HENNING and R.L. RICHARDSON. The chemistry of shale oil and its refined products. *In: ACS Symposium Series*, 1981, pp.315-326.
86. LEE, S. *Oil shale technology*. CRC Press, 1990.
87. LEE, S., J.G. SPEIGHT and S.K. LOYALKA. *Handbook of alternative fuel technologies*. crc Press, 2014.
88. MERRICK, D. *Coal combustion and conversion technology*. Macmillan, 1984.
89. KARR, C. *Analytical methods for coal and coal products*. Academic press, 2013.
- 90.
91. BAHNG, M.K., MUKARAKATE, C., ROBICHAUD, D.J., AND NIMLOS, M.R. Current technologies for analysis of biomass thermochemical processing: A review. *AnalyticaChimicaActa*, 2009, **651**(2), pp. 117-138.
92. BRIDGEWATER, A.V., MEIER, D., AND REDLEIN, D.,. An overview of fast pyrolysis of biomass. *Organic Chemistry*, 1999, **30**, pp.1479-1493.
93. LEA-LANGTON, A., N. GIANNAKEAS, G. RICKETT, V. DUPONT and M. TWIGG. Waste lubricating oil as a source of hydrogen fuel using chemical looping steam reforming. *SAE International Journal of Fuels and Lubricants*, 2010, **3**(2), pp.810-818.
94. LI, H., A. LEA-LANGTON, G.E. ANDREWS, M. THOMPSON and C. MUSUNGO. *Comparison of exhaust emissions and particulate size distribution for diesel, biodiesel and cooking oil from a heavy duty DI diesel engine*. 0148-7191. SAE Technical Paper, 2013.

95. MAURICE, L.Q., LANDER, H., EDWARDS, T., AND HARRISON, W.E. .
Advanced aviation fuels: a look ahead via a historical perspective. *Fuel*, 2001 **80**
pp.747-756.
96. EDWARDS, T., HARRISON, W.E., AND MAURICE, L.Q. . “Properties and Usage
of Air Force Fuel: JP-8.”. In: *Proceedings of the AIAA Aerospace Sciences
Meeting & Exhibit*, 2001, pp. 1-11
97. HAYNES, B.S.A.W., H. G. . “Soot Formation,” *Prog. Energy Combustion Science*,
1981 **7**, p. 229.
98. MINCHIN, S.T. "The Chemical Significance of Tendency to Smoke",. *Journal of the
Institute of Petroleum Technologists*, 1931 **17**, pp.102-120.
99. KEWLEY, J., & JACKSON, J.S. . "The Burning of Mineral Oils in Wick-Fed Lamps.".
Journal of the Institute of Petroleum Technologists, 1927 **13**, pp.364-382.
100. BELVOIR, V. *Petroleum Quality Information System Report, from Defense Energy
Support Center, Ft. Unpublished*, 2006.
101. CLARKE, A.E., HUNTER, T.G., GARNER, F.H The Tendency to Smoke of Organic
Substances on Burning. *Journal of the Institute of Petroleum Technologists*, 1946, **32**
pp.627-642.
102. MCCAIN, W.D. *The properties of petroleum fluids*. PennWell Books, 1990.
103. SPEIGHT, J.G. *The chemistry and technology of petroleum*. CRC press, 2014.
104. LO, W.-H., H.-Y. YANG and G.-T. WEI. One-pot desulfurization of light oils by
chemical oxidation and solvent extraction with room temperature ionic liquids. *Green
Chemistry*, 2003, **5**(5), pp.639-642.
105. SHIRAISHI, Y., K. TACHIBANA, T. HIRAI and I. KOMASAWA. Desulfurization
and denitrogenation process for light oils based on chemical oxidation followed by
liquid-liquid extraction. *Industrial & engineering chemistry research*, 2002, **41**(17),
pp.4362-4375.
106. CLARK, N.N., J.M. KERN, C.M. ATKINSON and R.D. NINE. Factors affecting
heavy-duty diesel vehicle emissions. *Journal of the Air & Waste Management
Association*, 2002, **52**(1), pp.84-94.

- 107.
108. SAITO, K., GORDON, A.S., WILLIAMS, F. A., STICKLE, W.F. A study of the early history of soot formation in various hydrocarbon diffusion flames. *Combustion Science and Technology*, 1991, **80**(1-3), pp.103-119.
109. MEGARIDIS, C.M. and R.A. DOBBINS. Comparison of soot Growth and Oxidation in Smoking and Non-Smoking Ethylene Diffusion Flames. *Combustion Science and Technology*, 1989 **66**(1).
110. CHEN, J., C. CASTAGNOLI and S. NIKSA. Coal Devolatilization During Rapid Transient Heating. Part 2. Secondary Pyrolysis. *Energy and Fuels*, 1992c, **6**, p.264
111. HAYNES, B. and H.G. WAGNER. Soot formation. *Progress in Energy and Combustion Science*, 1981, **7**(4), pp.229-273.
112. A.R. LEA-LANGTON, F.A.A., K.D. BARTLE, J.M. JONES, M POURKASHANIAN, A WILLIAMS, AND I.B. G. HUMPHRIES. Mechanism of the formation of smoke from the combustion of wood. *In: mediterranean Combustion Symposium*, , Rhodes, Greece. 2015, pp. 7-11.
113. BAEZA-ROMERO, M.T., J.M. WILSON, E.M. FITZPATRICK, J.M. JONES and A. WILLIAMS. In Situ Study of Soot from the Combustion of a Biomass Pyrolysis Intermediate□ Eugenol□ and n-Decane Using Aerosol Time of Flight Mass Spectrometry. *Energy & Fuels*, 2009, **24**(1), pp.439-445.
114. GLASSMAN, I. Soot formation in combustion processes. *In: Symposium (International) on Combustion*: Elsevier, 1989, pp.295-311.
115. FILIPPOV, A.V., M.W. MARKUS and P. ROTH. In-situ characterization of ultrafine particles by laser-induced incandescence: sizing and particle structure determination. *Journal of Aerosol Science*, 1999, **30**(1), pp.71-87.
116. FITZPATRICK, E.M.J., J. M., POURKASHANIAN, M., ROSS, A. B., WILLIAMS, A. and K.D. BARTLE. Mechanistic Aspects of Soot Formation from the Combustion of Pine Wood. *Energy & Fuels*, 2008, **22**(6), pp.3771-3778.

117. SMITH, O.I. Fundamentals of soot formation in flames with application to diesel engine particulate emissions. *Progress in Energy and Combustion Science*, 1981, **7**(4), pp.275-291.
118. AMANN, C.A. and D.C. SIEGLA. Diesel particulates—what they are and why. *Aerosol Science and Technology*, 1981, **1**(1), pp.73-101.
119. LEE, K.O., R. COLE, R. SEKAR, M.Y. CHOI, J. ZHU, J. KANG and C. BAE. *Detailed characterization of morphology and dimensions of diesel particulates via thermophoretic sampling*. SAE Technical Paper, 2001.
120. TREE, D.R. and D.E. FOSTER. *Optical measurements of soot particle size, number density, and temperature in a direct injection diesel engine as a function of speed and load*. 0148-7191. SAE Technical Paper, 1994.
121. PINSON, J.A., T. NI and T.A. LITZINGER. *Quantitative imaging study of the effects of intake air temperature on soot evolution in an optically-accessible DI diesel engine*. SAE Technical Paper, 1994.
122. LADOMMATOS N. AND ZHAO, H. "A guide to measurement of flame temperature and soot concentration in diesel engines using the two-color method—Part 1: Principles",. *SAE, Paper 941956 PA Society of Automotive Engineers, Warrendale*, 1994.
123. BRUCE, C.W., T.F. STROMBERG, K.P. GURTON and J. MOZER. Trans-spectral absorption and scattering of electromagnetic radiation by diesel soot. *Applied Optics*, 1991, **30**(12), pp.1537-1546.
124. DESANTES, J., V. BERMÚDEZ, J. GARCÍA and E. FUENTES. Effects of current engine strategies on the exhaust aerosol particle size distribution from a heavy-duty diesel engine. *Journal of Aerosol Science*, 2005, **36**(10), pp.1251-1276.
125. TREE, D.R. and K.I. SVENSSON. Soot processes in compression ignition engines. *Progress in Energy and Combustion Science*, 2007, **33**(3), pp.272-309.
126. WANG, H. and M. FRENKLACH. A detailed kinetic modeling study of aromatics formation in laminar premixed acetylene and ethylene flames. *Combustion and Flame*, 1997, **110**(1), pp.173-221.

127. MILLER, J.A. and C.F. MELIUS. Kinetic and thermodynamic issues in the formation of aromatic compounds in flames of aliphatic fuels. *Combustion and Flame*, 1992, **91**(1), pp.21-39.
128. BARTOK, W.S., A. F. ed. *Fossil fuel combustion*. New York, NY (USA); John Wiley and Sons Inc., 1991.
129. COLKET, M.B.S., D. J. . Reaction mechanisms for toluene pyrolysis. . In: *Symposium (International) on Combustion*, (1994, pp. 883-891.
130. CASTALDI, M.J., MARINOV, N. M., MELIUS, C. F., HUANG, J., SENKAN, S. M., PIT, W. J. & WESTBROOK, C. K. . Experimental and modeling investigation of aromatic and polycyclic aromatic hydrocarbon formation in a premixed ethylene flame. *Symposium (International) on Combustion*, 1996, **26**, pp. 693-702.
131. HEYWOOD, J.B. *Internal Combustion Engine Fundamentals* [online]. New York: McGraw-Hills, 1988.
132. CRUA, C. *Combustion Processes in a Diesel Engine*. . thesis, University of Brighon, 2002.
133. BARTOK, W.S., A. F. *Fossil fuel combustion*. [online]. New York, USA: John Wiley and Sons Inc., 1991.
134. HAYNES, B.S. "Soot and Hydrocarbons in Combustion," *Fossil Fuel Combustion-A Source Book* [online]. New York: John Wiley & Sons, Inc., 1991.
135. GLASSMAN, I. Soot formation in combustion processes. In: *Symposium (International) on Combustion: The Combustion Institute*, 1989, pp.295-311.
136. BULUSHEV, D.A.R., J.R.H. . Catalysis for conversion of biomass to fuels via Pyrolysis and gasification: A review. . *Catal. Today*, 2011, **171**, pp.1–13.
137. DRYER, F. and I. GLASSMAN. High-temperature oxidation of CO and CH₄. In: *Symposium (International) on Combustion: Elsevier*, 1973, pp.987-1003.
138. WESTBROOK, C.K. and F.L. DRYER. Simplified reaction mechanisms for the oxidation of hydrocarbon fuels in flames. *Combustion Science and Technology*, 1981, **27**(1-2), pp.31-43.

139. LEA-LANGTON, A.R., M.T. BAEZA-ROMERO, G.V. BOMAN, B. BROOKS, A.J.M. WILSON, F.A. ATIKU, K.D. BARTLE, J.M. JONES and A. WILLIAMS. A study of smoke formation from wood combustion. *Fuel Processing Technology*, 2015, **137**, pp.327-332.
140. BRIDGEWATER, A.P., G. Fast pyrolysis processes for biomass. . *Renewable and Sustainable Energy Reviews*, 2000, **4**(1), pp. 1–73.
141. S., S. *Pyrolysis* [online]. 2008. [Accessed 18-11-13]. Available from: <http://bioweb.sungrant.org/NR/rdonlyres/57BCB4D0-1F59-4BC3-A4DD-4B72E9A3DA30/0/Pyrolysis.pdf>.
142. MORTENSEN, P.M.G., J.D.; JENSEN, P.A.; KNUDSEN, K.G.; JENSEN, A.D. . A review of catalytic upgrading of bio-oil to engine fuels. . *Appl. Catal. A Gen.*, 2011, **407**, pp. 1–19.
143. OASMAA, A.C., S. . Fuel oil quality of biomass pyrolysis oils—State of the art for the end user. *Energy Fuels*, 1999, **13**, pp.914–921.
144. FRENCH, R.C., S. . Catalytic pyrolysis of biomass for biofuels production. *Fuel Process. Technol*, 2010 **91**, pp. 25–32.
145. MORTENSEN, P.M.G., J.D.; JENSEN, P.A.; KNUDSEN, K.G.; JENSEN, A.D. A review of catalytic upgrading of bio-oil to engine fuels. . *Appl. Catal. A Gen.*, 2011, **407**, pp. 1–19.
146. BRIDGEWATER, A.V. Production of high grade fuels and chemicals from catalytic pyrolysis of biomass. *Catal. Today*, 1996, **29**, pp.285–295.
147. MULLER-HAGEDORN, M.B., H.; KREBS, L.; MULLER, U. A comparative kinetic study on the pyrolysis of three different wood species. *J. Anal. Appl. Pyrolysis*, 2003, **68–69**, pp.231–249.
148. PATWARDHAN, P.R.S., J.A.; BROWN, R.C.; SHANKS, B.H. . Influence of inorganic salts on the primary pyrolysis products of cellulose. . *Bioresour. Technol.*, 2010, **101** pp.4646–4655.

149. BOATENG, A.A., MULLEN, C. A., GOLDBERG, N., HICKS, K. B., JUNG, H. G., AND LAMB, J. F. S. Bio-oils from the fast pyrolysis of switch grass forage. *Ind. Eng. Chem. Res.*, 2008, **47**, pp. 4115–22.
150. DIEBOLD, J.P. *A Review of the Chemical and Physical Mechanisms of the Storage Stability of Fast Pyrolysis Bio-oils*. . NREL/SR-570-27613, . 2000.
151. HUANG, F., LI, W., LU, Q. & ZHU, X. . Homogeneous catalytic hydrogenation of bio-oil and related model aldehydes with RuCl₂ (PPh₃)₃. . *Chem. Eng. Technol.*, 2009, **33**, pp. 2082–2088.
152. SHARMA, R.K., & BAKHSHI, N. N. . Catalytic upgrading of pyrolysis oil. *Energy Fuels* 1993, **7**, pp. 306–314.
153. SONG, Q., NIE, J., REN, M., GUO, Q. . Effective phase separation of biomass pyrolysis oils by adding aqueous salt solutions. . *Energy Fuels*, 2009, **23**, pp. 3307–3312
154. VISPUTE, T.P.H., G. W. . Production of hydrogen, alkanes and polyols by aqueous phase processing of wood-derived pyrolysis oils. . *Green Chem.*, 2009, **11**, pp. 1433–1445
155. XUE-SONG, Z., GUANG-XI, Y., HONG, J., WU-JUN, L., & HONG-SHENG D. . Mass production of chemicals from biomass-derived oil by directly atmospheric distillation coupled with co-pyrolysis. *Scientific Reports*, 2012, **3**, pp. 1-7.
156. ZHAOXIANG WANG; YUE PAN ; TING DONG, X.Z., TAO KAN, LIXIA YUAN, YOUSHIKUMI TORIMOTO, MASAYOSHI SADAKATA, QUANXIN LI Production of hydrogen from catalytic steam reforming of bio-oil using C12A7-O--based catalysts. . *Appl. Catal.*, 2007, **A 320**, pp.24–34
157. WARNECKE, R. Gasification of Biomass: comparism of fixed bed and fluidized bedgasifer. . *Biomass and Bioenergy*, 2000, **18**, pp. 489-487.
158. SUN, S., TIAN, H., ZHAO, Y., SUN, R., AND ZHOU, J.,. Experimental and Numerical studies of biomass flash pyrolysis in an entrained flow reactor. *Bioresources Technology*, 2010, **101**(10), pp.3678-3684.

159. LADE, J. The Cyclone: A Multifunctional Reactor for the Fast pyrolysis of biomass. *Industrial & Engineering Chemistry Research*, 2000, **39**(4), pp. 893-903.
160. DUPONT, C., COMMANDRE, J.M., GAUTHIER, P., BOISSONNET, G., SALVADOR, S., AND SCHWEICH, D. Biomass pyrolysis experiments in an analytical entrained flow reactor between 1073K and 1273K. *Fuel* 2008, **87** (7), pp.1155-1164.
161. SCOTT, D.S.M., P.; PISKORZ, J.; RADLEIN, D. J. . A second look at fast pyrolysis of biomass—the RTI process. *Anal. Appl. Pyrolysis*, 1999, **51**, pp.23-37.
162. BRIDGEWATER, A.V. Renewable fuels and chemicals by thermal processing of biomass. *Chem. Eng. J.*, 2003 **91**, pp.87-102.
163. BRIDGEWATER, A.V. Progress in Thermochemical Biomass Conversion. *Chemical Engineering Journal*, 2001, **9**(2-3), pp. 90-91.
164. NIU, M., ZHOU, W., YAN, Z., GUO, Q., LIANG, Q., WANG, F., AND YU, Z., . Multifractal detrended fluctuations analysis of combustion flames in four-burner impinging entrained- flow gasifier. *Chemical Engineering Journal*, 2008, **143**(1-3), pp.230-235.
165. ZHANG, L., XU, S., ZHO, W., LIU, S.,. Co-pyrolysis of biomass and coal in a free fall reactor. *Fuel*, 2007, **86**(3), pp.353-359.
166. GOYAL, H.B., SEAL, D., AND SAXENA, R.C., . Bio-fuels from thermochemical conversion of renewable resources: A review. . *Renewable and Sustainable Energy Reviews*, 2008, **12**, pp. 504-517.
167. K, S.V.L.A.J. ed. *The handbook of Biomass Combustion & Co-firing*, . London UK: eathscan, Washington, DC, 2008.
168. THOMAS, N. Combustion and Co-combustion of biomass : Fundamental Technology and primary measures for emission reduction. *Energy& Fuels*, 2003, **17**, pp.1510-1521.
169. A., J.J.M.D.L.I.B.T.G.P.M.W. An investigation of the thermal and catalytic behaviour of potassium in biomass combustion. *Proceeding of the Combustion Institute*, 2007, **31**(2), pp.1955–1963.

170. ARCOUMANIS, C., C. BAE, R. CROOKES and E. KINOSHITA. The potential of dimethyl ether (DME) as an alternative fuel for compression-ignition engines: A review. *Fuel*, 2008, **87**(7), pp.1014-1030.
- 171.
172. CORBITT, R.A. *Standard Handbook of Environmental Engineering* [online]. New York: McGraw-Hill Inc. , 1998.
173. VANDER WAL, R.L., TICICH, T. M. & STEPHENS, B.A. . Can soot primary particle size be determined using laser-induced incandescence? *Combustion and Flame*, 1999, **116**, pp. 291-296.
174. SMITH, O. Fundamentals of Soot Formation in Flames with Application to Diesel Engine Particulate Emissions. *Progress in Energy and Combustion Science*, 1981, **7**, pp.275-291.
175. DI STASIO, S. Electron microscopy evidence of aggregation under three different size scales for soot nanoparticles in flame. *Carbon*, 2001, **39**(1), pp.109-118.
176. SYMONDS, J.P., REAVELL, R., KINGSLEY, ST J. O., JASON, S. C., BRUCE, W. S., STUART, J. Diesel soot mass calculation in real-time with a differential mobility spectrometer. *Journal of Aerosol Science*, 2007, **38**(1), pp.52-68.
177. BOTERO, M.L., S. MOSBACH, AND M. KRAFT, . Sooting tendency of paraffin components of diesel and gasoline in diffusion flames. *Fuel*, 2014, **126**, pp. 8-15.
178. JOHNSON, T., R. CALDOW, A. PUCHER, A. MIRME and D. KITTELSON. *An Engine Exhaust Particle Sizer™ spectrometer for transient emission particle measurements*. TSI Incorporated; University of Tartu (EE); Center for Diesel Research, University of Minnesota (US), 2004.
179. MIRME, A., M. NOPPEL, I. PEIL, J. SALM, E. TAMM and H. TAMMET. Multi-channel electric aerosol spectrometer. In: *In Intern. Comm. for Cloud Phys. 11th Intern. Conf. on Atmosphere Aerosols, Condensation and Ice Nuclei, Vol. 2 p 155-159 (SEE N85-32596 21-47)*, 1984, pp.155-159.

180. KHALEK, I.A., D.B. KITTELSON and F. BREAR. *Nanoparticle growth during dilution and cooling of diesel exhaust: Experimental investigation and theoretical assessment*. 0148-7191. SAE technical paper, 2000.
181. LEERMAKERS, C. and M. MUSCULUS. In-cylinder soot precursor growth in a low-temperature combustion diesel engine: Laser-induced fluorescence of polycyclic aromatic hydrocarbons. *Proceedings of the Combustion Institute*, 2015, **35**(3), pp.3079-3086.
182. ECKBRETH, A.C. Effects of laser-modulated particulate incandescence on Raman scattering diagnostics. *Journal of Applied Physics*, 1977, **48**(11), pp.4473-4479.
183. MELTON, L.A. Soot diagnostics based on laser heating. *Applied Optics*, 1984, **23**(13), pp.2201-2208.
184. DEC, J.E., A.O. ZUR LOYE and D.L. SIEBERS. *Soot distribution in a DI diesel engine using 2-D laser-induced incandescence imaging*. 0148-7191. SAE Technical Paper, 1991.
185. ROTH, P. and A. FILIPPOV. In situ ultrafine particle sizing by a combination of pulsed laser heatup and particle thermal emission. *Journal of Aerosol Science*, 1996, **27**(1), pp.95-104.
186. WILL, S., S. SCHRAML and A. LEIPERTZ. Two-dimensional soot-particle sizing by time-resolved laser-induced incandescence. *Optics letters*, 1995, **20**(22), pp.2342-2344.
187. BLADH, H., P.-E. BENGTSSON, J. DELHAY, Y. BOUVIER, E. THERSSEN and P. DESGROUX. Experimental and theoretical comparison of spatially resolved laser-induced incandescence (LII) signals of soot in backward and right-angle configuration. *Applied Physics B*, 2006, **83**(3), pp.423-433.
188. KOCK, B.F., C. KAYAN, J. KNIPPING, H.R. ORTHNER and P. ROTH. Comparison of LII and TEM sizing during synthesis of iron particle chains. *Proceedings of the Combustion Institute*, 2005, **30**(1), pp.1689-1697.
189. KOOK, S., R. ZHANG, K. SZETO, L.M. PICKETT and T. AIZAWA. *In-flame soot sampling and particle analysis in a diesel engine*. SAE Technical Paper, 2013.

190. LEHRE, T., R. SUNTZ and H. BOCKHORN. Time-resolved two-color LII: size distributions of nano-particles from gas-to-particle synthesis. *Proceedings of the Combustion Institute*, 2005, **30**(2), pp.2585-2593.
191. VANDER WAL, R.L. Flame synthesis of Ni-catalyzed nanofibers. *Carbon*, 2002, **40**(12), pp.2101-2107.
192. HOFMANN, M., W.G. BESSLER, C. SCHULZ and H. JANDER. Laser-induced incandescence for soot diagnostics at high pressures. *Applied Optics*, 2003, **42**(12), pp.2052-2062.
193. VANDER WAL, R.L. Laser-induced incandescence: detection issues. *Applied Optics*, 1996, **35**(33), pp.6548-6559.
194. VANDER WAL, R.L. and K.A. JENSEN. Laser-induced incandescence: excitation intensity. *Applied Optics*, 1998, **37**(9), pp.1607-1616.
195. ROSS AB; LEA-LANGTON A; FITZPATRICK EM; JONES JM; WILLIAMS A; ANDREWS GE; LI H; BARTLE KD. Investigation of Pyrolysis of Hydrocarbons and Biomass Model Compounds Using a Micropyrolysis Flow Cell. . *Energy & Fuels*, 2011, **25**, pp. 2945 - 2955.
196. BOND, T.C., S.J. DOHERTY, D. FAHEY, P. FORSTER, T. BERNTSEN, B. DEANGELO, M. FLANNER, S. GHAN, B. KÄRCHER and D. KOCH. Bounding the role of black carbon in the climate system: A scientific assessment. *Journal of Geophysical Research: Atmospheres*, 2013, **118**(11), pp.5380-5552.
197. BØLLING, A.K., J. PAGELS, K.E. YTTRI, L. BARREGARD, G. SALLSTEN, P.E. SCHWARZE and C. BOMAN. Health effects of residential wood smoke particles: the importance of combustion conditions and physicochemical particle properties. *Particle and fibre toxicology*, 2009, **6**(29), p.20.
198. KENNEDY, I.M. The health effects of combustion-generated aerosols. *Proceedings of the Combustion Institute*, 2007, **31**(2), pp.2757-2770.
199. FITZPATRICK, E., K. BARTLE, M. KUBACKI, J. JONES, M. POURKASHANIAN, A. ROSS, A. WILLIAMS and K. KUBICA. The mechanism of the formation of soot

- and other pollutants during the co-firing of coal and pine wood in a fixed bed combustor. *Fuel*, 2009, **88**(12), pp.2409-2417.
200. FITZPATRICK, E., J. JONES, M. POURKASHANIAN, A. ROSS, A. WILLIAMS and K. BARTLE. Mechanistic aspects of soot formation from the combustion of pine wood. *Energy & Fuels*, 2008, **22**(6), pp.3771-3778.
201. FITZPATRICK, E., A. ROSS, J. BATES, G. ANDREWS, J. JONES, H. PHYLAKTOU, M. POURKASHANIAN and A. WILLIAMS. Emission of oxygenated species from the combustion of pine wood and its relation to soot formation. *Process safety and environmental protection*, 2007, **85**(5), pp.430-440.
202. WILSON, J., M. BAEZA-ROMERO, J. JONES, M. POURKASHANIAN, A. WILLIAMS, A. LEA-LANGTON, A. ROSS and K. BARTLE. Soot formation from the combustion of biomass pyrolysis products and a hydrocarbon fuel, n-decane: an aerosol time of flight mass spectrometer (ATOFMS) study. *Energy & Fuels*, 2013, **27**(3), pp.1668-1678.
203. SCHMIDL, C., I.L. MARR, A. CASEIRO, P. KOTIANOVÁ, A. BERNER, H. BAUER, A. KASPER-GIEBL and H. PUXBAUM. Chemical characterisation of fine particle emissions from wood stove combustion of common woods growing in mid-European Alpine regions. *Atmospheric Environment*, 2008, **42**(1), pp.126-141.
204. ROSS, A., S. JUNYAPOON, J. JONES, A. WILLIAMS and K. BARTLE. A study of different soots using pyrolysis–GC–MS and comparison with solvent extractable material. *Journal of analytical and applied pyrolysis*, 2005, **74**(1), pp.494-501.
205. FERGE, T., E. KARG, A. SCHRÖPPEL, K. COFFEE, H. TOBIAS, M. FRANK, E. GARD and R. ZIMMERMANN. Fast determination of the relative elemental and organic carbon content of aerosol samples by on-line single-particle aerosol time-of-flight mass spectrometry. *Environmental Science & Technology*, 2006, **40**(10), pp.3327-3335.
206. ELSASSER, M., C. BUSCH, J.R. ORASCHE, C. SCHÖN, H. HARTMANN, J.R. SCHNELLE-KREIS and R. ZIMMERMANN. Dynamic changes of the aerosol

- composition and concentration during different burning phases of wood combustion. *Energy & Fuels*, 2013, **27**(8), pp.4959-4968.
207. HEAL, M.R. and P. QUINCEY. The relationship between black carbon concentration and black smoke: a more general approach. *Atmospheric Environment*, 2012, **54**, pp.538-544.
208. ORASCHE, J.R., J.R. SCHNELLE-KREIS, C. SCHÖN, H. HARTMANN, H. RUPPERT, J.M. ARTEAGA-SALAS and R. ZIMMERMANN. Comparison of emissions from wood combustion. Part 2: Impact of combustion conditions on emission factors and characteristics of particle-bound organic species and polycyclic aromatic hydrocarbon (PAH)-related toxicological potential. *Energy & Fuels*, 2013, **27**(3), pp.1482-1491.
209. COLKET, M.B. and R.J. HALL. Successes and uncertainties in modeling soot formation in laminar, premixed flames. *In: Soot formation in combustion*. Springer, 1994, pp.442-470.
210. FRENKLACH, M. and H. WANG. Detailed mechanism and modeling of soot particle formation. *In: Soot formation in combustion*. Springer, 1994, pp.165-192.
211. MARICQ, M.M. Examining the relationship between black carbon and soot in flames and engine exhaust. *Aerosol Science and Technology*, 2014, **48**(6), pp.620-629.
212. SONG, J. and P.A. PENG. Characterisation of black carbon materials by pyrolysis–gas chromatography–mass spectrometry. *Journal of analytical and applied pyrolysis*, 2010, **87**(1), pp.129-137.
213. D'ANNA, A. and A. VIOLI. Detailed modeling of the molecular growth process in aromatic and aliphatic premixed flames. *Energy & Fuels*, 2005, **19**(1), pp.79-86.
214. RICHTER, H. and J.B. HOWARD. Formation and consumption of single-ring aromatic hydrocarbons and their precursors in premixed acetylene, ethylene and benzene flames. *Physical Chemistry Chemical Physics*, 2002, **4**(11), pp.2038-2055.
215. ROSS, A., A. LEA-LANGTON, E. FITZPATRICK, J. JONES, A. WILLIAMS, G. ANDREWS, H. LI and K. BARTLE. Investigation of pyrolysis of hydrocarbons and

- biomass model compounds using a micropyrolysis flow cell. *Energy & Fuels*, 2011, **25**(7), pp.2945-2955.
216. ROSS, A.B., J.M. JONES, S. CHAIKLANGMUANG, M. POURKASHANIAN, A. WILLIAMS, K. KUBICA, J.T. ANDERSSON, M. KERST, P. DANIHELKA and K.D. BARTLE. Measurement and prediction of the emission of pollutants from the combustion of coal and biomass in a fixed bed furnace. *Fuel*, 2002, **81**(5), pp.571-582.
217. OBERDÖRSTER, G. Pulmonary effects of inhaled ultrafine particles. *International archives of occupational and environmental health*, 2000, **74**(1), pp.1-8.
218. ORGANIZATION, W.H. Effects of air pollution on children's health and development: a review of the evidence. 2005.
219. SMOOKE, M., M. LONG, B. CONNELLY, M. COLKET and R. HALL. Soot formation in laminar diffusion flames. *Combustion and Flame*, 2005, **143**(4), pp.613-628.
220. JONES, J.M. Chemical fractionation of copper, lead and zinc in ombrotrophic peat. *Environmental Pollution*, 1987, **48**(2), pp.131-144.
221. JONES, J.M., LEA-LANGTON, A. R., MA, L., POURKASHANIAN, M., WILLIAMS, A. Pollutant Formation and Health Effects. In: *Pollutants Generated by the Combustion of Solid Biomass Fuels*. Springer London, 2014, pp.45-61.
222. A.R. LEA-LANGTON, F.A.A., K.D. BARTLE, J.M. JONES, M POURKASHANIAN and I.B. A WILLIAMS, G. HUMPHRIES. Mechanism of the formation of smoke from the combustion of wood. *Under review*, 2014, pp.1-31.
223. E.M. FITZPATRICK, A.B.R., J.M. JONES, A. WILLIAMS. Smoke produced from the Combustion of Biomass. In: *Proceedings of the 15th European Biomass Conference and Exhibition*, May 2007, Berlin. 2007, pp.7-11.
224. A.R. LEA-LANGTON, F.A.A., J.M. JONES, M POURKASHANIAN, A WILLIAMS, K.D. BARTLE,. Pyrolysis of soot from Biomass. *Under review with the journal of Analytical and Applied pyrolysis*, 2014, **xx**, pp.1-15.
225. COZIC, J., S. MERTES, B. VERHEGGEN, D.J. CZICZO, S. GALLAVARDIN, S. WALTER, U. BALTENSPERGER and E. WEINGARTNER. Black carbon enrichment

- in atmospheric ice particle residuals observed in lower tropospheric mixed phase clouds. *Journal of Geophysical Research: Atmospheres (1984–2012)*, 2008, **113**(D15).
226. AVAKIAN, M.D., B. DELLINGER, H. FIEDLER, B. GULLET, C. KOSHLAND, S. MARKLUND, G. OBERDÖRSTER, S. SAFE, A. SAROFIM and K.R. SMITH. The origin, fate, and health effects of combustion by-products: a research framework. *Environmental health perspectives*, 2002, **110**(11), p.1155.
227. SMEDLEY, J.M., A. WILLIAMS and A. MUTSHIMWONG. Soot deposition from ethylene/air flames and the role of aromatic intermediates. *In: Soot Formation in Combustion*. Springer, 1994, pp.403-416.
228. FRUSTERI, L., C. CANNILLA, K. BARBERA, S. PERATHONER, G. CENTI and F. FRUSTERI. Carbon growth evidences as a result of benzene pyrolysis. *Carbon*, 2013, **59**, pp.296-307.
229. RAVINDRA, K., R. SOKHI and R. VAN GRIEKEN. Atmospheric polycyclic aromatic hydrocarbons: source attribution, emission factors and regulation. *Atmospheric Environment*, 2008, **42**(13), pp.2895-2921.
230. SEATON, A., D. GODDEN, W. MACNEE and K. DONALDSON. Particulate air pollution and acute health effects. *The Lancet*, 1995, **345**(8943), pp.176-178.
231. SIEGRIST, J. Adverse health effects of high-effort/low-reward conditions. *Journal of occupational health psychology*, 1996, **1**(1), p.27.
232. SNAPE, C.E. and K.D. BARTLE. Definition of fossil fuel-derived asphaltenes in terms of average structural properties. *Fuel*, 1984, **63**(7), pp.883-887.
233. LI, D.D. and M.L. GREENFIELD. High internal energies of proposed asphaltene structures. *Energy & Fuels*, 2011, **25**(8), pp.3698-3705.
234. WALLER, P., A. WILLIAMS and K.D. BARTLE. The structural nature and solubility of residual fuel oil fractions. *Fuel*, 1989, **68**(4), pp.520-526.
235. KARIMI, A., K. QIAN, W.N. OLMSTEAD, H. FREUND, C. YUNG and M.R. GRAY. Quantitative evidence for bridged structures in asphaltenes by thin film pyrolysis. *Energy & Fuels*, 2011, **25**(8), pp.3581-3589.

236. MORGAN, T., P. ALVAREZ-RODRIGUEZ, A. GEORGE, A. HEROD and R. KANDIYOTI. Characterization of Maya crude oil maltenes and asphaltenes in terms of structural parameters calculated from nuclear magnetic resonance (NMR) spectroscopy and laser desorption– mass spectroscopy (LD– MS). *Energy & Fuels*, 2010, **24**(7), pp.3977-3989.
237. ROSS, A., S. JUNYAPOON, K. BARTLE, J. JONES and A. WILLIAMS. Development of pyrolysis–GC with selective detection: coupling of pyrolysis–GC to atomic emission detection (py–GC–AED). *Journal of analytical and applied pyrolysis*, 2001, **58**, pp.371-385.
238. QUIMBY, B.D., D.A. GRUDOSKI and V. GIARROCCO. Improved Measurement of Sulfur and Nitrogen Compounds in Refinery Liquids Using Gas Chromatography— Atomic Emission Detection. *Journal of chromatographic science*, 1998, **36**(9), pp.435-443.
239. MÖSSNER, S.G. and S.A. WISE. Determination of polycyclic aromatic sulfur heterocycles in fossil fuel-related samples. *Analytical chemistry*, 1999, **71**(1), pp.58-69.
240. BARTLE, K., S. HALL, K. HOLDEN, S. MITCHELL and A. ROSS. Analysis of oxygen-containing polycyclic aromatic compounds by gas chromatography with atomic emission detection. *Fuel*, 2009, **88**(2), pp.348-353.
241. SENUM, G.I. and R.T. YANG. Rational approximations of the integral of the Arrhenius function. *Journal of thermal analysis*, 1977, **11**(3), pp.445-447.
242. LEA-LANGTON, A., G. ANDREWS, K. BARTLE, J. JONES and A. WILLIAMS. Combustion and pyrolysis reactions of alkylated polycyclic aromatic compounds: The decomposition of ¹³C methylarenes in relation to diesel engine emissions. *Fuel*, 2015, **158**, pp.719-724.
243. M.K.SARMAH, A.B.A.A.D. Chemical characterization of *Bull. Material Sci.*, 2010, , **33**,, pp.509-515.
244. GARG, V.N., B.D. BHATT, V.K. KAUSHIK and K.R. MURTHY. Polycyclic Aromatic Hydrocarbons in C8 Isomer Aromatic Feed: Analysis by GC, GC/MS, and GC/FTIR Techniques. *Journal of chromatographic science*, 1987, **25**(6), pp.237-246.

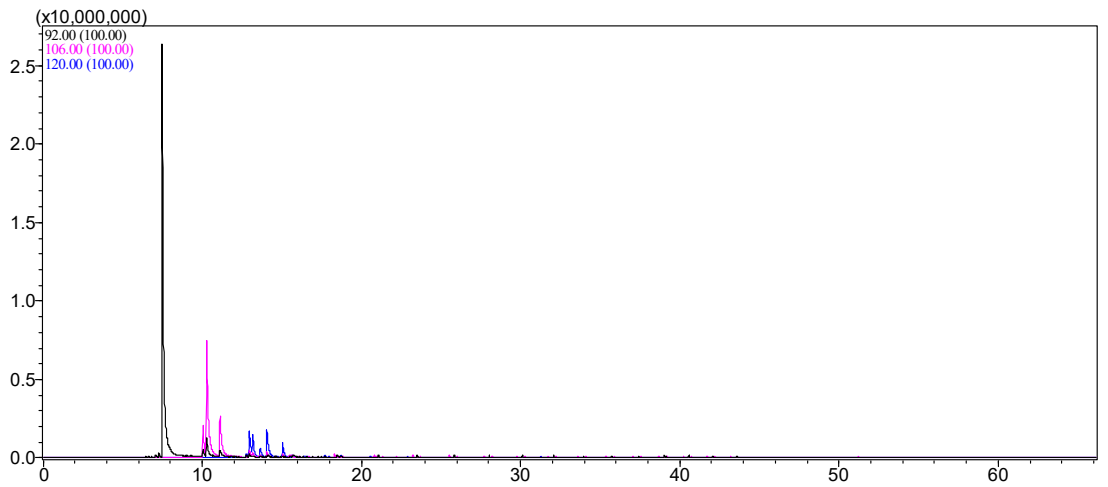
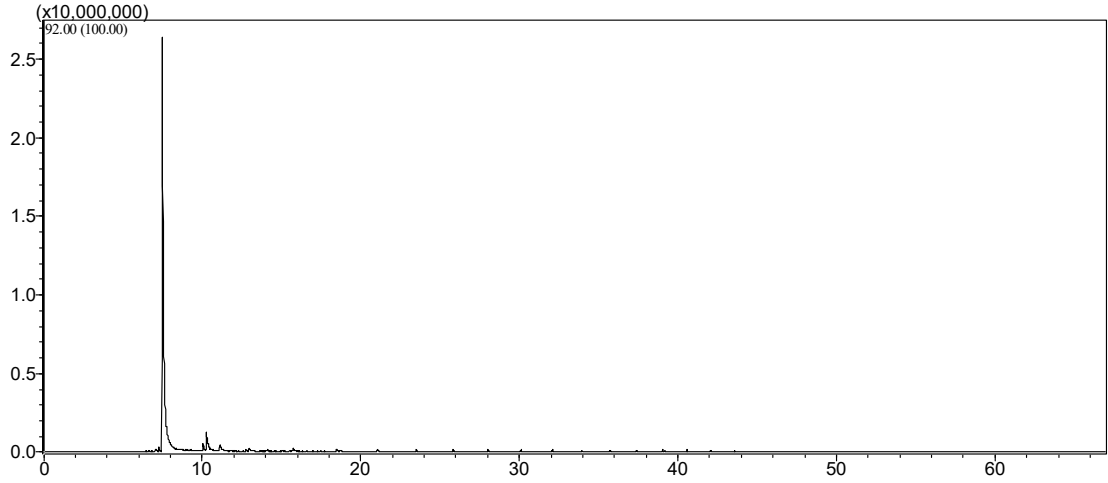
245. HECHT, S.S. Lung carcinogenesis by tobacco smoke. *International journal of cancer*, 2012, **131**(12), pp.2724-2732.
246. P.O.P., H.G.A. ed. *Polycyclic Hydrocarbons and Cancer* Tso Eds. ' ed. New York Academic Press, , (2012).
247. K.M.L.HOLDEN. *PhD Thesis*. thesis, University of Leeds (UK) 1997.
248. EASTMOND, D.A., G.M. BOOTH and M.L. LEE. Toxicity, accumulation, and elimination of polycyclic aromatic sulfur heterocycles in *Daphnia magna*. *Archives of Environmental Contamination and Toxicology*, 1984, **13**(1), pp.105-111.
249. REINKE, G., M. SWANSON, D. PAUSTENBACH and J. BEACH. Chemical and mutagenic properties of asphalt fume condensates generated under laboratory and field conditions. *Mutation Research/Genetic Toxicology and Environmental Mutagenesis*, 2000, **469**(1), pp.41-50.
250. GRAY, M.R., R.R. TYKWINSKI, J.M. STRYKER and X. TAN. Supramolecular assembly model for aggregation of petroleum asphaltenes. *Energy & Fuels*, 2011, **25**(7), pp.3125-3134.
251. RATKIEWICZ, A. Kinetics of 1, 6-hydrogen migration in alkyl radical reaction class. *Reaction Kinetics, Mechanisms and Catalysis*, 2013, **108**(2), pp.545-564.
252. RATKIEWICZ, A. and T.N. TRUONG. Kinetics of the C–C bond beta scission reactions in alkyl radical reaction class. *The Journal of Physical Chemistry A*, 2012, **116**(25), pp.6643-6654.
253. SIMMIE, J.M. Detailed chemical kinetic models for the combustion of hydrocarbon fuels. *Progress in Energy and Combustion Science*, 2003, **29**(6), pp.599-634.
254. SNAPE, C.E., K.D. BARTLE, I.O. AMAECHINA and D.G. MILLS. The chemical nature of material released from coal-derived asphaltenes by reprecipitation and cyclohexane extraction. *Fuel Processing Technology*, 1987, **16**(1), pp.89-96.
255. DAVIES, I.L., K.D. BARTLE, P.T. WILLIAMS and G.E. ANDREWS. On-line fractionation and identification of diesel fuel polycyclic aromatic compounds by two-dimensional microbore high-performance liquid chromatography/capillary gas chromatography. *Analytical chemistry*, 1988, **60**(3), pp.204-209.

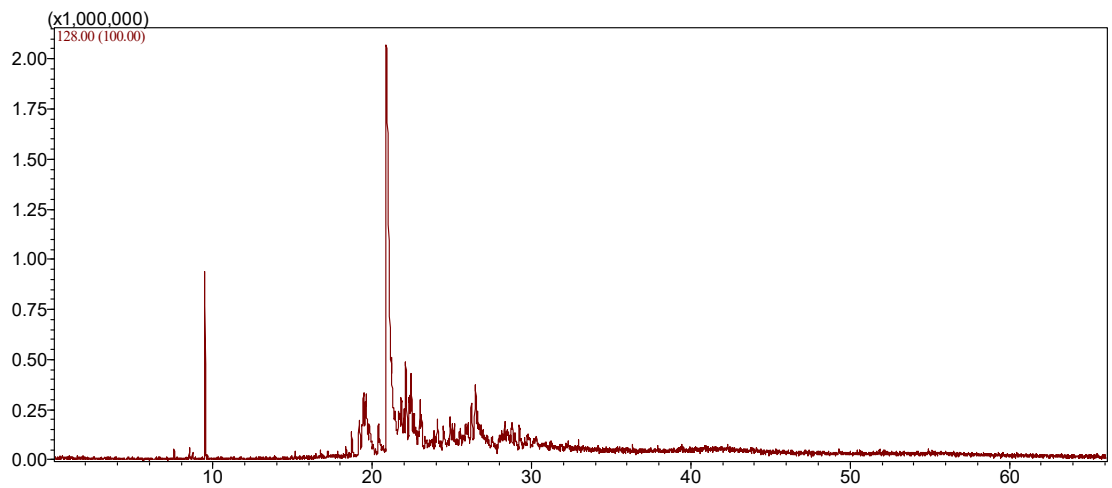
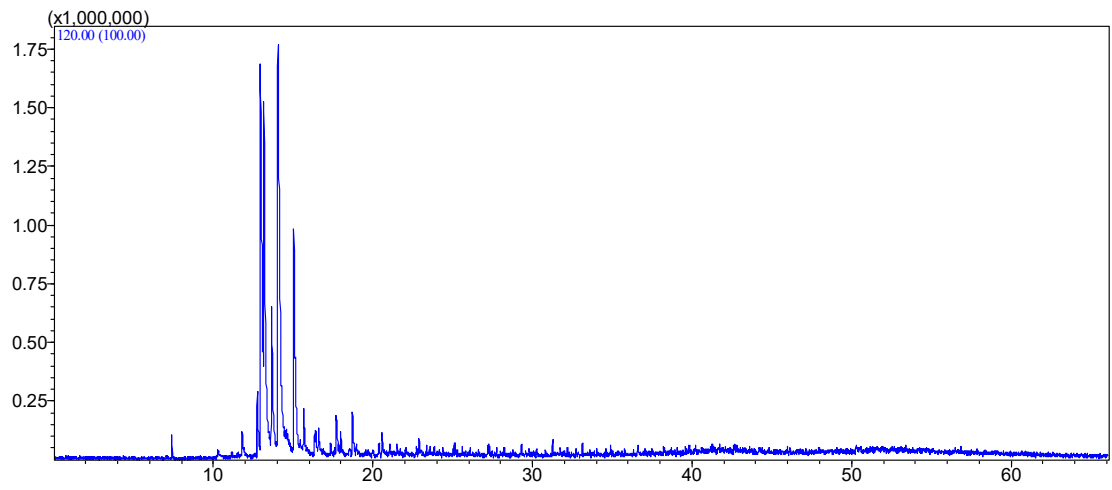
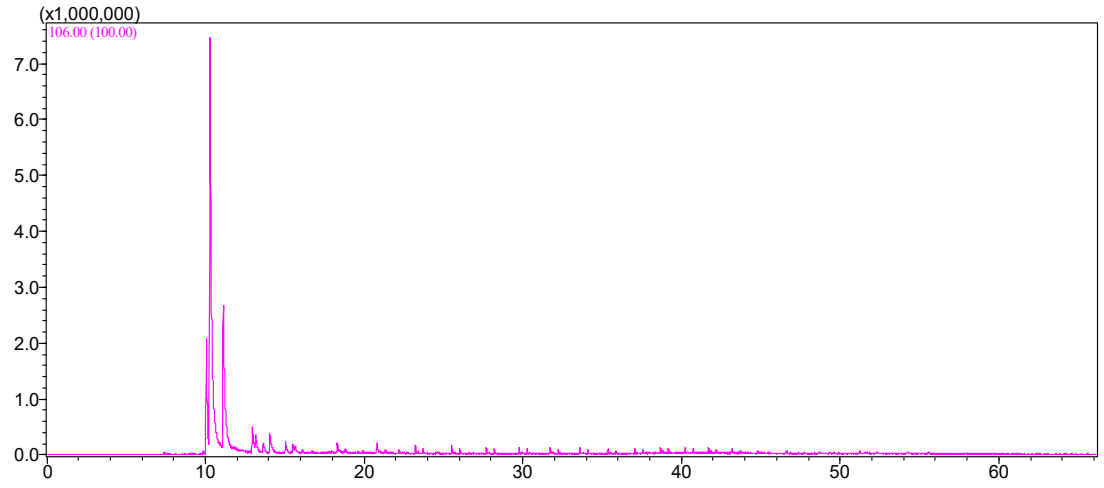
256. XIONG, Y. and A. GENG. Carbon isotopic composition of individual n-alkanes in asphaltene pyrolysates of biodegraded crude oils from the Liaohe Basin, China. *Organic Geochemistry*, 2000, **31**(12), pp.1441-1449.
257. WALDO, G.S., O.C. MULLINS, J.E. PENNER-HAHN and S. CRAMER. Determination of the chemical environment of sulphur in petroleum asphaltenes by X-ray absorption spectroscopy. *Fuel*, 1992, **71**(1), pp.53-57.
258. WALLACE, S., K. BARTLE, M. BURKE, B. EGIA, S. LU, N. TAYLOR, T. FLYNN, W. KEMP and W. STEEDMAN. Characterization of petroleum feedstocks for coal-oil co-processing. *Fuel*, 1989, **68**(8), pp.961-967.
259. BARTLE, K., S. BOTTRELL, M. BURKE, C. JONES, P. LOUIE, S.L. LU, J. SALVADO, N. TAYLOR and S. WALLACE. Co-refining of coal and petroleum: New analytical methods and results. *International journal of energy research*, 1994, **18**(2), pp.309-315.
260. PAYZANT, J., E. LOWN and O. STRAUSZ. Structural units of Athabasca asphaltene: the aromatics with a linear carbon framework. *Energy & Fuels*, 1991, **5**(3), pp.445-453.
261. LOEGEL, T.N., N.D. DANIELSON, D.J. BORTON, M.R. HURT and H.I. KENTTÄMAA. Separation of asphaltenes by reversed-phase liquid chromatography with fraction characterization. *Energy & Fuels*, 2012, **26**(5), pp.2850-2857.
262. SADIQ, M. and A. MIAN. Nickel and vanadium in air particulates at Dhahran (Saudi Arabia) during and after the Kuwait oil fires. *Atmospheric Environment*, 1994, **28**(13), pp.2249-2253.
263. ORGANIZATION, W.H. *The world health report 2002: reducing risks, promoting healthy life*. World Health Organization, 2002.
264. COOPER, D. Exhaust emissions from high speed passenger ferries. *Atmospheric Environment*, 2001, **35**(24), pp.4189-4200.
265. YANG, H.-H., W.-J. LEE, S.-J. CHEN and S.-O. LAI. PAH emission from various industrial stacks. *Journal of Hazardous Materials*, 1998, **60**(2), pp.159-174.
266. JANG, H.-N., Y.-C. SEO, J.-H. LEE, K.-W. HWANG, J.-I. YOO, C.-H. SOK and S.-H. KIM. Formation of fine particles enriched by V and Ni from heavy oil combustion:

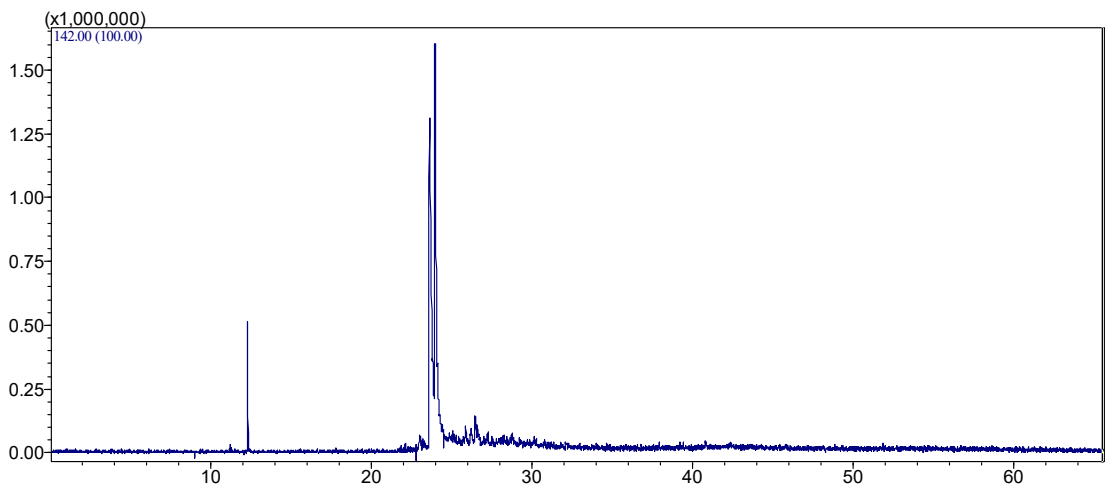
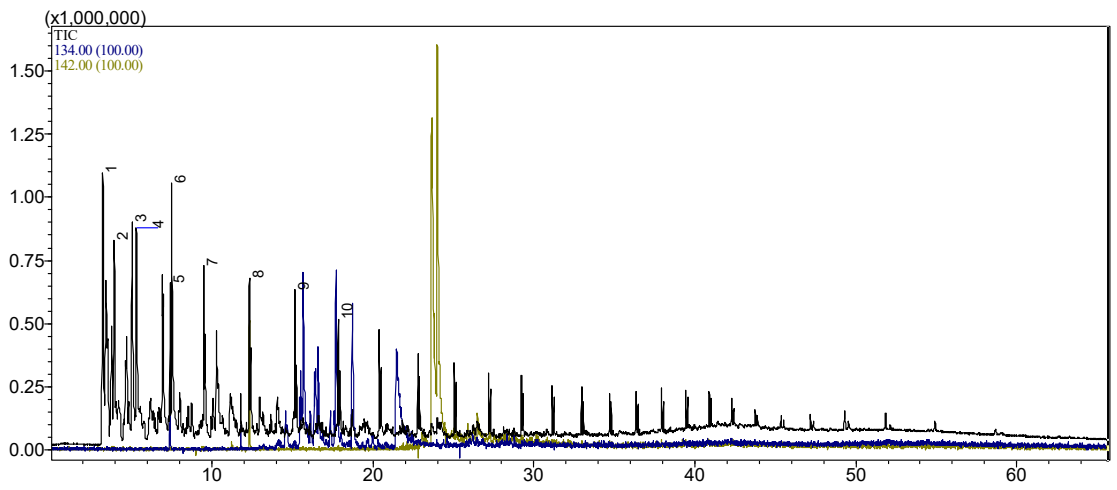
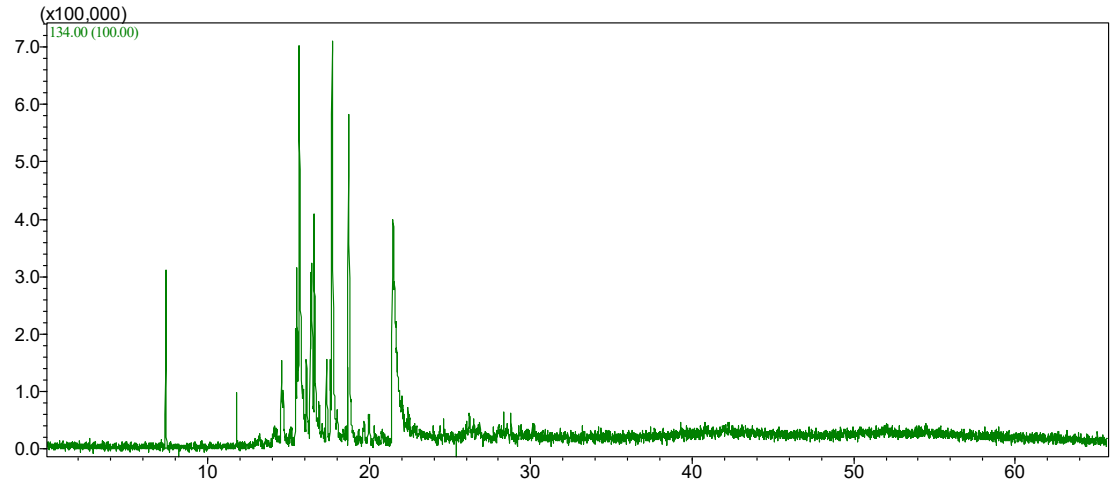
- Anthropogenic sources and drop-tube furnace experiments. *Atmospheric Environment*, 2007, **41**(5), pp.1053-1063.
267. ZENG, Y. and P.C. UDEN. High temperature gas chromatography–atomic emission detection of metalloporphyrins in crude oils. *Journal of High Resolution Chromatography*, 1994, **17**(4), pp.223-229.
268. GOUAL, L. *Petroleum asphaltenes*. INTECH Open Access Publisher, 2012.
269. HOSSEINNEZHAD, S., E.H. FINI, B.K. SHARMA, M. BASTI and B. KUNWAR. Physiochemical characterization of synthetic bio-oils produced from bio-mass: a sustainable source for construction bio-adhesives. *RSC Advances*, 2015, **5**(92), pp.75519-75527.
270. LEHTO, J., A. OASMAA, Y. SOLANTAUSTA, M. KYTÖ and D. CHIARAMONTI. Review of fuel oil quality and combustion of fast pyrolysis bio-oils from lignocellulosic biomass. *Applied Energy*, 2014, **116**, pp.178-190.
271. CENTER, D.E.S. *Petroleum Quality Information System Report*. Ft. Belvoir, VA 2006.
272. MANSOORI, G., T. JIANG and S. KAWANAKA. Asphaltene deposition and its role in petroleum production and processing. *Arab. J. Sci. Eng*, 1988, **13**(1), pp.17-34.
273. GOUAL, L. and A. FIROOZABADI. Measuring asphaltenes and resins, and dipole moment in petroleum fluids. *AIChE Journal*, 2002, **48**(11), pp.2646-2663.
274. ALBOUDWAREJ, H., J. BECK, W. SVRCEK, H. YARRANTON and K. AKBARZADEH. Sensitivity of asphaltene properties to separation techniques. *Energy & Fuels*, 2002, **16**(2), pp.462-469.
275. ALBOUDWAREJ, H., W. SVRCEK and H. YARRANTON. PVT investigation of asphaltene precipitation and redissolution from bitumens. *In: Canadian International Petroleum Conference: Petroleum Society of Canada*, 2002.
276. AKBARZADEH, K., A. HAMMAMI, A. KHARRAT, D. ZHANG, S. ALLENSON, J. CREEK, S. KABIR, A. JAMALUDDIN, A.G. MARSHALL and R.P. RODGERS. Asphaltenes—problematic but rich in potential. *Oilfield Review*, 2007, **19**(2), pp.22-43.
277. MULLINS, O.C., E.Y. SHEU, A. HAMMAMI and A.G. MARSHALL. *Asphaltenes, heavy oils, and petroleomics*. Springer Science & Business Media, 2007.

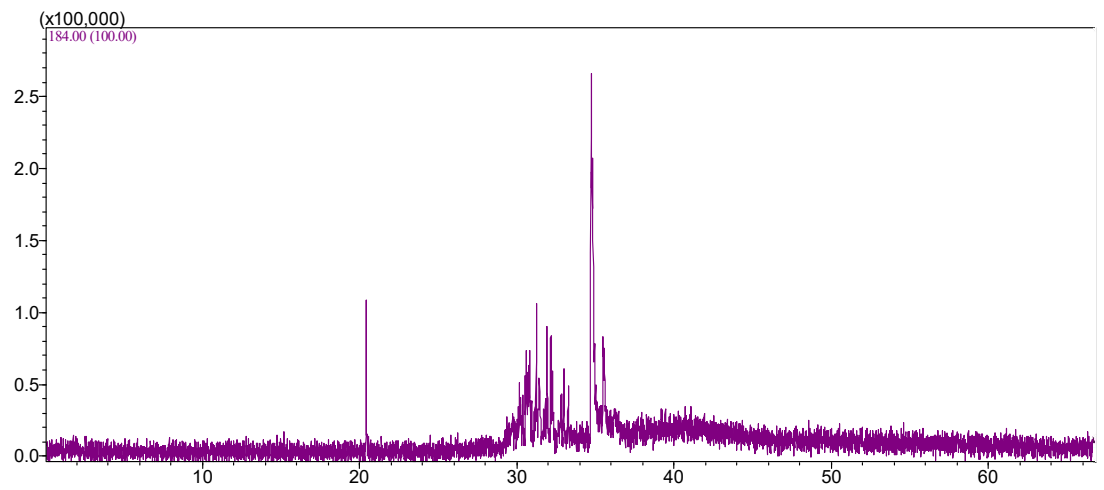
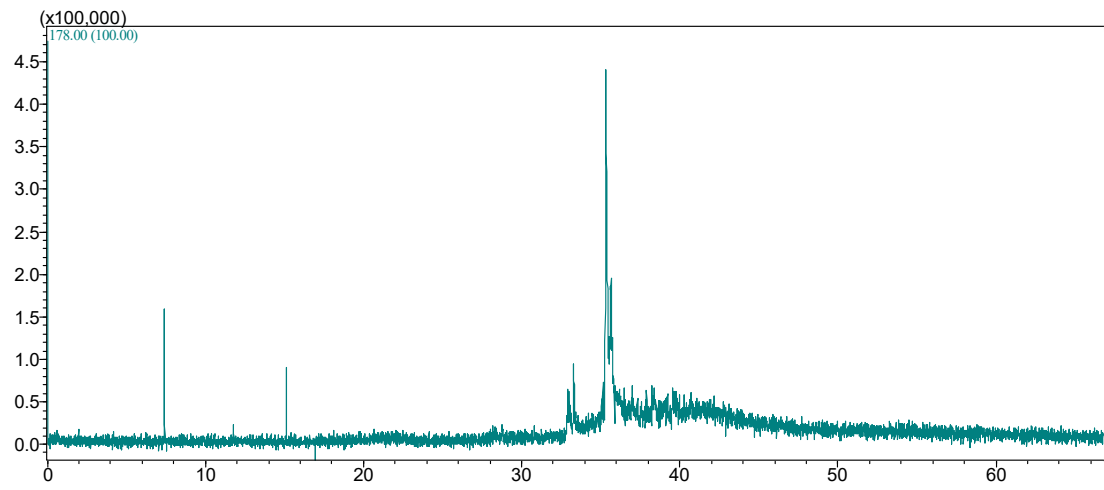
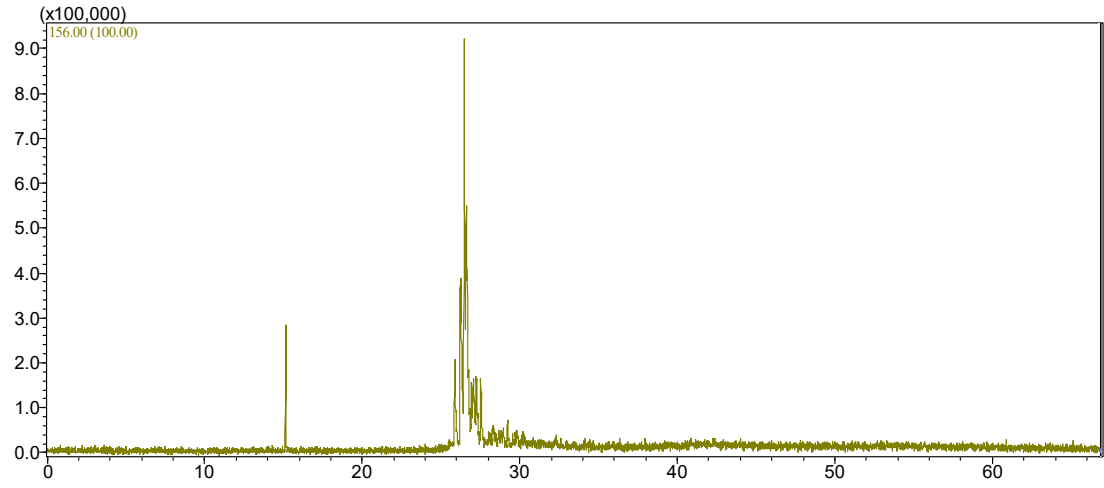
278. WILLIAMS, A. and M. POURKASHANIAN. The combustion of bitumen-water mixtures. *Journal of the Institute of Energy*, 1987, **60**(445), pp.209-211.
279. GIUNTOLI, J., W. DE JONG, S. ARVELAKIS, H. SPLIETHOFF and A. VERKOOIJEN. Quantitative and kinetic TG-FTIR study of biomass residue pyrolysis: Dry distiller's grains with solubles (DDGS) and chicken manure. *Journal of analytical and applied pyrolysis*, 2009, **85**(1), pp.301-312.
280. MANSARAY, K. and A. GHALY. Thermal degradation of rice husks in nitrogen atmosphere. *Bioresource technology*, 1998, **65**(1), pp.13-20.
281. DARVELL, L., J. JONES, B. GUDKA, X. BAXTER, A. SADDAWI, A. WILLIAMS and A. MALMGREN. Combustion properties of some power station biomass fuels. *Fuel*, 2010, **89**(10), pp.2881-2890.
282. LEYVA, C., J. ANCHEYTA, C. BERRUECO and M. MILLÁN. Chemical characterization of asphaltenes from various crude oils. *Fuel Processing Technology*, 2013, **106**, pp.734-738.
283. LEDESMA, E.B., C. CAMPOS, D.J. CRANMER, B.L. FOYTIK, M.N. TON, E.A. DIXON, C. CHIRINO, S. BATAMO and P. ROY. Vapor-Phase Cracking of Eugenol: Distribution of Tar Products as Functions of Temperature and Residence Time. *Energy & Fuels*, 2013, **27**(2), pp.868-878.
284. XU, Q., Z. ZHANG, S. ZHANG, F. WANG and Y. YAN. Molecular Structure Models of Asphaltene in Crude and Upgraded Bio-Oil. *Chemical Engineering & Technology*, 2014, **37**(7), pp.1198-1204.
285. STAŠ, M., D. KUBIČKA, J. CHUDOBA and M. POSPÍŠIL. Overview of analytical methods used for chemical characterization of pyrolysis bio-oil. *Energy & Fuels*, 2014, **28**(1), pp.385-402.
286. BALLESTER, J.M., N. FUEYO and C. DOPAZO. Combustion characteristics of heavy oil-water emulsions. *Fuel*, 1996, **75**(6), pp.695-705.
287. HOU, S.-S., F.M. RIZAL, T.-H. LIN, T.-Y. YANG and H.-P. WAN. Microexplosion and ignition of droplets of fuel oil/bio-oil (derived from lauan wood) blends. *Fuel*, 2013, **113**, pp.31-42.

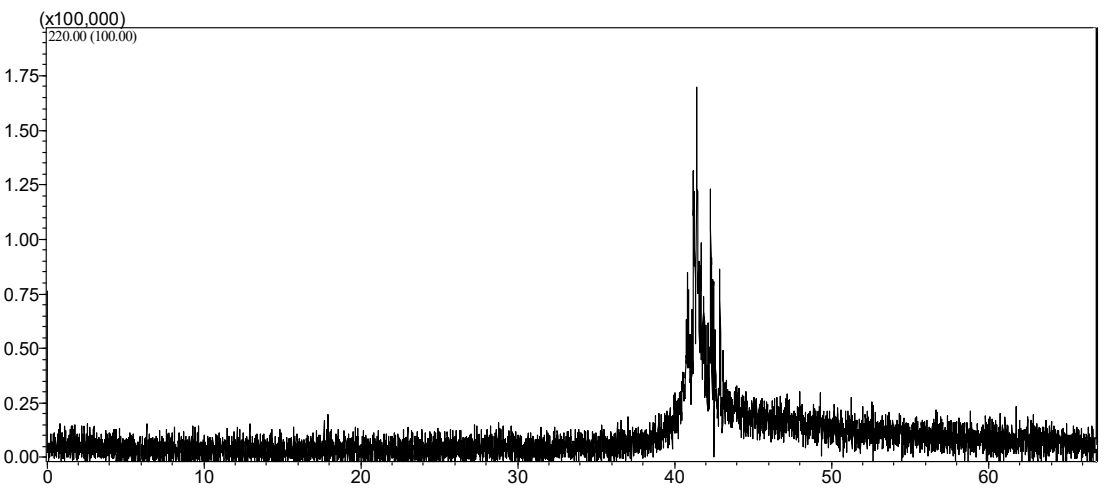
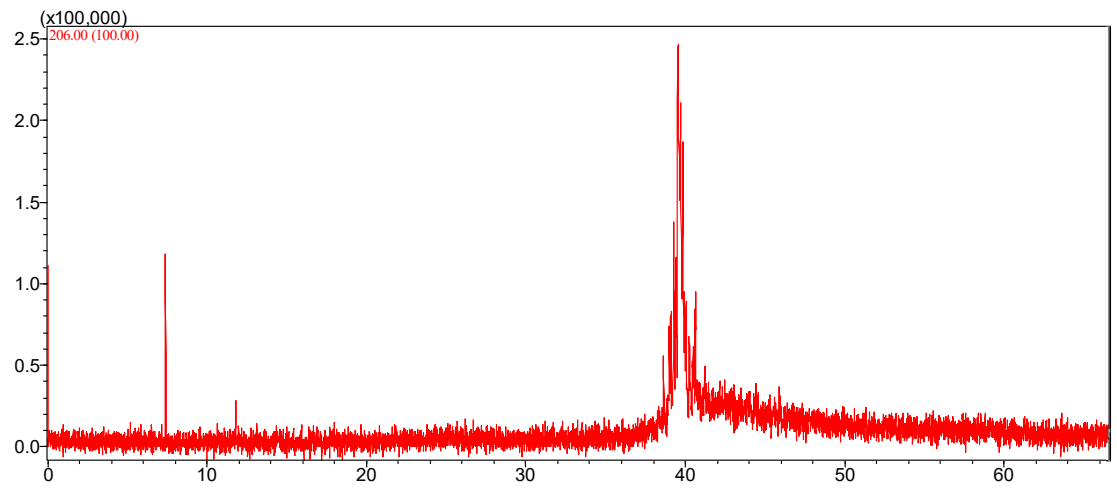
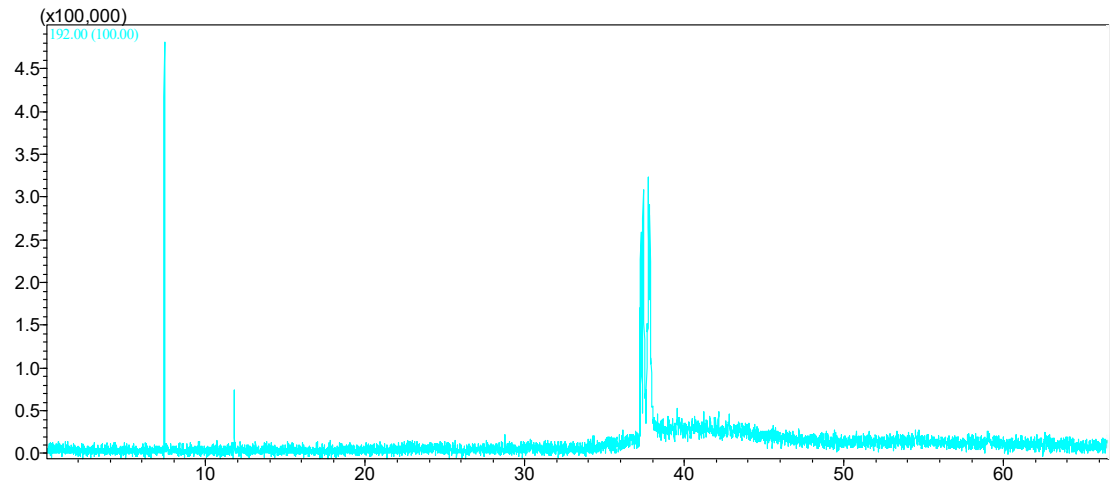
**Appendix A: Data interrogation for both Shell oil and heavy fuel oil
asphaltenes chromatograms showing different heavy molecular weight
compounds.**

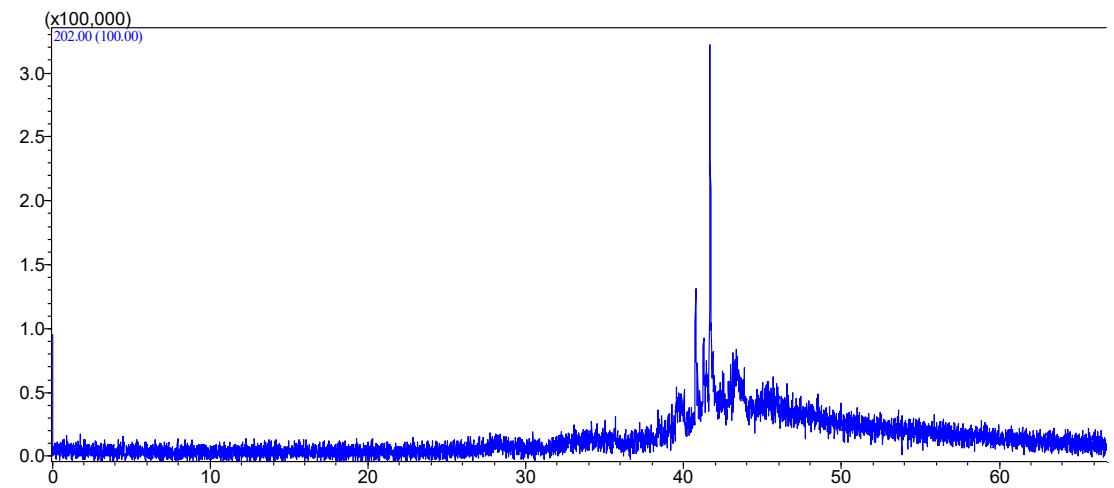
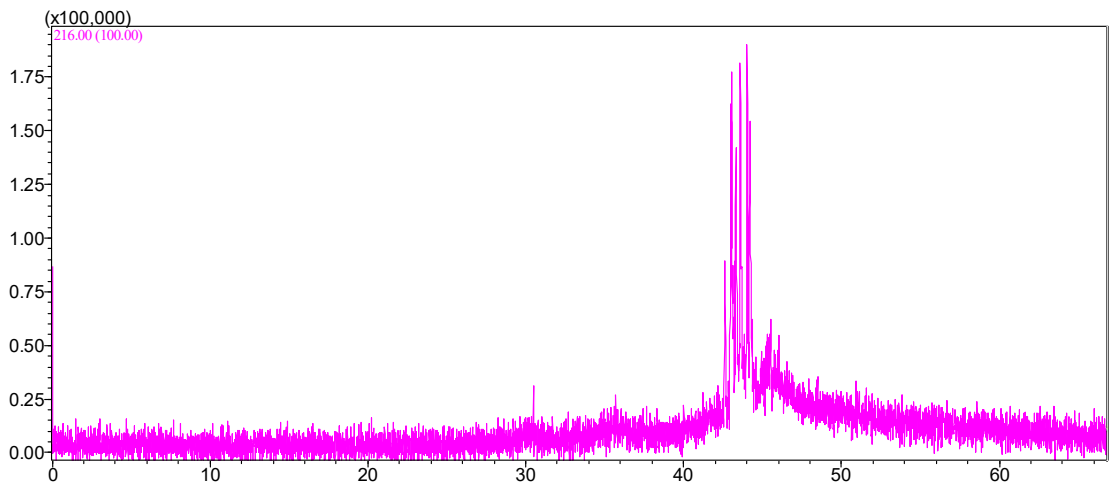
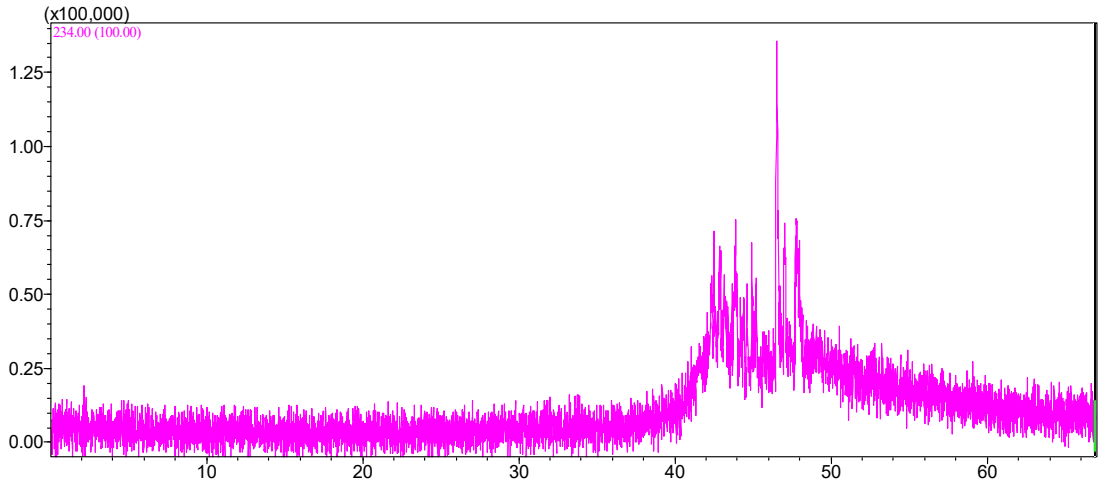


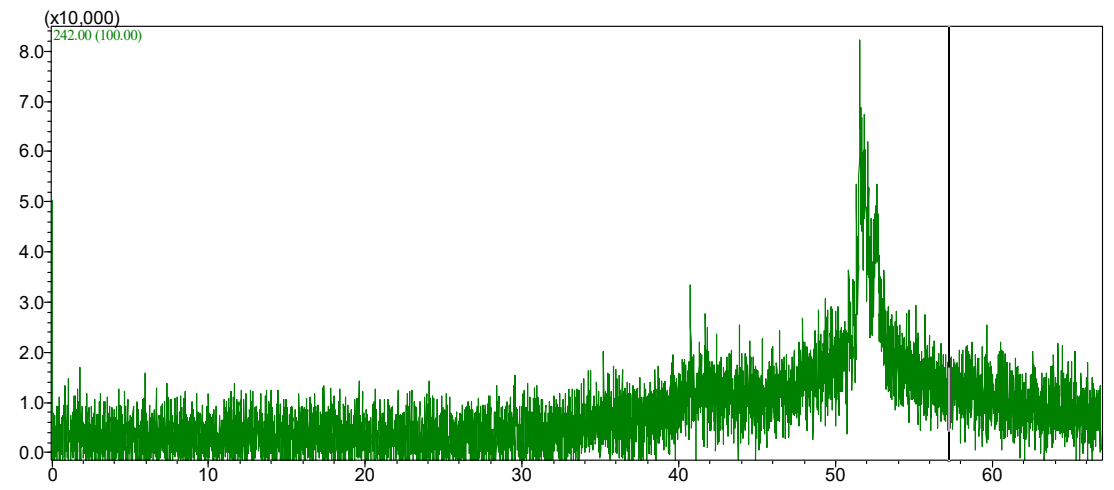
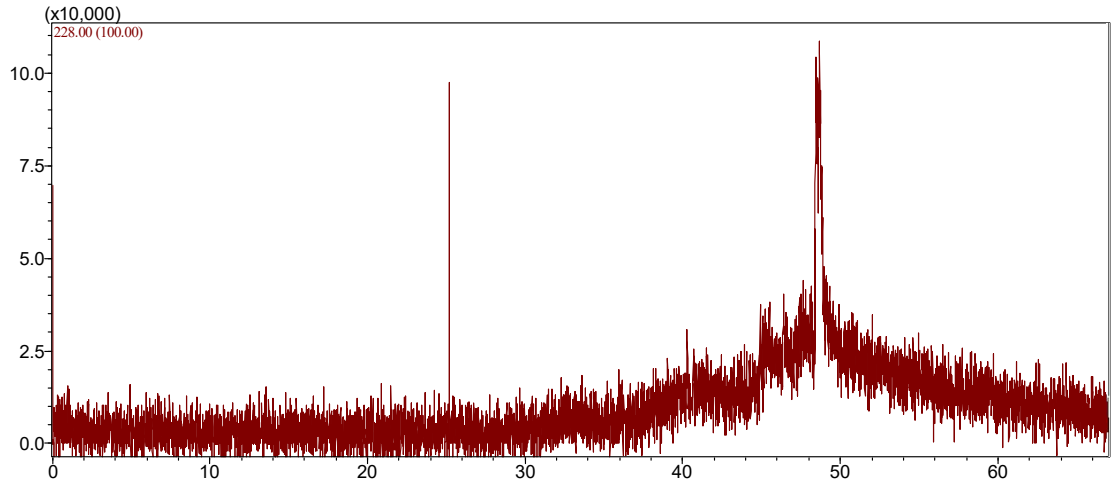




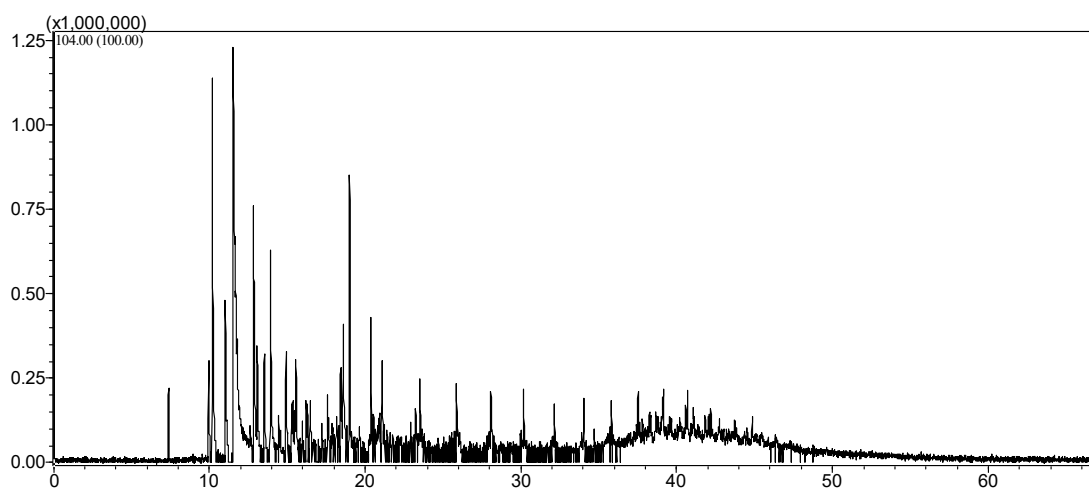




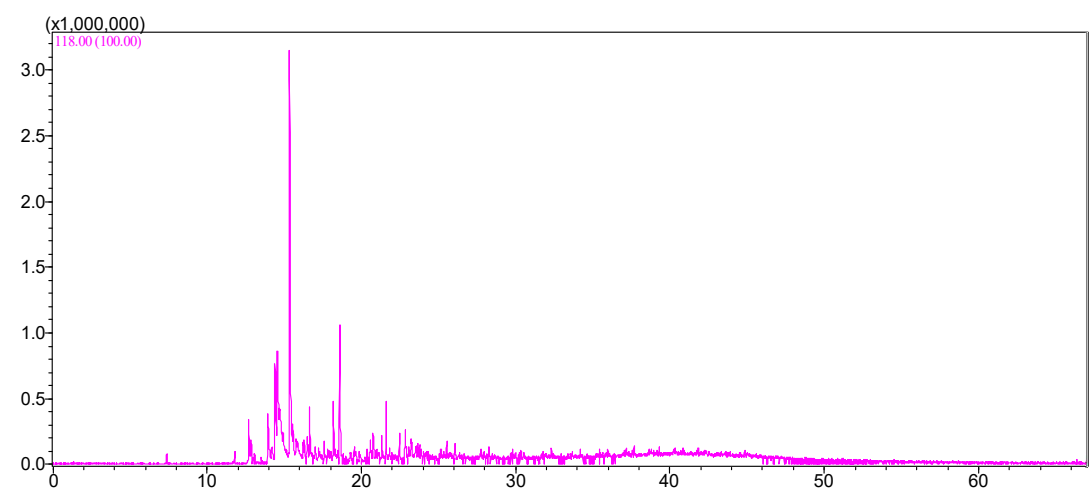




**Appendix B: Data interrogation for both Shell oil and heavy fuel oil
asphaltenes chromatograms showing different lower molecular weight
compounds.**



4-[(1E)-1,3-Butadienyl]-3,5,5-trimethyl-1-cyclohexene



Styrene, 2,4-dimethyl-

